

UNCLASSIFIED

AD 296 309

*Reproduced
by the*

**ARMED SERVICES TECHNICAL INFORMATION AGENCY
ARLINGTON HALL STATION
ARLINGTON 12, VIRGINIA**



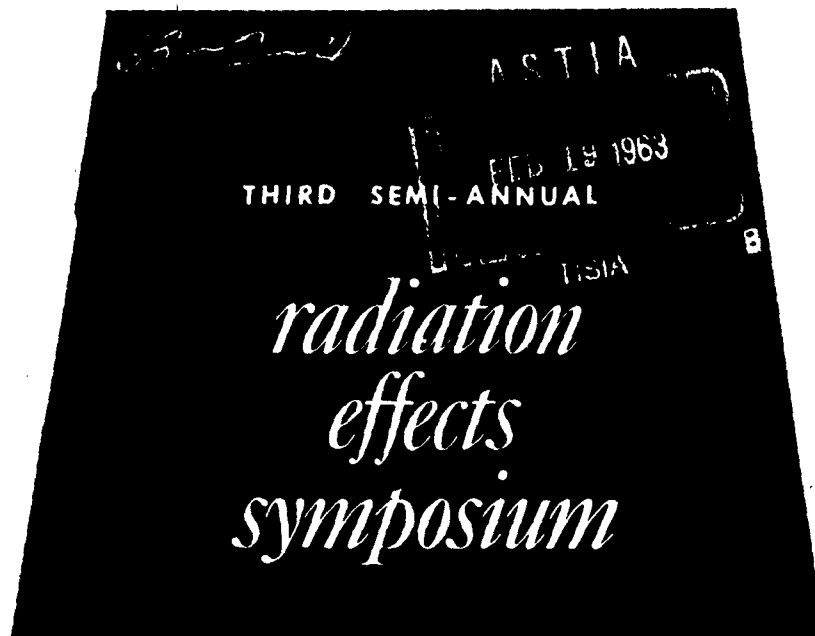
UNCLASSIFIED

NOTICE: When government or other drawings, specifications or other data are used for any purpose other than in connection with a definitely related government procurement operation, the U. S. Government thereby incurs no responsibility, nor any obligation whatsoever; and the fact that the Government may have formulated, furnished, or in any way supplied the said drawings, specifications, or other data is not to be regarded by implication or otherwise as in any manner licensing the holder or any other person or corporation, or conveying any rights or permission to manufacture, use or sell any patented invention that may in any way be related thereto.

296 309

4

of 6



\$21.00
p-351

Sponsored by Air Research and Development Command
UNITED STATES AIR FORCE

LOCKHEED NUCLEAR PRODUCTS
Lockheed Aircraft Corporation, Georgia Division

VOLUME 4 OF 6

Electronics and Semi-Conductors Papers

Third Semi-annual 28

radiation effects symposium

28-30 October 1958

Sponsored by**Air Research and Development Command
UNITED STATES AIR FORCE****LOCKHEED NUCLEAR PRODUCTS**LOCKHEED AIRCRAFT CORPORATION
GEORGIA DIVISION MARIETTA, GEORGIA

FOREWORD

The proceedings of the Third Semi-Annual ANP Radiation Effects Symposium, held at the Dinkler-Plaza Hotel in Atlanta, Georgia, October 28 through 30, 1958, are in six volumes. Each of the first five volumes presents the unclassified papers from one of the five sessions; the sixth volume presents classified papers from all five sessions.

Each volume contains a complete table of contents and an index of authors. Volume One contains a list of the names of all who attended the Symposium.

VOLUME 1

GENERAL SESSION

1. APPLICATION OF RADIATION EFFECTS DATA TO NUCLEAR AIRCRAFT PROBLEMS by ~~C. G. Collins, Aircraft Nuclear Propulsion Department, General Electric Company, Cincinnati, Ohio~~
2. RADIATION EFFECTS TESTING OF AIRCRAFT SUBSYSTEMS AND COMPONENTS AT AIR FORCE PLANT No. 67 FOR THE ANP PROGRAM by ~~W. L. Bridges, Lockheed Nuclear Products, Lockheed Aircraft Corporation, Georgia Division, Marietta, Georgia~~
3. *MISSION AND TRAFFIC CONTROL REQUIREMENTS FOR THE WS/125A by ~~James R. Burnett, Bendix Systems Division, Bendix Aviation Corporation, Ann Arbor, Michigan~~
4. NEW RADIATION TEST FACILITIES IN THE GENERAL ELECTRIC COMPANY by ~~S. S. Jones, Vallecitos Atomic Laboratory, General Electric Company, San Jose, California, and W. R. Langdon and T. T. Newlan, General Electric Company, Schenectady, New York~~
5. THE CONVAIR RADIATION EFFECTS TESTING SYSTEM by ~~J. W. Allen, Convair, A Division of General Dynamics Corporation, Fort Worth, Texas~~
6. RADIATION EFFECTS REACTOR by ~~W. T. Scarborough, Lockheed Nuclear Products, Lockheed Aircraft Corporation, Georgia Division, Marietta, Georgia~~
7. A DESCRIPTION OF A MULTI-KILOCURIE IRRADIATION FACILITY AND THE ASSOCIATED RADIATION DOSIMETRY by ~~R. E. Simpson, Lockheed Nuclear Products, Lockheed Aircraft Corporation, Georgia Division, Marietta, Georgia, and M. Z. Fainman, Mr. E. Krasnow, E. R. Rabin, C. R. Monahan, Inland Testing Laboratories and Cook Research, Morton Grove, Illinois~~
8. START-UP OF THE CRITICAL EXPERIMENT REACTOR by ~~M. A. Dewar, Lockheed Nuclear Products, Lockheed Aircraft Corporation, Georgia Division, Marietta, Georgia~~
9. REMOTE AREA MONITORING SYSTEM AT AIR FORCE PLANT No. 67 by ~~E. N. Lids, Lockheed Nuclear Products, Lockheed Aircraft Corporation, Georgia Division, Marietta, Georgia~~

* This paper is classified and is bound in Volume Six.

10. AREA MONITORING FOR RADIOACTIVITY by Roy Shipp, Lockheed Nuclear Products, Lockheed Aircraft Corporation, Georgia Division, Marietta, Georgia
11. LOGARITHMIC CIRCUITS FOR RADIATION DOSIMETRY by L. A. Turner, Lockheed Nuclear Products, Lockheed Aircraft Corporation, Georgia Division, Marietta, Georgia

VOLUME 2

DOSIMETRY AND NUCLEAR MEASUREMENTS

12. INFLUENCE OF ENERGY SPECTRA ON RADIATION EFFECTS by F. C. Malenschlein, Oak Ridge National Laboratory, Oak Ridge, Tennessee
13. CROSS SECTION AVERAGES FOR TYPICAL REACTOR SPECTRA by Walter R. Burrus and Russell P. Sullivan, Physics Department, Ohio State University, Columbus, Ohio
14. NUCLEAR UNITS AND MEASUREMENTS by R. S. Caswell and S. W. Smith, Atomic and Radiation Physics Division, National Bureau of Standards, Washington, District of Columbia
15. COMPARISON OF RADIATION EFFECTS IN DIFFERENT FACILITIES by W. T. Harper, Lockheed Aircraft Corporation, Lockheed Missile Systems Division, Palo Alto, California, and W. R. Burrus, Ohio State University, Columbus, Ohio
16. THE DETERMINATION OF NUCLEAR PARAMETERS FOR EXPERIMENTAL RADIATION EFFECTS by G. A. Wheeler, Convair, A Division of General Dynamics Corporation, Fort Worth, Texas
17. CALORIMETRIC DOSIMETRY PROGRAM AT LOCKHEED by Roger L. Gamble, Lockheed Nuclear Products, Lockheed Aircraft Corporation, Georgia Division, Marietta, Georgia
18. DOSIMETRY AND ENERGY DISTRIBUTION OF FAST NEUTRONS USING LI I by F. D. Schupp and S. L. Ruby, Radiation & Nucleonics Laboratory, Materials Engineering Department, Westinghouse Electric Corporation, East Pittsburgh, Pennsylvania

19. NEUTRON FLUX ENERGY DISTRIBUTION OF THE BNL REACTOR SHIELDING FACILITY by M. M. Weiss and M. M. Donnelly, Bell Telephone Laboratories, Whippany, New Jersey
20. THE EFFECTS OF NUCLEAR RADIATION ON SPARK GAPS by G. I. Duncan, Special Transformer Department, General Electric Company, Fort Wayne, Indiana, and J. C. Fraser and B. Valachovic, General Engineering Laboratory, General Electric Company, Schenectady, New York
21. RADIATION TESTING AND PROPERTIES OF A BORON NITRIDE DIELECTRIC CAPACITOR by G. R. Van Houten, T. C. O'Nan and J. T. Hood, P. R. Mallory and Company, Incorporated, Indianapolis, Indiana

VOLUME 3

AIRCRAFT SYSTEMS AND MATERIALS

22. THE PERFORMANCE OF IRRADIATED ELECTRONIC SYSTEMS BY ANALOG COMPUTER SIMULATION by V. C. Brown and N. M. Peterson, Convair, A Division of General Dynamics Corporation, Fort Worth, Texas
23. COMBINED TIME, TEMPERATURE, AND RADIATION EFFECTS ON ORGANIC MATERIALS by C. G. Collins, Aircraft Nuclear Propulsion Department, General Electric Company, Cincinnati, Ohio
24. RADIATION DAMAGE OF AIRPLANE TIRE MATERIALS by T. C. Gregson and S. D. Gehman, The Goodyear Tire and Rubber Company, Akron, Ohio
25. RADIATION EFFECTS ON FLIGHT CONTROLS SUBSYSTEM DESIGN by D. O. Gunson, Lockheed Aircraft Corporation, Georgia Division, Marietta, Georgia
26. PNEUMATICS - A TOOL FOR THE DESIGNER OF NUCLEAR POWERED AIRCRAFT by John A. Osterman, Lockheed Aircraft Corporation, Georgia Division, Marietta, Georgia

27. AIRCRAFT RADOME DESIGN PROBLEMS ASSOCIATED WITH A NUCLEAR ENVIRONMENT by Frank W. Thomas, Lockheed Nuclear Products, Lockheed Aircraft Corporation, Georgia Division, Marietta, Georgia
28. *EFFECTS OF HIGH ALTITUDE NUCLEAR DETONATIONS ON PROPAGATION OF ELECTROMAGNETIC WAVES by Samuel Horowitz and Lt. Richard Sugarman, U. S. Air Force Cambridge Research Center, Bedford, Massachusetts
29. *THE EFFECTS OF GAMMA RAY AND REACTOR IRRADIATIONS ON THE SENSITIVITY OF EXPLOSIVES by Paul W. Levy, Brookhaven National Laboratory, Upton, Long Island, New York, and J. V. R. Kaufman and James E. Abel, Explosives Research Section, Picatinny Arsenal, Dover, New Jersey
30. ON THE ENERGY LEVELS IN NEUTRON IRRADIATED SILICON by C. A. Klein and W. D. Straub, Research Division, Raytheon Manufacturing Company, Waltham, Massachusetts
31. EFFECT OF RADIATION ON THE CRITICAL SHEAR STRESS OF A METAL SINGLE CRYSTAL by C. E. Morgan, Convair, A Division of General Dynamics Corporation, Fort Worth, Texas
32. MEASUREMENT OF THE RANGE OF RECOIL ATOMS by R. A. Schmitt and R. A. Sharp, General Atomic, A Division of General Dynamics Corporation, San Diego, California
33. THE EFFECTS OF NUCLEAR ENVIRONMENT ON METALLIC AND NONMETALLIC MAGNETIC MATERIALS by E. I. Salkovitz and A. I. Schindler, U. S. Naval Research Laboratory, Washington, District of Columbia
34. *THE EFFECT OF NUCLEAR RADIATION ON COMMUNICATIONS SET AN/ARC-34 by D. L. Jacobs, Convair, A Division of General Dynamics, Fort Worth, Texas
35. RADIATION TESTING OF J-79 ORGANIC ENGINEERING MATERIALS AND COMPONENTS by D. E. Barnett, Aircraft Nuclear Propulsion Department, General Electric Company, Cincinnati, Ohio
36. *THE EFFECT OF NUCLEAR RADIATION DURING ESCAPE ON F-104 by F. L. Bouquet, Jr., Lockheed Aircraft Corporation, California Division, Burbank, California

* This paper is classified and is bound in Volume Six.

VOLUME 4

ELECTRONICS AND SEMI-CONDUCTORS

Contents:

37. THE EFFECTS OF RADIATION ON VARIOUS RESISTOR TYPES by ~~E. R. Pfaff and R. D. Shelton, Admiral Corporation, Chicago, Illinois~~
38. RADIATION EFFECTS IN COMPOUND SEMICONDUCTORS by ~~L. W. Aukerman and R. K. Willardson, Battelle Memorial Institute, Columbus, Ohio~~
39. A CRITICAL SURVEY OF RADIATION DAMAGE TO CIRCUITS by ~~W. W. Happ and S. R. Hawkins, Lockheed Aircraft Corporation, Lockheed Missile Systems Division, Palo Alto, California~~
40. RADIATION STABILIZATION OF TRANSISTOR CIRCUITS BY ACTIVE FEEDBACK by ~~S. R. Hawkins and W. W. Happ, Lockheed Aircraft Corporation, Lockheed Missile Systems Division, Palo Alto, California~~
41. COMPARISON OF NEUTRON DAMAGE IN GERMANIUM AND SILICON TRANSISTORS by ~~J. W. Easley, Bell Telephone Laboratories, Whippany, New Jersey~~
42. PULSED RADIATION EFFECTS IN SEMICONDUCTORS by ~~J. M. Denney, C. W. Perkins, and J. R. Wierske, Nuclear Electronics Department, Hughes Aircraft Company, Culver City, California~~
43. THE EFFECT OF VARIATION OF THE WIDTH OF THE BASE REGION ON THE RADIATION TOLERANCE OF SILICON DIODES by ~~Gerald C. Huth, Aircraft Nuclear Propulsion Department, General Electric Company, Cincinnati, Ohio~~
44. THE EFFECT OF NUCLEAR RADIATION ON COMMERCIAL SILICON DIODES by ~~John R. Crittenden, Aircraft Nuclear Propulsion Department, General Electric Company, Cincinnati, Ohio~~
45. EVALUATION OF SILICON DIODE IRRADIATION RESULTS IN TERMS OF MAGNETIC AMPLIFIER PERFORMANCE by ~~J. A. Russell, Aircraft Nuclear Propulsion Department, General Electric Company, Cincinnati, Ohio~~
46. GAMMA RADIATION EFFECTS IN SILICON SOLAR CELLS by ~~G. Enslaw, F. Junga, and W. W. Happ, Lockheed Aircraft Corporation, Lockheed Missile Systems Division, Palo Alto, California~~

47. THE EFFECTS OF NUCLEAR RADIATION ON POWER TRANSISTORS by ~~Frederick Gordon, Jr., U. S. Army Signal Corps, Research and Development Laboratories, Fort Monmouth, New Jersey~~

48. THE PERFORMANCE OF SOME ZENER REFERENCE ELEMENTS DURING EXPOSURE TO NUCLEAR RADIATION by ~~M. A. Xavior, Cook Research Laboratory Division, Cook Electric Company, Morton Grove, Illinois~~

49. EFFECTS OF ELECTRON BOMBARDMENT ON CADMIUM SULFIDE WHISKERS by ~~B. A. Kulp and D. C. Reynolds, Aeronautical Research Laboratory, Wright Air Development Center, Wright-Patterson Air Force Base, Ohio~~

VOLUME 5

LUBRICANTS AND PLASTICS

50. THE BEHAVIOR OF FUELS AND LUBRICANTS IN DYNAMIC TEST EQUIPMENT OPERATING IN THE PRESENCE OF GAMMA RADIATION by M. Z. Fainman, Inland Testing Laboratory, Morton Grove, Illinois
51. THE DEVELOPMENT OF NUCLEAR RADIATION RESISTANT SOLID FILM LUBRICANTS by William L. R. Rice and Lieutenant William L. Cox, Materials Laboratory, Wright Air Development Center, Wright-Patterson Air Force Base, Ohio
52. INTEREFFECTS BETWEEN REACTOR RADIATION AND MIL-L-7808C AIRCRAFT TURBINE OIL by F. A. Haley, Convair, A Division of General Dynamics Corporation, Fort Worth, Texas
53. DEVELOPMENT OF RADIATION-RESISTANT HIGH-TEMPERATURE LUBRICANTS by C. L. Mahoney, W. S. Saari, K. J. Sax, W. W. Kerlin, E. R. Barnum, P. H. Williams, Shell Development Company, Emeryville, California
54. ELECTRICAL EFFECTS OF HIGH-INTENSITY IONIZING RADIATION ON NONMETALS by V. A. J. Van Lint and P. H. Miller, Jr., General Atomic, A Division of General Dynamics Corporation, San Diego, California

55. STUDY OF RADIATION EFFECTS ON ELECTRICAL INSULATION by J. F. Hansen, Battelle Memorial Institute, Columbus, Ohio, and M. L. Shatzen, Lockheed Nuclear Products, Lockheed Aircraft Corporation, Georgia Division, Marietta, Georgia
56. A STUDY OF RADIATION EFFECTS ON FUEL TANK SEALANTS AND BLADDER CELL MATERIAL by M. L. Shatzen, Lockheed Nuclear Products, Lockheed Aircraft Corporation, Georgia Division, Marietta, Georgia, and R. S. Tope, C. W. Cooper, and R. G. Heiligmann, Sealants and Elastomers Division, Battelle Memorial Institute, Columbus, Ohio
57. THE EFFECT OF ELECTRON RADIATION ON THE COMPLEX DYNAMIC MODULUS OF POLYSTYRENE AND HIGH DENSITY POLYETHYLENE by R. H. Chambers, General Atomic, A Division of General Dynamics Corporation, San Diego, California
58. RADIATION RESISTANT SILICONES by E. L. Warrick, D. J. Fischer, and J. F. Zack, Dow Corning Corporation, Midland, Michigan
59. RADIATION EFFECTS ON ORGANO-SILICONS by T. W. Albrecht, Convair, A Division of General Dynamics Corporation, Fort Worth, Texas
60. EFFECTS OF GAMMA RADIATION ON FLUOROCARBON POLYMERS by Leo A. Wall, Roland E. Florin, and D. W. Brown, National Bureau of Standards, Washington, District of Columbia
61. *FAST NEUTRON ACTIVATION OF SEAPLANE MATERIALS by L. Brandeis Wehle, Jr., Michael D. D'Agostino, and Anthony J. Favale, Grumman Aircraft Engineering Corporation, Bethpage, Long Island, New York
62. EFFECTS OF NUCLEAR RADIATION ON CORK, LEATHER, AND ELASTOMERS by Chester J. De Zeih, Boeing Airplane Company, Seattle, Washington
63. THE "PLATE SHEAR METHOD" OF DETERMINING THE MODULUS OF RIGIDITY OF SANDWICH PANELS by R. R. Bauerlein, Convair, A Division of General Dynamics Corporation, Fort Worth, Texas
64. "O" RING TESTING IN A MIXED FIELD IRRADIATION by E. E. Kerlin, Convair, A Division of General Dynamics Corporation, Fort Worth, Texas

* This paper is classified and is bound in Volume Six.

65. RADIATION EFFECTS ON 23 SILICONE RUBBERS AT AMBIENT TEMPERATURE
by D. M. Newell, Convair, A Division of General Dynamics Corporation, Fort
Worth, Texas
66. *THE RADIATION ENVIRONMENT DUE TO ACTIVATION AND SCATTERING
EFFECTS NEAR BASED SEAPLANES by F. L. Bouquet, Jr., Lockheed Aircraft
Corporation, California Division, Burbank, California

* This paper is classified and is bound in Volume Six.

VOLUME 6

CLASSIFIED PAPERS

3. MISSION AND TRAFFIC CONTROL REQUIREMENTS FOR THE WS/125A
by James R. Burnett, Bendix Systems Division, Bendix Aviation Corporation,
Ann Arbor, Michigan
28. EFFECTS OF HIGH ALTITUDE NUCLEAR DETONATIONS ON PROPAGATION
OF ELECTROMAGNETIC WAVES by Samuel Horowitz and Lt. Richard Sugarman,
U. S. Air Force Cambridge Research Center, Bedford, Massachusetts
29. THE EFFECTS OF GAMMA RAY AND REACTOR IRRADIATIONS ON THE
SENSITIVITY OF EXPLOSIVES by Paul W. Levy, Brookhaven National Laboratory,
Upton, Long Island, New York, and J. V. R. Kaufman and James E. Abel,
Explosives Research Section, Picatinny Arsenal, Dover, New Jersey
34. THE EFFECT OF NUCLEAR RADIATION ON COMMUNICATIONS SET
AN/ARC-34 by D. L. Jacobs, Convair, A Division of General Dynamics,
Fort Worth, Texas

36. THE EFFECT OF NUCLEAR RADIATION DURING ESCAPE ON F-104 by
F. L. Bouquet, Jr., Lockheed Aircraft Corporation, California Division, Burbank,
California
61. FAST NEUTRON ACTIVATION OF SEAPLANE MATERIALS by L. Brandeis Wehle, Jr.,
Michael D. D'Agostino, and Anthony J. Favale, Grumman Aircraft Engineering
Corporation, Bethpage, Long Island, New York
66. THE RADIATION ENVIRONMENT DUE TO ACTIVATION AND SCATTERING
EFFECTS NEAR BASED SEAPLANES by F. L. Bouquet, Jr., Lockheed Aircraft
Corporation, California Division, Burbank, California

INDEX OF AUTHORS

NAME	PAPER NO.	NAME	PAPER NO.
1. Abel, J. E.	29	42. Hawkins, S. R.	39, 40
2. Albrecht, T. W.	59	43. Heiligmann, R. G.	56
3. Allen, J. W.	5	44. Hood, J. T.	21
4. Aukerman, L. W.	38	45. Horowitz, S.	28
5. Barnett, D. E.	35	46. Huth, G. C.	43
6. Barnum, E. R.	53	47. Jacobs, D. L.	34
7. Bauerlein, R. R.	63	48. Jones, S. S.	4
8. Bouquet, F. L.	36, 66	49. Junga, F.	46
9. Bridges, W. L.	2	50. Kaufman, J. V. R.	29
10. Brown, D. W.	60	51. Kerlin, E. E.	64
11. Brown, V. C.	22	52. Kerlin, W. W.	53
12. Burnett, J. R.	3	53. Klein, C. A.	30
13. Burrus, W. R.	13, 15	54. Krasnow, M. E.	7
14. Caswell, R. S.	14	55. Kulp, B. A.	49
15. Chambers, R. H.	57	56. Langdon, W. R.	4
16. Collins, C. G.	1, 23	57. Levy, P. W.	29
17. Cooper, C. W.	56	58. Lide, E. N.	9
18. Cox, Lt. W. L.	51	59. Mahoney, C. L.	53
19. Crittenden, J. R.	44	60. Maienschein, F. C.	12
20. D'Agostino, M. D.	61	61. Memhardt, C. R.	7
21. Denney, J. M.	42	62. Miller, P. H., Jr.	54
22. Dewar, M. A.	8	63. Morgan, C. E.	31
23. DeZei, C. J.	62	64. Naydan, T. T.	4
24. Donnelly, M. M.	19	65. Newell, D. M.	65
25. Duncan, G. I.	20	66. O'Nan, T. C.	21
26. Easley, J. W.	41	67. Osterman, J. A.	26
27. Enslow, G.	46	68. Perkins, C. W.	42
28. Fainman, M. Z.	7, 50	69. Peterson, N. M.	22
29. Favale, A. J.	61	70. Pfaff, E. R.	37
30. Fischer, D. J.	58	71. Rathbun, E. R.	7
31. Florin, R. E.	60	72. Reynolds, D. C.	49
32. Fraser, J. C.	20	73. Rice, W.L.R.	51
33. Gamble, R. L.	17	74. Ruby, S. L.	18
34. Gehman, S. D.	24	75. Russell, J. A.	45
35. Gordon, F., Jr.	47	76. Saari, W. S.	53
36. Gregson, T. C.	24	77. Salkovitz, E. I.	33
37. Gunson, D. O.	25	78. Sax, K. J.	53
38. Haley, F. A.	52	79. Scarborough, W. T.	6
39. Hansen, J. F.	55	80. Schindler, A. I.	33
40. Happ, W. W.	39, 40, 46	81. Schmitt, R. A.	32
41. Harper, W. T.	15	82. Schupp, F. D.	18

THE EFFECTS OF RADIATION ON VARIOUS RESISTOR TYPES*

by

E. R. Pfaff and R. D. Shelton

Admiral Corporation
Chicago, Illinois

ABSTRACT

A study of the effect of nuclear radiation on various types of resistors revealed interesting trends and several possible damage mechanisms, most of which seem to be associated with the boron content in the components. Film type resistors consisting of a glass core containing boron and a conducting film with no boron, showed greater damage when the film was thin (high resistance values). It is probable that in this case the (n, α) reaction in boron removed some of the atoms from the thin conducting film.

Resistors having a core with no boron but with a boron-carbon conducting film showed greater damage when the film was thick (low resistance values). It is conjectured that since, in this case, all of the boron is in the conducting film, there is more recoil energy deposited in the conducting layer having the thicker film.

Wire-wound resistors having a vitreous enamel coating had resistance changes greater than could be attributed to temperature coefficient or a change from a disordered to ordered arrangement in the wire. There is some evidence that the vitreous coating, sometimes containing a large amount of boron, changes density sufficiently to distort the wire and increase the resistance of the unit by as much as 6 percent.

*This work was supported by the United States Air Force through the Electronic Components Laboratory of Wright Air Development Center.

INTRODUCTION

The resistor types studied included wire-wound, composition, and film types. The irradiation facilities were the CP-5 reactor of the Argonne National Laboratory, the MTR of the National Reactor Test Station, and a 20,000 curie Co^{60} source. The approximate radiation fields of these facilities are summarized in Table 1. The period of irradiation was from one to three weeks.

In interpreting the effects of radiation on resistors, a number of possibilities need to be considered. The most probable cause of resistance change is associated with a change in the resistive element. There are possibilities of parallel leakage paths occurring because of a deterioration of core or coating material. Secondary effects may result from damage to coating layers and accelerated aging and corrosion.

Except in evacuated systems, there is always a cloud of ions surrounding electronic components in radiation fields, and if there are potential differences, small currents will flow. As a rule, these currents were of the order of millimicroamperes in our experiments, and were not important in our resistance measurements. It is possible to reduce these currents greatly by using conventional electrostatic shielding techniques and to reduce the volume of air from which ions are collected.

WIRE-WOUND RESISTORS

Figure 2 shows a typical wire-wound power resistor similar to those studied in this program.

Wire-wound resistors are usually considered to be quite radiation resistant. In general, the resistance increases with irradiation, and there are very few resistors which show a decrease in resistance. Manganin decreases in resistance due to temperature change but this change is very slight (15 parts per million). The power resistors usually consist of nickel-chromium alloy wire-wound on a ceramic tube and covered with a vitreous enamel. All of these constituents are radiation resistant. Wire-wound precision resistors fortunately show less change during irradiation than the power resistors.

Figure 3 shows the effect of reactor irradiation upon this type of wire-wound power resistor.

After studying the construction and the behavior of the wire-wound resistor, we have come to several conclusions. The general increase in resistance indicates that it is the wire, rather than the surrounding

TABLE 1

Irradiation Environment^a Provided by the Different
Facilities Available to Admiral

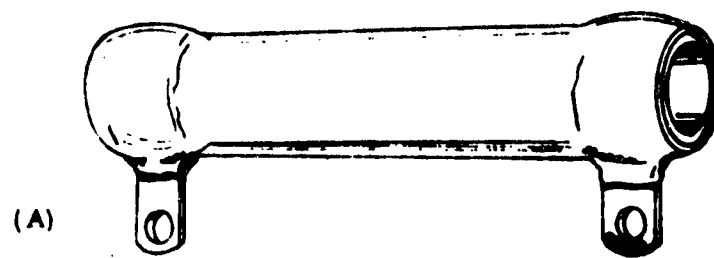
Facility	Thermal Neutron Flux		Epi-Cadmium Neutron Flux		Neutron ^b Flux Above 2.5 mev		Gamma ^c Flux	
Isotope Hole (CP-5)		2×10^{12}		3×10^9		1×10^8		1×10^{12}
Flux Converter ^d (CP-5)		1×10^{12}		1×10^{11}		1×10^{10}		1×10^{12}
⁶⁰ Co Source		0		0		0		1×10^{11}

^aAll fluxes are in particles/cm² sec

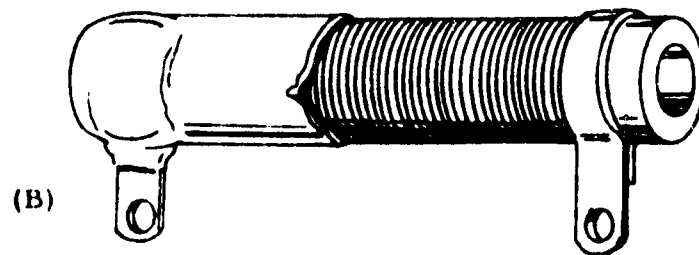
^bMeasured with sulfur threshold detectors

^cAn average energy of 1 mev was assumed

^dThe flux converter provides a fission environment



COMPLETED WIRE-WOUND RESISTOR



**CROSS SECTION VIEW SHOWING RESISTIVE
ELEMENT**

FIGURE 2

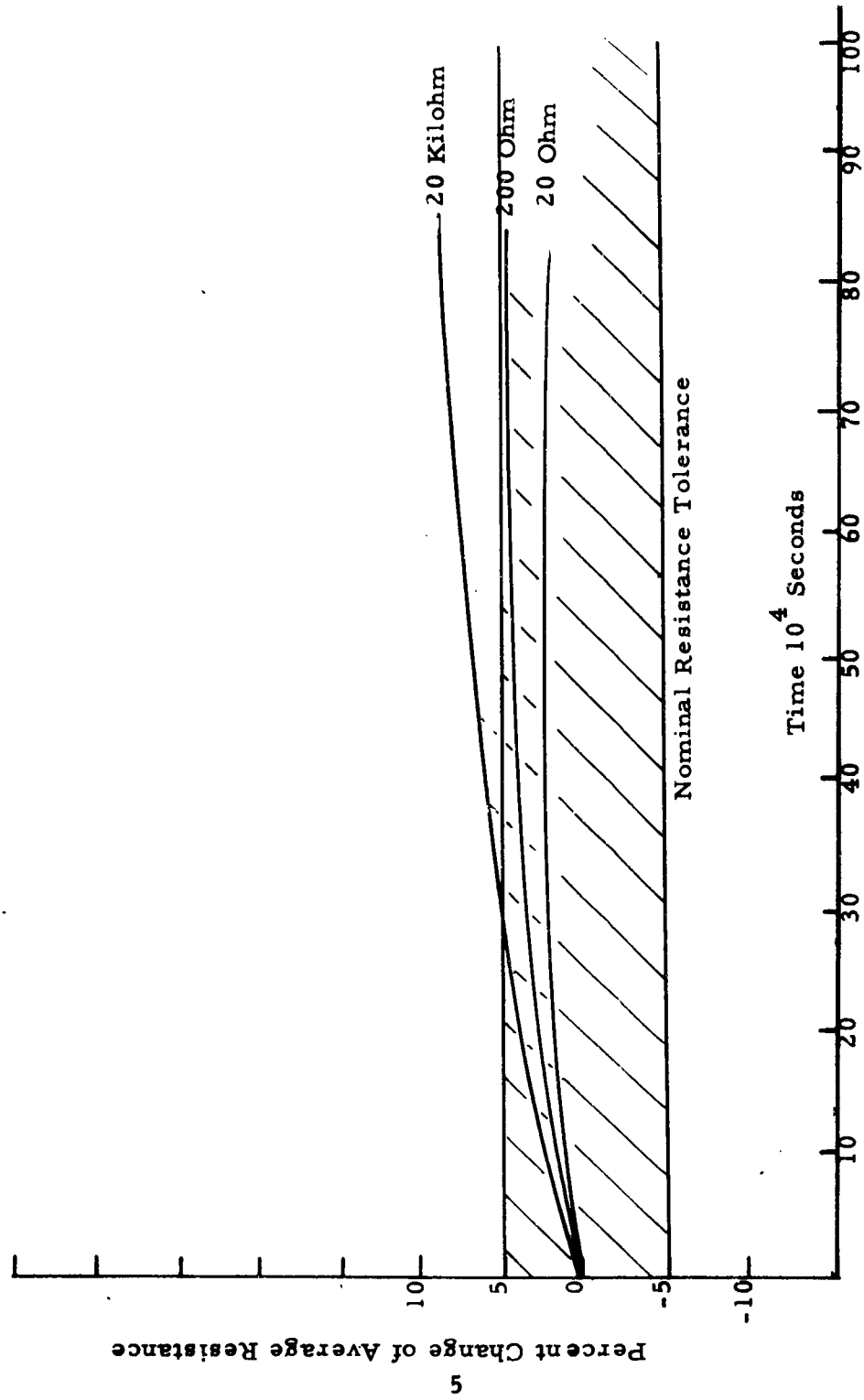


Figure 3 Percent Change of Average Resistance of RW31V Fixed Wire-Wound Power Resistors In-Pile

material, which is giving the effect. However, if we consider the work of others in the field, we cannot attribute all of the changes during irradiation to a change in the order-disorder state of the wire.

Mr. J. C. Wilson of ORNL has made studies of evenohm and inconel wire containing about 80% nickel and 20% chrome and found that radiation increases the resistance about 2% for a dose of 10^{19} fast neutrons per cm^2 and that copper shows practically no change for the same dose.

The initial state of the metal proves to be important in the radiation damage pattern and change in resistance under irradiation is believed to be connected with the order-disorder transitions in the metal. This resistance increase is the result of a change from a disordered to ordered arrangement. However, in the case of gold-copper alloys an increase of resistance due to irradiation is due to an order to disorder transition.

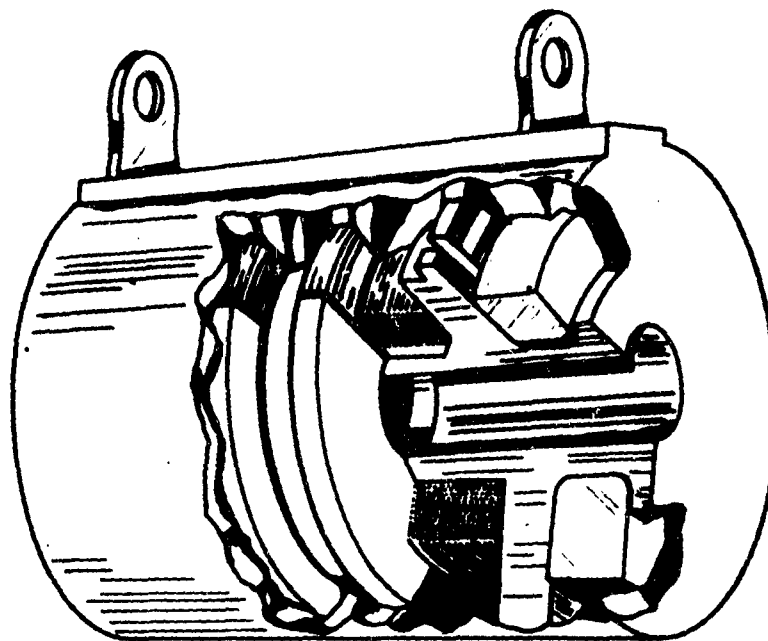
A discussion on this subject with Mr. Jim Howe, Director of Engineering at the Ohmite Mfg. Co., was very helpful. I learned that refiring this type of resistor to temperature of 1800° would often increase the resistance as much as 6%. This change is caused by the changing density of the vitreous enamel coating stretching the resistance wire.

Our experience with glass has shown that several types of glass tend to become more dense under irradiation, and we know that wire changes resistance when under stress. We suspect, therefore, that some of the change in resistance results from dimensional changes caused by radiation. The use of coating enamels with significant amounts of boron makes dimensional changes much more probable, since boron glass is known to be very susceptible to densification by neutron irradiation.

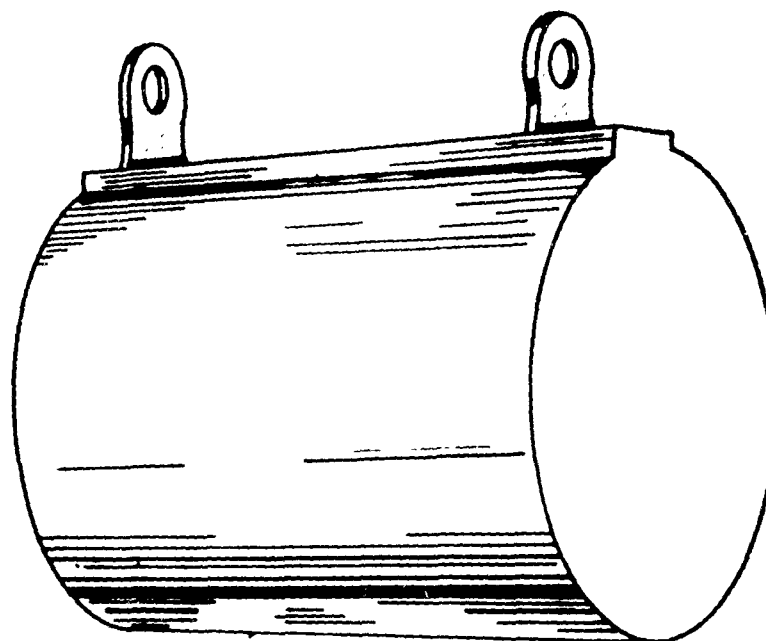
Samples of various types of glass supplied by Dr. Vaughn Culler of the Corning Glass Works, and irradiated by Admiral, underwent density changes of up to 1% for certain types which contained boron. Other samples containing no boron underwent density changes from 0 to .06%.

The precision wire-wound resistors, pictured in Figure 4, were bobbin wound, and the epoxy resin coating layer was not so closely integrated with the wire. The relatively small changes in the precision resistors during irradiation, as compared with the power resistors, may result from the different type of construction, as well as the different type of coating.

Figure 5 shows the effect of pile irradiation on this type of resistor.



(A)
CROSS SECTION OF MEPCO AFRT19 FIXED (PRECISION)
WIRE-WOUND RESISTORS



(B)
COMPLETED (ENCAPSULATED) RESISTOR

FIGURE 4

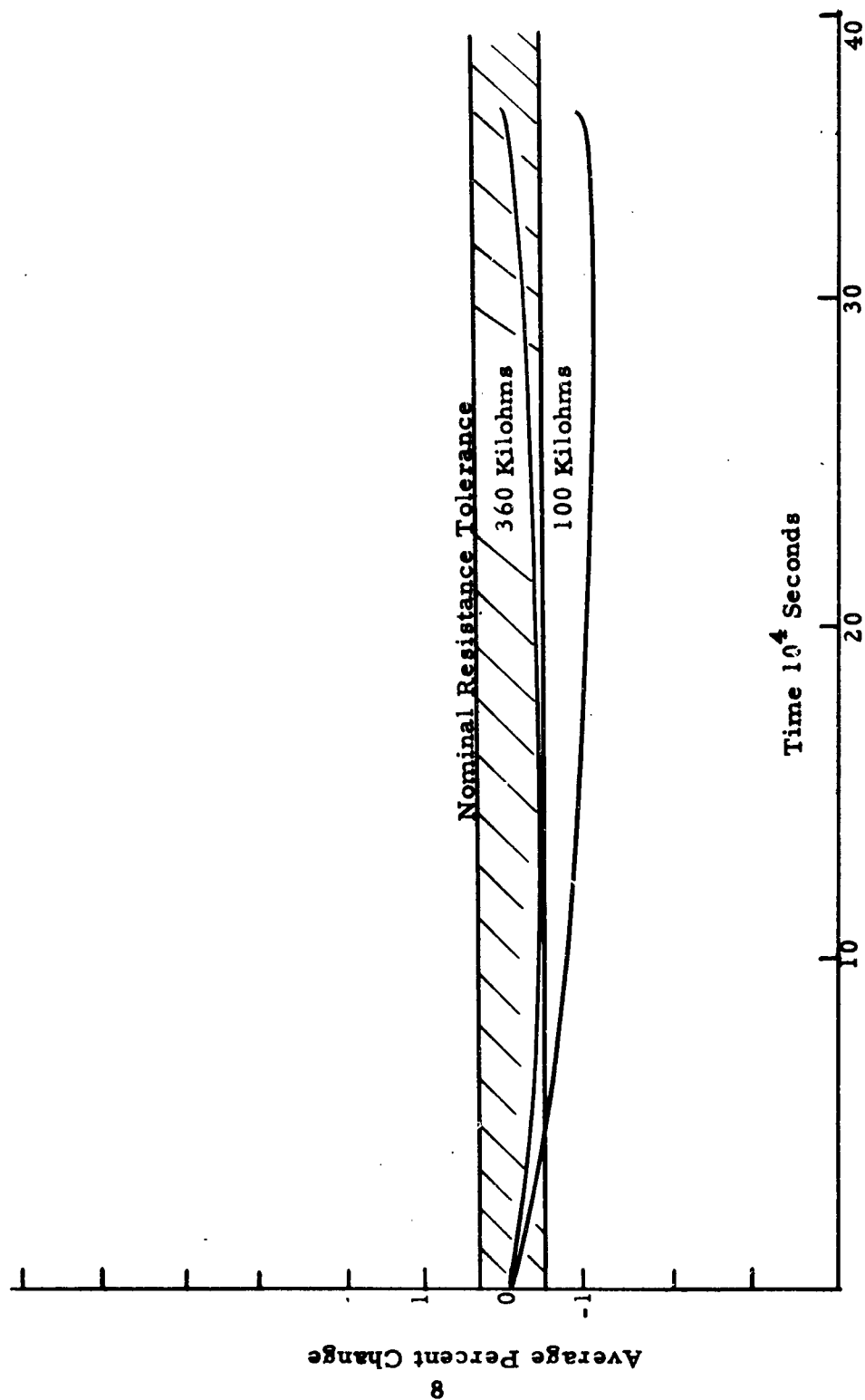


Figure 5 Average Percent Change from the Nominal Resistance Value of
AFRT 19 Precision Wire-Wound Resistors In-Pile

Figure 6 indicates that some damage did occur to the coating and that the slight changes that did occur may have been due to gas evolution, temperature, and in the case of the high resistance values, a change in resistance of the coating.

COMPOSITION RESISTORS

Composition resistors are the most unstable of all the resistor types and usually have the least rigid specifications on environmental and aging effects. In many experiments it has been impossible to separate the radiation effects from changes which normally occur with variations in humidity, temperature, and aging.

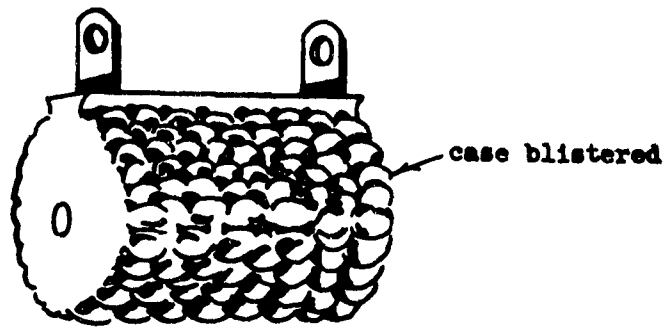
Most reactors operate with a carefully controlled external environment. However, severe temperature gradients sometimes exist within reactors as a result of radiation heating, and the humidity inside the reactor is considerably lower than that outside the reactor. The necessity of maintaining a supply of cooling air sometimes leads to a greater than usual air flow about the component.

Fixed composition style resistors consist of a pellet of a nearly homogeneous mixture of carbon and resin binders enclosed in a phenolic case. The resistors of larger nominal value appear to undergo a greater relative change during irradiation. This fact suggests either that the conducting carbon decreases in resistance or that elements of the resistor other than the carbon decrease in resistance.

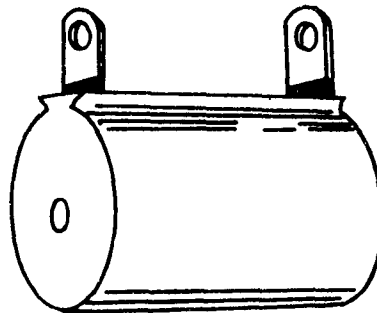
Our experience with a variety of dielectrics leads us to suspect both the resin binder and the phenolic case of contributing to the decrease in resistance. The extra leakage afforded by the deterioration of these dielectrics would be more strongly in evidence in the resistors of larger nominal value.

It is conceivable that the radiation causes a lower resistance rearrangement of the carbon, or that the pressure of gas liberated in the phenolic shell reduces the resistance of the pellet. It is more reasonable, however, to believe that the major part of the resistance change caused by radiation is attributable to changes in the resin binder and the phenolic case.

Figure 7 shows the effect of reactor irradiation on typical composition carbon resistors. As stated before, the normal changes due to aging are so great that it is difficult to determine if there is any radiation effect at all.



Post irradiation illustration of AFRT19E100R0D resistor



Pre irradiation illustration of AFRT19E100R0D resistor

FIGURE 6

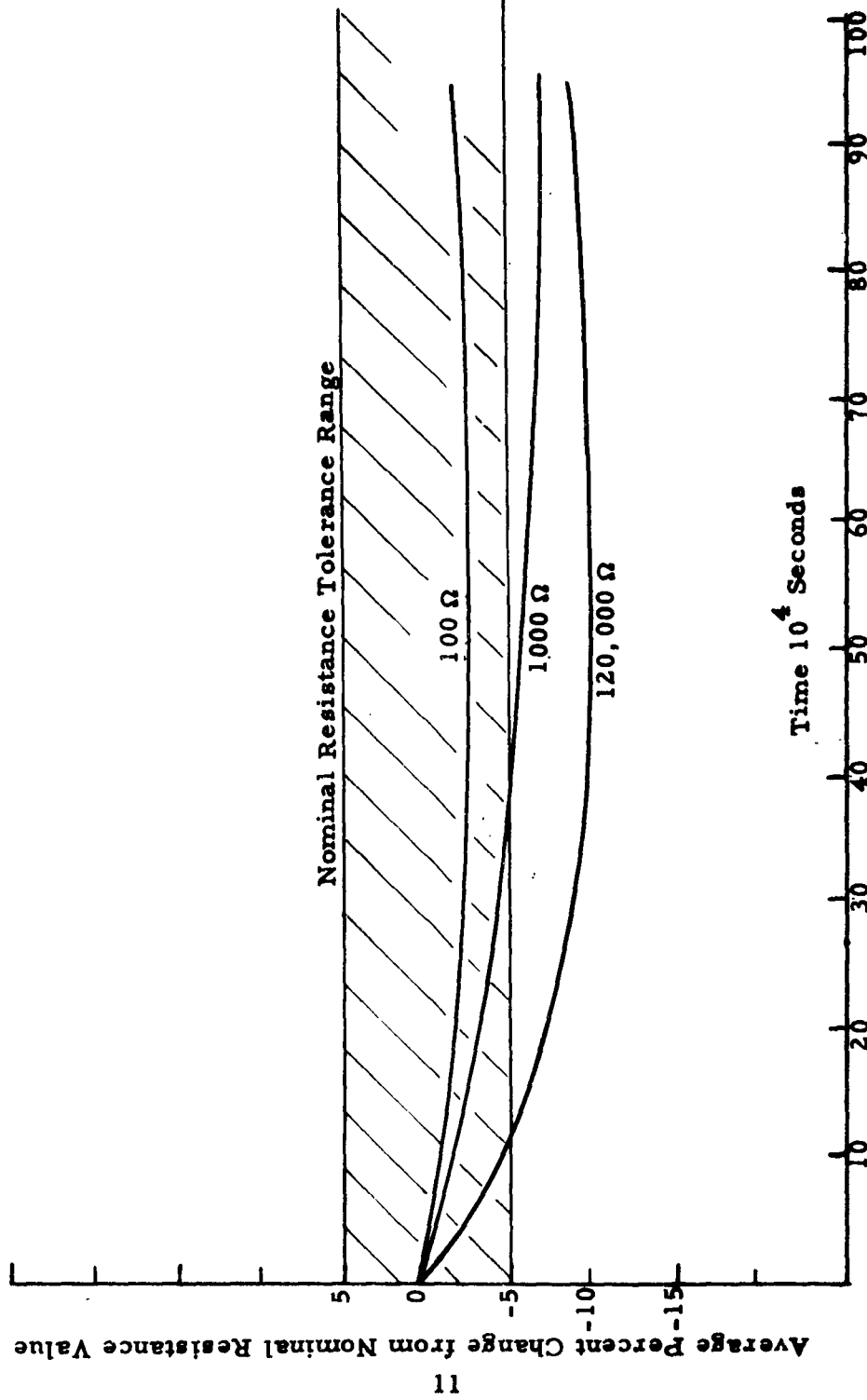


Figure 7 Average Percent Change from the Nominal Resistance Value of Five Percent Carbon Composition Resistors In-Pile

FILM RESISTORS

The conductive films of many film resistors have thicknesses of the same order of magnitude as the atomic displacements caused by radiation. Consequently, the transport of material into and out of the film becomes an important consideration in the study of radiation damage. It is easy to visualize that, the thinner the film, the more likely a recoil atom will be to leave the film. Likewise, the relative percent transport of foreign material into the film increases as the film becomes thinner.

Transmutation of atoms is not important in causing resistance changes. Even in electronic devices such as transistors, in which minute amounts of impurities are detectable, transmutation is considered to contribute only a small fraction of the total damage during a fast neutron irradiation. Although a film may contain boron, the percentage of atoms transmuted is too small to account for the observed resistance changes. For example, an atom with a capture cross section of 4,000 barns has a probability of 4×10^{-3} of being transmuted by an integrated flux of 10^{18} .

The capture of a neutron by a B^{10} nucleus results in a highly excited nucleus which splits into He^4 and Li^7 with an average total kinetic energy of 2.35 mev. These energetic recoils have low penetrating power and dissipate their energies in less than 0.001 inch.

Some of the film resistors have a glass core containing an appreciable amount of boron. It has been observed that glass exposed to soft x-radiation develops a chalky surface and that some types of glass exposed to nuclear radiation shrinks and increases in density. The surface effect on x-ray tubes occurs because a large amount of the soft radiation, not penetrating far beneath the surface, causes the surface glass, as it becomes more dense, to crack away from the main body of the glass, which is relatively unaffected.

Neutron absorption in boron glass is not uniform because of self-shielding, but is not strictly a surface effect. Since the distribution of neutron absorption is not uniform, the resulting densification is not uniform. Thus, strains are created in the glass.

The film resistors usually employ a very hard, thin film which is closely bound to a core material of glass or ceramic. If any deformations or cracks of the core occur, the effect should be transferred to the film. The absence of complete failures indicated that the core materials commonly used has remained intact. The gradual increase of resistance during irradiation implied that the film was becoming less conductive, either because of a disordering of the crystalline state or because of a

transport of material by radiation. The greater percentage increase in resistance of the higher resistance values indicated that the transport hypothesis was more reasonable, it being readily demonstrable that relative transport is greater for thinner films.

Figure 8 shows the effect of reactor irradiation on a group of resistors having a tin oxide coating on a pyrex glass core. The pyrex core contains a considerable amount of boron. I would like to call your attention to the fact that the amount of damage increases as the value of the resistor is increased, the higher resistance of course requires the use of a thinner film.

Figure 9 shows the damage resulting from reactor irradiation on typical boro-carbon film resistors. As in the case of the previous resistors, I think it is obvious that the damage is due to the displacement of atoms from the conducting film, and possibly a change in the crystalline structure of the conductor. It is interesting to note that these resistors have a boro-carbon film on a ceramic core containing no boron. In this case all of the boron is in the conducting film and the thinner the film the less boron in the resistor. Also in the case of a very thin conducting film containing boron, much of the recoil energy would be dissipated outside of the film. The resulting damage pattern is quite different, from the case where the boron is in the core, in that the higher value resistors show the least damage and the relatively thick film of the lower value resistors show the greater change.

Figure 10 shows the effect of reactor irradiation on crystalline carbon deposited film type of resistors. Since neither the film or the ceramic core contained any boron the spectacular damage associated with the two previously described resistors is not present. It is quite possible that the relatively slight change in these resistors may not be due to radiation damage.

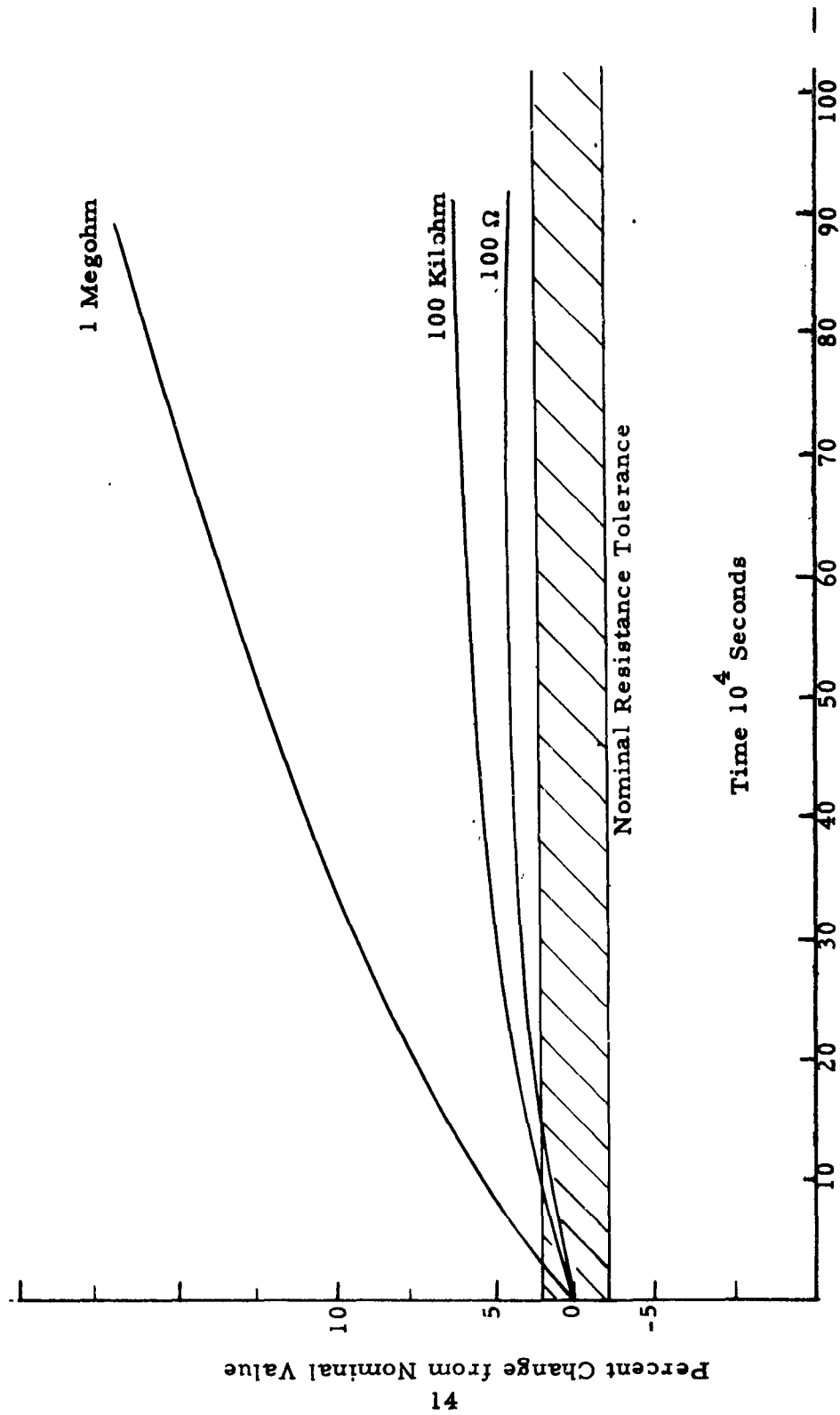


Figure 8 Average Percent Change from Nominal Resistance of Pyrex Core Stannic Oxide Film Resistors In-Pile

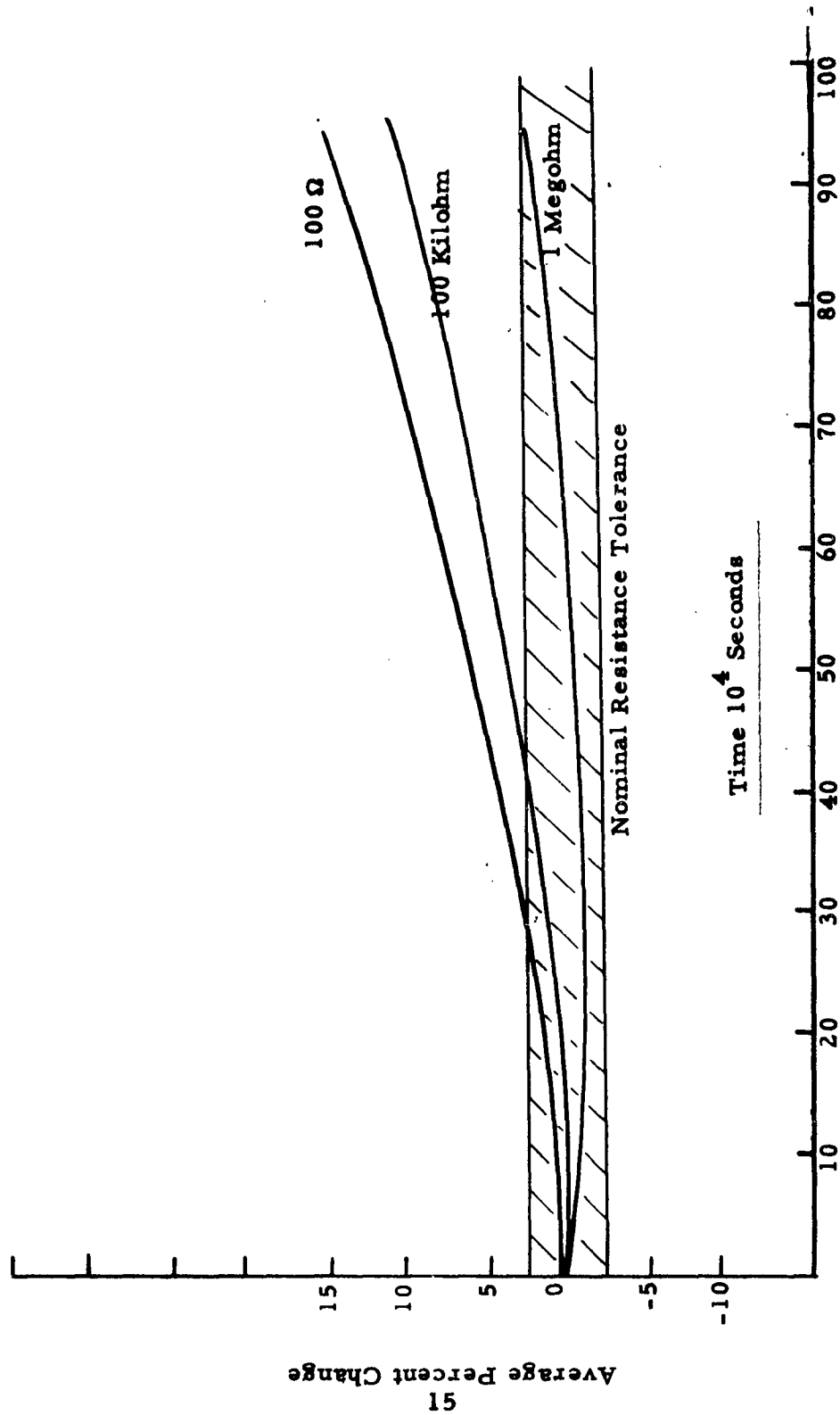


Figure 9 Average Percent Change from the Nominal Resistance Value of RN20 (Boro Carbon) Deposited Film Resistors In-Pile

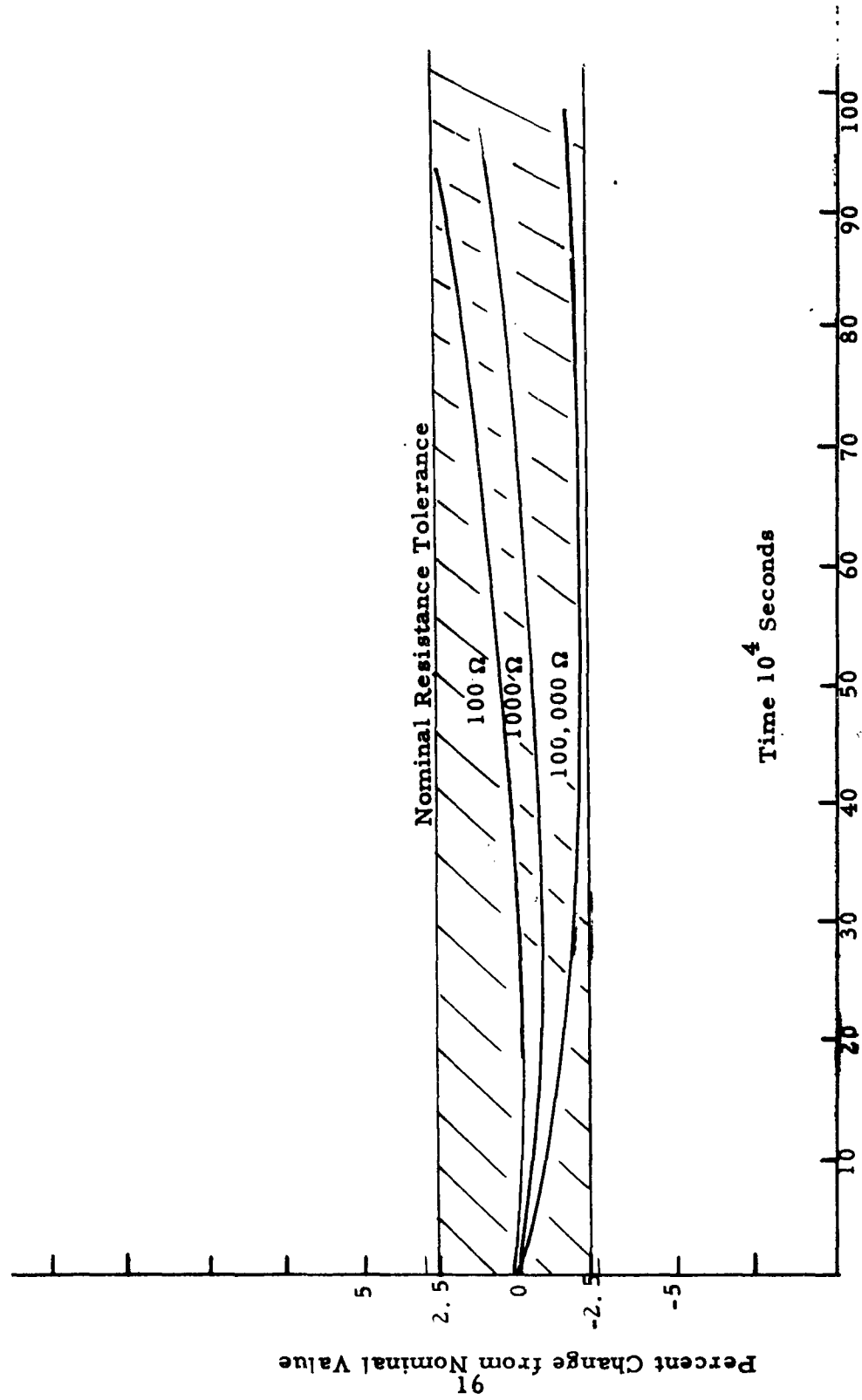


Figure 10 Average Percent Change from Nominal Resistance Value of RN20X
Crystalline Carbon Film Resistors In-Pile

RADIATION EFFECTS IN COMPOUND SEMICONDUCTORS^a

by

L. W. Aukerman and R. K. Willardson

Battelle Memorial Institute
Columbus, Ohio

The properties of semiconductor devices (such as transistors and rectifiers) depend strongly on minority-carrier lifetime, carrier concentration, and mobility. These parameters are strongly affected by nuclear irradiation. For the design of a device relatively insensitive to radiation damage, semiconductors composed of heavy atoms and having a high minority-carrier mobility and a large energy gap are desirable. The properties of several compound semiconductors, including AlSb, InP, GaAs, CdTe, and InSb, are compared with respect to the above criteria. Investigations of the effects of fast-neutron irradiation on these compounds are reported. Annealing and heat-treatment studies before and after irradiation are discussed.

INTRODUCTION

A study of the effects of energetic radiation on the electrical properties of semiconductors may be expected to provide valuable insight into the fundamental mechanisms of radiation effects, as well as to yield information which will be useful in the design of radiation-resistant devices. The electrical properties of semiconductors are essentially determined by crystal imperfections and are thus quite sensitive to defects produced by irradiation. For example, to change the residual resistivity of copper 10 per cent requires a fast-neutron flux of 10^{17} neutrons per cm^2 . But the resistivity of 0.1 ohm-cm germanium is increased 10 per cent by a flux of 10^{15} neutrons per cm^2 and the forward resistance of a silicon

^a This research was supported in whole or in part by the United States Air Force under Contract No. 33(616)-3747, monitored by the Aeronautical Research Laboratory, Wright Air Development Center.

conductivity-modulated rectifier is increased 10 per cent by a flux of only 4×10^{10} neutrons/cm².

Figure 1 shows a classic example of the changes in conductivity of a semiconductor¹, InSb, with fast-neutron bombardment.^a *N*-type InSb with an initially large carrier concentration, the upper curve, undergoes a monotonic decrease in conductivity and approaches a saturation value with large flux. The conductivity of the initially *p*-type specimen (lower curve) first decreases, goes through a minimum, and then increases, eventually approaching the saturation value of the *n*-type sample.

Hall-coefficient measurements indicate that on the low-flux side of the minimum the sample is *p*-type, and on the large-flux side of the minimum the sample is *n*-type. At first the concentration of holes is decreasing, and after the minimum the concentration of electrons is increasing. This behavior is understood to result from the fact that the defects introduced tend to produce *n*-type behavior of a certain electron concentration. Stated more precisely: bombardment produces donors and acceptors in equal concentrations, but the distribution of the energy levels associated with these donors and acceptors is such that most of the levels lie in the half of the forbidden band nearest the conduction band. In some semiconductors, for example germanium, this behavior is reversed, the distribution of the levels being such as to make a specimen *p*-type, regardless of its initial type. In silicon, the bombardment-produced levels are distributed quite symmetrically so that both *n*- and *p*-type specimens tend to become intrinsic (i. e., the carrier concentration approaches the lowest possible value). It is usually assumed that the vacancies are acceptors and the interstitials are donors.²

The mobility of the carriers is also affected by irradiation, since the defects, which are usually ionized, act as additional scattering centers. The changes in mobility are usually not as evident as the changes in carrier concentration. For example, in Figure 1, eventually the two curves should bend slightly downward due to the decrease in mobility. These two specimens did not receive enough bombardment for this effect to become noticeable.

The minority-carrier lifetime is even more sensitive to bombardment than the conductivity. This fact is illustrated by the extreme sensitivity to irradiation of the conductivity-modulated rectifier mentioned above. Figure 2 shows the changes in the reciprocal of minority carrier lifetime of *n*-type germanium³ and *p*-type silicon⁴ with neutron bombardment. Note the flux scale as compared with the flux scale of Figure 1.

^a Figures appear at the end.

The bombardment-produced defects act as recombination centers, i. e., they trap electrons and holes, allowing them to recombine. The magnitude of the change in lifetime depends on the number of defects introduced and the recombination cross section of the defects. The recombination cross section of the defects may vary widely from one material to another and may also depend on the type of irradiation to which the specimen is exposed. For example Figure 2 suggests that the recombination cross section of the defects produced by fast neutrons is considerably greater in silicon than in germanium (even allowing for the greater rate of producing defects in silicon).

DISPLACEMENTS IN DIATOMIC SOLIDS

The mechanism of radiation damage in semiconductors is frequently imagined as follows: an energetic particle strikes an atom, imparting part of its energy thereto. If the struck atom receives energy greater than a certain amount, called the threshold displacement energy, T_d , it will be dislodged from its lattice site, and may go on to dislodge other atoms from their sites. Eventually the dislodged atoms will settle into interstitial positions. It is sometimes assumed, for convenience, that the vacancies and interstitials are essentially randomly distributed. This is far from the truth, especially in the case of neutron bombardment, where the primary knock-on may receive an energy several thousand times the threshold displacement energy and tend to produce a large number of secondary vacancies and interstitials (see Table I). These secondary defects will mostly lie rather close to the primary event, so that the defects, in all likelihood, are produced in clumps or clusters rather than homogeneously.

Several different kinds of radiation-induced defects are possible in the case of compounds which would not occur in the case of elements. For example, in a diatomic compound composed of Type A and Type B atoms there would be produced vacant A sites as well as vacant B sites, and A interstitials as well as B interstitials. In addition an interstitial can have either A or B atoms as nearest neighbors. There would also be two types of replacements possible; an A atom on a B site and conversely. Thus eight different point defects can be created - two types of vacancies, four types of interstitials, and two replacement-type defects. In calculating the number of each of these defects introduced, the methods which apply to elements will not in general apply to compounds. Special methods^{6,7} have been developed for diatomic compounds, but in general the theoretical picture is far from complete.

Threshold displacement energies can be determined by plotting the rate of change of some bombardment-sensitive parameter as a function of the energy of the bombarding particles. Electrons are usually used for this experiment because monoenergetic beams can be obtained without too much difficulty and they penetrate farther than heavier particles (except neutrons). The energy of the bombarding electrons at which permanent changes start to occur can then be converted into the maximum energy imparted to an atom, T_m , and this should be the threshold displacement energy. The relation between the energy of the bombarding electrons, E , and T_m is as follows:

$$T_m = 557(E/m_0c^2) (E/m_0c^2 + 2)/A, \quad (1)$$

where T_m is expressed in electron volts, A is the atomic mass of the struck atom, m_0 the rest mass of an electron, and c the velocity of light ($m_0c^2 = 0.511$ Mev). In Figure 3 the carrier-removal rate $d\bar{n}/dN_e$ (the number of carriers per cm^3 removed for each incident electron per cm^2 , hence, the units are cm^{-1}) is plotted against T_m for two different semiconductors, germanium⁸, and InSb⁹. The threshold displacement energy for germanium is about 16 ev and for InSb about 6 ev. The threshold displacement energy of silicon¹⁰ is the same as that for germanium. Threshold determinations for silicon and germanium have also been made using minority-carrier lifetime as the bombardment-sensitive parameter.¹⁰

For certain practical purposes, for example the design of semiconductor devices to operate in radiation fields, it becomes desirable to minimize the effects of radiation. There may also be troublesome ionization effects to contend with, but this paper will be concerned only with the permanent rearrangements of the atoms of the crystal. In the mixed field of γ -rays and fast neutrons likely to be encountered near a reactor, by far the greatest amount of permanent damage to the bulk semiconductor material will be produced by the neutrons.

The maximum energy which can be imparted to an atom during a collision by a neutron of energy E is

$$T_m = [4A/(1+A)^2]E, \quad (2)$$

it being assumed that the collision is elastic. All energies up to T_m are equally probable so the average energy \bar{T} is $1/2 T_m$. Since the differential cross section is essentially independent of E one may write, for rather heavy atoms:

$$\bar{T} = 2 \bar{E}/A. \quad (3)$$

The average energy of the fast neutrons is approximately 1 Mev, thus, the average energy of the primary knock-ons will be greater than 10^4 ev. Knock-ons of this energy will produce many secondary displacements. The average number, $\bar{\nu}$, of secondary displacements per primary knock-on may be estimated by the following approximate formula providing the atomic weight is greater than about 30:

$$\bar{\nu} = \bar{T}/2T_d. \quad (4)$$

This expression is not valid for the lighter elements where much of the energy is dissipated in ionization.

Equations (3) and (4) indicate that the damage produced in heavy elements will be less than that produced in light elements, at least for materials of an atomic mass greater than that of silicon. Calculated values of $\bar{\nu}$ for several representative elements are presented in Table I. The threshold was assumed to be 25 ev, although the exact value of the threshold may depend on how the atom is incorporated in the lattice. The calculation of the number of displacements produced in a compound is somewhat complicated. E. M. Baroody¹¹ has shown that in the case of AlSb, although the aluminum is considerably lighter than the antimony, the number of secondary displacements produced by the aluminum primary knock-ons is approximately equal to those produced by the antimony primary knock-ons.

DEVICE CRITERIA

In the case of junction transistors Loferski¹² has shown that the effect of the damage on the volume recombination is the greatest source of malfunction. Here we are dealing with the injection of minority carriers through a narrow base region and it is important that the carriers do not recombine before they penetrate the base. Thus, the diffusion length, which is the product of the minority-carrier lifetime and the minority-carrier diffusion constant, must not become too small. Since bombardment decreases the lifetime it is desirable that the diffusion constant be as large as possible; or, since the mobility is proportional to the diffusion constant (the Einstein relationship), a large mobility is desirable. Several compound semiconductors have an extremely large mobility as compared with germanium or silicon (for example, InSb, InAs, and GaAs).

Another approach to the problem of radiation damage in semiconductor devices is to operate the device at a rather high temperature so

TABLE I. APPROXIMATE MEAN NUMBER OF
DISPLACED ATOMS PER PRIMARY
KNOCK-ON, $\bar{\nu}$, FOR FAST-NEUTRON
IRRADIATION OF VARIOUS
ELEMENTS^a

Average Energy of Neutrons, 1 Mev.

Substance	Atomic Weight	$\bar{\nu}$
Be	9	440
C (graphite)	12	900
Al, Si, P	27, 28, 31	~700
Ga, Ge, As	70, 73, 75	~300
Cd, In, Sb, Te	112, 115, 122, 128	~200
Au	197	140

^a For the method of calculation see Reference 5.

that the defects anneal out as fast as they are introduced. This requires a material with a large band gap. There are several compound semiconductors which satisfy this requirement, for example AlSb, GaAs, InP, GaP, CdTe, CdS, and SiC. All have an energy band gap exceeding that of silicon.

Preliminary annealing experiments carried out on unirradiated AlSb indicate that at temperatures greater than approximately 200°C thermal defects are introduced which tend to make *n*-type samples *p*-type and *p*-type samples more *p*-type. If these defects cannot be eliminated, this effect will seriously limit the applicability of AlSb to the problem of making radiation-resistant devices. At the present time it is not known whether these defects are inherent or whether they result from, say, impurities on the surface of the sample, or in the ambient atmosphere.

One may hope to find a material with a relatively large threshold displacement energy. This would be desirable since the number of displacements is inversely proportional to the threshold energy. The low threshold of InSb (a low-band-gap material) as compared with germanium and silicon suggests that there might possibly be a correlation between threshold and band gap; however, until more threshold experiments are performed on a variety of materials, this remains pure speculation. Finally, and possibly most important, one may look for a material in which the defects introduced by bombardment have a comparatively small recombination cross section.

To summarize, it appears that a small recombination cross section, relatively massive atoms, a relatively large mobility, and a large gap are desirable properties for minimizing the effects of permanent radiation damage to semiconductor devices. Unfortunately, there is little information available on recombination cross sections and threshold energies in compound semiconductors.

COMPARISON OF CARRIER-REMOVAL RATES

Table II shows a comparison of the rates at which carrier concentration is decreased by fast-neutron bombardment for several semiconductors. These removal rates correspond to carrier concentrations large enough that the position of the Fermi level is quite close to either the conduction band or the valence band. In this case the removal rate should be equal, to within a factor of about two, to the rate at which vacancy-interstitial pairs are introduced (one expects one to two carriers to be

TABLE II. APPROXIMATE CARRIER-REMOVAL
RATES FOR FAST-NEUTRON
BOMBARDMENTS

Material	N-Type $-\frac{dn}{d\phi},$ cm^{-1}	P-Type $-\frac{dp}{d\phi},$ cm^{-1}	Final Type	Laboratory	Average Total Cross Section, barns	Calculated ^a Rate of V-I Pair Production, cm^{-1}
Ge	3.2	2.9	P	ORNL	4	50
Si	--	5	Intrinsic	ORNL	4	
AlSb	2	1.5	N	Battelle	5	70
GaAs	1.2	--	Intrinsic	Battelle	4.5	
InP	0.7	--	P	Battelle	4.5	
CdTe	--	0.44	N	Battelle	5.5	

^a Using a threshold of 25 ev.

removed per V-I pair). The comparison is rather crude because of the uncertain relation which exists between the carrier-removal rate and the rate of generating the defects. There is also considerable uncertainty in the removal rates listed because of difficulty in accurately determining the fast-neutron flux. Nevertheless, there does seem to be some correlation, as suggested by Table II, between removal rates and atomic mass. For example silicon, the lightest element, has the highest removal rate, and CdTe, composed of the heaviest elements, has the lowest.

It is perhaps more meaningful to compare the order of magnitude of the carrier-removal rates with the calculated rates of generation of defects shown in the last column for germanium and AlSb. We see that there is well over an order of magnitude discrepancy. On the other hand, agreement between the removal rates and the calculated rates of generating displacements, within a factor of two or three, is obtained when other bombarding particles such as electrons, alpha particles, or deuterons, are used. The discrepancy which seems to be present in all cases of neutron bombardments might be associated with the fact that a very large number of secondaries are produced in a very small volume near each primary event, so that the effectiveness of the displacements in removing carriers is considerably lessened from what it would be if they were distributed uniformly throughout the total volume of the crystal. Additional evidence for this type of inhomogeneity will be presented below.

BOMBARDMENT OF AlSb AND GaAs

The change in conductivity of an initially *p*-type AlSb sample and an initially *n*-type GaAs sample is shown in Figure 4. The AlSb, which goes through a very definite minimum, was *n*-type after the bombardment. If the defects are uniformly distributed and if the ionization due to γ -rays and fast neutrons is negligible, the minimum conductivity should correspond approximately to the intrinsic conductivity. The intrinsic conductivity for AlSb, at the temperature of irradiation, 386°K, is of the order of 10^{-7} ohm⁻¹cm⁻¹. The minimum conductivity of this sample was over four orders of magnitude greater than this value. The GaAs sample, on the other hand, does approach its intrinsic conductivity. The intrinsic conductivity for GaAs is of the order of 10^{-6} ohm⁻¹cm⁻¹ at the bombardment temperature, assuming the mobility has been lowered by about an order of magnitude by the bombardment. This is not due to ionization, since both samples were irradiated simultaneously at approximately the same position in the beam tube of the reactor. We conclude that the

minimum of the AlSb sample is determined by inhomogeneity, either initially present or produced by the irradiation.

Another p-type AlSb sample was irradiated with enough flux to greatly decrease the conductivity but not enough to convert it to n-type (i.e., the bombardment was stopped on the low-flux side of the minimum in conductivity). The temperature dependence of the Hall coefficient, resistivity, magnetoresistance mobility, and Hall mobility is shown in Figure 5. The Hall mobility is defined as the ratio of the Hall coefficient to the resistivity. The magnetoresistance mobility, μ_ρ , is proportional to the square root of the magnetoresistive ratio and was calculated by the following formula:

$$\frac{\rho_H - \rho_0}{\rho_H} = \frac{9\pi}{16} \mu^2 H^2 \left(1 - \frac{\pi}{4}\right),$$

where ρ_0 is the resistivity without magnetic field

ρ_H is the resistivity in the presence of a transverse magnetic field

H is the field strength (emu).

Before the irradiation the Hall mobility and the magnetoresistance mobility were of the same order of magnitude, as one would expect. However, after the bombardment the Hall mobility is about two orders of magnitude lower than the magnetoresistance mobility at 200°K and has an anomalously large temperature dependence. This rather strange behavior can be explained qualitatively in terms of the inhomogeneous distribution of defects mentioned above. For the purpose of simplifying the discussion, imagine that the density of the defects is very great inside a small sphere of radius a, and that the density of defects outside these spheres, or "islands", is much smaller and essentially uniform. Before the sample has converted, the volume inside the spheres will be n-type and the bulk will be p-type.

Now, there are two possible explanations. First, let us assume that the lines of current flow are not appreciably altered by the spheres of intense damage. In this case the Hall field inside the n-type spheres will oppose that of the bulk of the specimen. This will result in an appreciable lowering of the measured Hall coefficient and an increase in the magnetoresistance ratio from the values which would be obtained if these concentrated regions were not present. However, the conductivity will not be greatly affected, so that the Hall mobility will be considerably lower than the magnetoresistance mobility.

In the second explanation we assume that the lines of current flow do not penetrate the spheres of intense damage; i. e., the holes are deflected from these regions because of the space charges which must be present in the vicinity of the p - n junction separating the two regions. In this case the Hall coefficient and magnetoresistance are not affected, but the conductivity is lowered considerably. This assumption leads to the same qualitative result, namely, that the Hall mobility will be considerably lower than the magnetoresistance mobility.

To differentiate between these two mechanisms will require further experimental and theoretical investigations. However, it is to be expected that the first mechanism would be the most likely explanation if the radius of the spheres is quite large (10^{-3} to 10^{-4} cm) and the transition from p - to n -type is gradual. If the spheres are much smaller the second mechanism should apply.

If the spheres result from the intense damage in the vicinity of each primary knock-on one expects their radii to be quite small. For example, if a primary knock-on produced approximately 1000 progeny, or approximately 10 generations, and if the average distance which a knock-on must travel before producing another knock-on is the order of 1 unit cell or, say, 10 Å, the radius a would be the order of 100 Å or 10^{-6} cm.

We can obtain a crude experimental estimate of this radius by assuming that the total volume occupied by the spheres is approximately equal to the volume not occupied by the spheres when the flux, ϕ_1 , is large enough to produce the mobility anomaly. This gives

$$N_0 \sigma_t \phi_1 (4\pi a^3) = 1/2,$$

where N_0 is the number of atoms per cm^3

σ_t is the scattering cross section for the neutron collisions.

(The quantity $N_0 \sigma_t \phi_1$ is the total number of primary events per cm^3 .)

Taking 5 barns for σ_t , 4×10^{22} for N_0 , and 1×10^{18} for ϕ_1 , one obtains a $\approx 6 \times 10^{-7}$ cm.

This would suggest that the regions of intense damage have radii of roughly 60 Å, which is a fairly reasonable conclusion.

Another property which would be strongly affected by the type of inhomogeneity described above is the thermoelectric power. The contributions of the n - and p -type regions to the over-all thermal voltage would oppose each other, and the measured thermoelectric power would be considerably smaller than predicted on the basis of the conductivity. Either

of the two mechanisms considered above would imply an abnormally low thermoelectric power, since no current flows through the sample during the measurement of thermoelectric power.

Thermoelectric-power measurements on a p-type AlSb sample, before and after irradiation, illustrate this fact very clearly. Table III lists the magnetoresistance mobility, Hall mobility, thermoelectric power, and conductivity at 200°K for a p-type AlSb sample before irradiation, and after an exposure of 1.3×10^{18} neutrons/cm².

TABLE III. ELECTRICAL CHARACTERISTICS OF AN AlSb SAMPLE BEFORE AND AFTER IRRADIATION

	$\phi = 0$	$\phi = 1.3 \times 10^{18}$ neutrons/cm ²
Magnetoresistance Mobility, cm ² /volt-sec	360	92
Hall Mobility, cm ² /volt-sec	357	27
Thermoelectric Power, μv/°K	+225	+5
Conductivity, ohm ⁻¹ cm ⁻¹	26	0.18

We see that the fractional decrease in thermoelectric power is comparable with that of the conductivity. On the other hand, if the defects were homogeneously distributed, the thermoelectric power would increase as the carrier concentration decreased. It must be emphasized that the models described above are quite tentative and should not be taken too seriously until they have stood the test of considerably more experimentation. Nevertheless, they should serve to illustrate that certain of the bulk properties of semiconductors may be seriously affected by this type of inhomogeneity – much more so than would be expected from the assumption that the defects are homogeneously distributed.

SUMMARY

Compound semiconductors appear promising as radiation-resistant devices; however, more information is needed on threshold displacement

energies and recombination cross sections. The nonhomogeneous nature of the damage created by fast neutrons in semiconductors is revealed by means of the Hall coefficient, magnetoresistance ratio, and the thermoelectric power. In some cases the size of the damaged regions can be estimated.

ACKNOWLEDGMENTS

We wish to express our sincere gratitude to F. J. Reid of Battelle who was responsible for much of the early work on AlSb, including the measurements on the specimens which show the mobility anomaly. We also wish to thank Dietrich Langer of the Aeronautical Research Laboratory, Wright Air Development Center, with whom we have had stimulating discussions, and R. Miller and J. Moody of Battelle who made many of the measurements. We are indebted to the Sponsors of the Compound Semiconductor Research Group at Battelle for the samples of high-purity GaAs and AlSb.

REFERENCES

1. Cleland, J. W., and Crawford, J. H., Jr., Phys. Rev., 95, 1177 (1954).
2. James, H. M., and Lark-Horovitz, K., Z. Physik. Chem., 198, 107 (1951).
3. Curtis, O. L., Cleland, J. W., Crawford, J. H., Pigg, J. C., J. Appl. Phys., 28, 1161 (1957).
4. Beck, R. W., Paskell, E., Peet, C. S., "Effects of Fast Neutron Irradiation on Electron Lifetime in P-Type Silicon", Electrochem. Soc. Meeting, April, 1958.
5. Dienes, G. J. and Vineyard, G. H., "Radiation Effects in Solids", Interscience (1957).
6. Harris, E. G., "The Disordering of Polyatomic Solids by Neutrons", Naval Research Laboratory Report 4807.

REFERENCES
(Continued)

7. Baroody, E. M., "Theoretical and Experimental Studies Concerning Radiation Damage in Selected Compound Semiconductors", WADC Technical Report 57-593 (September, 1957); To be published.
8. Brown, W. L. and Augustyniak, W. M., Bull. Am. Phys. Soc., Ser. II, 2, 156 (1957).
9. Eisen, F. H., Bickel, P. W., and Sosin, A., "Third Quarterly Progress Report on Radiation Damage Studies in Compound Semiconductors to Wright Air Development Center", Contract No. AF 33(616)-3924.
10. Rappaport, P. and Loferski, J. J., Phys. Rev., 100, 1261 (1955).
11. Baroody, E. M., "Second Interim Progress Report on Theoretical and Experimental Studies Concerning Radiation Damage in Selected Compound Semiconductors to Wright Air Development Center", Contract No. AF 33(616)-3747 (December 29, 1956).
12. Loferski, J. J., J. Appl. Phy., 29, 35 (1958).

FIGURE LEGENDS

- Figure 1. Change in Conductivity of *N*- and *P*-Type InSb with Fast-Neutron Bombardment. Taken from Reference 1.
- Figure 2. Minority-Carrier Lifetime as a Function of Integrated Fast-Neutron Flux for Germanium and Silicon. Taken from References 3 and 4.
- Figure 3. Carrier-Removal Rate of InSb and Germanium as a Function of the Maximum Energy Imparted to an Atom. Taken from References 7 and 8.
- Figure 4. Conductivity Versus Fast-Neutron Flux for *P*-Type AlSb and *N*-Type GaAs. The Experiment was Carried Out at 113°C.
- Figure 5. Temperature Dependence of Resistivity, Hall Mobility, Hall Coefficient, and Magnetoresistance Mobility of *P*-Type AlSb after it has Received a Total Bombardment of 1.5×10^{18} Neutrons/cm².

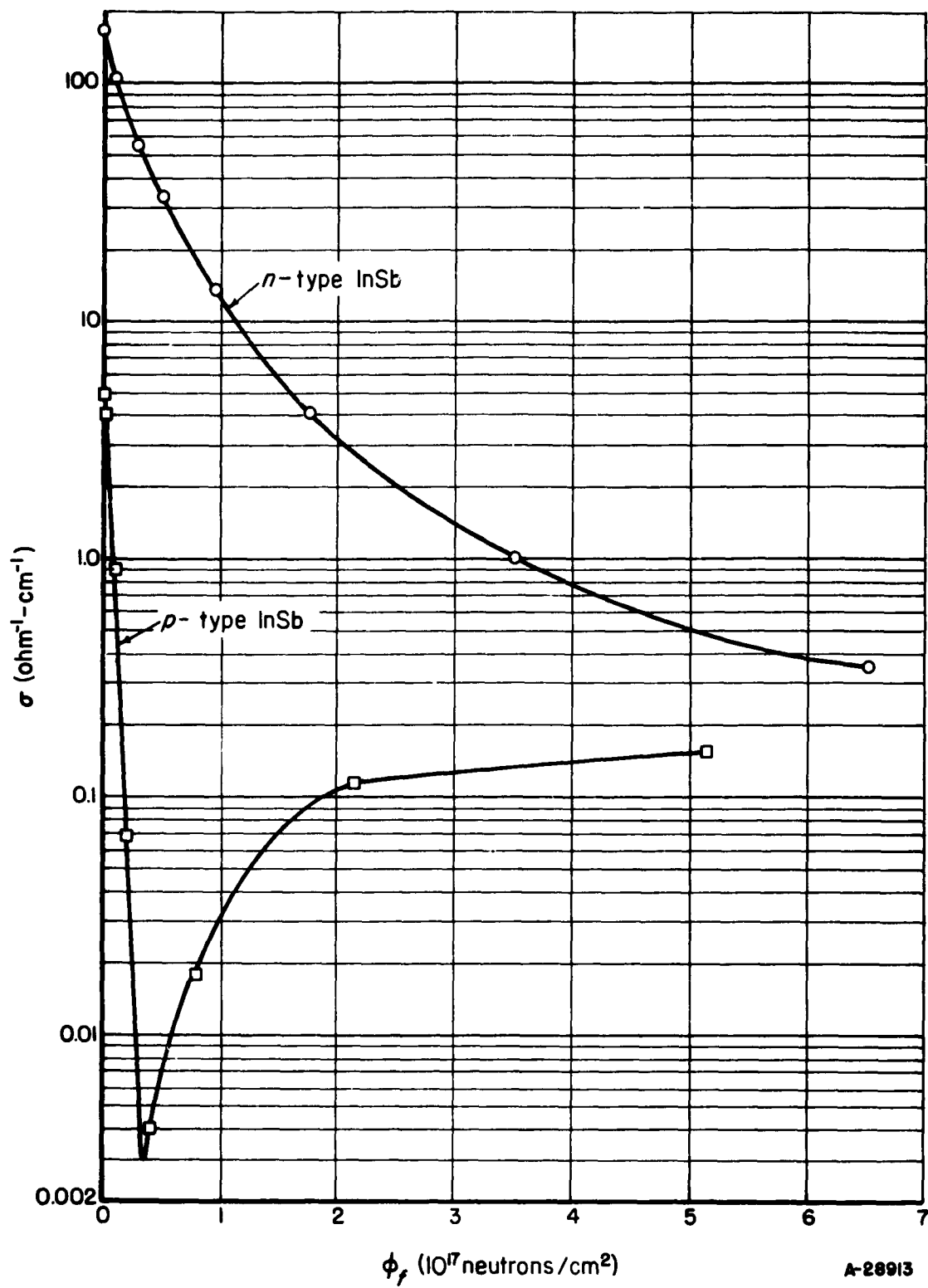


FIGURE I.

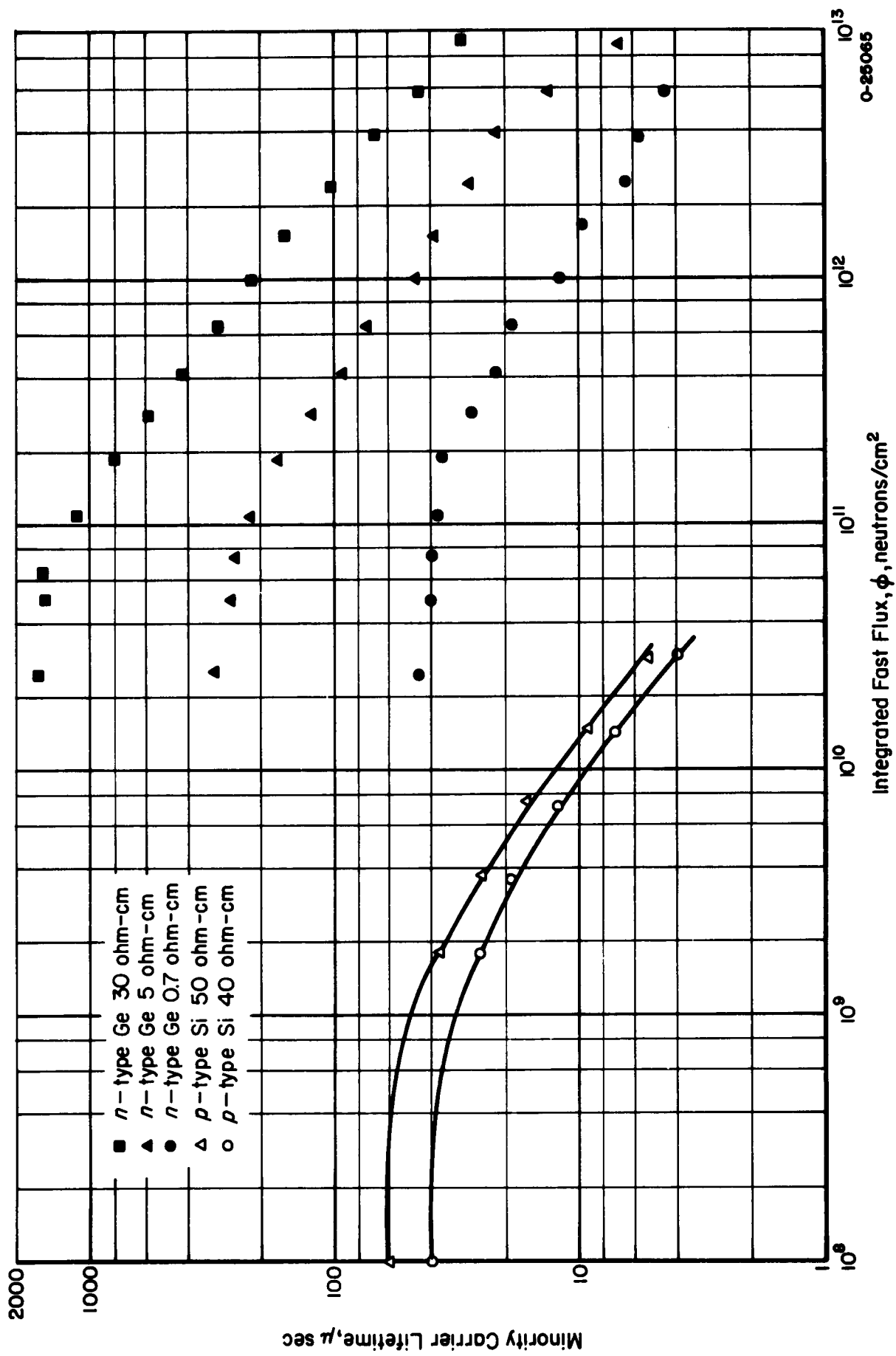


FIGURE 2.

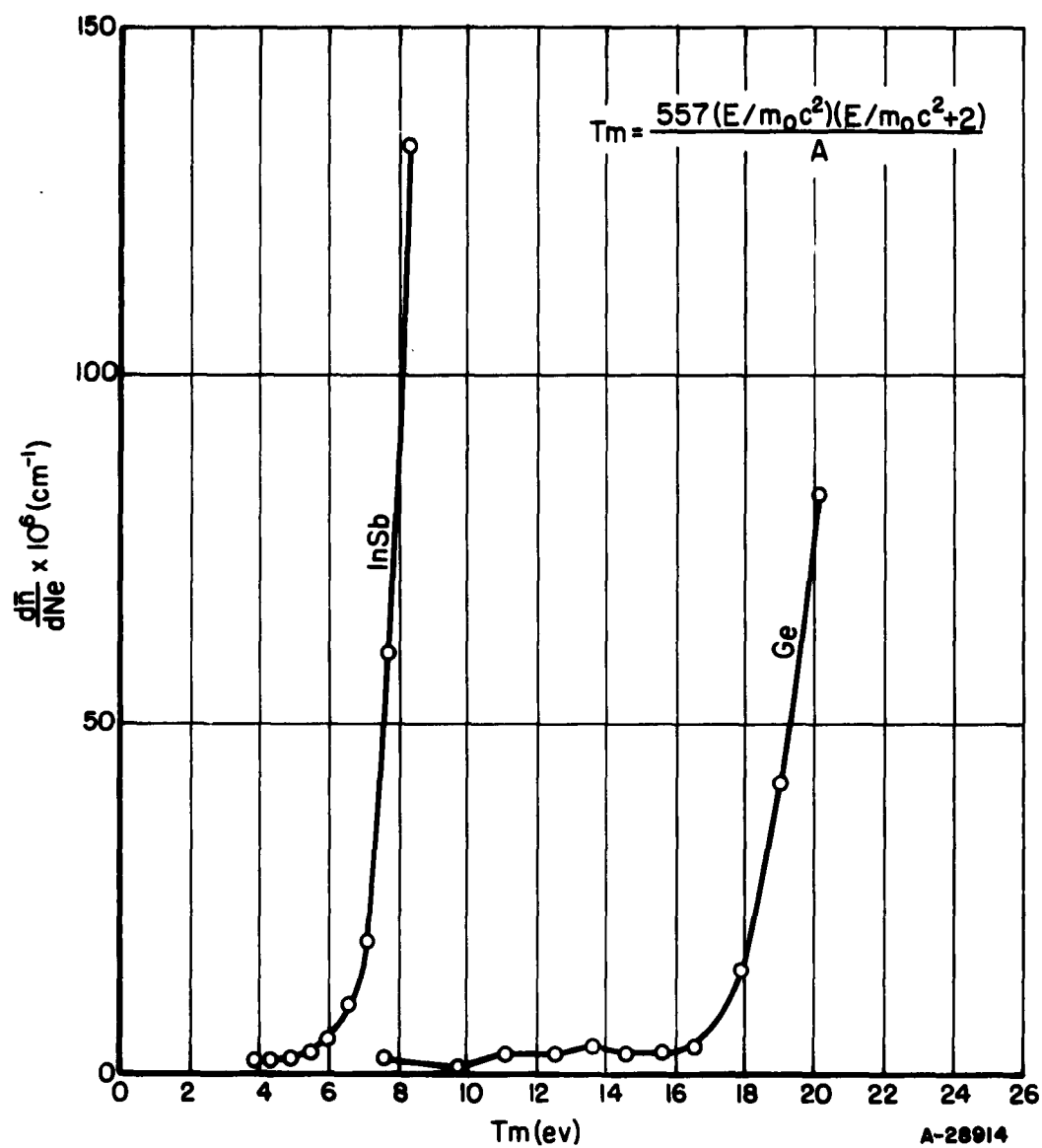


FIGURE 3.

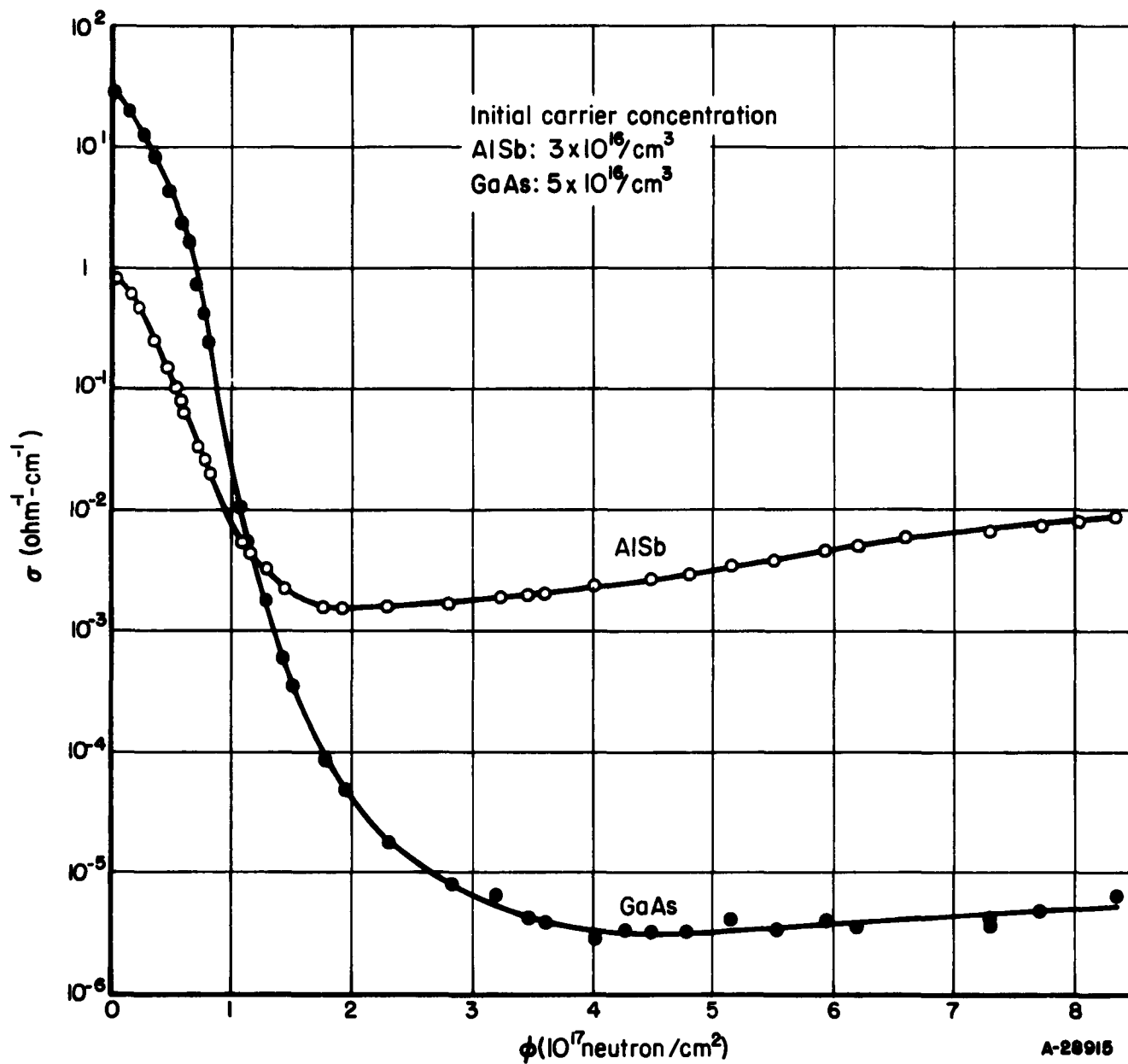


FIGURE 4.

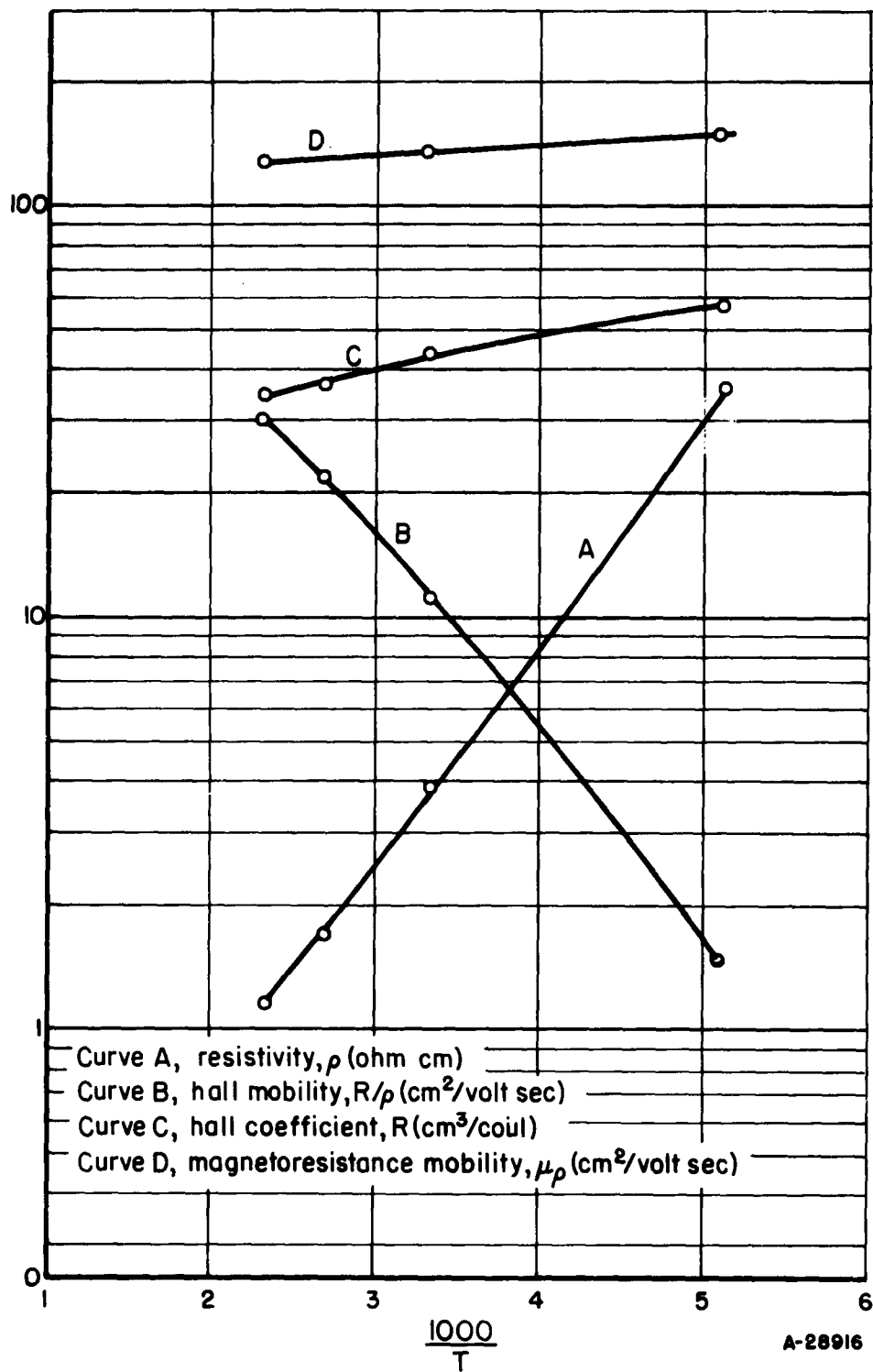


FIGURE 5.

A CRITICAL SURVEY OF
RADIATION DAMAGE TO CIRCUITS

by
W. W. Happ and S. R. Hawkins*

ABSTRACT

A critical survey was undertaken to investigate factors affecting circuit performance in the presence of damage producing radiations. Experimental work in progress consists of irradiating several types of circuits, such as multivibrators and blocking oscillators by gamma radiation with a 100-curie Cobalt-60 source. Causes of failure of the circuits tested thus far were traced primarily to the deterioration of semiconductor devices. This preliminary work is being used as a basis for planning investigations of other selected circuits, both under gamma and neutron irradiation.

* Lockheed Aircraft Corporation, Missile Systems Division,
Palo Alto, California

SECTION 1.0 SCOPE OF INVESTIGATION

1.1 FLUX-DOSE PLOTS

To more fully outline the scope and limitations of this investigation and to plan future work it is advisable to plot on logarithmic coordinate scales the following quantities:

- (a) Dose; the total number of particles or quanta traversing a unit of area. The unit of dose for gamma radiation is the roentgen, defined in Appendix A. Since the dimensions of dose are number of particles per unit volume \times velocity \times time, the dose for neutron radiation may be referred to as nvt.
- (b) Flux; the number of particles or quanta traversing a unit area per unit time. The units of flux are roentgen/hr or particles/cm²/sec.

If flux is plotted versus dose, as shown in Fig. 1.1, 1.2 and 1.3, then for an irradiation of constant flux the lines which are inclined at a constant angle denote time intervals. These plots provide a ready reference giving the order of magnitude of radiation. The graphs show that the magnitude of flux as well as dose extends over several decades.

The specific aims of this investigation, then, are:

- (a) Exposure of various types of transistor circuits to gamma, fast neutron, and slow neutron radiation
- (b) Analysis of the effects encountered in order to determine which components within the circuit are most critical
- (c) A study of the effects during irradiation as well as before and after effects
- (d) An effort to determine whether the controlling factor is rate of irradiation or integrated irradiation, or both.

1.2 GAMMA IRRADIATION

According to Steele (1956) irradiation by Cobalt-60 gamma rays at fluxes in excess of 10^3 r/hr, and in doses greater than 10^6 r, is necessary to induce temporary and permanent effects on transistor parameters. At this time it is believed that most transistors will be severely affected between 10^7 and 10^8 roentgens, while total destruction of most transistors occurs above 10^8 roentgens. Referring to Fig. 1.1, it follows that with a 100-curie source, permanent destruction of most transistors can be expected after about 1000 hours of irradiation, while failure to operate becomes more and more probable between 100 and 1000 hours.

Experiments in this report were made with a 100-curie source. With the 1000-curie source becoming available the irradiation times can be reduced by a factor of about 10, thus requiring an irradiation time of only 100 hours to approach the dose required for permanent destruction of all transistors.

A nomograph giving the gamma flux for various source strengths (in curies) at various distances for a Cobalt-60 point source is given in Fig. 1.4. A diagram of this type serves as an aid to setting up experiments with an isotope source.

1.3 FAST NEUTRON IRRADIATION

According to Pigg and Robinson (1956) each incident high energy neutron removes 3.2 electrons in germanium while Cobalt-60 gamma rays remove 1.4×10^{-3} electrons per incident photon. Also it has been found that 0.02 electrons are removed for each incident thermal neutron. On the basis of these figures, it is estimated that the ratio of the damage produced by fast neutrons to slow neutrons to gamma rays is 2300:16:1. If we assume a similar relationship for permanent damage to transistors, then, according to Fig. 1.1, if total destruction can be expected to occur at gamma doses of 10^8 roentgens (1.6×10^{17} photons/cm²), we can assume that total destruction will also occur at integrated fast neutron fluxes above 10^{14} neutrons/cm². These figures correspond fairly well to experimental data reported by Steele (1956), Behrens and Shaul (1958), and data obtained in this laboratory.

From study of this experimental data, we can expect damage to transistors to begin to show effects at integrated fluxes of between 10^{11} and 10^{12} nvt (neutrons/cm²) with serious damage occurring between 10^{12} and 10^{13} nvt, and total destruction occurring between 10^{13} and 10^{14} nvt (Fig. 1.2).

Since our present Po-Be neutron source has a maximum flux of about 10^5 nv (neutrons/cm²), an irradiation time of more than 10^8 seconds or 1160 days is required before total destruction of a transistor can be expected. Irradiation time of at least 10^6 sec or 11.6 days should be required before any effect at all can be expected. With Lockheed's Van de Graaff

generator total destruction can be expected after about 10^4 seconds, or approximately 3 hours, provided the neutron energy distribution is comparable with that available at a reactor.

The Vallecitos power reactor, and also the Materials Test Reactor, is likely to cause total destruction of transistors in a matter of minutes or even seconds, as shown by Fig. 1.2.

For this reason consideration is being given to performing certain tests at these sites. The operating costs computed on an hourly basis at the Vallecitos reactor at this time are substantially higher than those of the Material Test Reactor; however, our required irradiation times are short enough to warrant frequent use of this nearby facility.

The high minimum neutron fluxes involved at the Material Test Reactor, render measurements during irradiation very difficult as can be seen from Fig. 1.2. Tentatively, the Vallecitos reactor, and, in certain cases Lockheed's Van de Graaff generator, are recommended in preference to the Materials Test Reactor for neutron irradiation. (For further facility discussion see 1.5)

1.4 SLOW NEUTRON IRRADIATION

At this time we know of no systematic study of the effects of thermal neutrons on semiconductor devices. Following the reasoning in paragraph 1.3, one might expect total destruction of transistors at doses above 10^{15} nvt, provided the crystal is directly exposed. Obviously, the required dosage is much higher if shielding and scattering are involved. The apparent lack of knowledge of radiation damage by thermal neutrons may make further investigations in this area desirable.

1.5 FACILITIES

The availability of the gamma and neutron sources is based mainly upon geographical location and ease of access as well as the maximum workable flux densities. An idea of the relative magnitudes of the various sources can be seen from examination of Fig. 1.1, 1.2, 1.3 and Table 1.1.

A complete list of neutron and gamma irradiation facilities in operation, being built or planned has been compiled by Martens and Minuth (1957).

TABLE 1.1
MAXIMUM GAMMA AND NEUTRON FLUXES FROM
IRRADIATION FACILITIES UNDER CONSIDERATION

SOURCE	MAXIMUM FLUX		Gamma (r/hr)
	Fast Neutrons (n/cm ² /sec)	Thermal	
LMSD Co ⁶⁰ (100 curie)			10 ⁵
LMSD Co ⁶⁰ (1000 curie) (to be delivered)			10 ⁶
Stanford Research Institute Co ⁶⁰ (1000 curie)			.8 x 10 ⁶
MTR (Materials Test Reactor) Spent-Fuel Gamma Source National Reactor Testing Station, Idaho Falls, Idaho			10 ⁷
LMSD Po-Be	10 ⁵		
LMSD Van de Graaff Generator	10 ⁹		
Experimental Power Reactor Vallicitos, Calif.	10 ¹⁰	10 ¹¹	
MTR, National Reactor Testing Station	2.5 x 10 ¹⁴	5 x 10 ¹⁴	10 ⁹
ETR, National Reactor Testing Station	1.5 x 10 ¹⁵	4 x 10 ¹⁴	

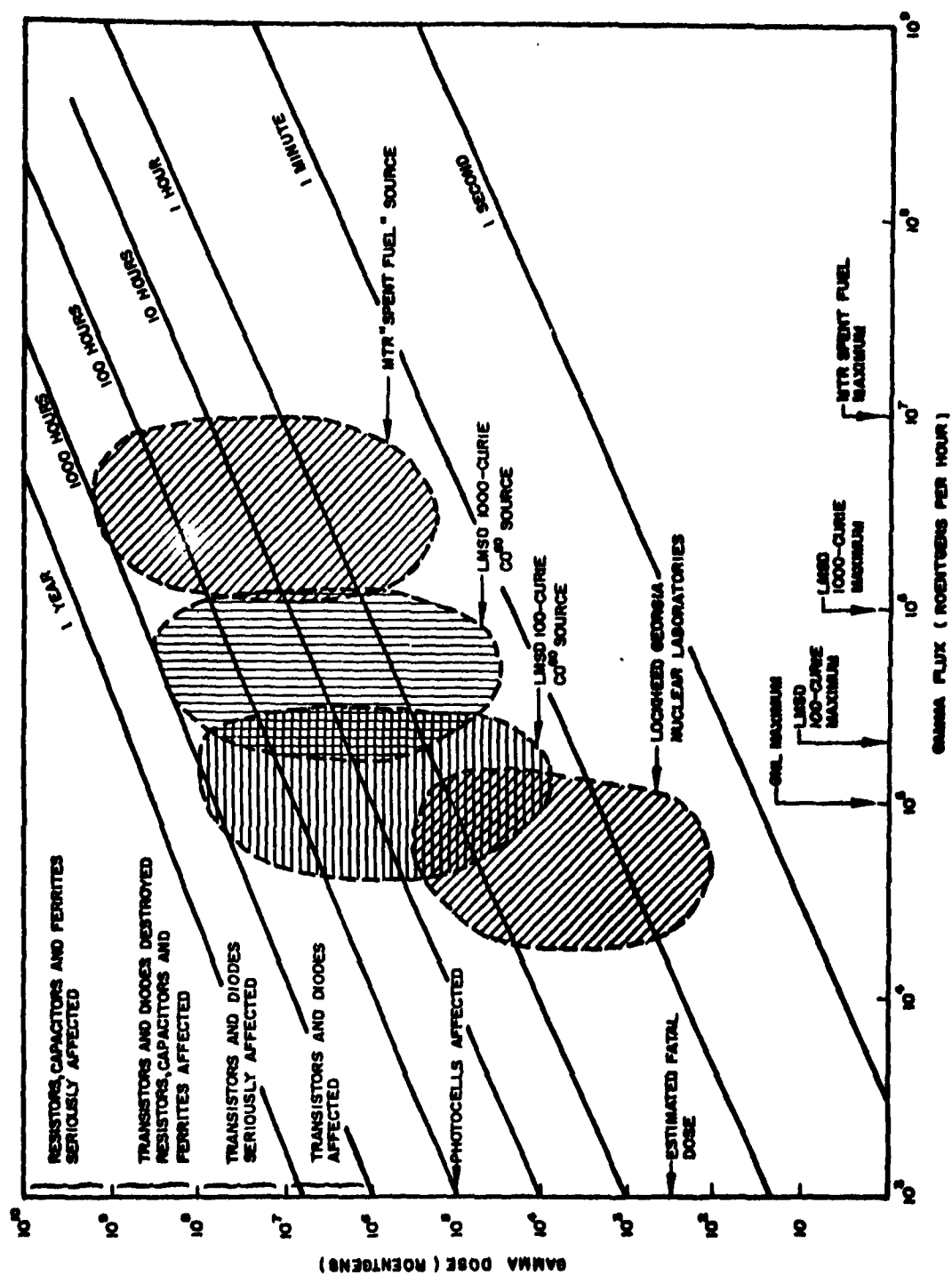


Fig. 1-1 Approximate Limits of Gamma Investigations

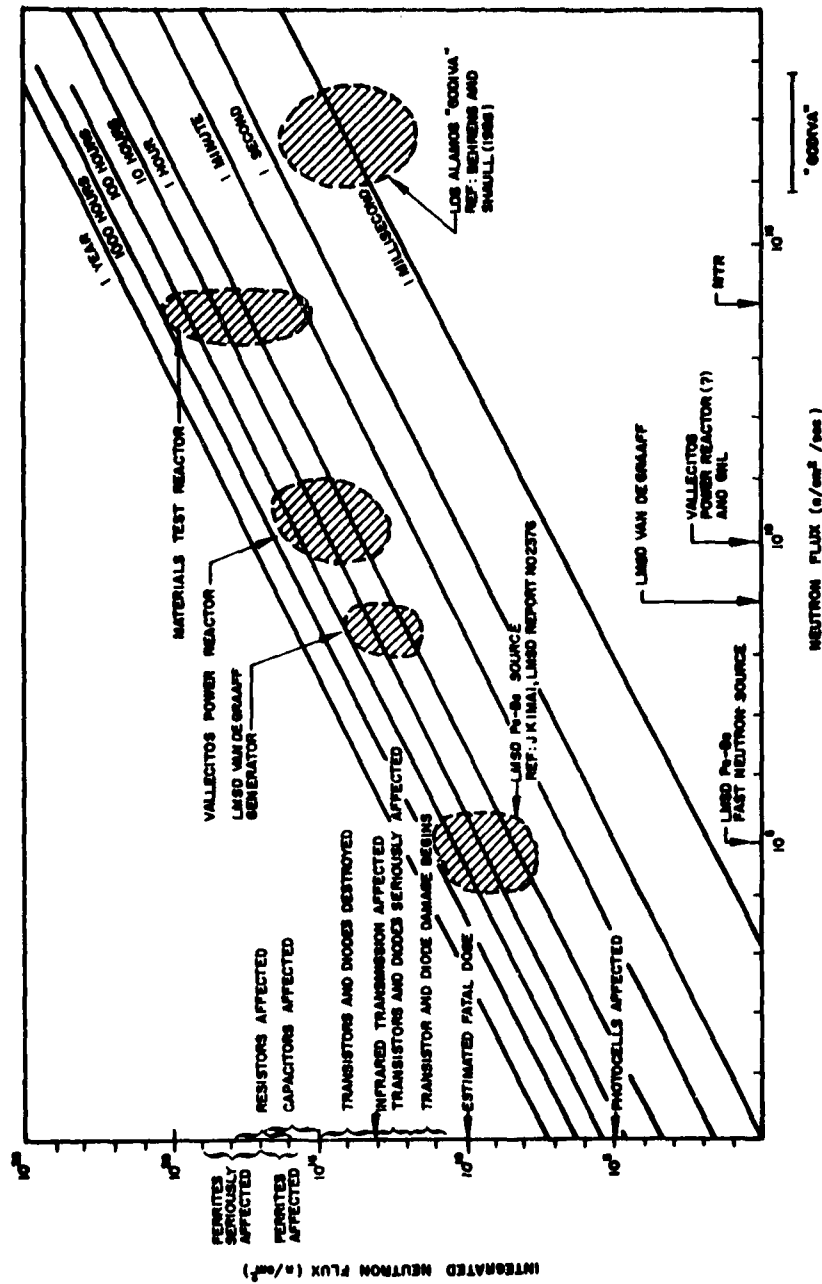


Fig. 1-2 Approximate Limits of Fast Neutron Investigations

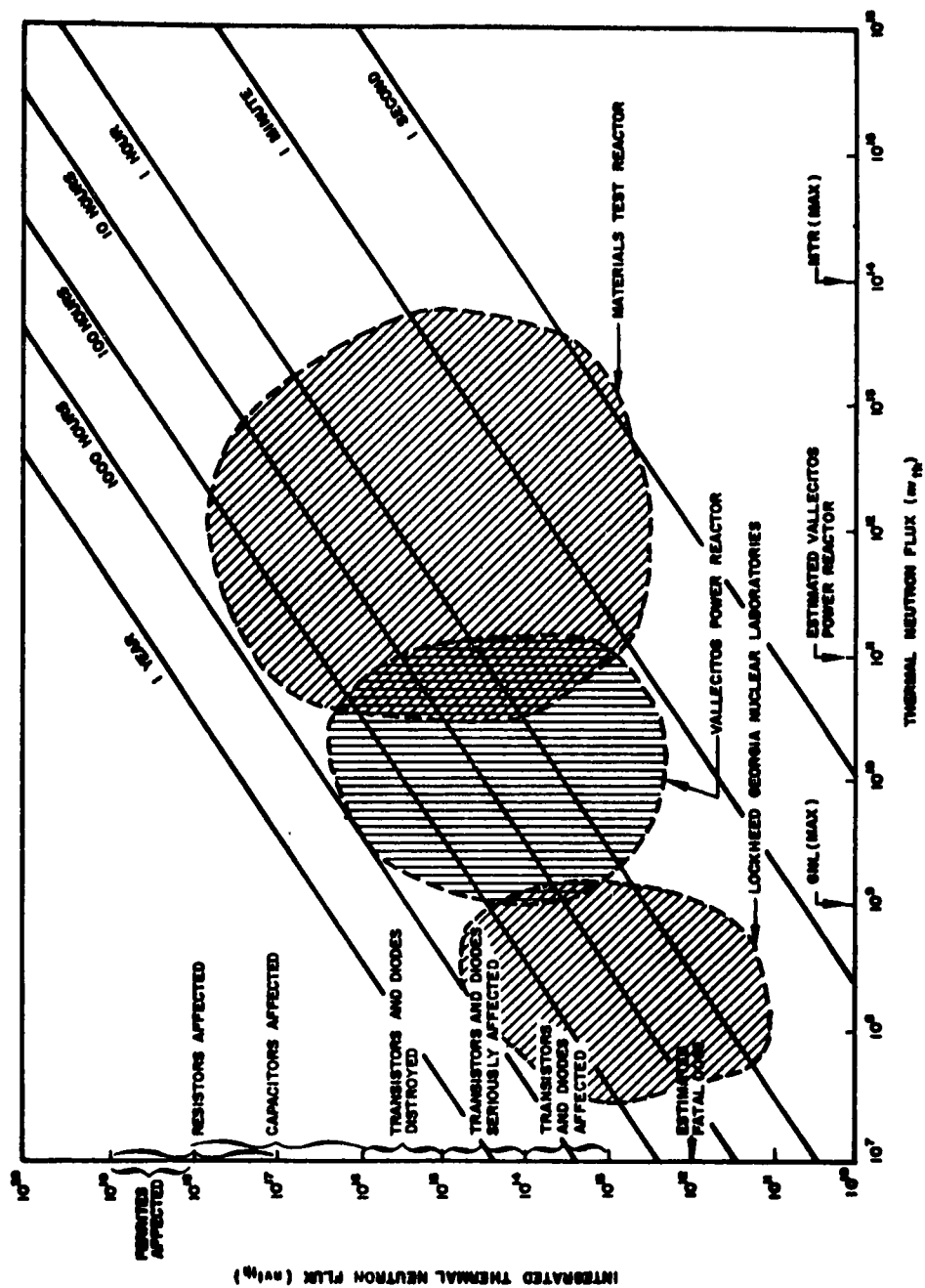


Fig. 1-3 Approximate Limits of Thermal Neutron Investigations

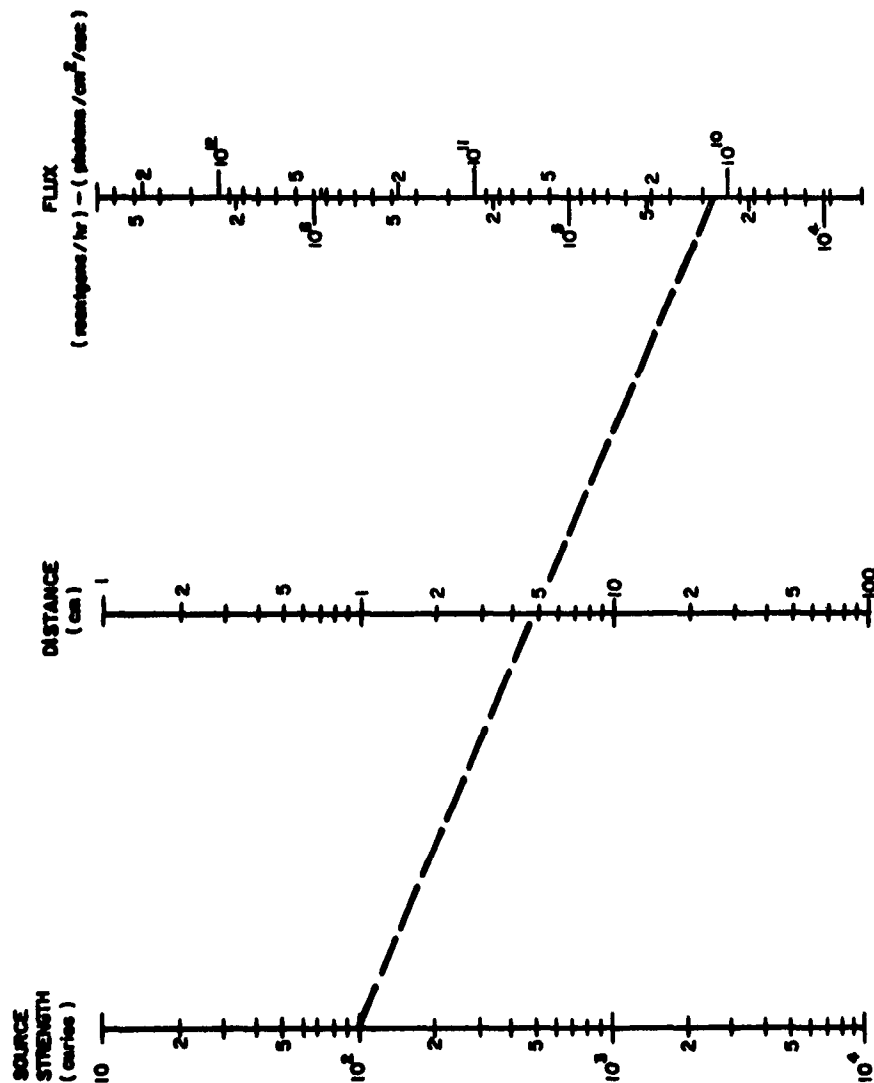


Fig. 1-4 Nomograph: Gamma Flux vs Source Strength at Various Distance for Cobalt-60 Point Source

SECTION 2.0

CIRCUITS PROPOSED FOR INVESTIGATION

2.1 AMPLIFIERS

Since nearly all types of circuits are in some way derived from the basic amplifier, an analysis of the effects of nuclear irradiation on an amplifier stage will give valuable information on what to expect in the more complicated circuitry. The types of amplifier and their corresponding properties which should be studied are:

A. Low Frequency Amplifiers

- (1) Degenerative: the use of negative feedback to counteract the radiation damage to the circuit.
- (2) Regenerative: the effect of radiation damage on the stability of the circuit.

B. High Frequency and Pulse Amplifiers

- (1) The deterioration of frequency response.
- (2) The deterioration of gain.

It appears worthwhile to examine the feasibility of compensating radiation damage by methods similar to those used in circuits compensated for variations in temperature.

2.2 OSCILLATORS

It is proposed to determine how the frequency, amplitude and distortion of various types of oscillators are affected and at what radiation doses these circuits fail to function within the specified limits. It is planned to investigate the following types of oscillators.

- (a) RL, RC, LC oscillators of various design; to determine the sensitivity of each to radiation damage and, if necessary, to propose methods on how each circuit may be improved.
- (b) Crystal controlled oscillators. It is expected that crystal controlled oscillators will present a challenging problem for investigation; particularly if the close tolerance on the frequency deviation must be maintained. It may be possible to develop techniques which compensate for radiation damage in a manner similar to temperature compensation. A metallographic study of the nature of the damage to the crystal may be of value to assess the expected effects of radiation on the circuit performance.

2.3 SWITCHING CIRCUITS

Switching circuits should be investigated extensively since these types of circuits are widely used. The types of switching circuits which should be investigated are:

- (1) Multivibrators; to determine dosage at which the circuits fail to switch; to examine the extent and by what mechanism switching time and other circuit parameters are affected.
- (2) Blocking oscillators; to determine the dosage at which the circuit will fail to trigger or to oscillate and to what extent the waveform is affected.

- (3) Other circuits using semiconductor devices, such as logic and pulse shaping circuits.

It appears particularly desirable to analyze the deterioration of the switching action in terms of the corresponding changes of device parameters. This analysis may then lead to the design of circuits which partially compensate for radiation damage.

2.4 CHOICE OF COMPONENTS

Reid, Moody and Willardson (1957), as well as Messenger and Spratt (1957), have pointed out that, in general, silicon semiconductor devices are more susceptible to radiation damage than corresponding types of germanium devices. It was further shown that the npn transistors are more susceptible than the pnp type. It is desirable to investigate circuits using both germanium and silicon devices and pnp as well as npn transistors, since the nature of the radiation damage can be more closely interpreted in circuits using the more sensitive devices, and in view of the limited flux obtainable from the radiation sources now available to us.

2.5 LIMITS OF OPERATION

The term limit of operation requires clarification. For instance, radiation damage may affect the circuits as follows:

- (1) The circuit may change in a specified parameter beyond the permissible limit, depending upon the function of the circuit.
- (2) The circuit may fail in its principal function in the presence of radiation.
- (3) Circuit components may have suffered permanent damage to an extent that the circuit will not perform its function even after the radiation source is removed.

In Table 2.1 an estimate of the limits of operation is given by assuming the order of magnitude of the limit of operation, as defined in (1), (2) or (3) above to be roughly the same. This somewhat loose use of the term limit of operation appears justified, since the failure of circuit components can only be specified statistically. Thus for a single circuit, variations in the limit of operation by a factor of ten are likely to be the rule rather than the exception.

TABLE 2.1
ESTIMATE OF LIMITS OF OPERATION FOR SELECTED CIRCUITS

Circuit	Sensitive Parameter	Estimated Limit of Operation		
		Gamma	Neutron Radiation	
			Fast	Slow
(a) Multivibrator	Triggering level	$10^8 r$	$10^{13} nvt$	$10^{15} nvt$
(b) Transistor magnetic core circuit	Triggering level	$10^7 r$	$10^{12} nvt$	$10^{14} nvt$
(c) Pulse shaping circuit	Saturation resistance	$10^7 r$	$10^{12} nvt$	$10^{14} nvt$
(d) Crystal oscillator	Frequency	$10^6 r$	$10^{11} nvt$	$10^{13} nvt$
(e) Amplifier	Gain, distortion, noise	$10^7 r$	$10^{12} nvt$	$10^{14} nvt$

SECTION 3.0

RESULTS OF PRELIMINARY WORK

3.1 MEMORY CORE DRIVER

Two memory core driver circuits consisting of a transistor blocking oscillator and power amplifier have been irradiated with a gamma flux of about 3×10^4 r/hr. The total irradiation time was 380 hours and gave a gamma dose slightly in excess of 10^7 r.

A schematic diagram of the circuit and specifications on its operation are given in Fig. 3.1. The purpose of the circuit is to drive a string of ferrite memory cores. In order that each stage could be evaluated, each circuit was monitored at the output of the blocking oscillator and the output of the power amplifier during irradiation. It should be noted that each stage is normally in a non-conducting state and becomes saturated when the blocking oscillator is triggered by an input pulse so that the entire circuit functions as a switch. The ferrite-core load was omitted from the circuit since it provides a very low impedance after the switching action has taken place and since it has little effect upon the action of the blocking oscillator.

3.1.1 Arrangement for Testing

The experimental arrangement for testing the two memory core-drivers is illustrated in Fig. 3.2(a). This arrangement includes provisions for testing the two circuits with a single pair of leads from the hot cell using remote control techniques. Fig. 3.2(b) also shows the position of the circuits relative to the gamma source. Since the transistors were placed approximately 5cm. from the gamma source it can be seen from Fig. 1.4 that

the gamma flux at this distance is approximately 3×10^4 r/hr. This estimate is probably reliable to within 50%, allowing for self-absorption and the geometry of the gamma source.

3.1.2 Circuit Performance

The circuit parameters monitored during irradiation of the memory core-driver were the following:

- (a) Minimum triggering level
- (b) Pulse width at monitors "A" and "B"
- (c) Pulse rise times at monitor "A" and "B"
- (d) Pulse decay time at monitors "A" and "B"
- (e) Pulse amplitude at monitors "A" and "B"

These quantities are plotted as functions of dosage in Fig. 3.3. Interpretations of these results are also given. These curves are intended to show the trend of these parameters during irradiation and should not be taken as exact.

"Before" and "after" photographs of the pulse waveforms are shown in Fig. 3.4. It is interesting to note from the photographs that, although, the pulse width narrowed and the decay time increased, the waveform in general appears to have improved during irradiation.

Further investigations with this circuit will be carried out with the 1000 curie Cobalt-60 gamma source when it arrives. It is expected that the total dose with this source will approach 10^8 r after 100 hours.

3.2 FERRITE CORE LOGIC CIRCUIT

Several ferrite core logic circuits have been constructed and are to be tested under radiation. This circuit is a two-state memory device which is

being used extensively in many applications. Figure 3.5 (a) shows that this circuit consists of a single transistor and a ferrite core. The ferrite core, which has a square hysteresis-loop similar to that shown in Fig. 3.5(b), provides the memory function. The transistor serves as a driving element, a buffer and also supplies the output power. An analysis of this circuit was given by Guterman and Carey (1955).

The circuit parameters to be monitored on this circuit during irradiation include:

- (a) The "set" function efficiency, or the minimum current required to cause the ferrite core to completely change states
- (b) The "reset" function efficiency, or the minimum current or voltage amplitude required to start the blocking oscillator action which causes the circuit to reset itself to the original state
- (c) The minimum width of the reset pulse
- (d) The minimum supply voltage necessary for the reset function to operate
- (e) The maximum repetition rate of the set and reset sequence

In order to interpret the changes in this circuit during irradiation, several type 2N332 transistors will be irradiated while this or other circuits are under irradiation. In this manner the changes in circuit parameters during irradiation can be correlated with the observed changes in transistor parameters.

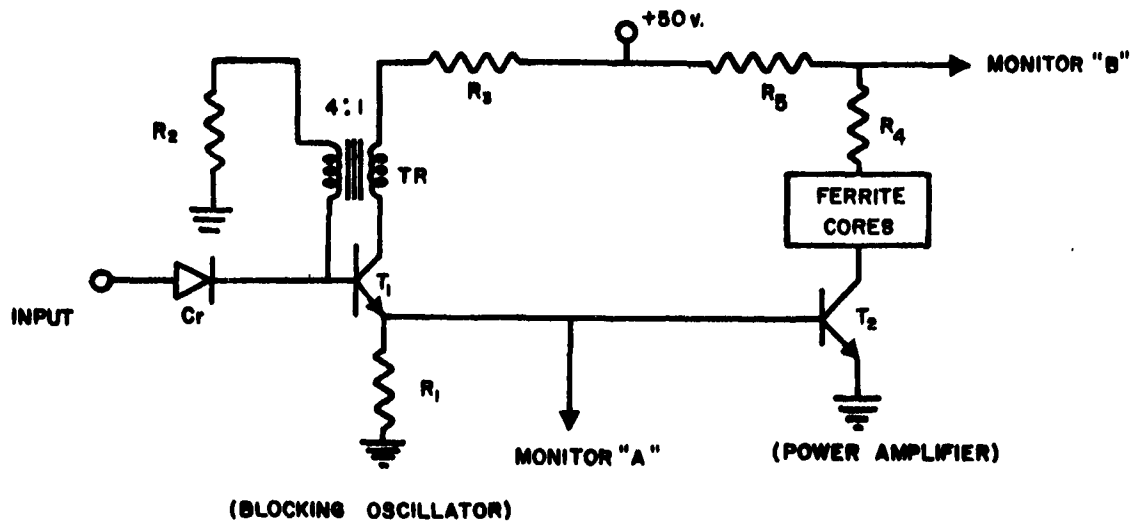
3.3 MULTIVIBRATOR

The bi-stable multivibrator circuit shown in Fig. 3.6 has been constructed and is now being irradiated with the Lockheed Cobalt-60 gamma source. The circuit will be irradiated for about 350 hours with an estimated gamma flux of 3×10^5 r/hr to provide a gamma dose in excess of 10^8 r.

Four 2N338 transistors, which are the type used in this circuit, have been irradiated simultaneously with another experiment now in progress. Curves of beta, the common-emitter forward transfer current ratio (h_{fe}) versus gamma dose, are shown in Fig. 3.7. It can be seen from these curves that the multivibrator action is expected to fail after approximately 350 hours of irradiation since the triggering level is a function of beta. Curves for I_{co} , the collector-base leakage current versus gamma dose for these transistors, are shown in Fig. 3.8. These curves show an indication of the expected change of the cutoff currents of the circuits during irradiation.

The circuit parameters which we expect to monitor during irradiation include:

- (a) Minimum triggering voltage
- (b) Switching times (rise and decay times)
- (c) Operating points (saturation and cutoff currents)
- (d) Minimum supply voltage required for 100% triggering.



CIRCUIT SPECIFICATIONS

R_1 = 20 ohms, 1/2 w, 5%

R_2 = 910 ohms, 1/2 w, 5%

R_3 = 20 ohms, 1/2 w, 5%

R_4 = 20 ohms, 1/2 w, 5%

R_5 = 10 ohms, 1/4 w, 1%

Cr = Radio receptor IN 658 (Substituted for Texas Instruments IN 645)

T_1 = Texas Instruments 2N 498

T_2 = Texas Instruments 2N 389

TR = Pulse engineering strattan 10 mh; Type EF 71-2250

OPERATING SPECIFICATIONS (Ideal):

Input: 10 microseconds, 3-5 volt pulse
pulse repetition frequency: 1000 pps

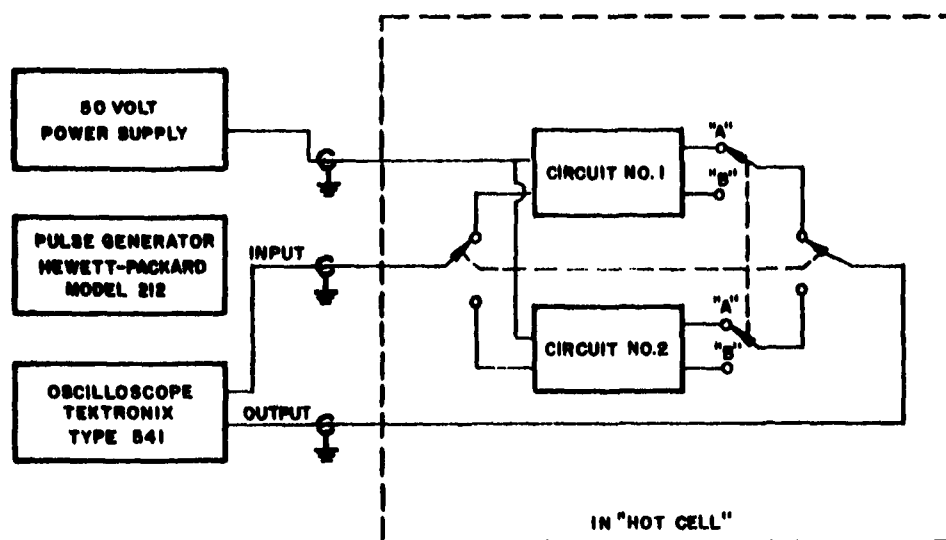
Output:

Monitor 'A' ; 10 microseconds, 10 volt pulse

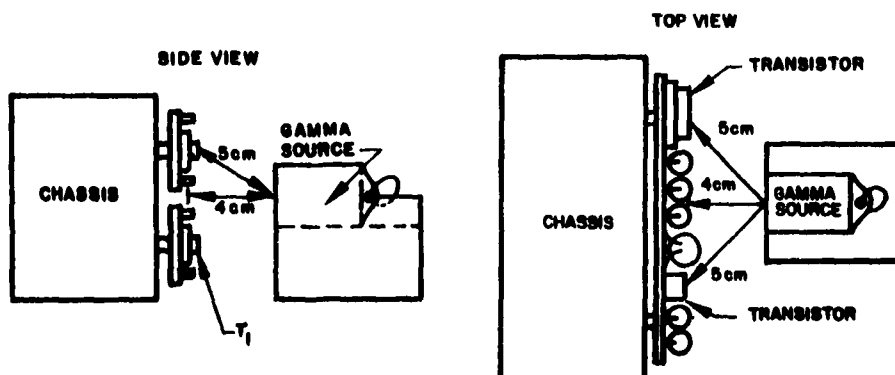
Monitor 'B' ; 10 microseconds, 15 volt pulse

Both stages are non-conducting until blocking oscillator is triggered.

FIG. 3.1 Magnetic Core Driver Schematic Diagram and Specifications



(a) Set-up for Remote Control Test of Several Limited Circuits as Used for Multivibrator Evaluation

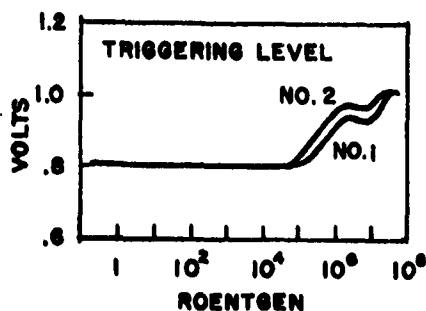


(b) Relative Position of Irradiation Source and Components irradiated

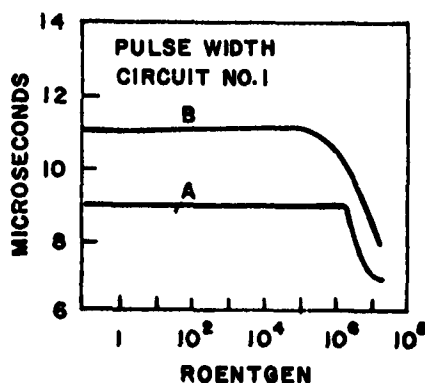
Fig. 3-2 Experimental Set-up for Memory Core Driver Test

CIRCUIT PARAMETERS vs DOSAGE

PROBABLE CAUSES



Increase in triggering levels is caused by a decrease in beta. This is caused by a reduction of the minority carrier lifetime which is the result of an increase in the number of recombination centers in the base region. Increase in triggering level is necessary to compensate for decrease in the gain of the amplifier section of the blocking oscillator. The "dip" in the triggering level is not understood.



Output "A":

Decrease of pulse width is caused by a decrease in the back resistance of the diode allowing escape of charge from the base region of T_1 . Inductance increase in coil, increase in input capacitance in the transistor and changes in the resistance of R_2 are ruled out.

Output "B":

Storage time of T_2 is decreased due to increase of recombination centers in the base region which causes a decrease of the "pulse stretching" effect of the power amplifier.

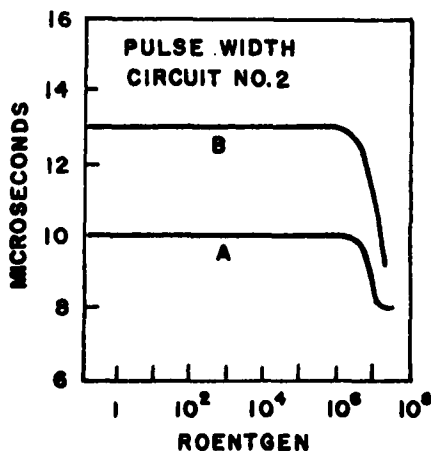
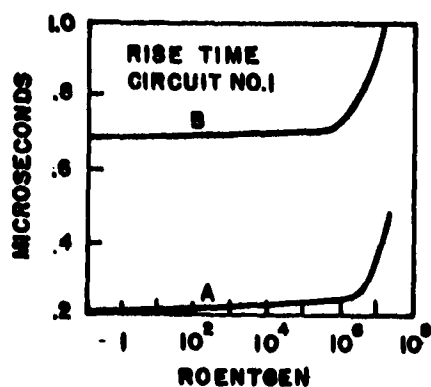


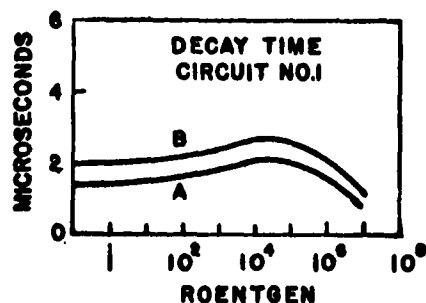
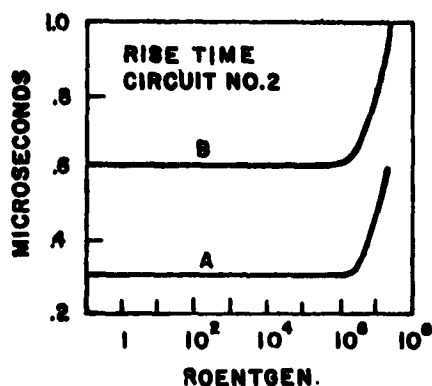
Fig. 3-3 Variation of Memory Core Driver Circuit Parameters

CIRCUIT PARAMETERS vs DOSAGE

PROBABLE CAUSES



Increase in rise time is due to an increase in the effective input capacitance of T_1 . Increase of recombination centers in the base region causes the effective input capacitance to increase since more time is required to saturate the base region with charge carriers. This effect is more prominent in T_2 than in T_1 due to the difference in base widths.

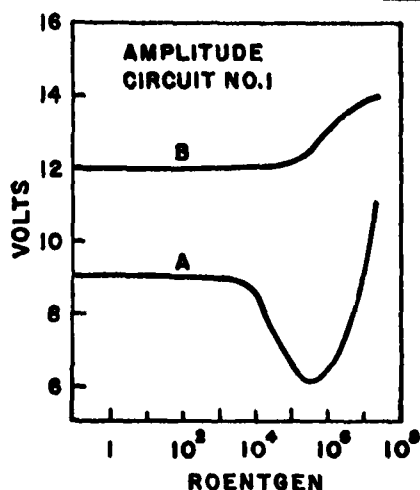
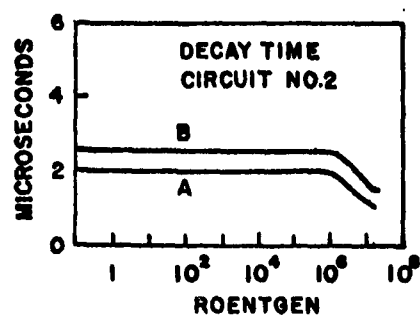


Decrease in decay time is due to an increase in recombination centers in the base region of T_1 . This change is reflected in the power amplifier. The initial increase in the decay time in circuit is followed by a decrease is not understood at this time.

Fig. 3-3 (cont) Variation of Memory Core Driver Circuit Parameters

CIRCUIT PARAMETERS vs DOSAGE

PROBABLE CAUSES



Output "A": Initial decrease in amplitude is due to an increase in I_{CO} indicating poor operating point stabilization. The increase in amplitude which follows is due to a decrease in the saturation resistance of T_1 . Decrease in saturation resistance is due to an increase in the number of recombination centers in the base region of T_1 , which reduces the minority carrier lifetime.

Output "B": Increase in amplitude is due to decrease in saturation resistance of T_2 . Operating point of T_2 is very well stabilized due to low resistance in the base circuit.

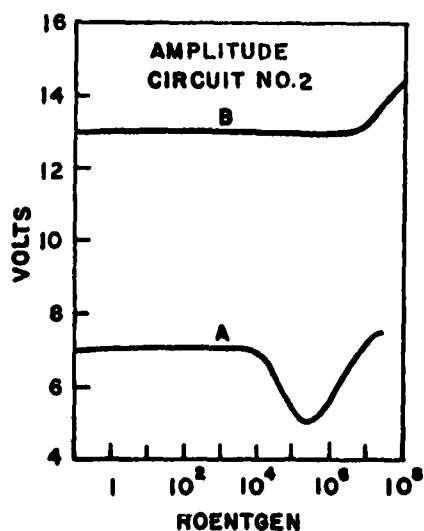
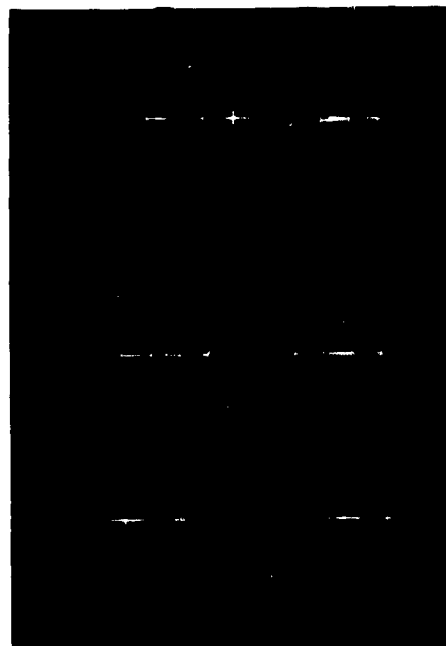


Fig. 3-3 (cont) Variation of Memory Core Driver Circuit Parameters



BEFORE IRRADIATION
 HORIZONTAL SCALES: ALL $5\mu\text{s}/\text{DIV.}$
 VERTICAL SCALES
 TOP: 2V/DIV
 MIDDLE: 5V/DIV
 BOTTOM: 5V/DIV



AFTER 1.2×10^7 ROENTGENS
 HORIZONTAL SCALES: $5\mu\text{s}/\text{DIV.}$
 VERTICAL SCALES: 5V/DIV.

Fig. 3.4 Memory Core Driver Waveforms

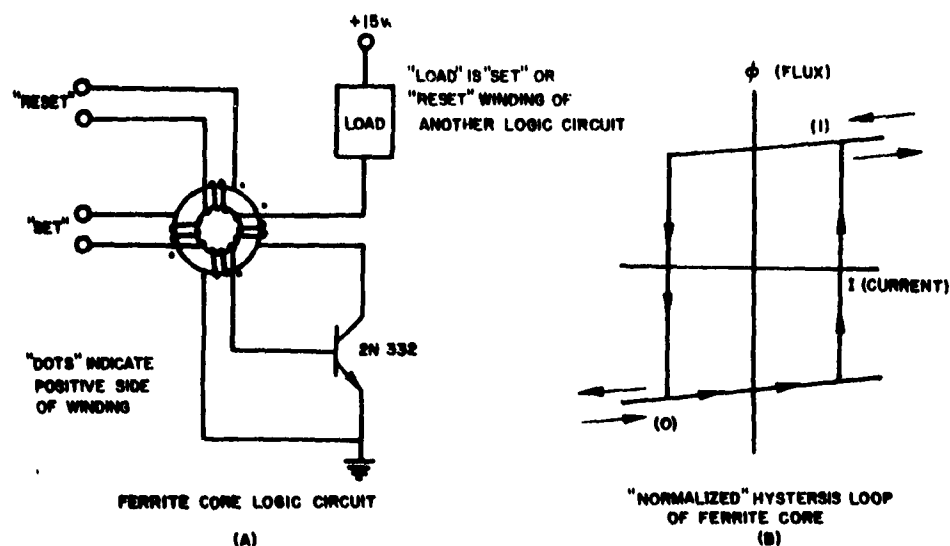


Fig. 3-5 Ferrite Core Logic Circuit

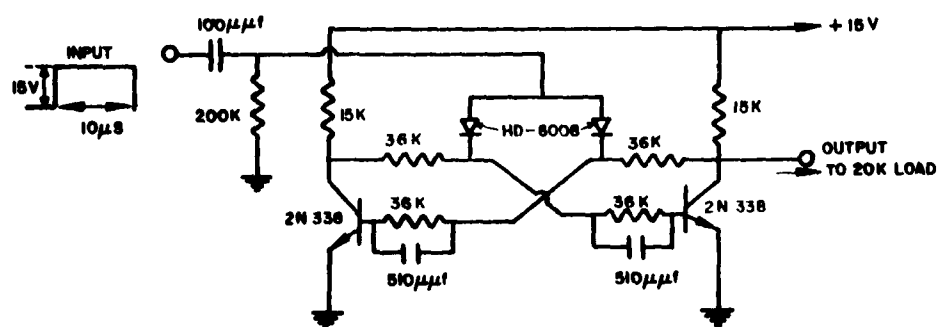


Fig. 3.6 Bistable Multivibrator (Flip-Flop)

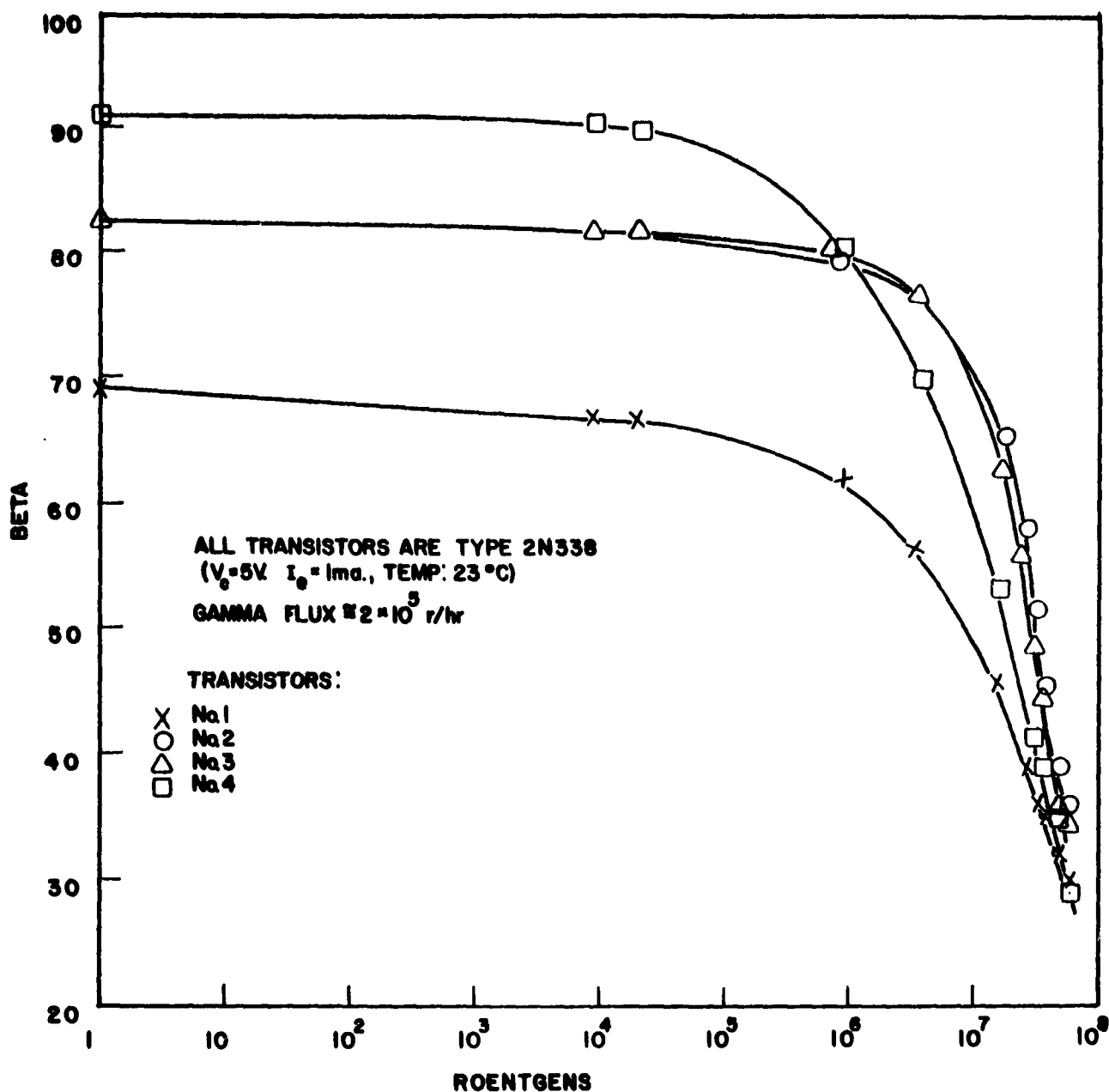


Fig. 3-7 Common Emitter Forward Current Ratio (Beta) vs Gamma Dose

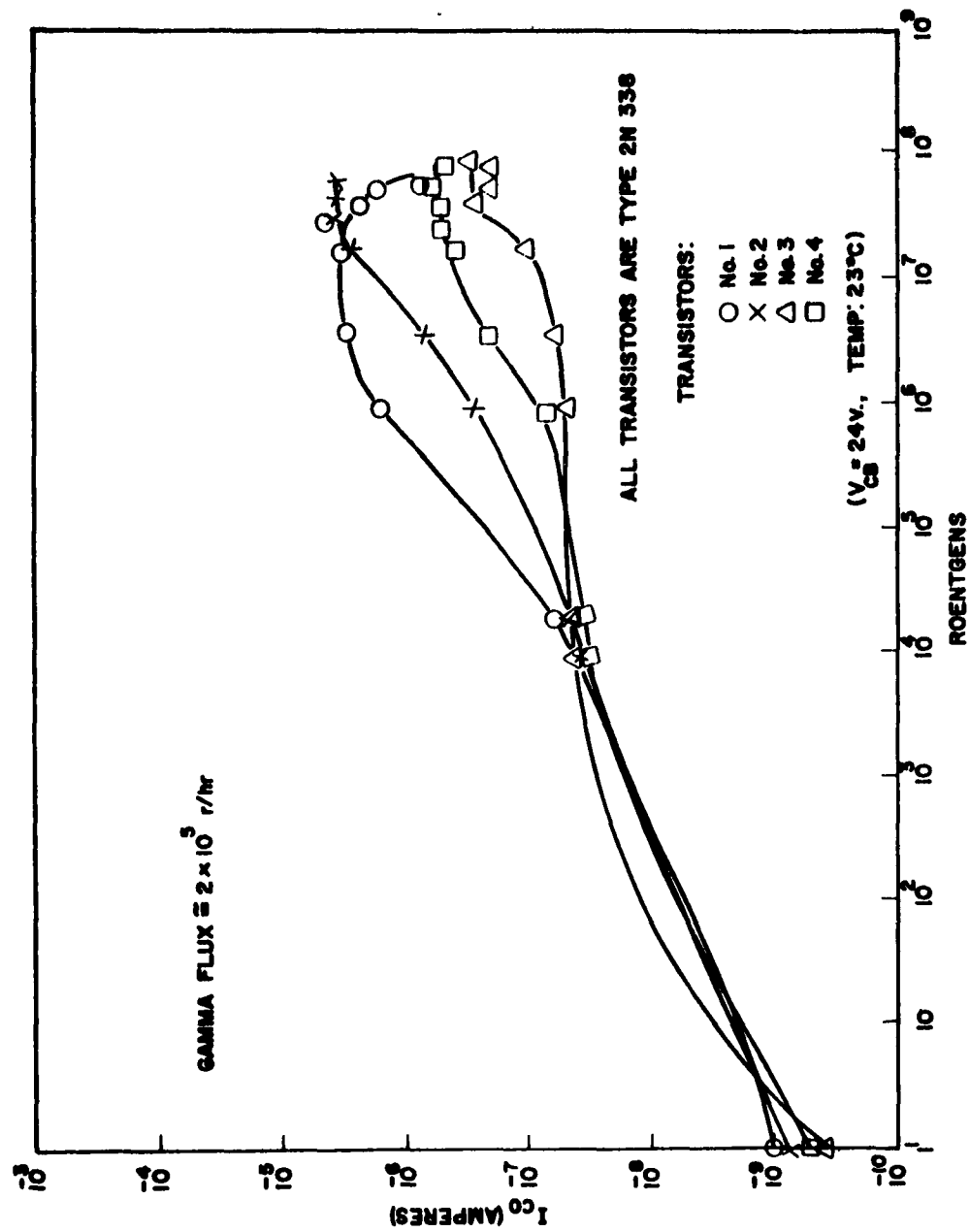


Fig. 3-8 Leakage Current (I_{CO}) vs Gamma Dose

SECTION 4.0

INTERPRETATION OF EXPERIMENTAL RESULTS

4.1 SEARCH FOR THE WEAKEST CIRCUIT COMPONENT

The operation of electronic circuits in the presence of radiation depends primarily upon:

- (a) The circuit components, in particular the one or two most sensitive components such as a transistor or a diode
- (b) the circuit design, which determines the effect of the most Sensitive components on circuit performance
- (c) The required stability of each circuit parameter, specified by the function of the circuit and the desired reliability of performance

In the circuits under consideration in Section 3, semiconductor devices were found to be the most sensitive components. If semiconductor devices can be improved in structure or if their performance can be improved by circuit design, other components will likely determine the effect of radiation damage on the circuit. In addition the circuit may be affected by radiation induced damage which is independent of circuit components. An example would be leakage currents produced by conducting surface layers. It is, therefore, advisable to examine the cause of failure and to locate the weakest circuit components.

4.2 RELIABILITY

The reliability of a circuit may be assessed by investigating experimentally the circuit parameters upon which the operation of the circuit depends. The permissible variation of each critical circuit parameter should then be defined by establishing limits of tolerance.

It is often desirable to specify permissible variations on those components which affect the critical circuit parameters. Conversely, if the variation of deterioration of the most sensitive components is known, this will provide criteria for the selection of these components to allow the designer to meet the required tolerances for each circuit parameter.

Parameters of manufactured devices often vary by a factor of two, due to production spreads. It is, therefore, desirable to specify each parameter by: (1) an average value and, (2) its deviation from this average. Thus circuit parameters as well as components must be treated as statistical variables, limiting the significance of any measurement on any individual unit.

A question then arises regarding size of a significant sample. In view of the inherent spread in device parameters, it appears reasonable to use a sample size as given in Table 4.1.

To illustrate the procedures used, assume that we wish to obtain an estimate of the deterioration of "beta" of a transistor. From data presented in Fig. 3.7, assume that the average is to be given by the 50 percentile within a factor of two, while the range need not be better known than by an order-of-magnitude estimate and should be specified by 1% failure as the lower limit and 1% survival as the upper limit. From Table 4.1 a sample size of about four is recommended for the accuracy specified.

From Fig. 3.7 one obtains the transistor performance as a function of dose for a sample of four units and, in particular, the dose at which the transistor must be derated by 10%, 20% or 50%. A corresponding probability plot based on a sample of four units is shown in Fig. 4.1 with "derating" as a running parameter. The median can be read off with a probable error which is well within a factor of two. The limit of failure and the limit of

survival, both taken at the one percentile level, must be obtained from Fig. 4.1 by extrapolation. The reliability of these extrapolated values is only indicative of the order-of-magnitude.

Derating curves are presented in Fig. 4.2 (here the median is shown more accurately than the upper and lower limits). The sample size selected to obtain Fig. 4.1 and Fig. 4.2 provides a satisfactory starting point for a design theory. To obtain curves useful for practical design of circuits, a sample of double or four times this size is probably desirable.

4.3 DESIGN THEORY FOR CIRCUIT STABILIZATION

Considerable progress has been made on a design theory to stabilize the gain of an amplifier stage of transistor circuits by active feedback. Since this work will form the subject of a separate report, it will only be briefly mentioned here.

The simultaneous deterioration of similar transistors due to radiation damage is employed to stabilize circuit characteristics by using one transistor as a feedback element. The relative merit of a number of circuit configurations are examined on the basis of overall current and voltage amplification, battery requirements, transistor symmetry, and similar factors. The requirement of both stabilization and amplification are simultaneously satisfied for the common-emitter configuration which uses a transistor in the common-collector configuration as a feedback element. Design curves for this configuration are devised for typical cases to illustrate the usefulness of this method of stabilization.

It is planned to verify experimentally this method of radiation stabilization by designing and testing a number of circuits with active feedback.

We have examined to a lesser extent other aspects of a design theory for stabilization against radiation damage. These include:

- (a) Operating point stabilization
- (b) Simultaneous temperature and radiation stabilization
- (c) Reliability of circuit performance under radiation
- (d) Sensitivity of circuit parameters to radiation damage
- (e) Design of circuits to operate in the presence of radiation

TABLE 4.1

APPROXIMATE SAMPLE SIZE NECESSARY TO OBTAIN, (1) THE AVERAGE AND
(2) THE DEVIATION WITHIN A
DESIRED ACCURACY

Accuracy Desired	(1) Average	(2) Deviation or Range
Accuracy of estimate not ascertainable	1	2
Estimate within an order of magnitude	2	4
Estimate within a factor of two	4	8
Estimate within about 50%	8	16
Estimate within about 20%	16	32
Estimate within about 1/N	$(N + 1)^2$	$2 (N + 1)^2$

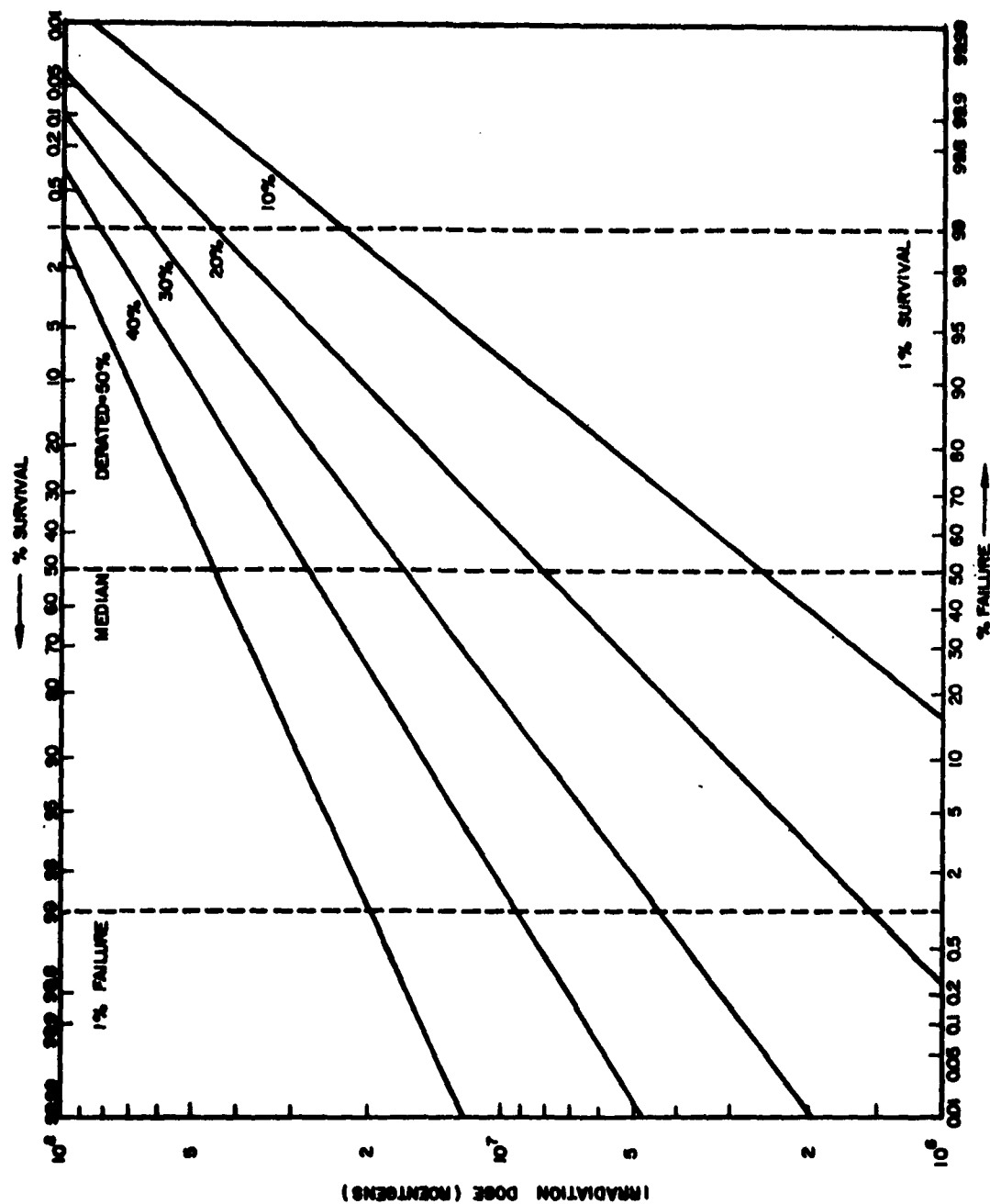


Fig. 4.1 Failure Analysis for Derated h_{fe} of 2N 338 Transistor ($N = 4$)

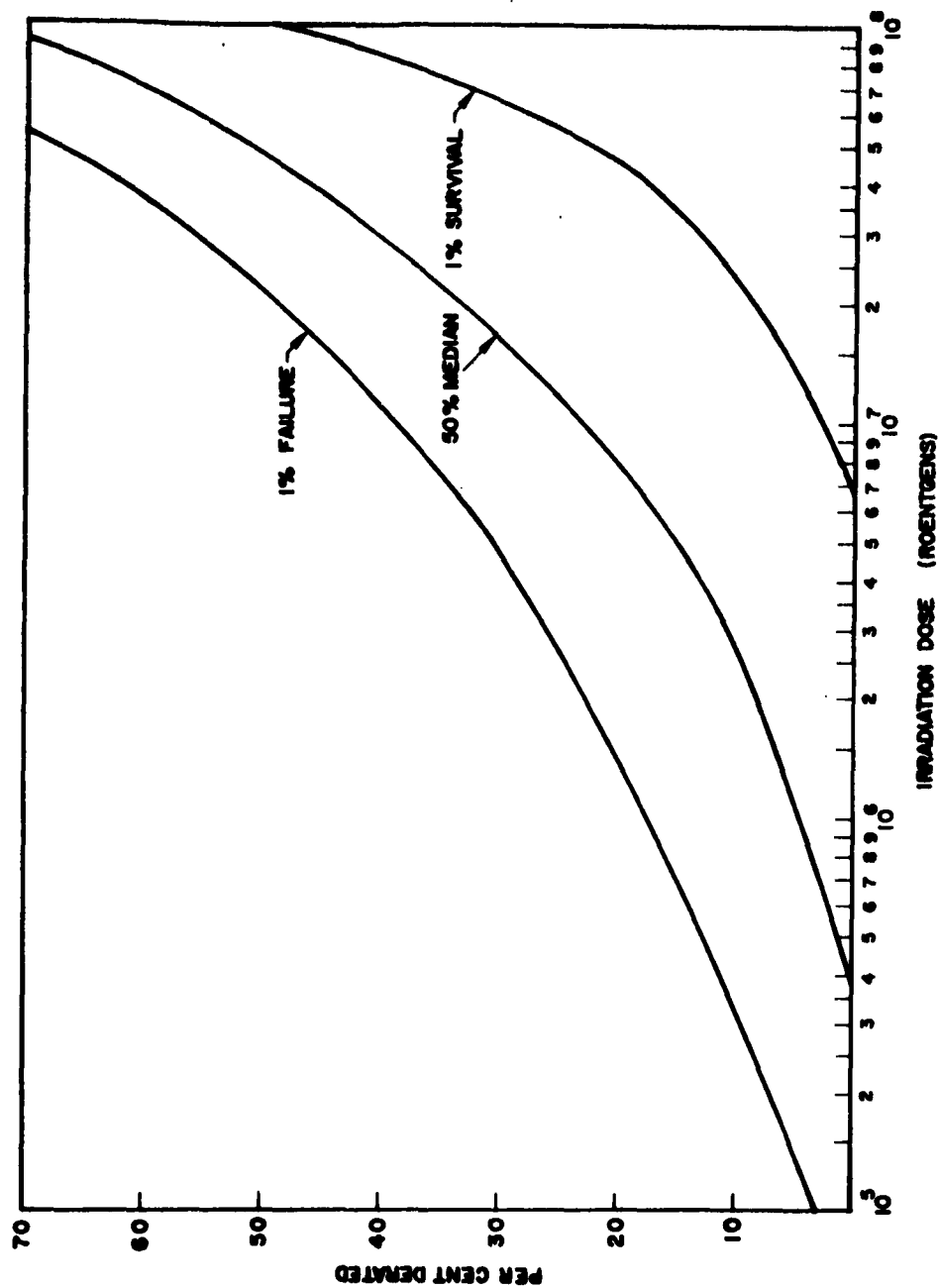


Fig. 4.2 Failure Analysis of Derated h_{fe} of 2N 338 Transistors ($N = 4$)

APPENDIX **CONVERSION FACTORS FOR THE DOSIMETRY COMPUTATIONS**

Flux = (particals/volume) x (velocity)

in the cgs system:

Flux = photons/cm²/sec for gamma or x-rays

= neutrons/cm²/sec or nv for neutrons

1 roentgen/hr = 5 x 10⁵ photons/cm²/sec

for 1 Mev gamma photons

Dose = (particals/volume) x (velocity x (time)

= Flux x Time

in the cgs system:

Dose = photons/cm² for gamma or x-rays

= neutrons/cm² or nvt for neutrons

1 roentgen = amount of gamma or x-ray radiation which will produce 1 esu of charge as ions per cubic centimeter of air under standard conditions

For Cobalt-60:

Energies of gamma photons = 1.17 and 1.33 Mev

1 roentgen = 1.6 x 10⁹ photons/cm²

1 r/hr = 4.44 x 10⁵ photons/cm²/sec

Flux (r/hr) = 6.63 x 10³ N_c/r²

Where

N_c = strength of Co⁶⁰ source in curies

r = distance from source

1 curie = 3.7 x 10¹⁰ disintegration/sec.

BIBLIOGRAPHY

- 1955 S. S. Guterman and W. M. Carey, Jr., "A Transistor-Magnetic Core Circuit A New Device Applied to Computing Techniques". IRE Convention Record, Vol. III, part 4, p. 84.
- 1956 J. C. Pigg and C. C. Robinson, "Radiation Effects in Semiconductor Devices". Proc. Transistor, p. 77, New York University Press.
- 1956 H. L. Steele, Jr., "Effects of Gamma Radiation on Transistor Parameters", Proc. Transistor Reliability Symposium, p. 96, New York University Press.
- 1957 G. C. Messenger and J. P. Spratt, "The Effects of Neutron Irradiation on Germanium and Silicon", Philco Report No. 276, Philco Research Division.
- 1957 Reid, Moody and Willardson, "The Effects of Nuclear Radiations on Semi-conductor Materials", Report from the Radiation Effects Information Center, Battelle Memorial Institute.
- 1957 J. H. Martens and F. G. Minuth, "Selected List of Neutron and Gamma Irradiation Facilities in Operation; Being Built, or Planned". Technical Information Service, USAEC. Available from Supt. of Documents, USGPO, Washington 25, D. C., (price 60 cents).
- 1958 J. K. Imai, "Preliminary Study of Radiation Damage to Silicon Transistors", LMSD Report No. 2376.
- 1958 W. V. Behrens and J. M. Shaul, "The Effects of Short Duration Neutron Radiation on Semiconductor Devices", Proc. IRE 46, 3, 601.

ACKNOWLEDGEMENT

The authors of this report wish to express their appreciation to Mr. K.R. Morsette, who assisted in the experimental measurements and, also, for his many other valuable suggestions.

Mrs. Ruth Kaluza's clerical assistance in preparing the report as well as compiling the data is also gratefully acknowledged.

LMSD-5031
29 August 1958

RADIATION STABILIZATION OF
TRANSISTOR CIRCUITS BY ACTIVE FEEDBACK

by

S. R. Hawkins and W. W. Happ

Lockheed Aircraft Corporation
Missile Systems Division
Sunnyvale, California

RADIATION STABILIZATION OF TRANSISTOR CIRCUITS BY ACTIVE FEEDBACK

by
S.R. Hawkins and W.W. Happ
Lockheed Missile Systems Division
Sunnyvale, California

The simultaneous deterioration of similar transistors due to radiation damage is employed to stabilize circuit characteristics by using one transistor as a feedback element. The relative merits of a number of circuit configurations are examined on the basis of over-all current and voltage amplification, battery requirements, transistor symmetry, and similar factors. The requirements of both stabilization and amplification are simultaneously satisfied for the common-emitter configuration using a transistor in the common-collector configuration as a feedback element. Design curves for this configuration are given for typical cases to illustrate the usefulness of this method of stabilization. Operating point stabilization is briefly discussed.

INTRODUCTION

1.1 Scope of Investigation

The forthcoming use of nuclear power sources in aircraft, rockets, and other vehicles is expected to create new and challenging problems in the use of electronic circuits. In particular, circuits employing semiconductor devices in strong nuclear radiation fields will involve problems likely to become critical.

This report presents the effects and a means of stabilizing transistor circuitry against nuclear radiation damage. The method presented here depends primarily upon the use of feedback stabilization with an active element. For this purpose a transistor is used in the feedback circuit. It is desirable, as will be shown, that the feedback transistor be identical to that used in the basic amplifier.

One of the most pronounced effects of nuclear radiation on transistors is the variation of "beta", the common-emitter forward current ratio (h_{fe}). The purpose of this method of stabilization is to minimize the effect of this variation.

Relationships giving the parameter variations of the compensated circuits in terms of the "beta" of the individual transistors are derived. From these relationships typical design curves are computed. The circuit performance with active feedback is compared to that of a similar circuit using passive feedback stabilization and to that of one using no feedback.

Some aspects of operating point stabilization are also discussed.

In the Appendix the relationships for compensated networks are derived using signal flow-graph analysis.

1.2 Radiation Effects on Circuitry

The following types of nuclear radiations are primarily responsible for variations in circuit parameters which lead in some cases to failure:

1. Gamma radiation
2. Thermal or "slow" neutron radiation
3. Epicadmium or "fast" neutron radiation.

These are the types of radiations which are found in various proportions in the vicinity of a nuclear reactor depending upon the amount and type of shielding which is present.

A comprehensive account of radiation effects in solids is given by Dienes and Vineyard (1957). Radiation effects on electronic components are being continually summarized and abstracted by the Radiation Effects Information Center of the Battelle Memorial Institute.

The effects of nuclear irradiations on transistors have been investigated by Pigg and Robinson (1956), Steele (1956), Messenger and Spratt (1958), and others. From the above investigations the following facts of particular interest to this investigation can be stated:

1. In most circuits the semiconductor devices are most vulnerable to nuclear irradiation.
2. Damage or impairment of circuit operation may be of two types:
 - a. Permanent damage caused by disruption of atomic structure which is cumulative with time.
 - b. Temporary damage, such as ionization, which permits the circuit to return to normal operation a short time after the radiation source is removed.
3. The extent of damage incurred is dependent upon the energy of the particles, the type of radiation, and the accumulated dose.
4. While the extent of damage depends upon a large number of factors, an estimate of the relative ionization allows a comparison of the temporary damage caused by the three types of nuclear radiations. According to Pigg and Robinson (1956) fast neutrons remove approximately 2300 times as many electrons

as gamma rays and approximately 14 times as many electrons as slow neutrons. Hence the ratio of fast neutrons, to gamma photons, to slow neutrons, necessary for each to produce the same temporary damage, is 1:14:2300.

5. Damage due to gamma irradiation is mostly temporary.
6. Damage due to neutron irradiation is mostly permanent.

1.3 Radiation Effects on Transistor Parameters

The transistor parameters which appear to be most sensitive to nuclear irradiation are beta, the common-emitter forward current ratio (h_{fe}), and the collector to base leakage current (I_{CO}). Nuclear irradiation also causes reduction of the breakdown and "punch-through" voltages of a transistor. Variations that occur in other parameters are usually quite small and can, in most cases, be neglected.

The collector to base leakage current I_{CO} usually rises very quickly to a saturation level which is dependent upon the rate of irradiation. This effect can be attributed to initial surface ionizing effects. I_{CO} then continues to increase at a rate which is a function of the accumulated dose, until the bulk ionization rate equals recovery rate of the transistor. Experimental curves of I_{CO} vs gamma dose for one type of silicon transistor and two types of germanium transistors are shown in Fig. 1.1. These curves agree fairly well both theoretically and experimentally with Pigg and Robinson (1956) and Steele (1956).

At this time it has become fairly well established that beta decreases monotonically with neutron dose for silicon transistors. However, in many cases, beta of germanium transistors increases initially and then decreases monotonically with radiation dose. Experimental curves illustrating variations of beta with gamma dose for the above mentioned silicon and germanium transistors are shown in Fig. 1.2.

According to Messenger and Spratt (1957), n-type germanium is least sensitive to radiation damage followed by p-type germanium, n-type silicon, and p-type silicon, in that order. This is based upon a "damage constant" given for these materials which gives a measure of their sensitivity to neutron irradiations. Since the base is considered to be the most critical region of the transistor, one can conclude that within a given frequency or power classification, pnp-germanium transistors should be least sensitive to nuclear irradiation followed by npn-germanium, pnp-silicon, and npn-silicon transistors in that order. Other factors such as size and geometry of the device, thickness of the base region, and manufacturing process, must be taken into consideration when choosing a particular type of transistor for use in a nuclear environment.

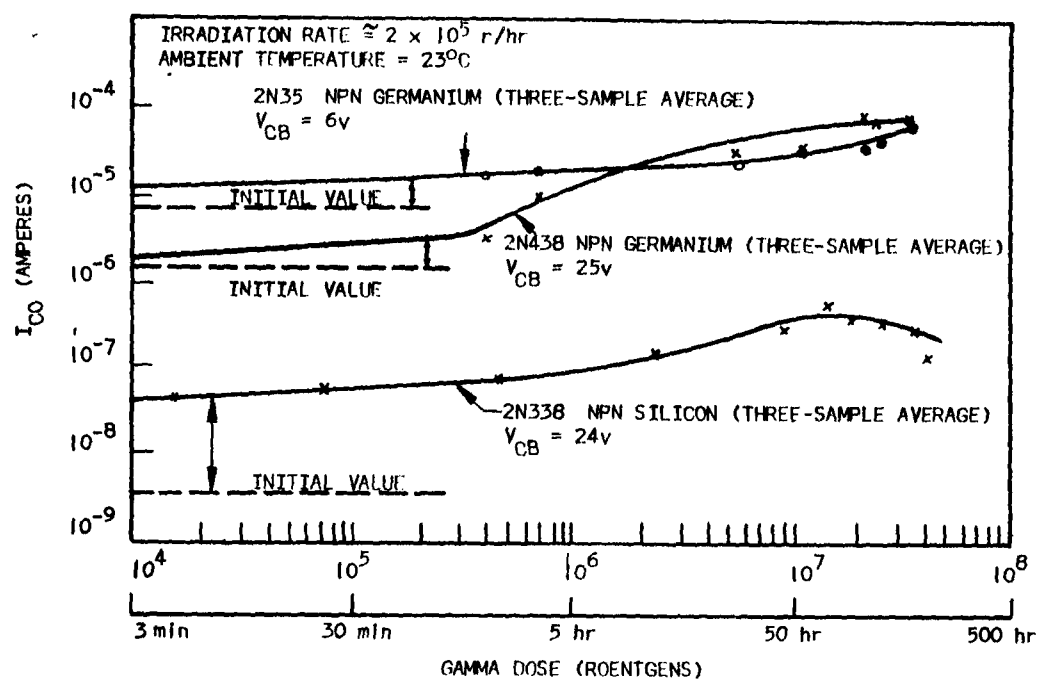


Fig. 1.1 Leakage Current (I_{CO}) vs Gamma Dose

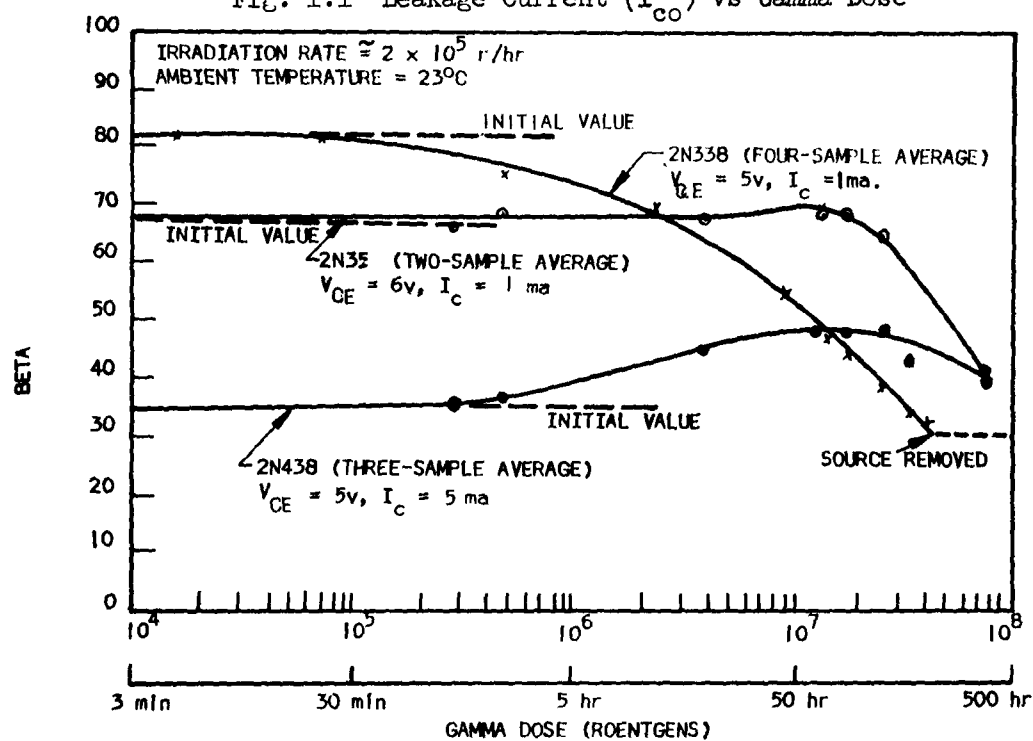


Fig. 1.2 Forward Current Ratio (Beta) vs Gamma Dose

1.4 Techniques for Circuit Stabilization

There are many techniques which can be employed to stabilize transistor circuit performance against changes in beta. Many of the techniques now employed for temperature stabilization, for example, can be directly applied to radiation stabilization. Other methods for radiation stabilization will no doubt be discovered when radiation problems become more acute. Some of the stabilization methods which seem to show promise are:

1. Techniques such as the use of base current feedback, as described by Boxall (1957), which make the over-all circuit performance independent of the parameter changes of a sensitive element.
2. Compound transistor arrangements such as those given by Darlington* and Boxall (1957).
3. Feedback stabilization methods such as those described by Lo (1955), Hunter (1956), Ghandi (1953), and Guggenbuhl and Schneider (1956).
4. Active feedback stabilization techniques such as suggested in this paper where the deterioration of a device in the feedback network compensates for deterioration in the amplifying device.

It is noteworthy that most temperature stabilization techniques are directed toward improving the stability of the operating point of the transistor rather than its gain. This is understandable since beta has a tendency to increase with temperature rather than decrease and thus there will always tend to be gain in the device, provided the operating point is stabilized. However, continued use of a transistor in a radiation environment will ultimately result in complete deterioration of beta, and it would seem therefore that more emphasis will probably be placed upon this type of stabilization.

1.5 Operating Point Stabilization

It can be seen from Fig. 1.1 that the behavior of I_{CO} in radiation environments is similar in many respects to that encountered in temperature environments. For this reason, techniques for stabilization of the operating point against temperature changes such as those given by Shea (1957) and Lo (1955) can also be used for stabilizing against radiation. Methods which take advantage of the increase of the leakage currents in a semiconductor diode should be particularly suitable.

Since thermistors are not particularly sensitive to radiation damage, the use of these devices in combined temperature and nuclear environments offers the possibility of stabilizing circuits against changes of I_{CO} due to temperature, independently of those changes due to nuclear radiation.

* Patent No. 2,663,806 assigned to Bell Labs.

2. FEEDBACK STABILIZATION

2.1 Advantages of Active Feedback Stabilization

Although most passive feedback stabilization techniques are simple to realize in practice as well as easy to analyze theoretically, they present a serious disadvantage when used for stabilization against large changes in beta such as are encountered in strong radiation fields. Namely, while the gain of the circuit is being drastically affected, the feedback ratio does not change appreciably when the feedback circuit is purely resistive. Figure 1.2 shows that if identical transistors are used in both the feedback circuit and the basic amplifier the feedback ratio should change at a rate identical to that of the uncompensated amplifier. Thus the circuit designer can be reasonably assured that, despite production spreads, the simultaneous deterioration of identical transistors due to radiation damage should produce the desired stabilizing effect. It is possible to stabilize effectively transistor circuits against changes in beta by using a suitably matched transistor as a feedback element. If non-identical transistors are used the circuit designer must give careful consideration to the choice of transistors to be assured that the feedback will change in the desired manner.

2.2 Active Feedback Stabilizing Circuits

An example of an amplifier with active feedback is illustrated in Fig. 2.1. The purpose of the resistance R_F in series with the active feedback element is to regulate the negative feedback and hence to determine the degree of stabilization.

In the analysis which follows, the active elements (transistors in this case) and the over-all stabilized amplifier stage are described by hybrid parameters as follows:

h - parameters for the basic or uncompensated element.

h' - parameters for the feedback element.

H - parameters for the compensated or combined network.

A derivation of these and all subsequent formulas is given in the Appendix, using signal flow-graphs; derivations by other methods are more lengthy.

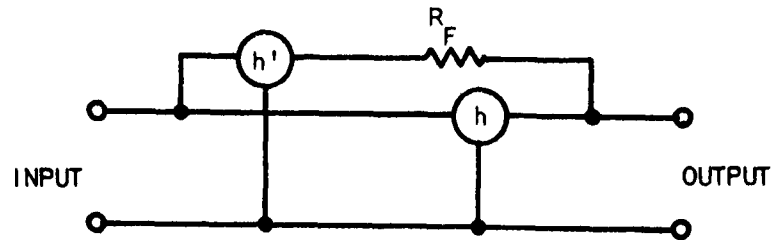


Fig. 2.1 Amplifier with Single-loop Active Feedback

The hybrid parameters for the circuit of Fig. 2.1 are:

- (1) $H_i = h_i (R_F + h_i') / D$
- (2) $H_r = (R_F h_r + h_i' - h_i h_f) / D$
- (3) $H_f = (R_F h_f + h_i' - h_i h_r) / D$
- (4) $H_o = h_o + (1/D) (1 + h_i h_o - h_r h_r' - h_f h_f' - R_F h_r h_o' h_f + h_r h_o' h_f h_i)$
 where $D = R_F (1 + h_i h_o') - h_i h_r' h_f + h_i h_r' h_f + h_i (1 + h_i h_o)$.

This treatment is somewhat similar to that of Ghandi (1957) on the Darlington Compound Connection for Transistors.

3. APPLICATION TO A TRANSISTOR AMPLIFIER

3.1 Possible Configurations

If transistors are used in the basic active feedback amplifier shown in Fig. 2.1, it is seen that there are nine possible standard configurations. This is because each transistor has three standard configurations, i.e., common-base, common-emitter, common-collector. There are many more non-standard or "hybrid" configurations which could be used if one or both of the transistors are used in a non-standard configurations (e.g., common-base with the collector input). The nine degenerative configurations and a few of the more important characteristics of each are presented in Table 3.1. Only the dynamic characteristics are considered here. Biasing considerations are discussed in Section 3.5.

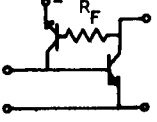

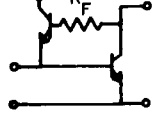
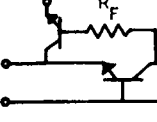
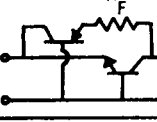

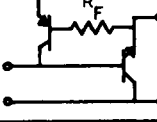
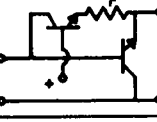

3.2 The Common-emitter Configuration with Common-collector Feedback

Referring to Table 3.1, it can be seen that for most applications the common-emitter configuration with the feedback transistor used as common-collector (hereafter referred to as common-emitter, common-collector) offers certain advantages over the other over-all configurations. This configuration offers both voltage and current amplification with a high degree of stabilization against changes in beta which none of the others can offer. The reason for this can be seen from the following considerations:

1. The common-emitter configuration in the basic uncompensated amplifier is the only one that offers simultaneous current and voltage amplification.
2. Only when the feedback transistor is used as common-collector is the voltage feedback ratio less than unity for any value of R_F . Thus voltage amplification is always possible with this over-all configuration.

This configuration is also one in which identical transistors can be used with a single power supply. It is unlikely that a complementary pair of pnp and npn transistors could be found which exhibit similar degradation of beta under radiation (see Section 1.3). Though such combinations might seem to offer useful properties in the convenience of biasing, the over-all ac parameters could not be held to any calculable limits.

TABLE 3-1.
STANDARD OVERALL CONFIGURATIONS AND THEIR CHARACTERISTICS

CONFIGURATION		Schematic Diagram	PREDICTED CHARACTERISTICS				Remarks
Amplifier	Feedback		Voltage Amplification	Current Amplification	Input Impedance	Output Impedance	
Common Emitter	Common Emitter		Poor	Good	High	Medium to Low	Not recommended due to difficult biasing requirements. Improper phase relationships for complimentary transistors.
	Common Base		Poor	Fair	High	Medium to Low	Use of identical transistors requires complicated biasing arrangement.
	Common Collector		Fair	Fair	Medium	Medium	Recommended for radiation stabilization. Chosen for demonstration of method in text.
Common Base	Common Emitter		Poor	Very Poor	Low	Medium	Requires two batteries
	Common Base		Poor	Poor	Low	Medium	Improper phase relationships for identical transistors.
	Common Collector		Good	Very Poor	Low	Medium	Not recommended due to complicated bias requirements. Improper phase relationships with complimentary transistors.
Common Collector	Common Emitter		Poor	Fair to Poor	High	Medium	Use of identical transistors gives improper phase relationships.
	Common		Poor	Fair	High	Medium to Low	May be difficult to get correct bias on feedback transistor. Improper phase relationships with complimentary transistors.
	Common Collector		Poor	Fair to Poor	High	Medium	Not recommended due to difficult bias requirements. Improper phase relationships for identical transistors.

3.3 Computation of Typical Design Curves for Active Feedback Stabilization

The H-parameters for the common-emitter, common-collector configuration can be calculated as follows, using equations (1) to (4) (and Table 3.2).

$$(5) \quad H_i = h_{ie} (R_F + h_{ic}) / D$$

$$(6) \quad H_r = (R_F h_{re} + h_{ic} - \beta h_{ie}) / D$$

$$(7) \quad H_f = (\beta R_F + h_{ic} - h_{ie} h_{rc}) / D$$

$$(8) \quad H_o = h_{oc} + (1/D) \left[1 + h_{ie} h_{oe} - h_{re} h_{rc} - \beta (\beta + 1) - h_{re} h_{oc} \beta (R_F + h_{ie}) \right]$$

where

$$D = R_F (1 + h_{ie} h_{oc}) - h_{ie} h_{rc} \beta - h_{ic} (1 + h_{ie} h_{oc})$$

and

$$h_{fe} = \beta$$

$$h_{fc} = \beta + 1$$

TABLE 3.2*
CONFIGURATION

PARAMETER	COMMON BASE	COMMON EMITTER	COMMON COLLECTOR
h_i	40 ohms	200 ohms	2000 ohms
h_r	4×10^{-4}	16×10^{-4}	1
h_f	$-\frac{\beta}{\beta + 1}$	β	$-(\beta + 1)$
h_o	1×10^{-6} mho	50×10^{-6} mho	50×10^{-6} mho

* Source: Shea (1957)

Figures 3.1, 3.2, 3.3, and 3.4 show typical variations of the over-all H-parameters with different values of the beta of the identical transistors. The numerical values of Table 3.2 were used for the parameters of the identical transistors in the computation of these curves.

The expressions for the current and voltage gains of the active feedback compensated amplifier are derived in the Appendix. These derivations assume an ideal signal generator and the effects of the source impedance are neglected. The voltage gain of the compensated amplifier is

$$(9) \quad A_{vH} = H_f R_L / H_i + R_L (H_i H_o - H_r H_f)$$

and the current gain is

$$(10) \quad A_{iH} = H_f / (1 + H_o R_L)$$

where R_L is the load resistance.

The power gain is thus,

$$(11) \quad P_H = A_{vH} A_{iH}$$

Typical curves for A_{iH} , A_{vH} , and P_H as functions of beta are shown in Figs. 3.5, 3.6, and 3.7 for load resistances of 120 Ω , 1K Ω , and 10K Ω , and $R_F = 100K \Omega$.

3.4 Comparison of Active and Passive Techniques

It is of interest to compare the active feedback amplifier with a similar amplifier using only passive feedback. A much-used amplifier of this type is obtained by removing the active element from the feedback network shown in the circuit of Fig. 2.1, leaving only a resistance between the input and output.

The hybrid parameters for an amplifier with a resistance R_F' between the input and output are:

$$(12) \quad H_i' = h_i R_F' / Z$$

$$(13) \quad H_r' = (R_F' h_r + h_i) / Z$$

$$(14) \quad H_f' = (R_F' h_f - h_i) / Z$$

$$(15) \quad H_o' = h_o + (1 - h_r) / Z$$

where

$$Z = R_F' + h_i$$

Since H_f' is the only parameter dependent upon the forward transfer current ratio (h_f), this quantity is plotted in Fig. 3.3 for the common-emitter configuration for various values of R_F' . The values of R_F' were chosen such that $H_f' = H_f$ when $\beta = 50$. The transistor parameters given in Table 3.2 were used

in the calculations. It is seen from Fig. 3.3, that to obtain the same degree of stabilization achieved by the use of active feedback, values of R_F' must be chosen which would render the amplifier useless.* This is due to the excessive amount of collector voltage fed back to the base. This trouble is not encountered with active feedback, due to the large values of R_F' that can be used and the small voltage amplification of the common collector feedback transistor.

From the foregoing statements and Figs. 3.1 to 3.7, the following observations are made:

1. For active feedback stabilization, all of the H-parameters are functions of beta, while with passive feedback stabilization, only H_F' is a function of beta.
2. The short-circuit input impedance is decreased by active feedback but increases as beta decreases.
3. The open-circuit feedback ratio is greatly increased when active feedback is used. However, H_r decreases while beta decreases.
4. Active feedback with identical transistors results in a greater stabilization of the current amplification factor.
5. The open circuit output admittance is increased by active feedback. However, H_o decreases as beta decreases.
6. From Fig. 3.5, it can be seen that for small load resistances active feedback provides very little voltage gain stabilization. However, as the load resistance R_L is increased, the voltage gain becomes more stabilized with very little sacrifice in gain. To realize the same degree of stabilization with the passive technique we have used would require the sacrifice of essentially all of the original voltage gain.
7. Fig. 3.6 shows that the amplifier current gain can be made very stable against changes in beta if a corresponding sacrifice in current gain can be tolerated. It can be seen that for certain values of R_F the current gain will actually be made to increase while beta decreases. One can see from equation 10 and Fig. 3.4 that this is a result of the behavior of H_o . This effect cannot be obtained with the passive technique we have used since H_o' is not a function of beta.
8. It can be seen from Fig. 3.7 that the power gain of a transistor amplifier can be made highly stable against changes in beta by the use of active feedback. However, considerable power gain must be sacrificed in order to obtain this high degree of stabilization.

*Application of passive feedback, by means of an un-bypassed emitter resistor, requires large resistances which also render the amplifier useless.

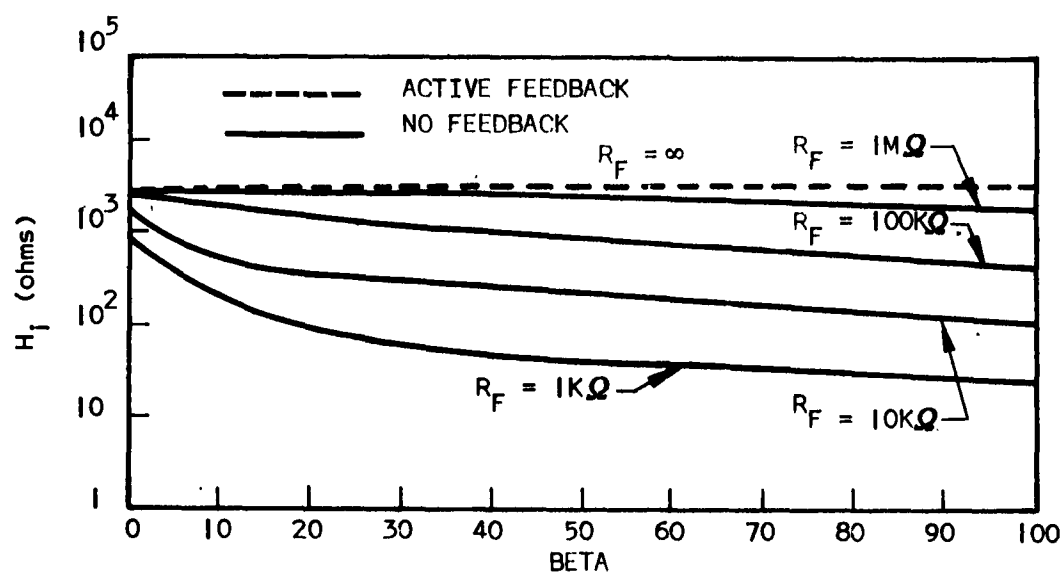


Fig. 3.1 Short Circuit Input Impedance vs Beta

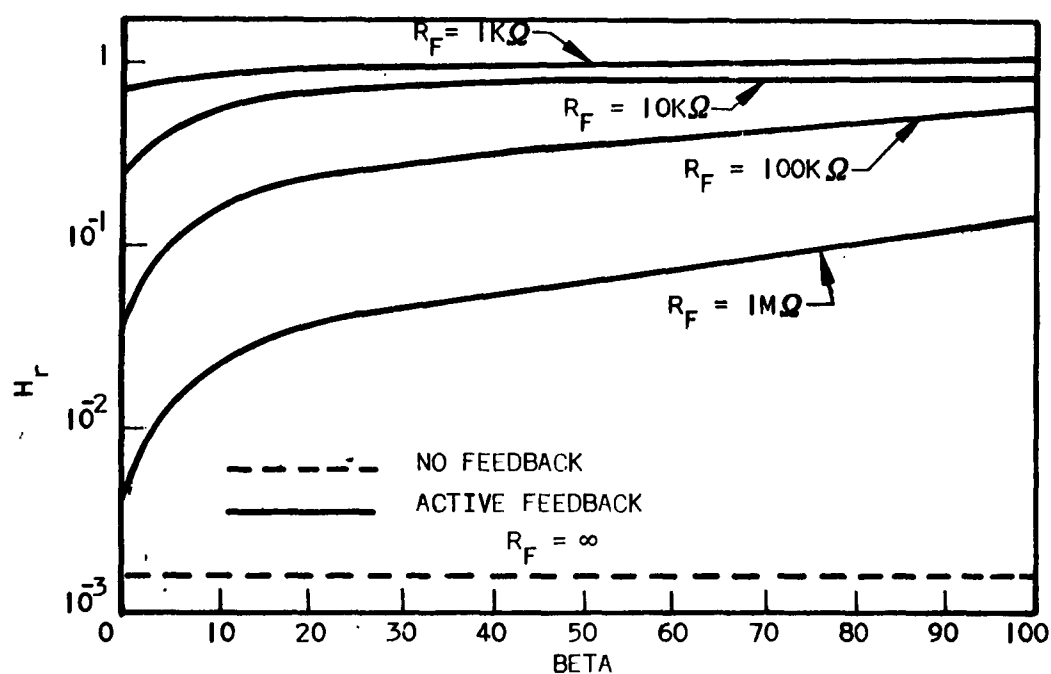


Fig. 3.2 Open Circuit Feedback Ratio vs Beta

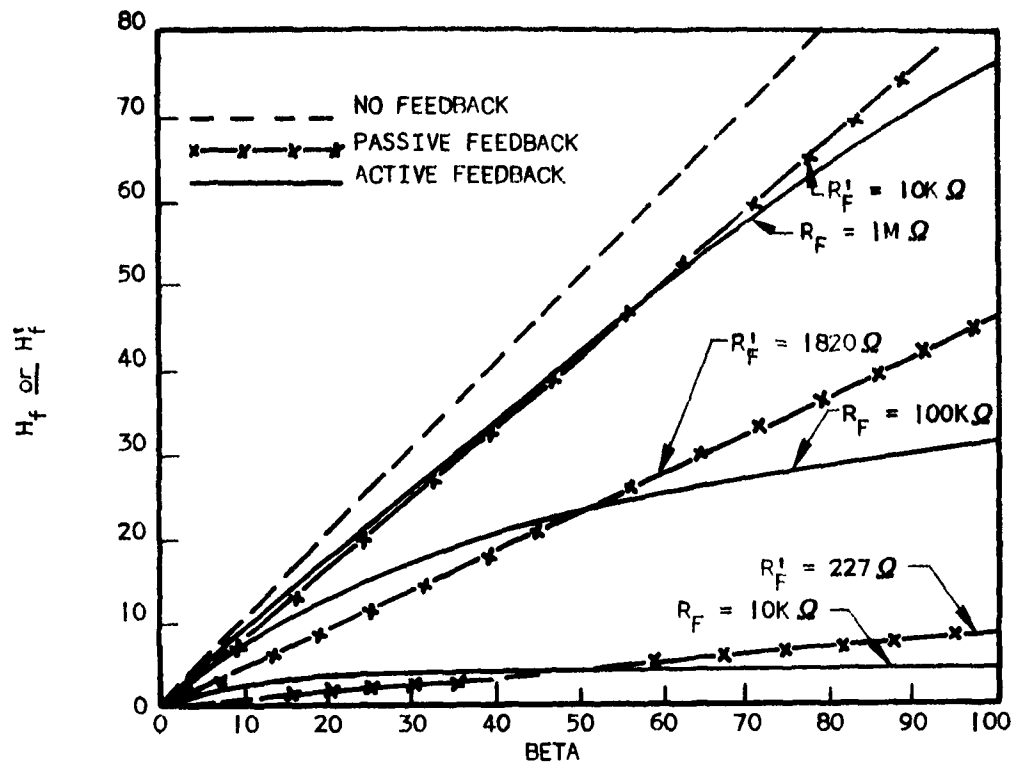


Fig. 3.3 Overall Current Amplification Factor vs Beta

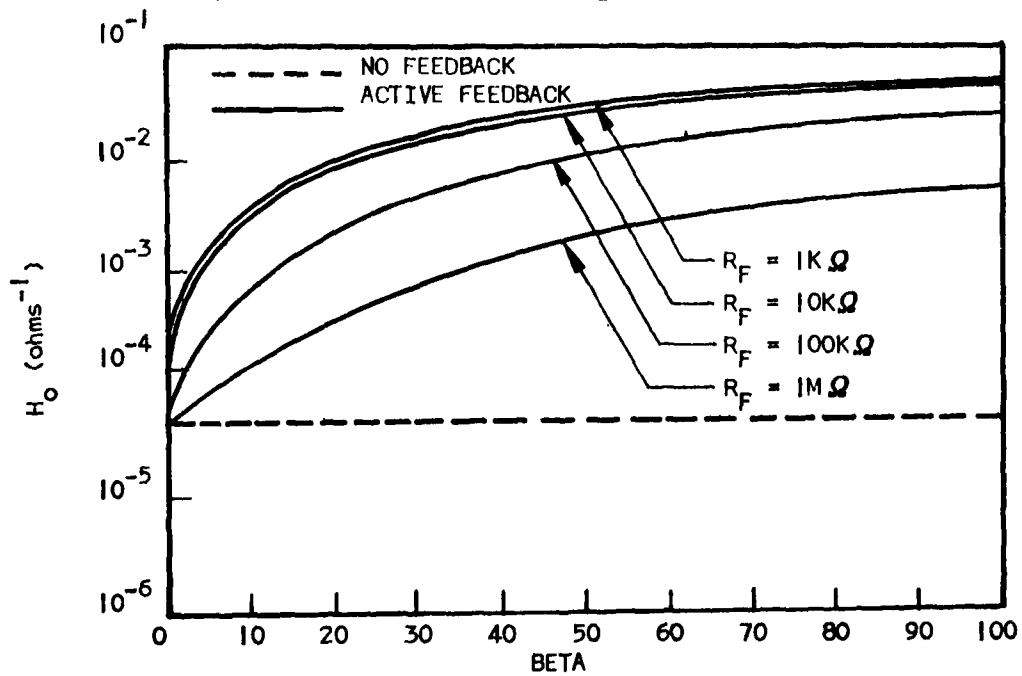


Fig. 3.4 Open Circuit Output Admittance vs Beta

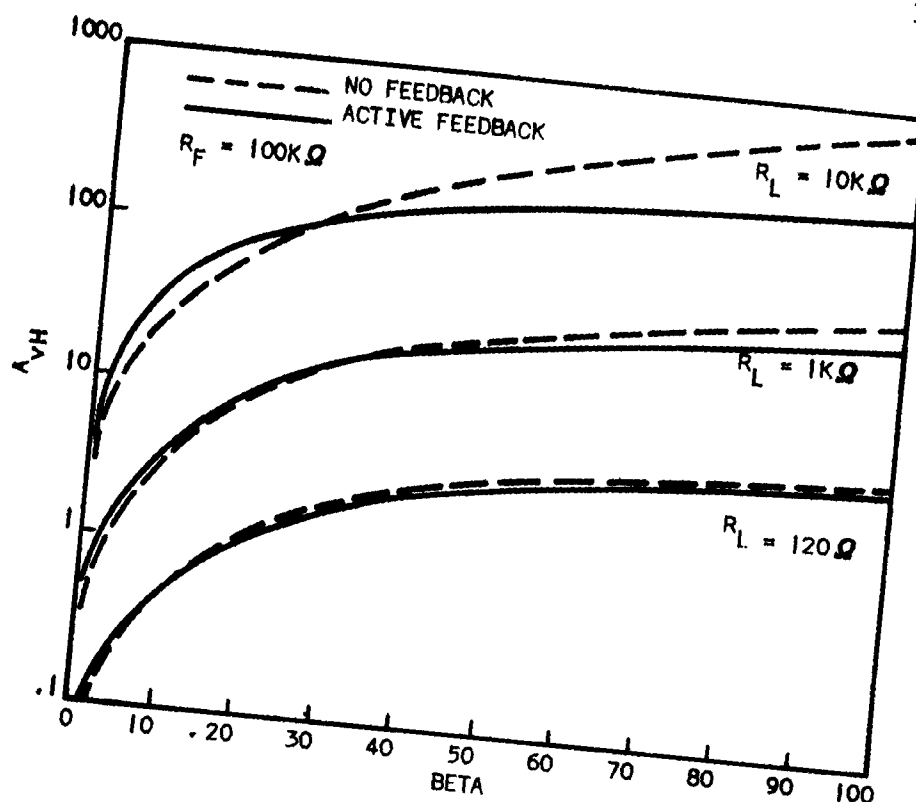


Fig. 3.5 Voltage Gain vs Beta

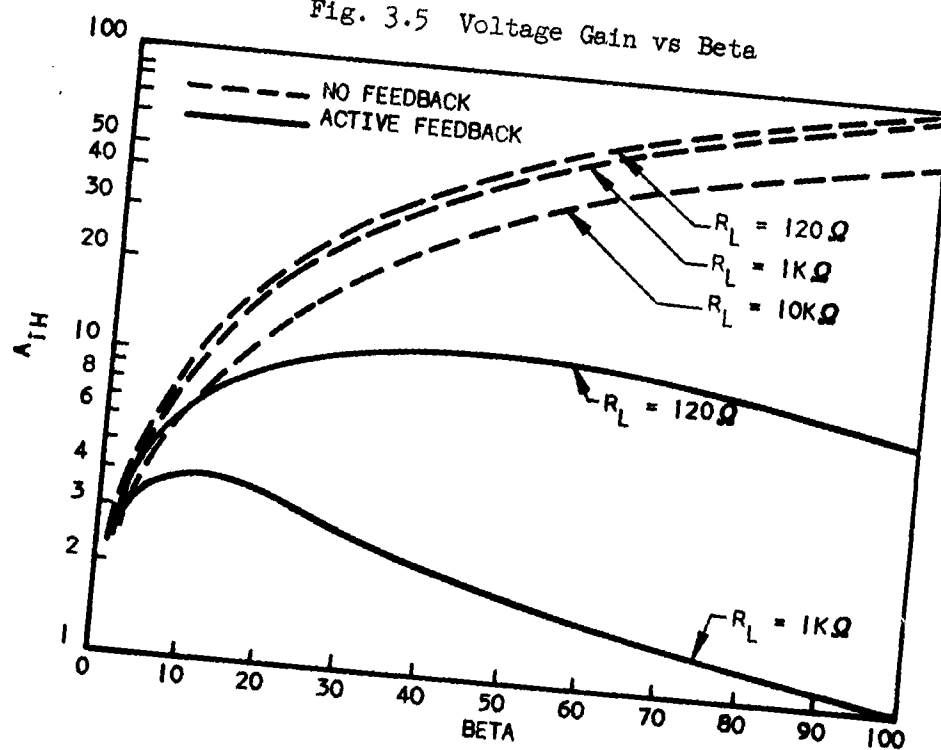


Fig. 3.6 Current Gain vs Beta

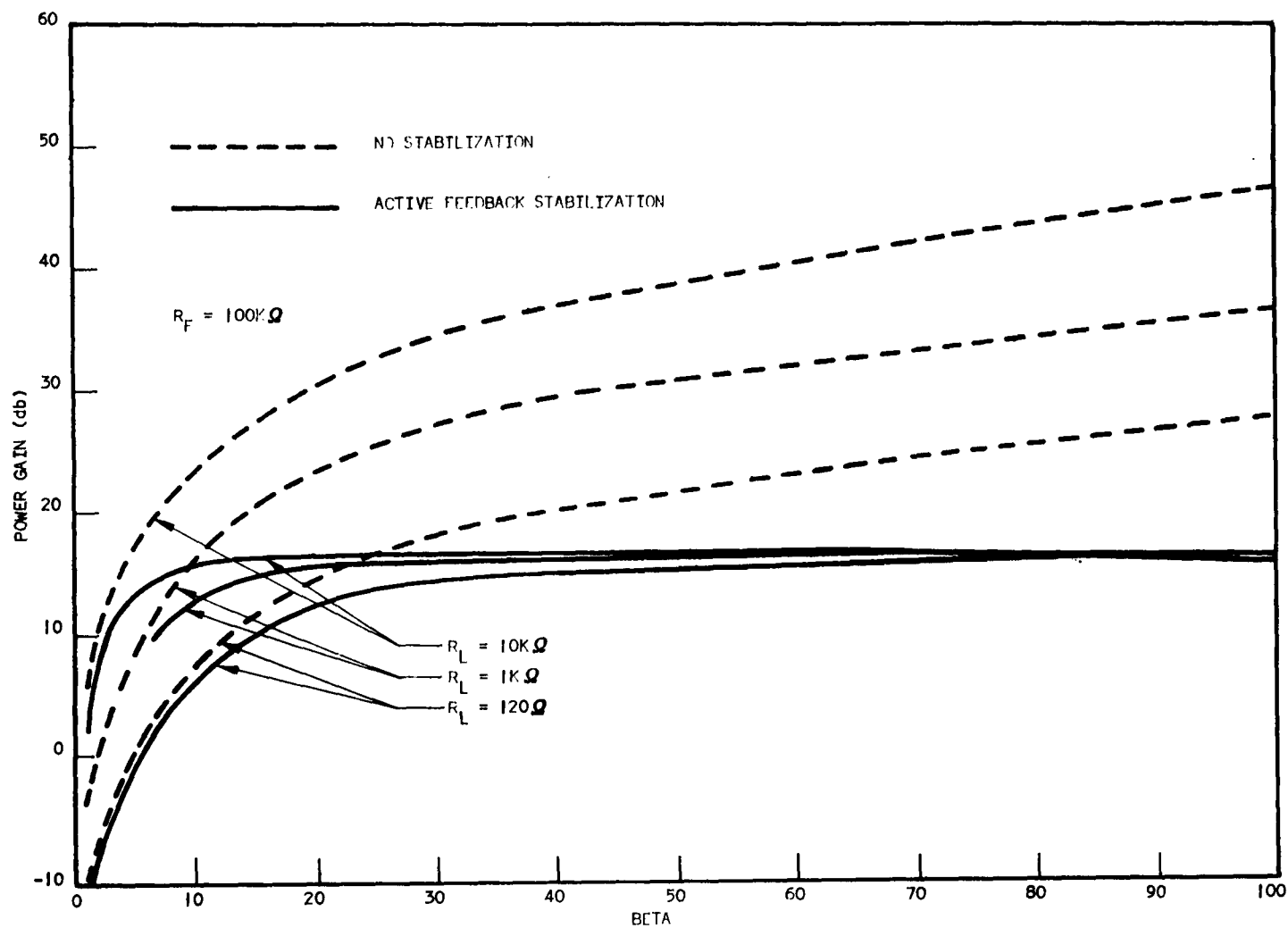


Fig. 3.7 Power Gain vs Beta

3.5 Design Considerations

The common-emitter, common-collector configuration was chosen to illustrate the technique of radiation stabilization by use of identical transistors in an active feedback arrangement. However, choice of one of the other configurations shown in Fig. 2.1 may be desirable in certain applications. Special care must be taken, however, to be sure that the phase relationships are correct (i.e., that the circuit is degenerative). For example, the use of identical transistors in the common-emitter, common-emitter arrangement results in a regenerative rather than a degenerative amplifier. Use of complementary transistors in this arrangement results in the proper phase relationship. However, a very complicated biasing problem is encountered.

Thus far, only the ac characteristics of the single-stage active feedback amplifier have been considered. Even though the determination of the proper biasing conditions and required circuitry are a necessary part of any amplifier design, this problem is not considered within the scope of this paper. However, it should be noted that if no additional circuitry other than a load resistance is used in the circuits of Fig. 2.1, the degree of stabilization which can be attained will be dictated by the biasing requirements of the transistors involved.

In order to minimize the effects of an increase of input impedance with decrease in β , the active feedback amplifier stage should be driven from a signal source with a fairly high output impedance. Maintaining an impedance match between the inputs and outputs of successive active feedback compensated stages may prove to be difficult but not impossible since both H_i and $1/H_o$ increase as β decreases. However, when a close impedance match between stages is required, this method of stabilization should probably be avoided.

As long as identical transistors are used with the method of radiation stabilization described in the preceding sections, the circuit designer can be reasonably assured that the β s of the transistors will deteriorate in an identical manner in a given radiation flux. When non-identical transistors are used, considerable care should be taken to be assured that the radiation characteristics of both transistors are known, if the performance of the compensated circuit is to be predicted.

4. EXPERIMENTAL VERIFICATION OF STABILIZATION DESIGN THEORY

4.1 Test on Common-emitter, Common-collector Amplifier

A test was made on a common-emitter, common-collector amplifier using 2N338 transistors which were very nearly identical. A 90-curie Co 60 gamma source was used which provided a flux (dose rate) of approximately 3×10^5 r/hr. The test was halted after an irradiation time of 138 hours, or about 4×10^6 r.

Figure 4.1 shows the variations in the short circuit current gains of both the individual transistors and the compensated amplifier with gamma dose. Notice that the betas of the identical transistors deteriorated almost identically. It is seen that H_F can be made very stable up to approximately 10 roentgens. However, the compensated amplifier cannot function beyond the point at which the transistor action is completely destroyed. This point is approximately 10^8 roentgens for Type 2N338 transistors.

Figure 4.2 shows the variations of the voltage, current and power gains of the amplifier with $R_F = 490 \text{ K } \Omega$ and a $5 \text{ K } \Omega$ load resistance. The amplifier was driven from a $100 \text{ K } \Omega$ signal source. Notice the increase in the current and power gains between 10^5 and 10^6 roentgens. A study of Figures 3.6, 3.7 and 4.1 will show that this effect was predicted by the design theory for certain values of load resistances.

5. SUMMARY:

As more and better information on the behavior of transistors in nuclear environments is reported, it is becoming well established that one of the more serious effects is the ultimate deterioration of beta. Thus, techniques for radiation stabilization against changes in beta are needed which will allow circuits to operate over longer periods of time. However, no stabilization method is of use after the transistor action is destroyed by the radiation field. It is then up to the transistor designer to find ways to make transistors more radiation resistant. Until then, there is no known way other than shielding, to make transistor circuits operate indefinitely in strong radiation fields.

The method of radiation stabilization proposed in this report takes advantage of the fact that identical transistors have a tendency to deteriorate identically in radiation fields. In this method, power gain is sacrificed in order to stabilize an amplifier against the deterioration of beta, thus increasing its useful operating time in radiation fields.

The advantages of the particular circuit chosen to illustrate the proposed active feedback arrangement are obvious from Figures 3.3, 3.6 and 3.7. However, Figures 3.1, 3.2 and 3.4 show some of the advantages of using passive current feedback. Other methods undoubtedly have other advantages. Choice of the most suitable method depends of course on the circuit requirements.

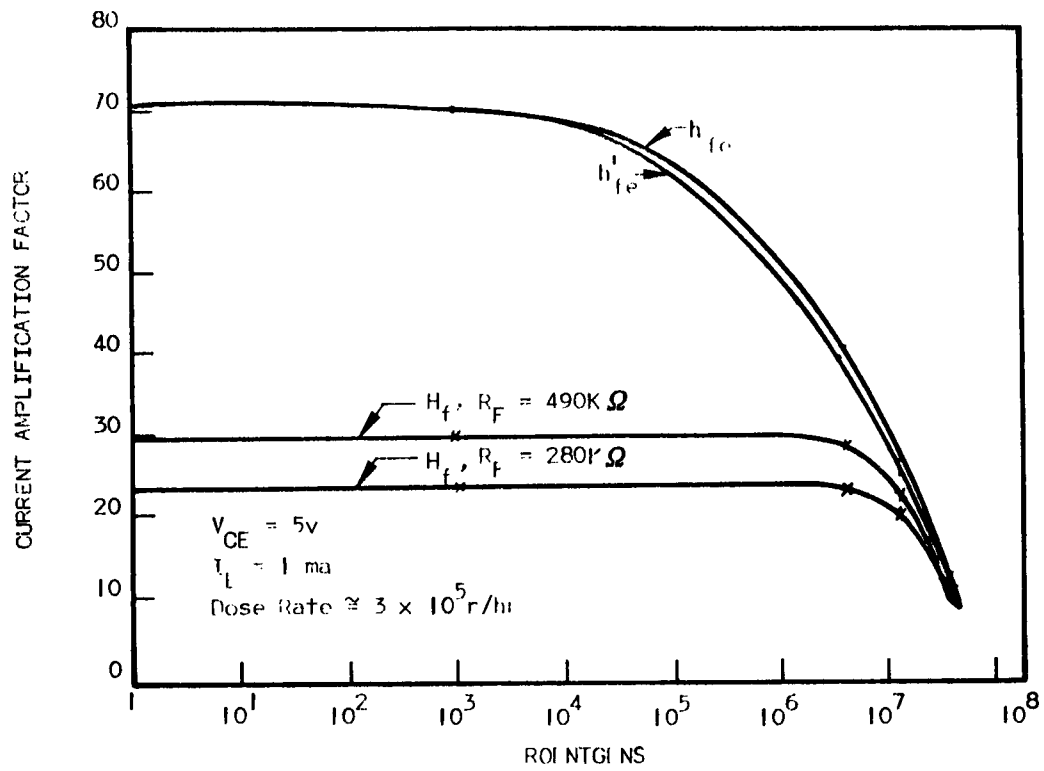


Fig. 4.1 Current Amplification Factor vs Gamma Dose

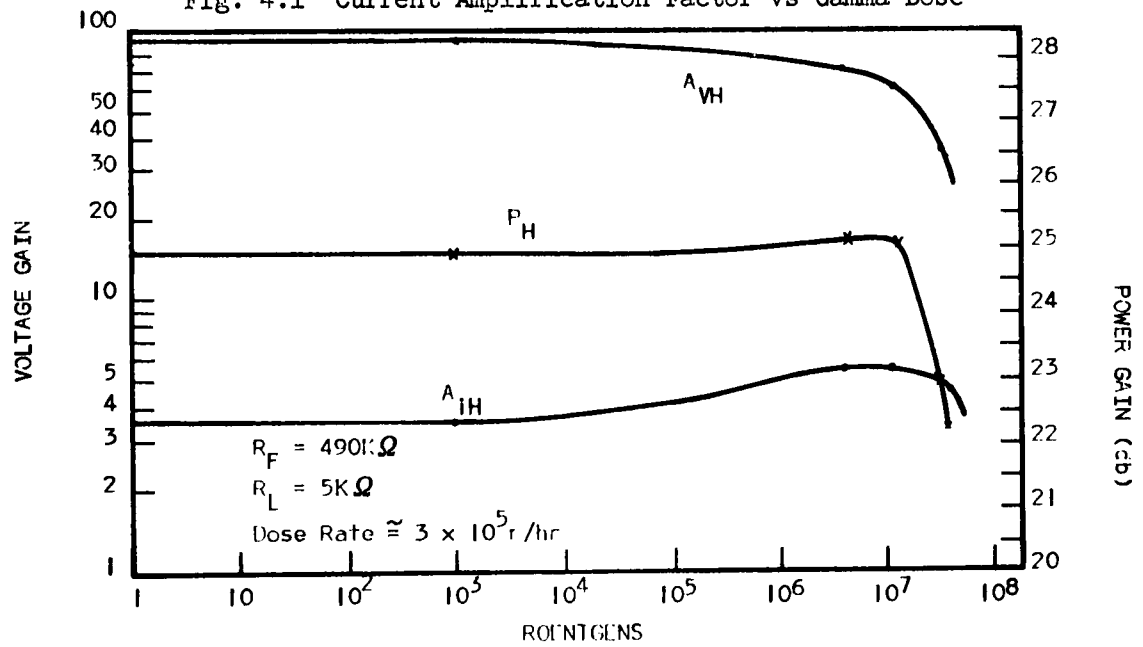


Fig. 4.2 Voltage, Current and Power Gain vs Gamma Dose

Most methods of operating point stabilization for temperature can be applied directly to radiation stabilization. Due to the nature of the radiation damage, it is expected that new and better methods will be developed for radiation environments.

ACKNOWLEDGMENTS

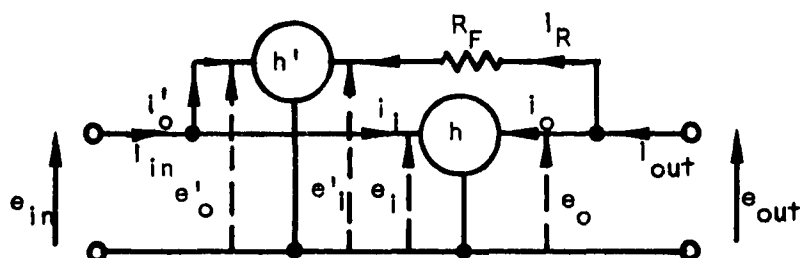
The authors express their appreciation to Mr. T.R. Nisbet for his many helpful suggestions and criticisms, Mr. K.R. Morsette for his assistance in the experimental measurements, and to Mrs. Ruth Kaluza for clerical assistance.

APPENDIX DERIVATION OF FORMULAS

I. Overall h-parameters

A. Active feedback

The general single-loop active feedback amplifier circuit is shown below:



From the diagram the following relationships are obtained:

$$e_{in} = e_i = e_o'$$

$$i_{in} = i_i + i_o'$$

$$e_{out} = e_o$$

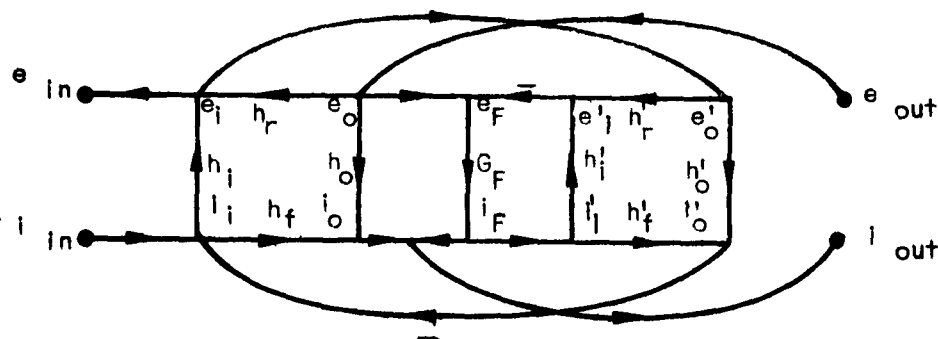
$$e_f = e_o - e_i = i_i R_F$$

$$e_{out} = e_o = e_i + i_R R_F$$

$$i_{out} = i_o + i_R$$

$$I_F = i_i$$

From these relationships we obtain the signal flow-graph* shown below:



From the flow-graph the following loops are identified:

$$L_1 = -h_i h'_o$$

$$L_2 = h_i h'_r h'_f G_F$$

$$L_3 = -h'_i G_F$$

$$L_1 L_3 = h_i h'_i h'_o G_F$$

where $G_F = 1/R_f$

Using the non-touching loop rule we have:

$$H_1 = \left. \frac{e_{in}}{i_{in}} \right|_{e_{out}} = h_1 (1 - L_3) / (1 - L_1 - L_2 - L_3 + L_1 L_3)$$

$$H_r = \left. \frac{e_{in}}{e_{out}} \right|_{i_{in}} = \left[h_r (1 - L_3) - h_i h'_f G_F \right] / (1 - L_1 - L_3 + L_1 L_3)$$

$$H_f = \left. \frac{i_{out}}{i_{in}} \right|_{e_{out}} = \left[h_f (1 - L_3) - h_i h'_r G_F \right] / (1 - L_1 - L_2 - L_3 + L_1 L_3)$$

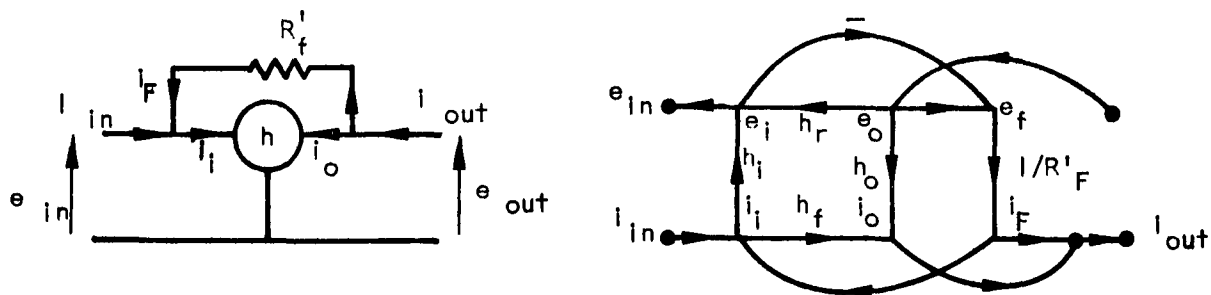
$$H_o = \left. \frac{i_{out}}{e_{out}} \right|_{i_{in}} = h_o + \left[G_F (1 - L_1) - G_F (h_r h'_r + h_f h'_f) - h_r h'_o h'_f (1 - L_3) \right] / (1 - L_1 - L_2 - L_3 + L_1 L_3)$$

which are the relationships given in section 2.2 .

*Readers who are unfamiliar with signal flow-graph analysis can refer to Mason (1953), Truxal (1955), Lorens (1956), and Happ (1957, 1958) treatment of the subject.

B. Passive Feedback

The passive feedback circuit used in paragraph 3.4 and its associated signal flow-graph are shown below:



we can see from the flow-graph that the only loop is:

$$L = - h_i / R'_F .$$

Thus, we see that the overall hybrid parameters are:

$$H_i' = h_i / (1 - L)$$

$$H_r' = (h_r + h_i / R'_F) / (1 - L)$$

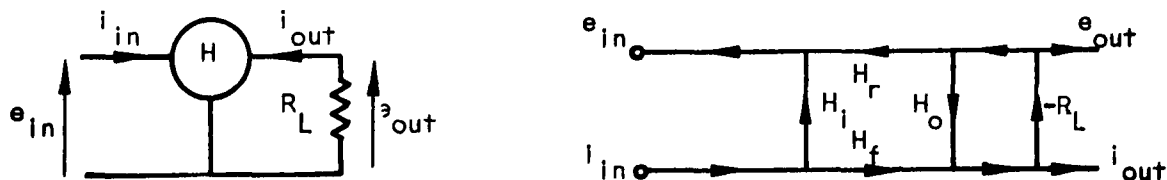
$$H_f' = (h_f - h_i / R'_F) / (1 - L)$$

$$H_o' = \left[h_o (1 - L) + (1 - h_r) / R'_F \right] / (1 - L)$$

which reduce to the equations given in paragraph 3.4

II. Amplifier Gain

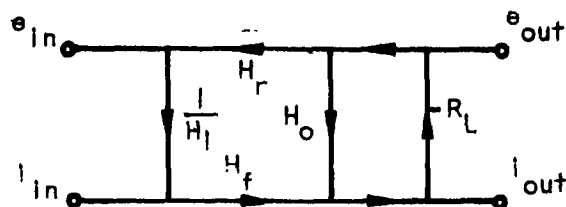
The current gain of the active feedback amplifier is calculated from the diagram and its corresponding flow-graph shown below:



The current gain is readily obtained from the flow-graph as:

$$A_{iH} = H_i / (1 + H_o R_L) \quad 19$$

The voltage gain can be obtained by reversing the path from i_{in} to e_{in} flow-graph:



The following loops can be identified:

$$L_1 = -H_o R_L \quad L_2 = \frac{R_L H_r H_f}{H_1}$$

The voltage gain can thus be seen to be:

$$A_{vH} = - (H_f R_L / H_1) / (1 - L_1 - L_2)$$

$$= - H_f R_L / \left[H_1 + R_L (H_1 H_o - H_r H_f) \right]$$

The power gain is thus:

$$P_H = A_{vH} A_{iH}$$

REFERENCES

- 1953 Ghandi, S.K., "Transistor Feedback Amplifiers", Proc. Natl. Electronics Conf., 9, 738-747
- 1953 Mason, J.S., "Feedback Theory-Some Properties of Signal Flow Graphs", Proc. IRE 41, 9, 1144
- 1955 Lo, A.W., et al, Transistor Electronics, New York, Prentice-Hall
- 1955 Truxal, Automatic Feedback Control Systems Synthesis, New York, McGraw-Hill
- 1956 Guggenbühl and Schneider, "Zur Stabilisierung des Gleichstromarbeitspunktes von Flächentransistoren", Archiv der Elektrischen Übertragung, 10 (1956) , 361 - 375.
- 1956 Hunter, L.P., Handbook of Semiconductor Electronics, New York, McGraw-Hill
- 1956 C.S. Lorens, Theory and Applications of Flow Graphs, Ph.d. Dissertation, Mass. Inst. of Tech.
- 1956 Pigg, J.C. and Robinson, C.C., "Radiation Effects in Semiconductor Devices", Proc. of the Transistor Reliability Symposium, New York Univ. Press
- 1956 Steele, H.L., "Effects of Gamma Radiation on Transistor Parameters", Proc. of the Transistor Reliability Symposium, New York Univ. Press
- 1957 Boxall, F.S., "Base Current Feedback in Transistor Power Amplifier Design", IRE Convention Record, Part 2. pp. 20-26
- 1957 Dienes, G.T. and Vineyard, G.H., Radiation Effects in Solids, New York, Interscience Publishers
- 1957 Ghandi, S.K., "Darlington's Compound Connection for Transistors", Trans. IRE, CT-4, 3. 291-292
- 1957 Happ, W.W., "Signal Flow Graphs", Proc. IRE 45, 9, 1293
- 1957 Shea, R.F., et al, Transistor Circuit Engineering, New York, Wiley & Sons
- 1958 Happ, W.W., "A New Teaching Aid: Flow Graphs", Lockheed MSD Report #2416
- 1958 Messenger, G.C. and Spratt, J.P., "The Effects of Neutron Irradiation on Germanium and Silicon", Proc. IRE, 46, 6, 1038-1044

COMPARISON OF NEUTRON DAMAGE IN GERMANIUM AND SILICON TRANSISTORS^a

by

J. W. Easley

Bell Telephone Laboratories, Incorporated
Whippany, N. J.

Quantitative comparison of the neutron bombardment sensitivity of germanium transistors to that of silicon transistors must include consideration of the mean time for minority carriers to traverse the base region of the structures being compared. Analysis shows that, for transistors of comparable carrier-transport-factor frequency cutoff, germanium transistors should be capable of receiving fast-neutron exposures which are one to two orders of magnitude greater than those permissible for silicon devices before current-gain degradation becomes critical for typical circuit applications. Experimental data are presented for both germanium and silicon transistors which are in good agreement with the analysis.

INTRODUCTION

Various¹⁻⁵ investigators have reported measurements of silicon and germanium transistor current gain during and after exposure to combined neutron and gamma flux. These measurements have demonstrated that silicon transistors are, in general, more sensitive to radiation than are germanium transistors. Loferski³, Messenger and Spratt⁴, and Easley and Dooley⁵ have reported analysis of the bombardment behaviour of current gain through inclusion of conductivity and carrier-lifetime behaviour in essentially equivalent formulations of existing transistor design theory. The major portion of reported data has been in qualitative agreement with these

^aThis work has been supported by the Air Force through Wright Air Development Center, Contract AF33(600)-32662.

analyses. In two instances^{4,5}, values of the lifetime associated with recombination centers introduced in germanium by neutron bombardment have been obtained from current gain measurements which are in approximate agreement with values obtained by direct measurement^{6,7}.

The intent of this paper is to express the bombardment dependence of current gain in an approximate form of general applicability, to discuss representative experimental results with particular attention to the extent of quantitative correlation with analysis, to discuss the associated problem of quantitative estimation of transistor bombardment behaviour, and to emphasize the magnitude of the greater bombardment sensitivity of silicon compared to germanium transistors.

The approximate range of maximum permissible exposure, based on an arbitrary criterion of a reduction in common emitter gain to 70% of initial value, is indicated in the following examples. A silicon alloy-junction moderate-power transistor with a transport-factor frequency cutoff, f_{β} , of approximately 1 megacycle has an estimated exposure limit of 1×10^{11} fast-neutrons, whereas a diffused-base structure with an f_{β} of approximately 100 megacycles has a limit of 2.5×10^{12} fast neutrons. A germanium alloy-junction high-power transistor with f_{β} equal to about 0.2 megacycles has an estimated exposure limit of 4×10^{11} fast neutrons whereas a germanium diffused structure with f_{β} of the order of 500 megacycles has a limit which is estimated to be of the order of 5×10^{15} fast neutrons. This wide range of exposure limits of over four decades results predominantly from the range among device types in values of the quotient $\bar{\tau}/\tau_b$ where $\bar{\tau}$ is the mean time for minority carriers to traverse the base layer and τ_b is the lifetime associated with the bombardment induced recombination centers in the base region. The lower range of exposure limits for silicon transistors, which overlaps that of germanium, is due to the more rapid bombardment reduction of carrier lifetime in Si⁸ than in Ge^{6,7}.

ANALYSIS

The analysis is restricted to the neutron bombardment induced change in current gain which, for the greater number of transistors, determines the upper limit of permissible fast neutron exposure. Further, for all silicon structures and npn

germanium structures the change in carrier lifetime is the dominant cause of failure and is therefore the mechanism considered here. In certain pnp germanium structures of high f_α the change in base region conductivity may constitute a failure mechanism if the initial conductivity is insufficiently high. The latter mechanism will not be considered here. Although no adequate experimental evidence has been reported to date, it is generally assumed that changes in electrical characteristics due to changes in surface properties are predominantly of gamma bombardment origin. For the gamma to neutron ratios associated with fission-like bombardment sources it appears^{3,4,9} that for "clean" devices the surface-origin contribution to changes in current gain may be neglected.

The current gain may be expressed as $\alpha = \beta \gamma \alpha^*$, the product of the transport factor, the injection efficiency and the collector multiplication factor. The transport factor can be expressed approximately as:

$$\beta \approx (1 - \frac{\bar{\tau}}{\tau}) \quad (1)$$

where $\bar{\tau}$ is the mean time for carriers to traverse the base layer

Since

$$\tau^{-1} = \tau_0^{-1} + \tau_b^{-1}(\phi) \quad (2)$$

where τ_0 is the initial effective minority carrier lifetime of the base region, $\tau_b(\phi)$ is the lifetime corresponding to bombardment-induced recombination centers, and ϕ the integrated neutron flux,

$$\alpha(\phi) \approx \alpha_0 - \gamma \alpha^* \frac{\bar{\tau}}{\tau_b} \quad (3)$$

It has been experimentally verified^{6,7,8} that

$$\tau_b \approx a \phi^{-1} \quad (4)$$

where a is a constant which depends on the base material and the injection level. It is reasonable to assume that α^* and $\bar{\tau}$ are independent of ϕ to values of ϕ corresponding to substantial reduction of β and that γ is a slowly varying function of ϕ compared to the factor $\frac{\bar{\tau}}{\tau_b}$. Therefore the dependence of current gain on integrated flux is given by

$$\alpha(\phi) \approx \alpha_0 - \gamma \alpha^* \bar{\tau} a^{-1} \phi \quad (5)$$

The expected form of the bombardment curve $\alpha(\phi)$ is then a straight line of slope $-\gamma \alpha^* \bar{\tau} a^{-1}$, as shown in Fig. 1.

For normal transistor structures $\gamma \approx 1$ and $\alpha^* \approx -1$ so that expression (5) can be simplified to

$$\alpha(\phi) \approx \alpha_0 - \bar{\tau} a^{-1} \phi \quad (6)$$

For the simplest structures of uniform base resistivity

$$\bar{\tau} = \frac{W^2}{2D} \quad (7)$$

where W is the width of the base region. Moll and Ross¹⁰ have discussed the dependence of $\bar{\tau}$ on the distribution of base-layer resistivity and have determined values for a number of resistivity distributions.

EXPERIMENTAL METHOD

Bombardment curves of current gain have been obtained from measurements of $(1-\alpha)$ concurrent with irradiation. A fission-plate source at the Brookhaven National Laboratory reactor, shown schematically in Figure 2, was employed for the irradiations. Aspects of the method which are significant in examining the correlation between observed behaviour and that calculated from the analysis are the temperature history of the samples during bombardment, the experimental uncertainty in the determination of α , and the measurement of the neutron flux magnitude and its energy spectrum.

The temperature of the transistors was monitored throughout the bombardments by a thermocouple soldered to the header of one of the ten devices measured during a given bombardment. For all transistors measured, the collector body was in good thermal contact with the header and the recorded temperature was constant to within $\pm 0.2^\circ\text{C}$, including the times of insertion into and removal from the flux. The upper limit of experimental error in the measured value of $(1-\alpha)$ is estimated to be approximately 3% so that the uncertainty in α is of the order of a few tenths of a percent. Consequently the variation in α due to temperature changes and the experimental uncertainty of the measured values are negligible.

The major source of experimental error in the data of the bombardment curves is in the integrated neutron flux measurement and therefore in the scale factor of the integrated flux coordinate. In the exposure facility employed the flux of fast-neutrons with energy greater than 1 kev was 1.2×10^9 neutron-cm⁻² -sec⁻¹ and the gamma dose-rate was 1.6×10^4 R/hr. The relative flux was obtained from a thermocouple enclosed in a boron bead located in proximity to the source plate. The emf of the thermocouple is proportional to the fission rate in the source plate and therefore to the fast-flux at the samples. In all bombardments wafers of 2 ohm-cm Ge were exposed with the transistors and the measured conductivity changes were employed to normalize the relative flux values to standard method foil activation measurements of the flux magnitude from previous bombardments. A value of "fast neutron flux" obtained directly from the measured conductivity changes in conjunction with the data of Cleland et al¹¹ yields an integrated flux value 20% lower than that obtained directly by foil activation. This difference is less than the estimated experimental uncertainty in the measurements.

DATA AND CORRELATION

Representative data are shown in plots of current gain α vs. integrated fast neutron flux ϕ in Figures 3, 4, 5 and 6.

Silicon

Figure 3 shows the behavior of five S1 diffused emitter diffused base transistors of the same type (2N560) described by L. E. Miller¹². The approximations of equation (6) are expected to be valid for this unit and the observed slopes are approximately constant over the range of bombardment, in agreement with these assumptions. The mean value of $d\alpha/d\phi$ for

fourteen samples of this type if -4.38×10^{-15} neutron⁻¹ cm² with an average deviation from the mean of 0.73×10^{-15} . The mean carrier transit time for these units as determined from f_{α} measurements is considered to be approximately 2.5×10^{-9} sec so that a value of the constant a of equation (4) of 5.7×10^5 neutron-cm⁻² μsec is obtained for the p-type base material of these structures at an injection level of the order of 10^{15} cm⁻³.

Figure 4 shows the behavior of three 2N560 transistors (units 1, 2, and 3) and three 2N338 (units 7, 9, and 10) for the initial portion of a bombardment. The constant slope of α vs. Φ prevails from zero integrated flux. The 2N338 units exhibit higher initial values of α than do the 2N560 but show a $\frac{d\alpha}{d\Phi}$ which is on the average 30% greater in absolute value. Although no qualitative correlation has been made, this is attributed to a higher initial lifetime and greater mean transit time of the 2N338. This qualitative difference is consistent with the different fabrication modes of the two devices.

In addition to the quantity $(1-\alpha)$, concurrent measurements of C_c , I_{co} and the collector reverse $V_c - I_c$ characteristic were obtained. The collector capacity and breakdown voltage exhibit no change from exposures sufficient to drastically reduce current gain, which is consistent with the known dependence of carrier concentration on neutron bombardment⁸. No apparent bombardment-induced changes in the surface properties of these specific device types were evident.

Germanium

Figure 5 shows representative data of α vs. Φ for germanium-alloy npn transistors of moderate frequency characteristics. The simplicity of the alloy structure compared to more complex transistor forms, as represented by the Si units discussed, admits of the possibility of a more detailed correlation between analysis, directly measured material properties, and observed behavior. A program of this nature is being currently pursued, and a portion of the data⁹ is employed here in order to make a comparison of the "radiation resistance" of germanium and silicon transistors. The curves shown have been selected to include units exhibiting common-base frequency cutoff values, f_{α} , over a wide range. Except for the related

variation in base-width, the structures are nominally identical. The base region resistivity is approximately 2.8 ohm-cm and the injection level of the measurements was

approximately $5 \times 10^{13} \text{ cm}^{-3}$ at the emitter edge of the base so that any correction to the low current level approximation of equation (6) should be small. The approximately constant slope of α vs. ϕ deduced from equation (6) is again evident. Since the transport factor frequency cutoff f_β is inversely proportional to $\bar{\tau}$ and as for these units $f_\beta = f_\alpha$, equation (5) or (6) predicts a constant product $(d\alpha/d\phi) \times f_\alpha$. Values of f_α range from 7.8 megacycles for unit 7 to 1.4 megacycles for unit 2 and the product of measured quantities $(d\alpha/d\phi) \times f_\alpha$ is constant within a 10% average deviation from the mean for the 5 units shown. This is in good agreement with the analysis. From the observed slopes and f_α values the constant a is evaluated as 2.0×10^7 neutrons $\text{cm}^{-2}\text{-sec}$.

Figure 6 is a plot of α vs. ϕ for the initial portion of the bombardment shown in Figure 5. A scatter of points occurs for units 2 and 3 during the first 5 minutes of bombardment. It is likely that the erratic behaviour is noise of surface origin. Also shown on Figure 6 is the median slope for the 2N560 silicon transistors. This slope is approximately equal to that of the germanium unit number 3, which has an f_α of 2.3 megacycles. Consequently, if the observed $d\alpha/d\phi$ of the Ge and Si units are normalized to equal $\bar{\tau}$, the current gain of the Si units decreases at a rate approximately 35 times that of Ge units.

DISCUSSION

The linear dependence of α on ϕ , exhibited by the bombardment curves of both Ge and Si is consistent with expressions (5) and (6) and therefore the underlying assumptions. In addition, values of the constant a of equation (4) as obtained from these curves are in approximate agreement with direct measurement values obtained by other investigators, particularly for Ge. Table I shows values of a which have been reported, and indicates a maximum variation in Ge values by a factor of about 2 and in Si by a factor of about 10.

A portion of the difference in values of a can be attributed to differences in fast neutron flux measurement and specification. However, the same absolute determination is involved in the values of columns III, IV, and V and the uncertainty in the relative determination among the bombardments

involved should be small. Further, some normalization or comparison of flux specification to that of column I data has been made by those reporting the values in the other columns.

In the case of Ge, all values reported were either obtained at low injection levels or have been extrapolated to low injection and should therefore permit comparison. The values shown in column I are not reported values of Curtis et al^{6,7} but are approximate values corresponding to the resistivity range applicable to columns II and IV as obtained by extrapolation of the reported values according to a Shockley-Read¹³ $\tau(\rho)$ dependence.

For Si the comparison cannot be as direct since the determinations from transistor-gain bombardment behaviour were obtained at high injection levels whereas those of Wertheim⁸ pertain to low injection. Further, the reported value obtained from α vs. Φ loci and equation (6) represent an average value over a region in which equilibrium carrier density, excess carrier density, and mobility are not uniform or simply-varying. Comparing values of column III and IV, for which the flux specification is identical, the device-measurement value is somewhat lower than might be estimated on the basis of the ratio of injection levels of approximately 10^3 . If expression (6) is assumed to be an adequate approximation, then the sole source of experimental error involved in the comparison is in the average value of \bar{t} , which has an estimated uncertainty of less than approximately 30%. The values reported by Messinger and Spratt⁴ are "low-injection level" values obtained by extrapolation from the measured emitter current variation of $(d\alpha/d\Phi)$ and the values of columns II and III are therefore not in agreement.

On the basis of these data, the qualitative difference between α values and therefore values of $(\partial\alpha/\partial\Phi) \times \bar{t}^{-1}$ for Si and Ge transistors is clear. The value of the ratio $(\alpha)_{Ge}/(\alpha)_{Si}$ appears to lie in the range of approximately 100 to 10 depending primarily on the relative injection levels.

SUMMARY

Analysis indicates that transistor current gain should decrease with neutron bombardment according to the relation

$$\alpha(\Phi) = \alpha_0 - \gamma \alpha a^{-1} \bar{t} \Phi$$

where $\bar{\tau}$ is the mean time for carriers to traverse the base region and a is a constant which depends on the base material and injection level.

The constant a is defined by the relation

$$\tau_b = a \phi^{-1}$$

where τ_b is the carrier lifetime corresponding to bombardment induced recombination centers. The observed experimental behaviour of $\alpha(\phi)$ is in qualitative agreement with the above relationship and values of a determined from experimental $\alpha-\phi$ loci are in approximate agreement with the direct measurement values that have been reported.

Currently reported data indicate that values of the ratio $(a)_{\text{Ge}}/(a)_{\text{Si}}$ can be expected to lie in the range of approximately 100 to 10. The specific value in this range corresponding to any given comparison depends primarily on relative injection level. Consequently if the rate of decrease of current gain with neutron bombardment is normalized to equal $\bar{\tau}$, Si transistors can be expected to degrade at rates which are approximately 10 to 100 times greater than those for Ge. If semiquantitative consideration of the effect of injection level is considered, estimates of current gain degradation rate can be made to considerably better than an order of magnitude.

REFERENCES

1. Gillis, R. C. and Tarzwell, J. W., "Resistance of Silicon Transistors to Neutron Bombardment", 1957 IRE WESCON Convention Record part 3.
2. Keister, G. L. and Stewart, H. V., "The Effect of Nuclear Radiation on Selected Semiconductor Devices", Proc. IRE, Vol. 45, No. 7 (1957).
3. Loferski, J. J., "Analysis of the Effect of Nuclear Radiation on Transistors", Journal of Applied Physics Vol. 29, January, 1958.
4. Messenger, G. C., and Spratt, J. P., "The Effects of Neutron Irradiation on Germanium and Silicon" Proc. IRE, Vol. 46 June, 1958.
5. Easley, J. W. and Dooley, J. A., "Irradiation of Germanium Alloy Transistors", AGET Symposium on Nuclear Radiation Effects on Semiconductor Devices and Materials, N. Y. February, 1957.
6. Curtis, Cleland, Crawford and Pigg, "Effect of Irradiation on the Hole Lifetime in n-Type Germanium", Journal of Applied Physics, Vol. 28, No. 10 (1957).
7. Curtis, O. L. and Cleland, J. W., "Investigation of Minority Carrier Recombination in Irradiated Germanium", Bulletin of the American Physical Society, Vol. 3, No. 1 January, 1958.
8. Wertheim, G. K., "Neutron Bombardment Damage in Silicon", Bulletin of the American Physical Society, Vol. 3, No. 2 March, 1958.
9. Unpublished data, J. W. Easley and J. A. Dooley.
10. Moll, J. C. and Ross, I. M., "The Dependence of Transistor Parameters on the Distribution of Base Layer Resistivity", Proc. IRE, Vol. 44, January 1956.
11. Cleland, J. W., Crawford, J. H., and Pigg, J. C., Physical Review, 98 (1955).

12. Miller, L. E., "The Design and Characteristics of a Diffused Silicon Logic Amplifier Transistor", 1958 IRE WESCON Convention.
13. Shockley, W. and Read, W. T., Jr., "Statistics of the Recombinations of Holes and Electrons", Physical Review, Vol. 87, September 1952.

TABLE I

Values of the constant $a = \tau_b \phi$ in units of neutrons cm^2 sec for reported data.

Column	I	II	III	IV	V
	Curtis et al. ^{6,7} (See Note 1)	Messenger- ⁴ Spratt	Wertheim ⁸	Easley	Easley - Dooley ⁹
n - Ge	5.9×10^7	$5.0 \pm 2.0 \times 10^7$			2.1×10^7
p - Ge	4.0×10^7	$2.4 \pm 0.4 \times 10^7$			1.8×10^7
n - Si		$2.8 \pm 0.8 \times 10^6$	3.9×10^5		
p - Si		$3.2 \pm 1.1 \times 10^6$	4.3×10^5	5.7×10^5	

Note 1.

These are not the measured values reported by Curtis et al but are approximate values corresponding to approx. 2.5 ohm-cm material which is the resistivity range applicable to column II and V. These values were obtained from the reported values according to a Shockley - Read $\tau(\rho)$ dependence.

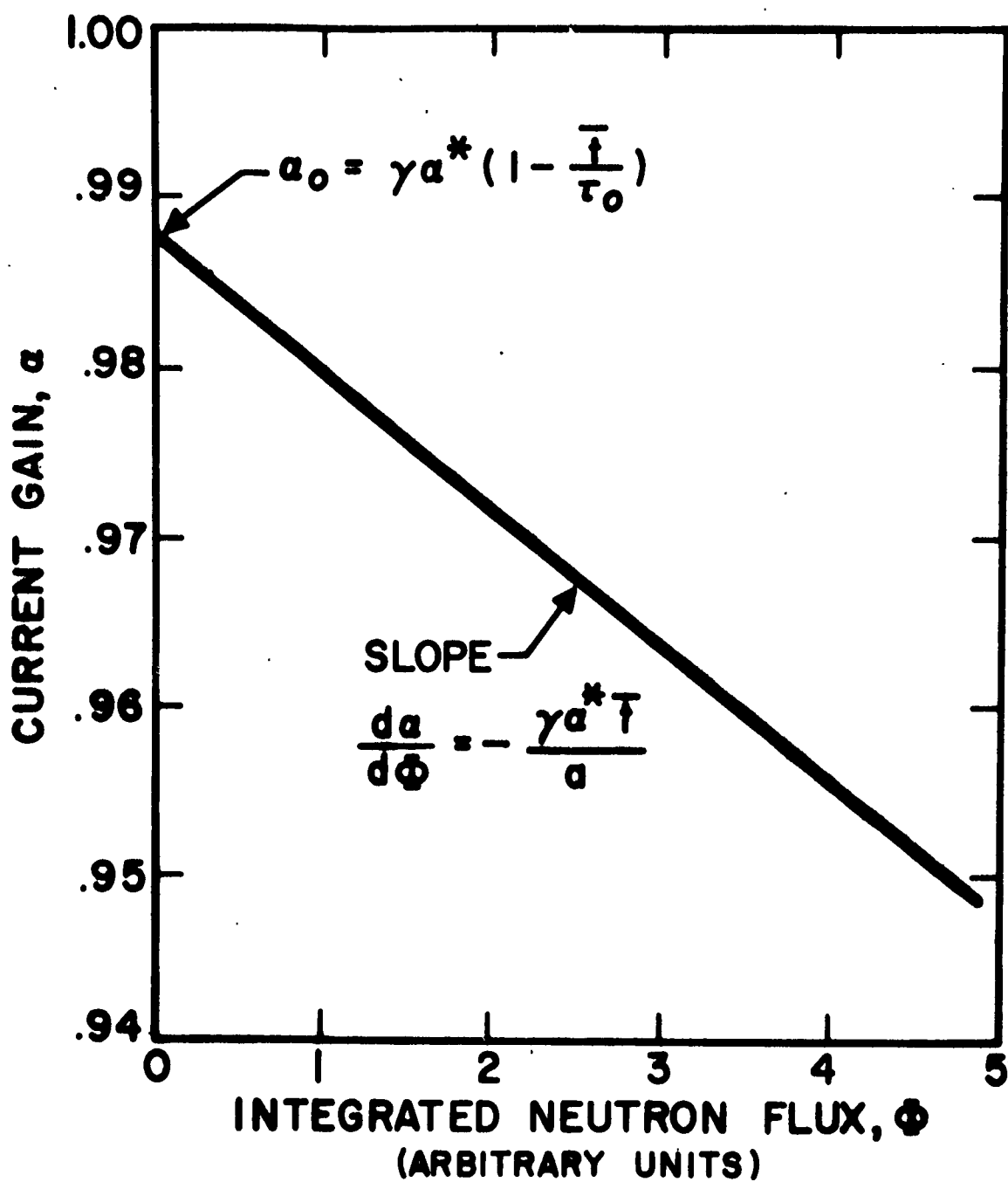


Figure 1. Theoretical form of α vs Φ according to equation (1).

SCHEMATIC REPRESENTATION OF SHIELDING FACILITY

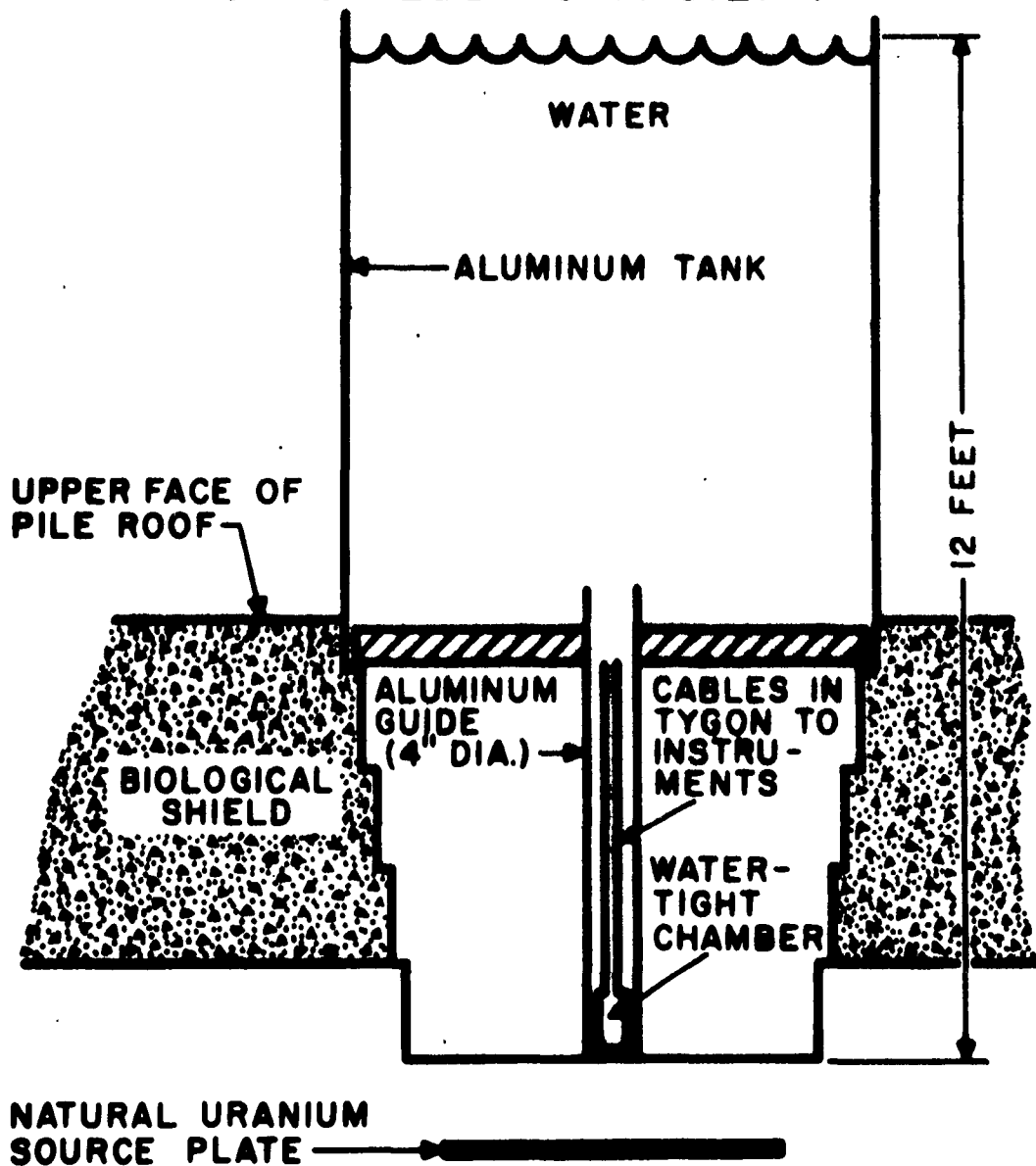


Figure 2. Schematic representation of shielding facility at the Brookhaven National Laboratory reactor.

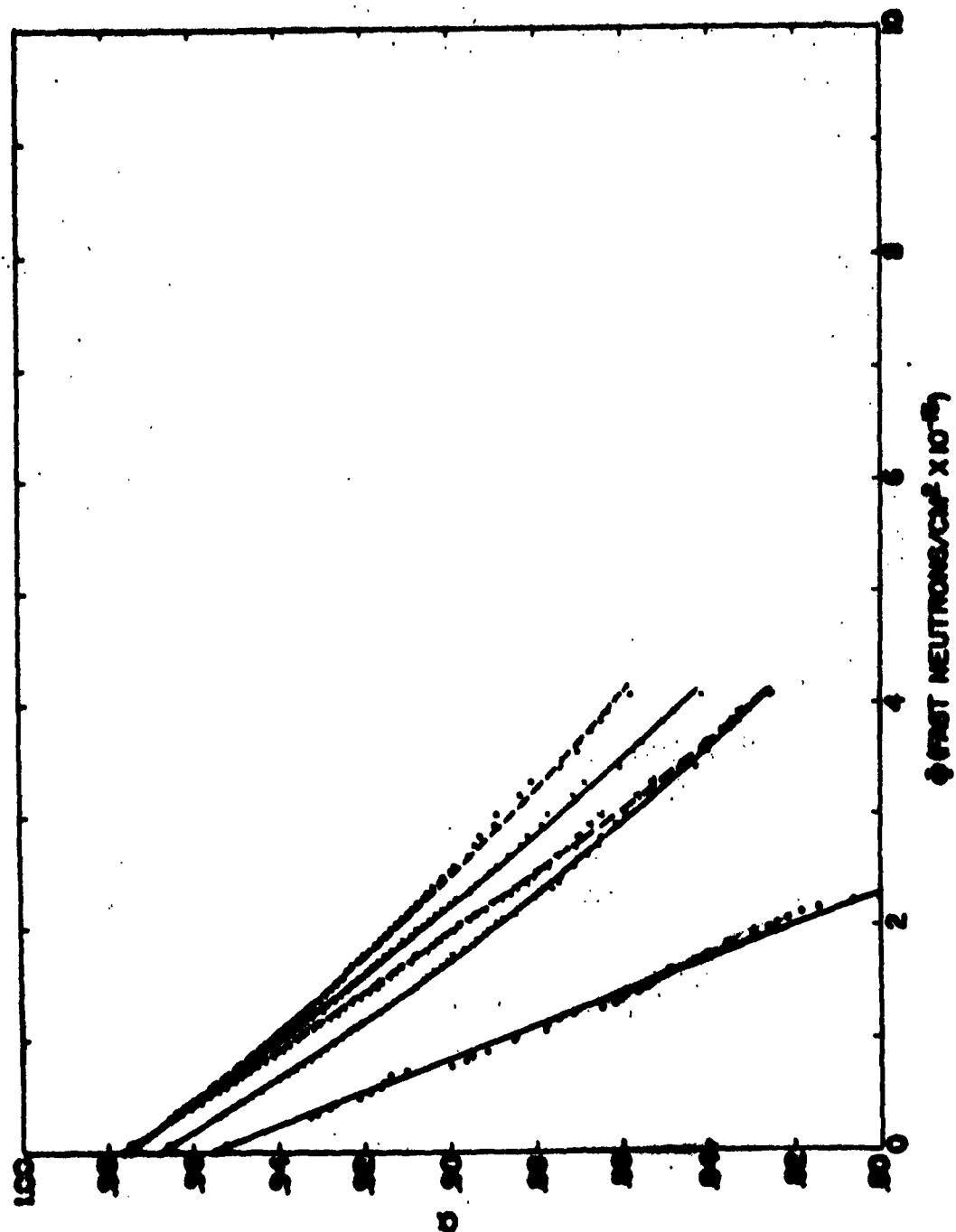


Figure 3. Representative experimental α vs ϕ curves for five Si 2N560 transistors. The remaining nine curves for the total sample all lie within the region bounded by the upper four curves and have been omitted to permit display of individual curves.

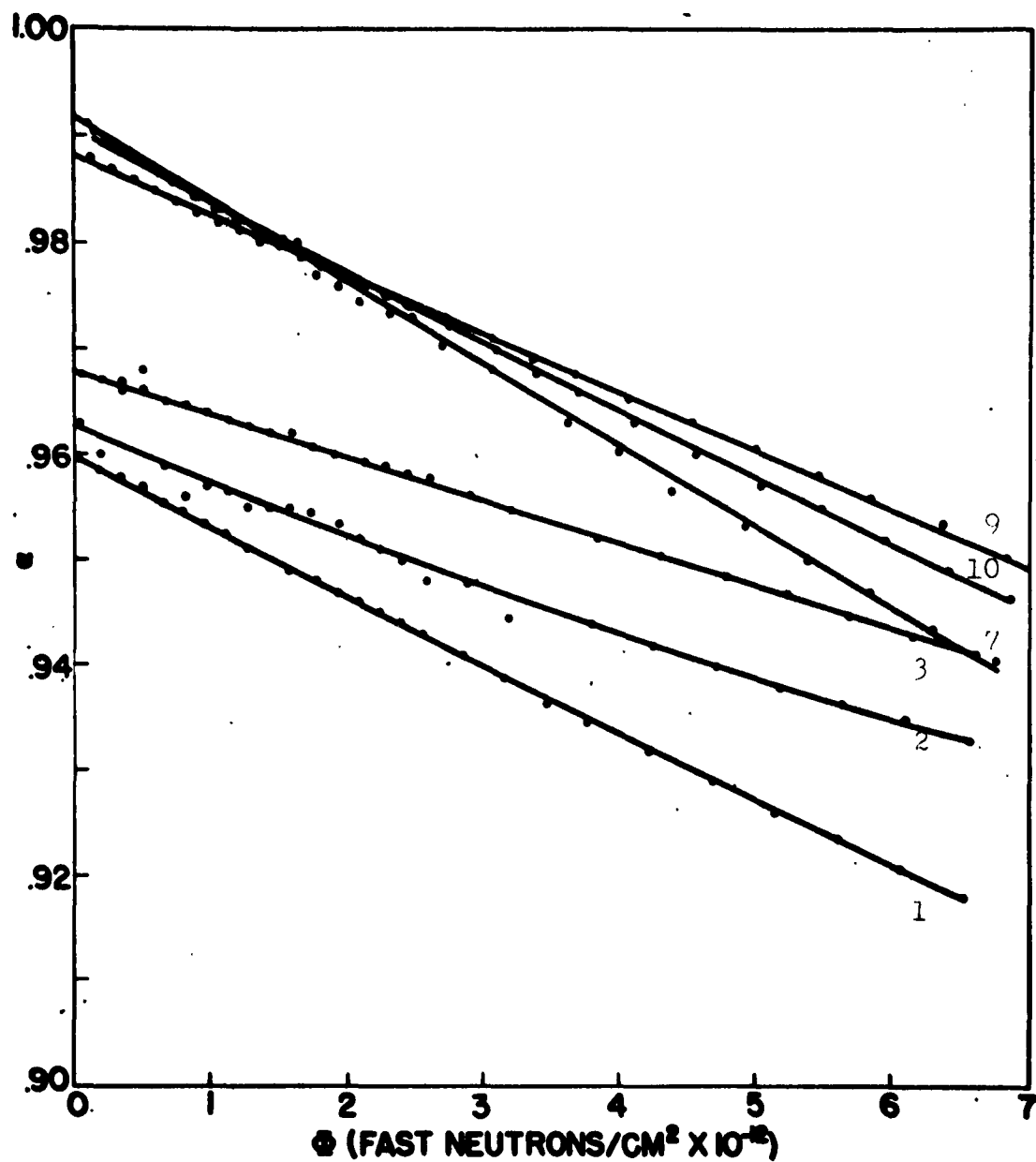


Figure 4. Curves of α vs Φ for three Si 2N560 transistors (units 1, 2 and 3) and three 2N338 (units 7, 9 and 10) for the initial portion of a bombardment.

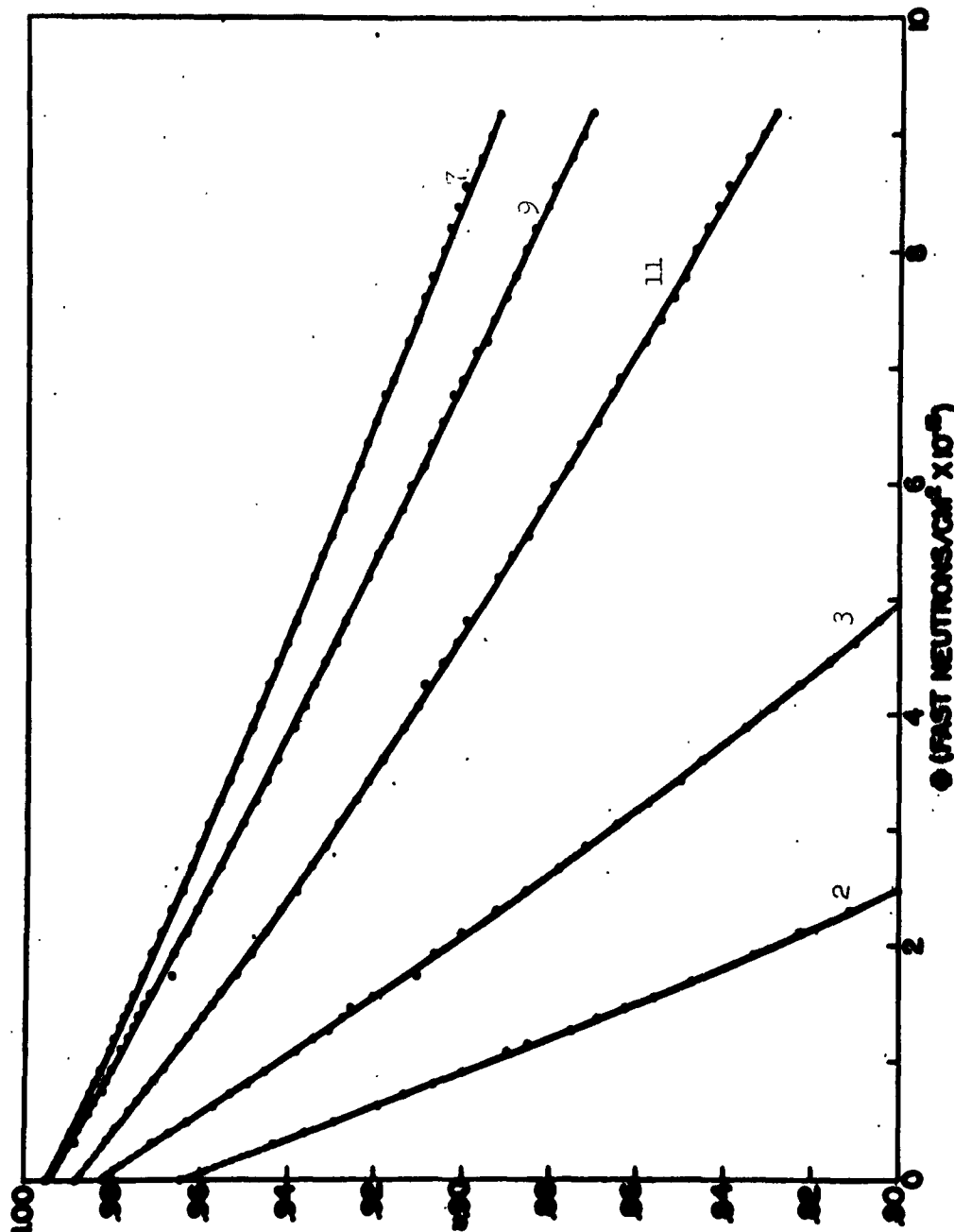


Figure 5. Representative experimental α vs Φ curves for Ge alloy-junction transistors. The slight positive curvature is tentatively attributed to the annealing during bombardment of defects acting as recombination centers. This suggests that a portion of the neutron bombardment induced defects anneal at room temperature in times of the order of 10^2 minutes.

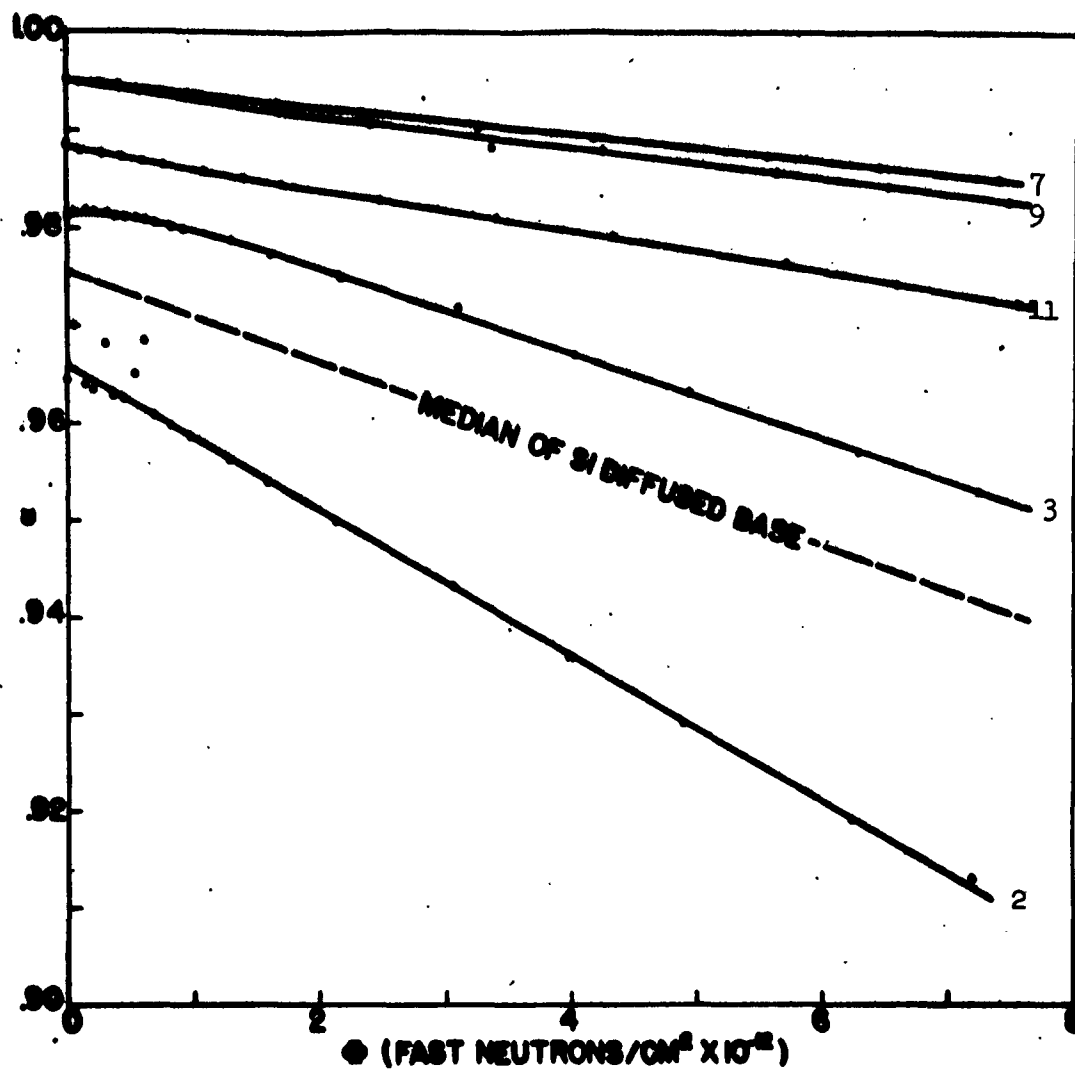


Figure 6. Curves of α vs Φ for the initial portion of the bombardment shown in Figure 5. The median transport factor frequency cutoff for the S1 units is approximately 35 times that of unit 3.

PULSED RADIATION EFFECTS IN SEMICONDUCTORS

by

J. M. DENNEY, C. W. PERKINS, and J. R. WIENEKE

**Nuclear Electronics Department
Hughes Aircraft Company
Culver City, California**

Typical semiconductors were exposed to pulsed neutron, electron and gamma fluxes. The effects of these exposures on the electrical properties of the semiconductors was observed during the radiation pulse. These radiation effects will be described and compared with analysis. Attention will be given to some of the differences between transient and residual radiation effects in semiconductors.

This paper was not available for publication.

THE EFFECT OF VARIATION OF THE WIDTH OF THE BASE REGION ON THE RADIATION TOLERANCE OF SILICON DIODES

By Gerald C. Huth
General Electric Company
Aircraft Nuclear Propulsion Department
Cincinnati 15, Ohio

ABSTRACT

Results are presented of experiments which were conducted to determine the effect of varying the width of the base region of a silicon diode on the radiation tolerance of the device as gauged by increase in voltage drop at forward bias. Reasonable agreement is shown between experimentally determined change in forward characteristic and behavior predicted from theoretical considerations - specifically considering the effect of degraded minority carrier lifetime. Devices irradiated (forty in number) were of the alloy junction type based on the configuration of the General Electric LN-538 rectifier. Their over-all behavior is discussed including the near exponential increase found in forward voltage drop, and the retention of reasonable reverse characteristics of all units during irradiation.

I. INTRODUCTION

In a radiation field consisting of neutron and gamma radiation, effects on the electrical properties of silicon resulting from the interactions of neutrons of sufficient energy (approximately 225 ev) to cause atomic displacements have been shown to be the factor limiting the life of solid state electronic devices containing this material⁽¹⁻⁵⁾. In the dosage range where devices possess useful characteristics the effect of gamma radiation is generally negligible. The neutron threshold dosage for the observance of these effects on device characteristics depends upon the sensitivity of the characteristic to property changes in the silicon crystal, but it is generally within the broad range from 10^{10} to 10^{12} n/cm² (epicadmium neutrons). Initial characteristic changes are due predominantly to degradation of the minority carrier lifetime property of the silicon and in the case of rectifiers these changes will in general be of sufficient magnitude to cause failure of the device. With further increase in neutron dosage (and thus increasing density of recombination and trapping centers) silicon resistivity begins to increase until approximate intrinsicity is reached in the vicinity of 10^{17} n/cm². A dosage range is thus obtained from 10^{10} to 10^{17} n/cm² dominated at the onset by decreasing minority carrier lifetime and at higher dosages by increasing resistivity where it will be possible to operate silicon semiconductor devices - the exact failure dosage dependent upon the sensitivity of device design to these basic property changes.

For the case of the silicon rectifier or diode, the result of decreased minority carrier lifetime is a decrease in current flow in the conducting or forward biased direction. It is this degradation of the forward characteristic that will probably cause failure in most circuits. It was the purpose of this work to determine the effect of varying one physical parameter of a diode - the effective width of the base region - which it was expected would reduce the effect of lifetime and resistivity changes on the forward characteristic. For this purpose one type of device - the 1N-538 alloy junction rectifier - was chosen as the basic study unit and modified only with respect to the width of the base region. The results of the irradiation of these modified devices and the correlation of these results with behavior predicted using basic device equations will be presented in this report.

II. THEORY

For a diode containing high resistivity silicon, the relationship⁽⁶⁾ between the voltage drop at forward bias E_f of the device and the effective base width W assuming constant current is given by:

$$E_f = (1 + \cosh \frac{W}{L}) \frac{E_{f0}}{2} \quad (1)$$

Where: L = Diffusion length for minority carriers
 E_{f0} = Forward voltage drop for W/L small, i.e. before irradiation

In design of practical rectifiers base width is intentionally made small in comparison with minority carrier diffusion length or in other words, the ratio W/L is initially very small. It is this ratio, or more specifically, minority carrier diffusion length, that will be affected by irradiation.

The effect of fast neutron bombardment as stated previously is to introduce defects into the semiconductor lattice, these defects acting as trapping and recombination centers for minority carriers - and it is precisely injected minority carriers which account for the bulk of forward conduction in a diode. Minority carrier diffusion length and lifetime are reduced, the two properties being related by:

$$L = \sqrt{D\tau} \quad (2)$$

where D is the diffusion coefficient for minority carriers and τ their lifetime. It remains to relate these properties to neutron dosage and the effect of varying the width of the base region on the radiation behavior of voltage drop at forward bias of a diode will be calculable. Loferski⁽⁷⁾, among others⁽⁸⁾, has found that minority carrier lifetime degrades under irradiation according to the following reciprocal relationship:

$$\frac{1}{\tau} = \frac{1}{\tau_0} + K\phi t \quad (3)$$

Where: τ = Minority carrier lifetime at radiation dosage ϕt
 τ_0 = Initial minority carrier lifetime
 ϕt = Neutron dosage
 K = An empirical constant which can be determined by observing the decay of τ in semiconductor crystals

The use of equations (1), (2), and (3) therefore, enables calculation of increase in forward voltage drop at constant current with increasing radiation dosage if the value of K is known. The value of this constant reflects among other factors, the method of neutron dosimetry used, with a value of approximately 10^{-7} neutron $^{-1}$ sec $^{-1}$ cm 2 reported when episcadmium neutron fluxes are measured. As will be shown later a value of 10^{-8} is applicable when neutron fluxes are measured as in this work, i.e. by exposing cobalt foils inside of boral shielding(a). It should be noted that a precise value for this constant will not be necessary here since we are interested in showing on only a relative rather than an absolute basis how a reduction in base thickness improves behavior under irradiation.

The approach taken here will be to assume a specific forward voltage drop as the failure point for the device. The neutron dosage necessary to increase the voltage drop to this point can then be calculated. This dosage will be termed the radiation tolerance of the diode. Radiation tolerances will be calculated for various base widths to illustrate the effect of varying this parameter.

The neutron dosage where E_f reaches four volts at a forward current I_f of one hundred milliamperes will be considered failure. From equation (1) the W/L ratio which corresponds to this failure point is 3.2 using a value of 0.6 volt for E_{f0} for a silicon alloy junction device at this current. If now a base width of .004 inches is assumed, the minority carrier diffusion length for this value of W/L is 3×10^{-3} cm. From equation (2) the corresponding minority carrier lifetime is 7×10^{-7} sec. (assuming no change in the diffusion coefficient) yielding from equation (3) a value for the radiation tolerance of a diode with this base width of 1.4×10^6 K $^{-1}$. By insertion of an appropriate value for K the tolerance in units of neutrons/cm 2 can be obtained. Using similar calculations for other base widths the family of curves of Figure 1 can be generated. It should be noted that different values for K merely change the placement but not the shape of the curve. From a practical standpoint it can be seen from this figure that a reduction in the width of the base by a factor of ten results in an increased radiation tolerance of approximately a factor of one hundred.

 (a) This method of measuring neutron flux was used because it was the best available method of assuring accuracy in dosage determinations between successive irradiations.

III. EXPERIMENTAL

Since it is mandatory in a study of the effects of varying base width that all other device parameters remain constant, one diode type - the 1N-538 alloy-junction diode - was chosen as the study vehicle. All devices for irradiation were produced under laboratory conditions for control purposes, however, there were no intentional deviations from the normal production processes for this unit. The alloy junction 1N-538 itself is a medium current rectifier containing high resistivity n-type silicon (approximately 25 ohm-cm) with the junction formed by alloying with aluminum. The donor impurity is phosphorous and the normal device silicon has a lifetime before incorporation into the device of 100 microseconds.

The effective base width of the standard 1N-538 is .0045 inches. Base widths were produced for irradiation of .0045, .0017, .0010, and .0008 inches, the .0008 inch value being the minimum it was possible to achieve reproducibly using the alloying technique. All silicon used in fabrication of these units was from the same crystal, no attempt being made as would be done in practical rectifier design to increase peak inverse voltage of the thin base width units by decreasing silicon resistivity. Forward rather than reverse characteristics were of concern here. The point of note is that design of thin base width devices could be optimized to provide higher peak inverse voltages than the units fabricated for these irradiations.

All irradiations were conducted in the ORNL-X-10 Graphite Reactor. A special tube inserted into the reactor allowed insertion and removal of experiments with the reactor at power thus facilitating relative accuracy in dosimetry measurements. A shield fabricated of boral sheet (one half inch thickness) surrounded the irradiation position in the reactor. Direct current measurements of the diode characteristic were made.

Ten devices of each base width were fabricated and five each were irradiated at temperatures of 30° and 150°C. A summary of the results of the behavior of the forward characteristics of the devices irradiated at 30°C is presented in Figure 2. These data are plotted to show the agreement with the curve of theoretical behavior (dashed curve) generated previously, a value of 10^{-8} being used for the constant to normalize the curve to the experimental results. The deviation among the five diodes comprising each irradiation is indicated.

Forward characteristic behavior of diodes irradiated at 30°C is compared with the results of irradiations of identical devices at 150°C in Figure 3. Increase in radiation tolerance is seen to be small - less than a factor of two - in the case of the diodes with wider base regions while for thinner base width devices this factor increases to four or greater. In general, it can be said, however, that operation of silicon devices at elevated temperatures (150°C is about the practical maximum operating temperature for currently produced silicon devices) will not greatly increase tolerance to neutron bombardment.

At a constant forward current of 100 milliamperes, behavior of the forward voltage drop with increasing neutron dosage of all of the diodes irradiated at 300°C is shown in Figures 4, 5, 6, and 7. The near exponential increase predicted previously can be seen. Figures 8, 9, 10, and 11 are similar plots for all devices irradiated at 150°C. A slight "knee" or deviation from the behavior at 300°C can be seen in these figures indicating the slight amount of thermal annealing of radiation-induced defects that is occurring. It should be noted in Figure 11 that only one of the five diodes (unit #1) with 0.0008 inch base width remained operative throughout the irradiation. A furnace excursion early in the test raised the temperature in the irradiation position to over 200°C and thermally destroyed four of the units.

As mentioned previously, reverse characteristics of all units were measured during irradiations. In general, reverse currents were observed to increase with decreasing width of the base region as expected, however, no drastic increases due to irradiation were seen in any of the units. The general pattern of reverse current behavior under irradiation is a moderate increase followed by a continual decrease (probably associated with decreasing lifetime) which persists to well beyond the dosage where the device has been rendered useless due to forward characteristic degradation. A portion of the over-all increase is due to transient ionization, reverse current dropping to a lower value if irradiation ceases - as during a reactor shutdown.

The behavior of the reverse current of individual diodes of the four base widths irradiated at 300°C are shown in Figures 12, 13, 14, and 15. A constant inverse voltage of 100 volts is assumed. Similar plots for diodes irradiated at 150°C are presented as Figures 16, 17, 18, and 19. Inverse voltages for these units are as shown on the figures. The abrupt decreases in reverse current seen in a number of the figures correspond to reactor shutdowns which occurred during a number of the longer irradiations.

IV. CONCLUSIONS

The effect of reducing the width of the base region of a diode on the radiation-induced degradation of forward characteristic of the device has been predicted on the basis of minority carrier lifetime degradation. This predicted behavior has been verified within reasonable limits by the experimental results obtained by irradiating diodes fabricated to be identical in all respects with the exception of base width.

Irradiation of a large number of these devices under conditions of strictly controlled temperature and nuclear environment indicates that their behavior under irradiation is predictable, i.e. increase in diode forward voltage drop is nearly exponential and reverse characteristics are reasonably stable. The deviation which was observed in the behavior of the forward characteristics of diodes with the same base width is probably a measure of the degree of control of base thickness possible with the alloying technique.

The possibility is thus presented of optimizing the design of semiconductor diodes and rectifiers for use in radiation fields by reducing the width of the base region to the minimum value which will maintain desired electrical characteristics. Improved control of base thickness during fabrication would additionally probably minimize deviation in behavior under irradiation among otherwise identical units. It has been mentioned that this improved degree of control is possible when junctions are formed by the diffusion process. The diffused junction device offers other additional advantages in the form of increased peak inverse voltages and the possibility of attainment of even thinner base regions. Indeed recent data^(a) obtained from the irradiation of electrically identical diffused and alloy junction diodes indicate that the diffused junction device possesses an improved radiation tolerance over the alloy variety by greater than a factor of five. From this it would seem that the optimized device for use in radiation fields may well consist of a thin base and a diffused junction.

(a) Recent as yet unpublished data obtained at GE-ANP.

REFERENCES

1. M. A. Xavier, The Behavior of Semiconductor Junction Rectifying Devices Exposed to Nuclear Radiation, Thesis, Illinois Institute of Technology, Chicago, Illinois, January, 1958.
2. J. W. Easley, Radiation Effects on Semiconductors, NARF 51-19T, FZK-9118, Vol. 4.
3. P. Rappaport, Minority Carrier Lifetime in Semiconductors as a Sensitive Indicator of Radiation Damage, Phys. Rev. 94, pp. 1409-1410, 1954.
4. J. J. Loferski, Analysis of the Effect of Nuclear Radiation on Transistors, National Conference on Aeronautical Electronics, IRE, pp. 357-363, 1957.
5. M. A. Xavier, Series of Reports, Research to Determine the Effects of Nuclear Radiation on Semiconductor Electronic Devices, AF Contract 33(616)-3776.
6. M. W. Aarons, On the Forward Characteristics of a PI Ohmic Contact Rectifiers and Its Variation with Lifetime Degradation, General Electric Advanced Semiconductor Laboratory, R58EGP26, May 27, 1958.
7. P. Rappaport and J. J. Loferski, Phys. Rev. Vol. 100, p. 126 (1955).
8. General Electric Company, Advanced Semiconductor Laboratory, unpublished results.

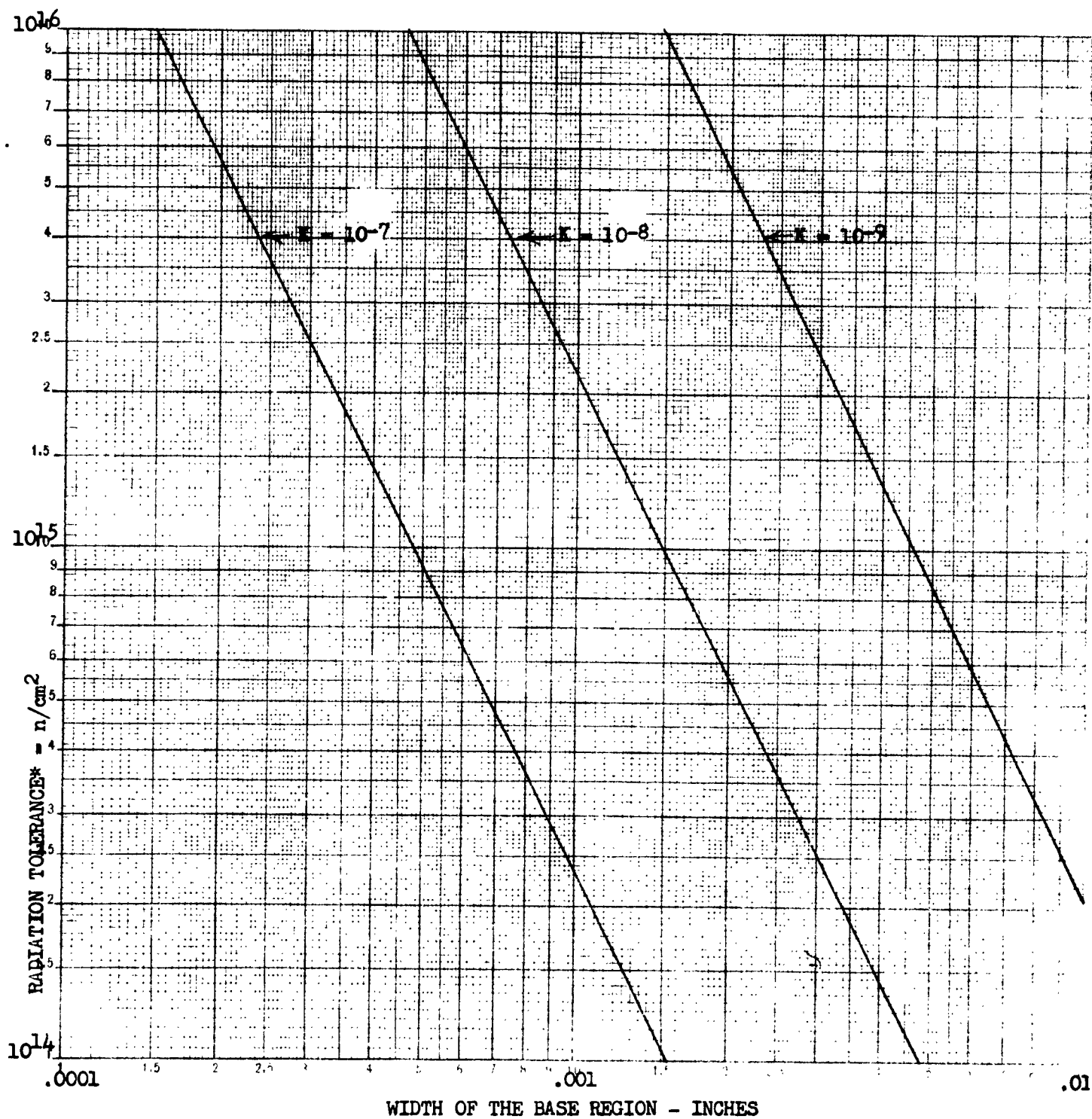


FIGURE 1

CALCULATED BEHAVIOR OF THE RADIATION TOLERANCE OF SILICON DIODES AS A
FUNCTION OF WIDTH OF THE BASE REGION

*Radiation tolerance is defined as the neutron dosage necessary to degrade E_f to 4 volts
at a forward current of 100 milliamperes.

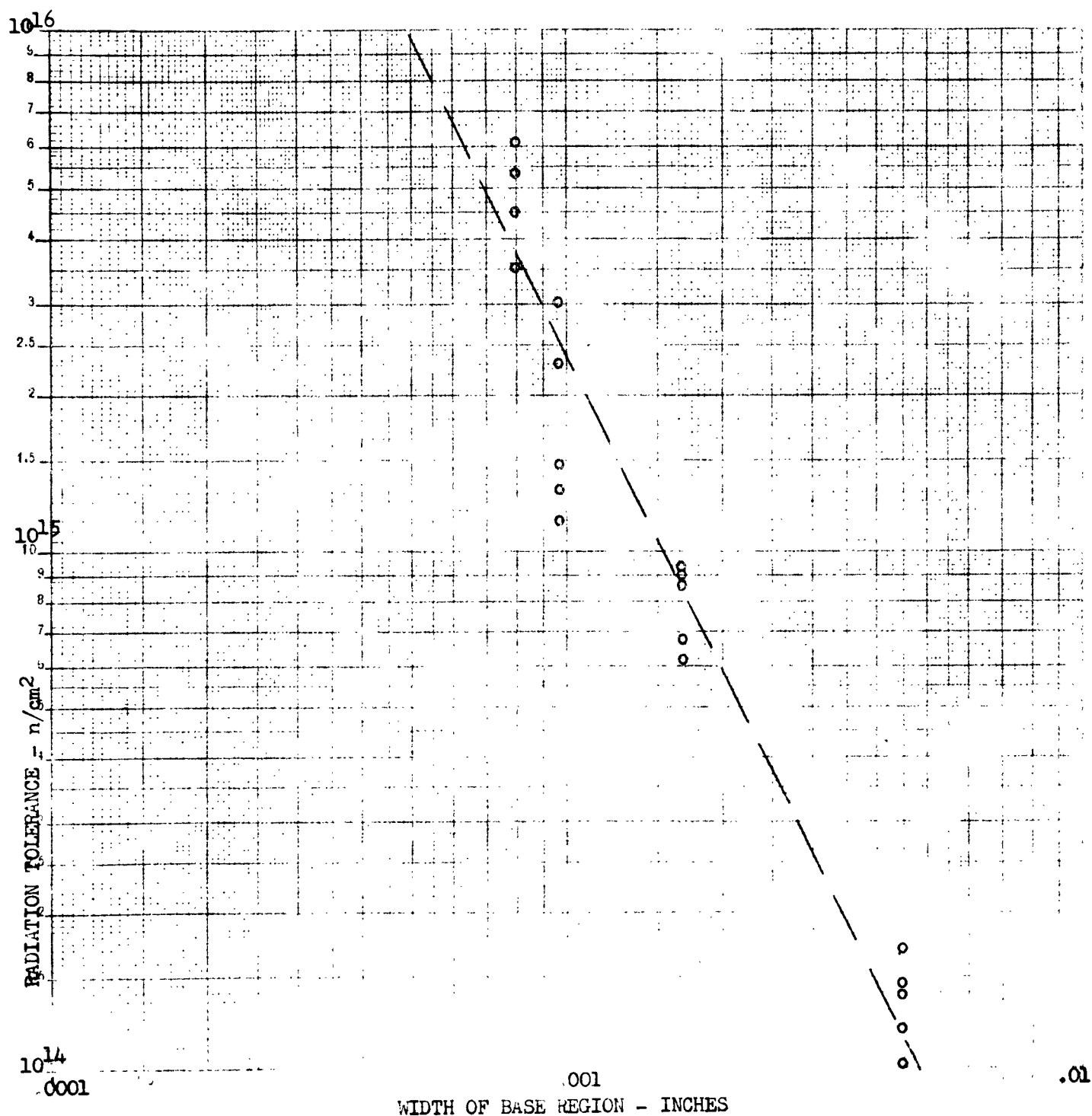


FIGURE 2
SUMMARY OF EXPERIMENTAL RESULTS - COMPARISON WITH
PREDICTED BEHAVIOR

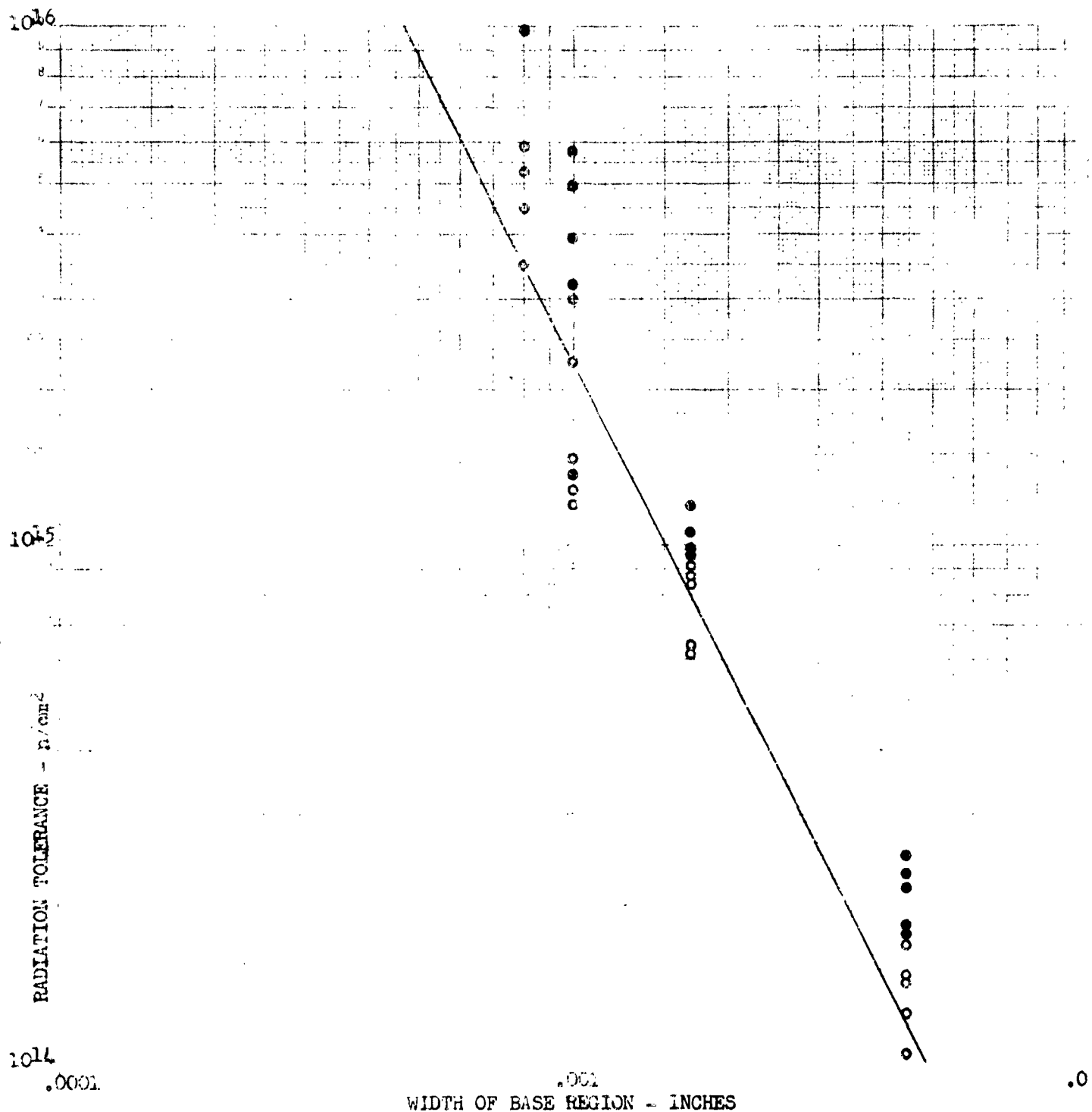
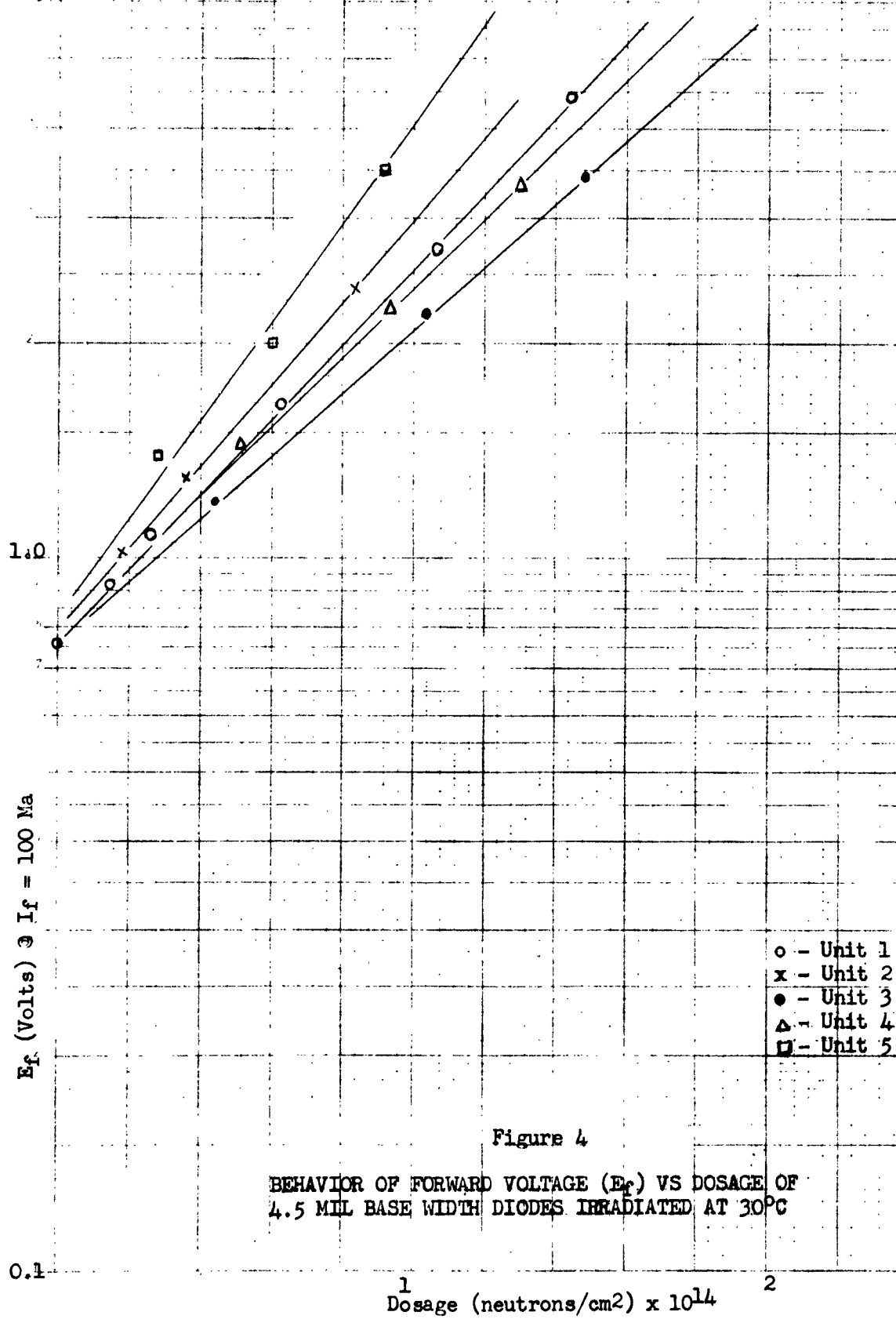
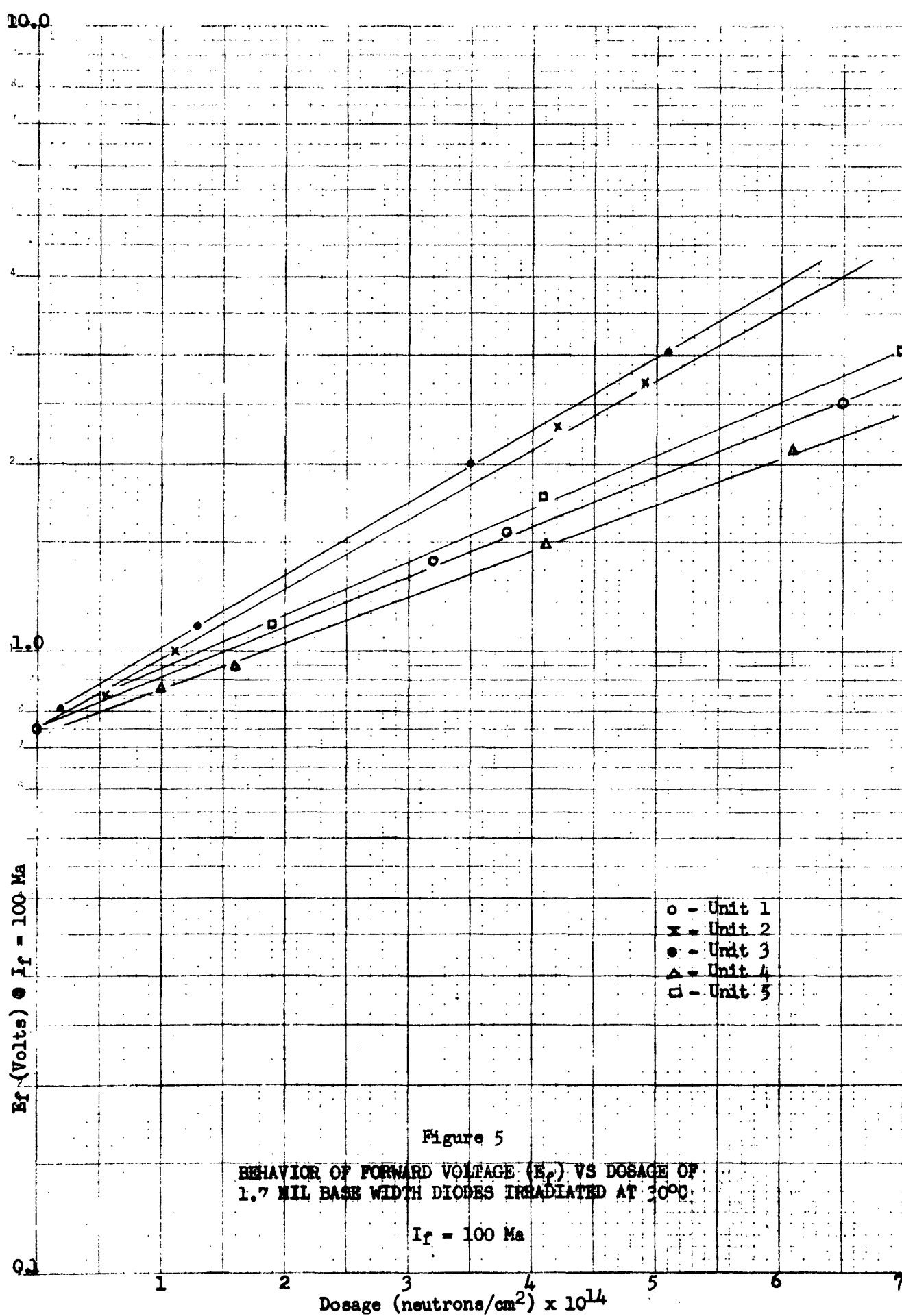


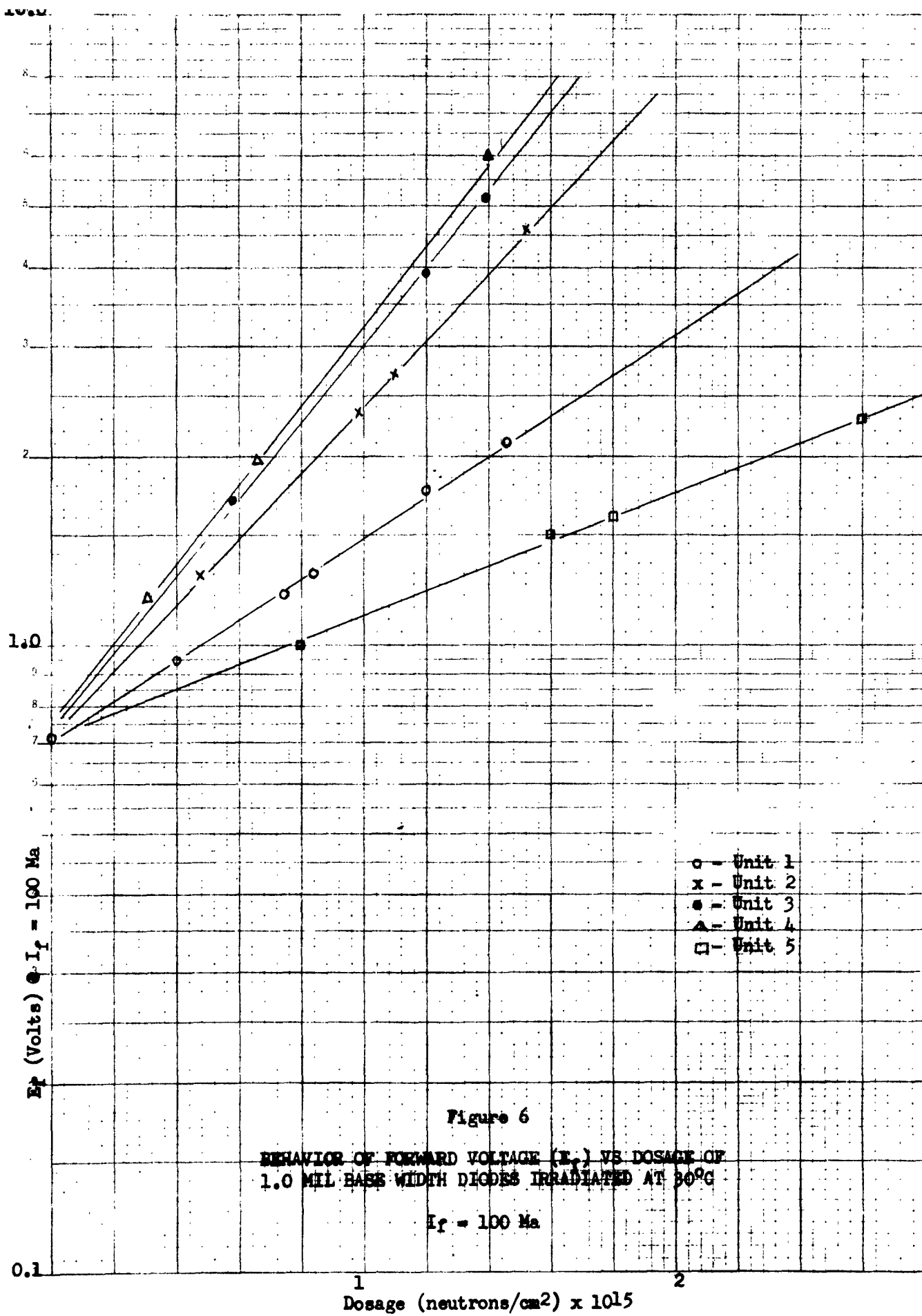
FIGURE 3

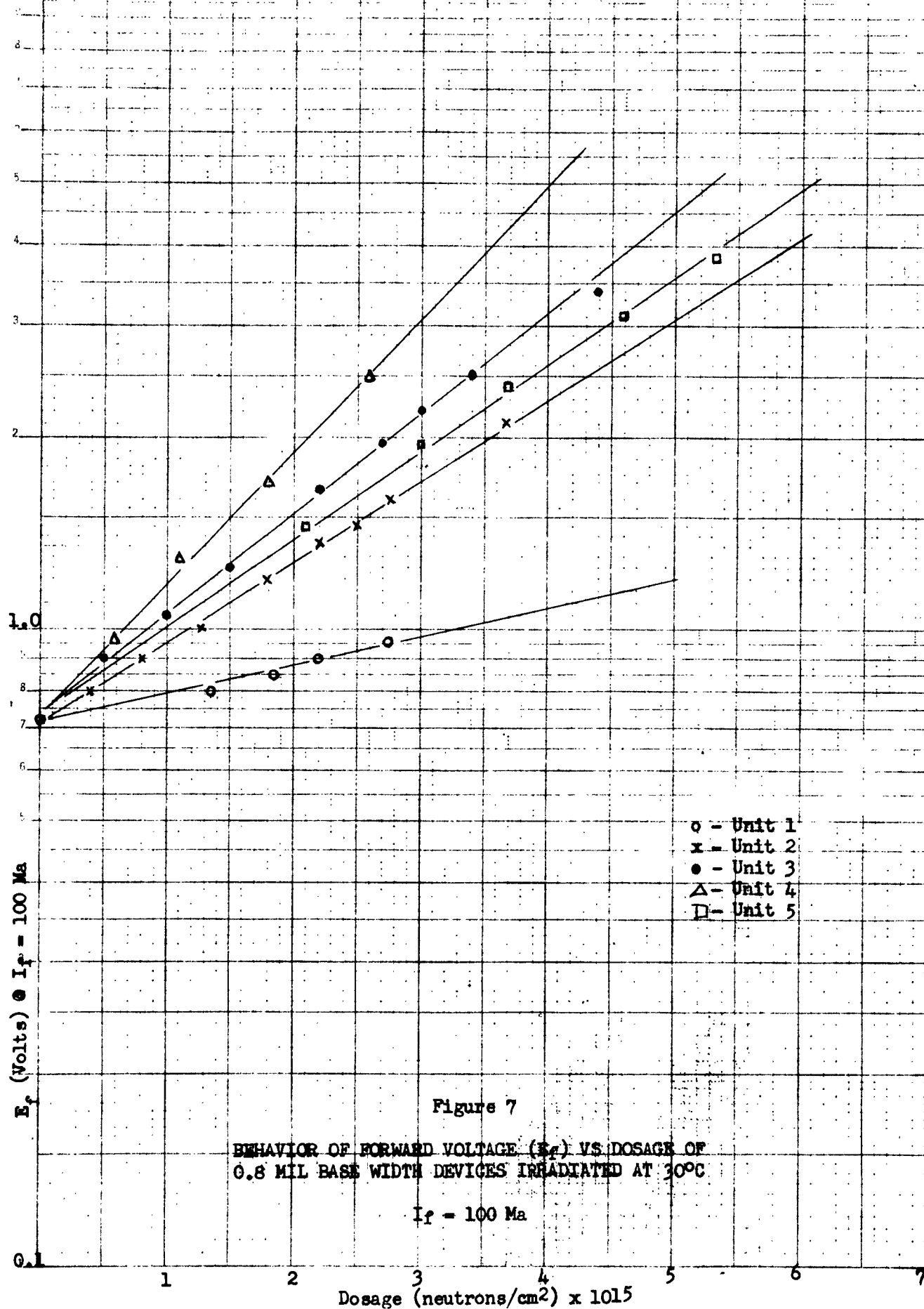
EFFECT OF IRRADIATION AT ELEVATED TEMPERATURE ON THE RADIATION TOLERANCE OF SILICON DIODES

- = Irradiated at 30°C
- = Irradiated at 150°C

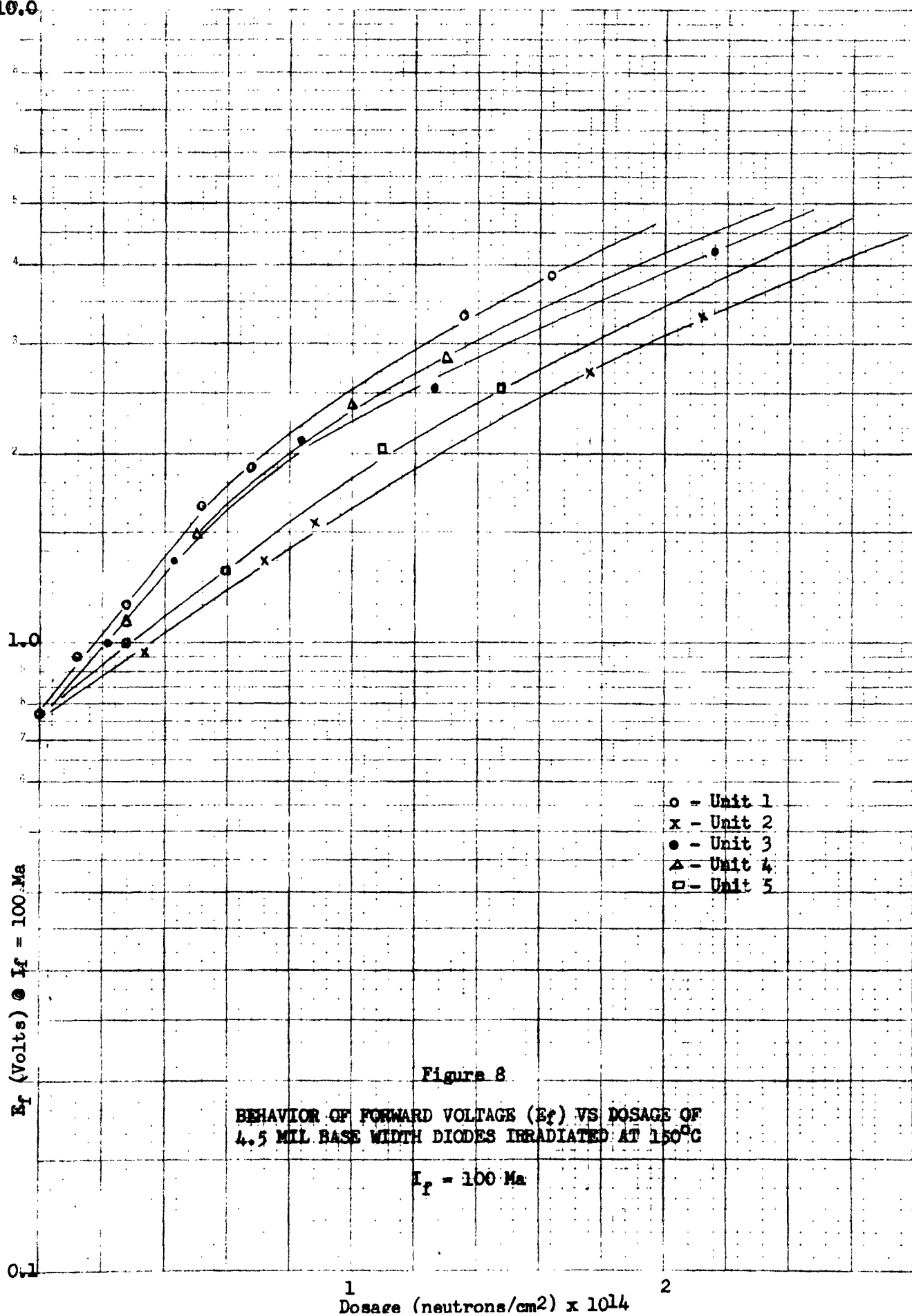


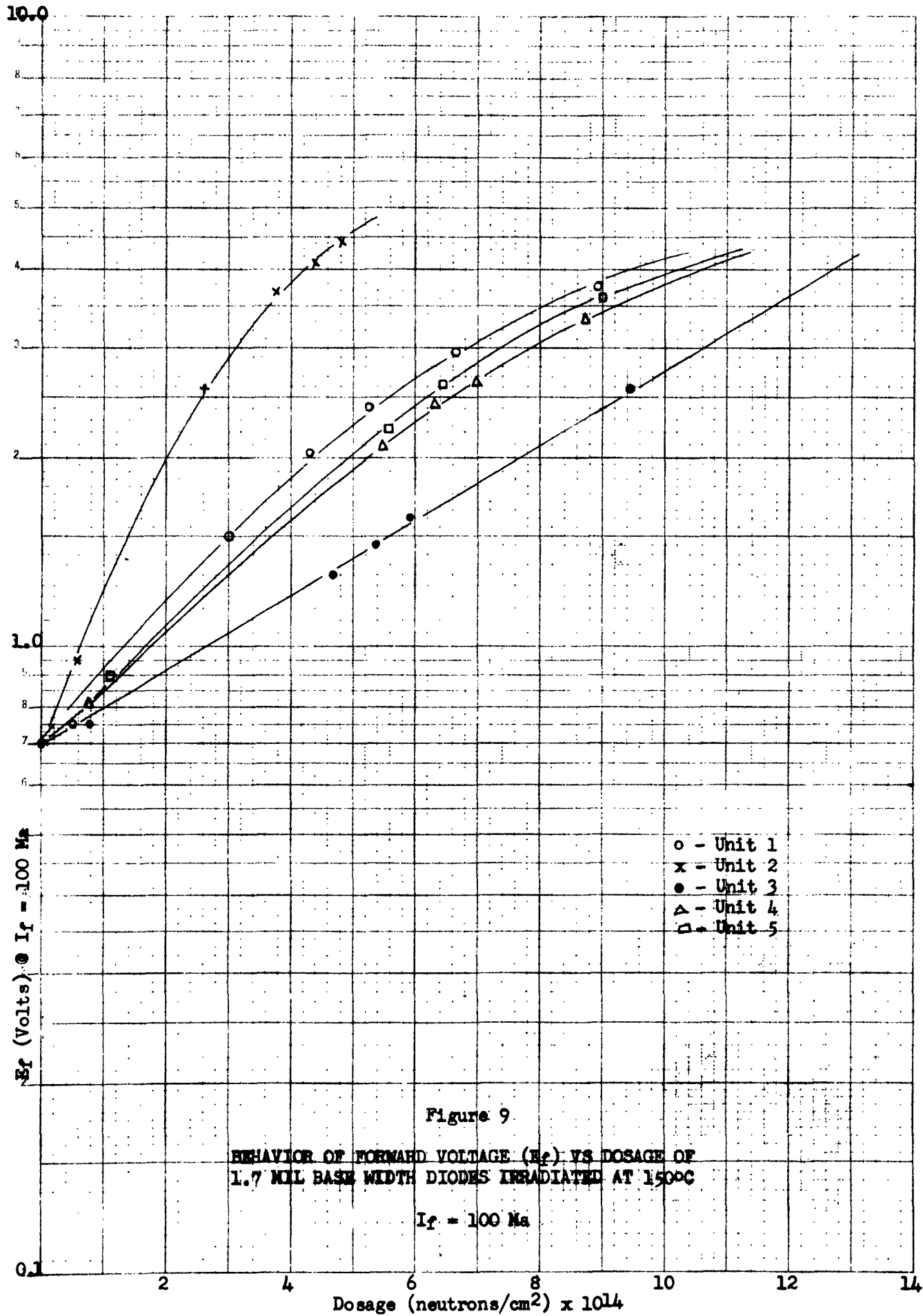






10.0





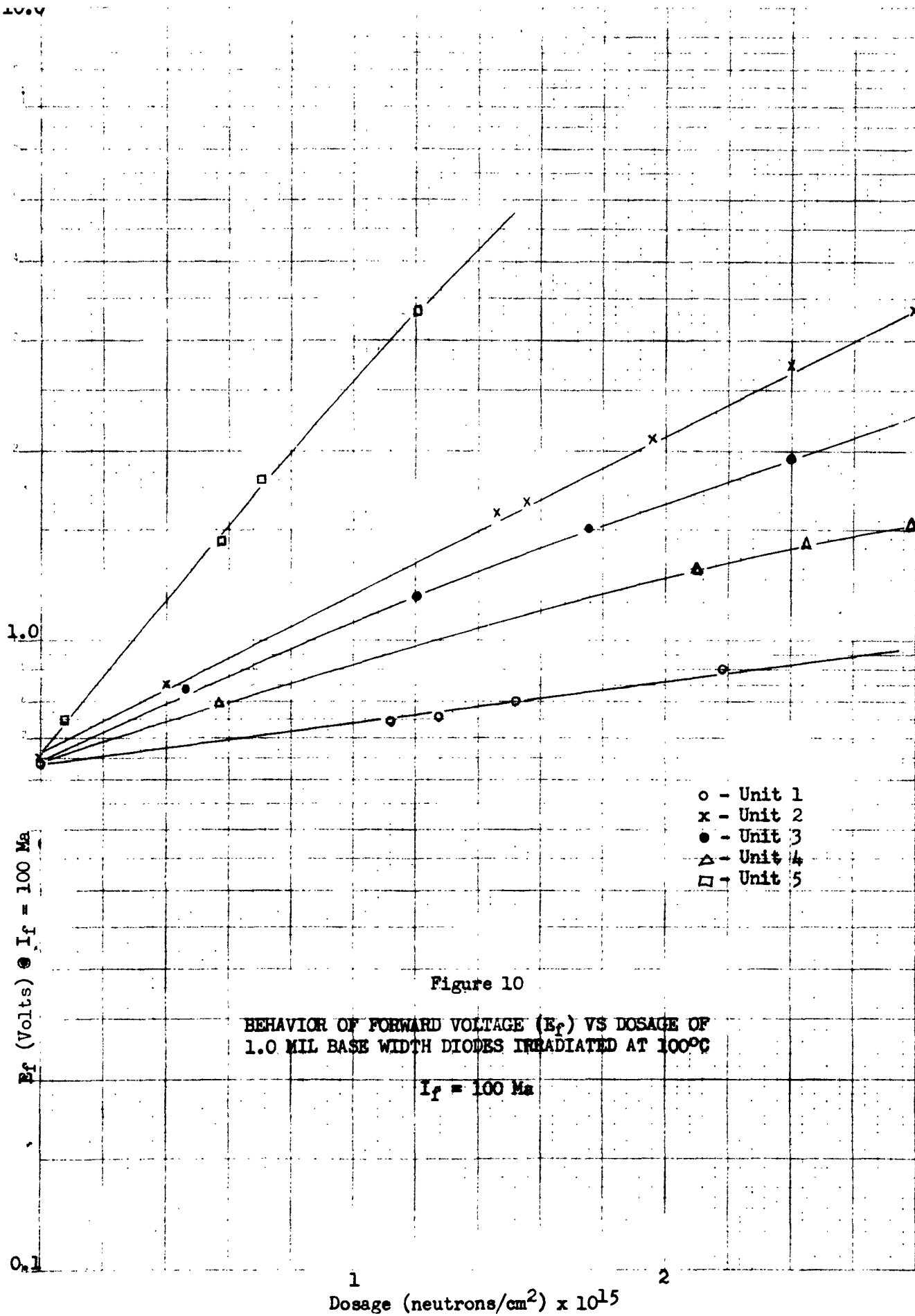
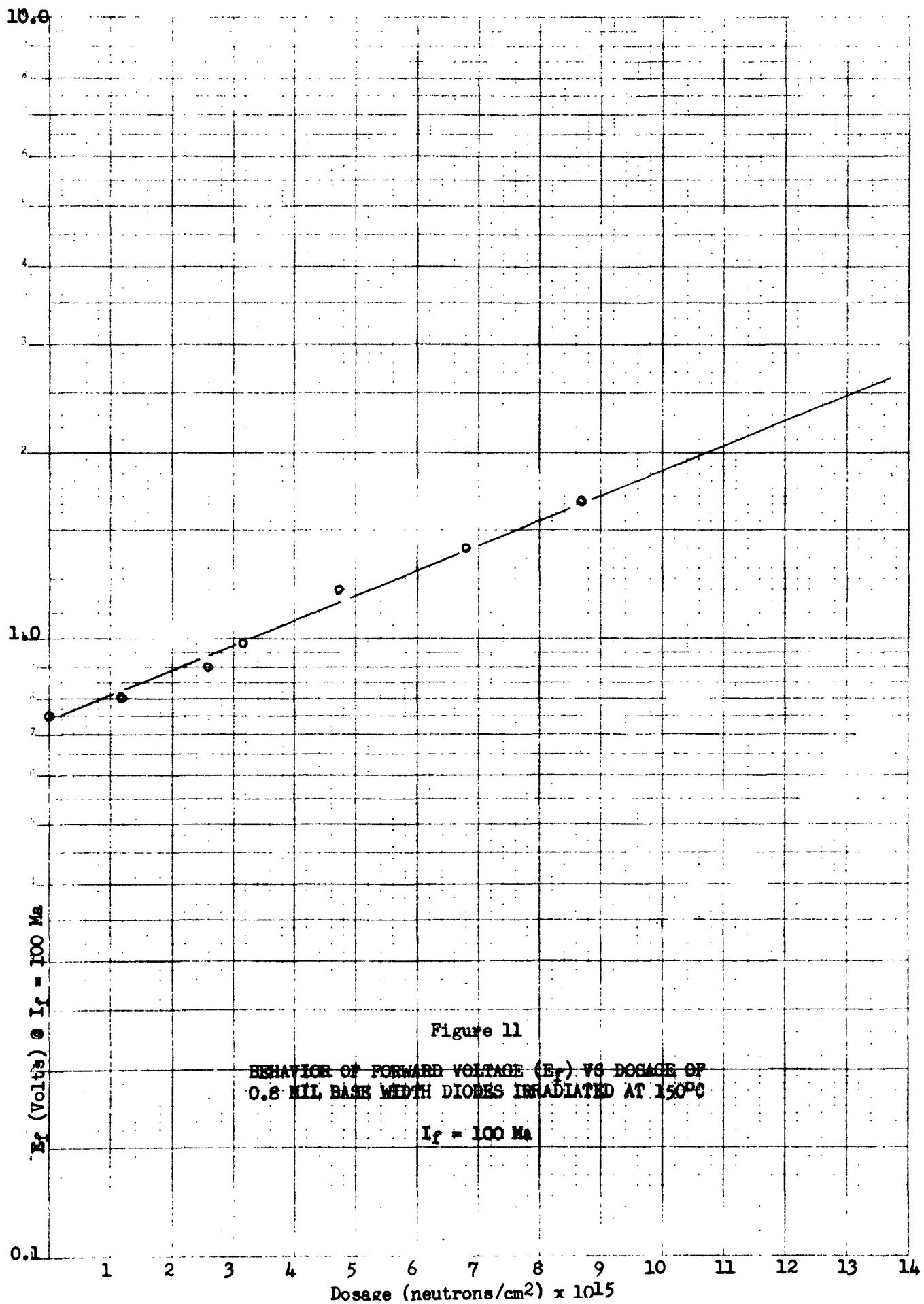


Figure 10

BEHAVIOR OF FORWARD VOLTAGE (E_f) VS DOSAGE OF
1.0 MIL BASE WIDTH DIODES IRRADIATED AT 100°C

$I_f = 100 \text{ Ma}$



10.0

Figure 12

BEHAVIOR OF REVERSE CURRENT (I_R) VS DOSAGE OF
4.5 MIL BASE WIDTH DIODES IRRADIATED AT 30°C

 $E_R = 200V$

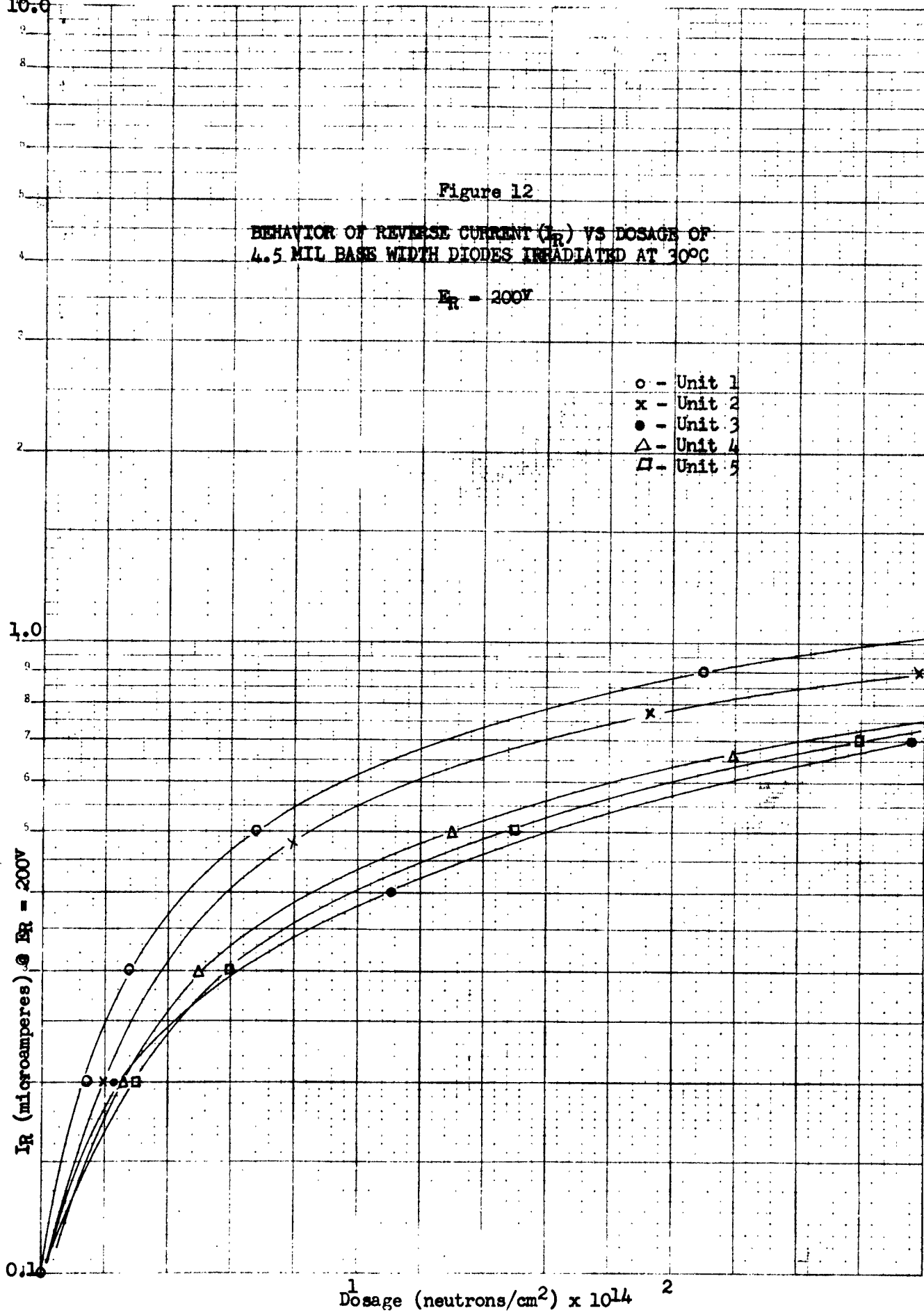
- - Unit 1
- x - Unit 2
- - Unit 3
- △ - Unit 4
- - Unit 5

1.0

 I_R (microamperes) @ $E_R = 200V$

0.10

Dosage (neutrons/cm²) x 10¹⁴ 2



10.0

Figure 13

BEHAVIOR OF REVERSE CURRENT (I_R) VS DOSAGE OF
1.7 MIL BASE WIDTH DIODES IRRADIATED AT 30°C

 $E_R = 100V$

○ - Unit 1
x - Unit 2
● - Unit 3
△ - Unit 4
□ - Unit 5

1.0

 I_R (microamperes) $E_R = 100V$

0.1

2

4

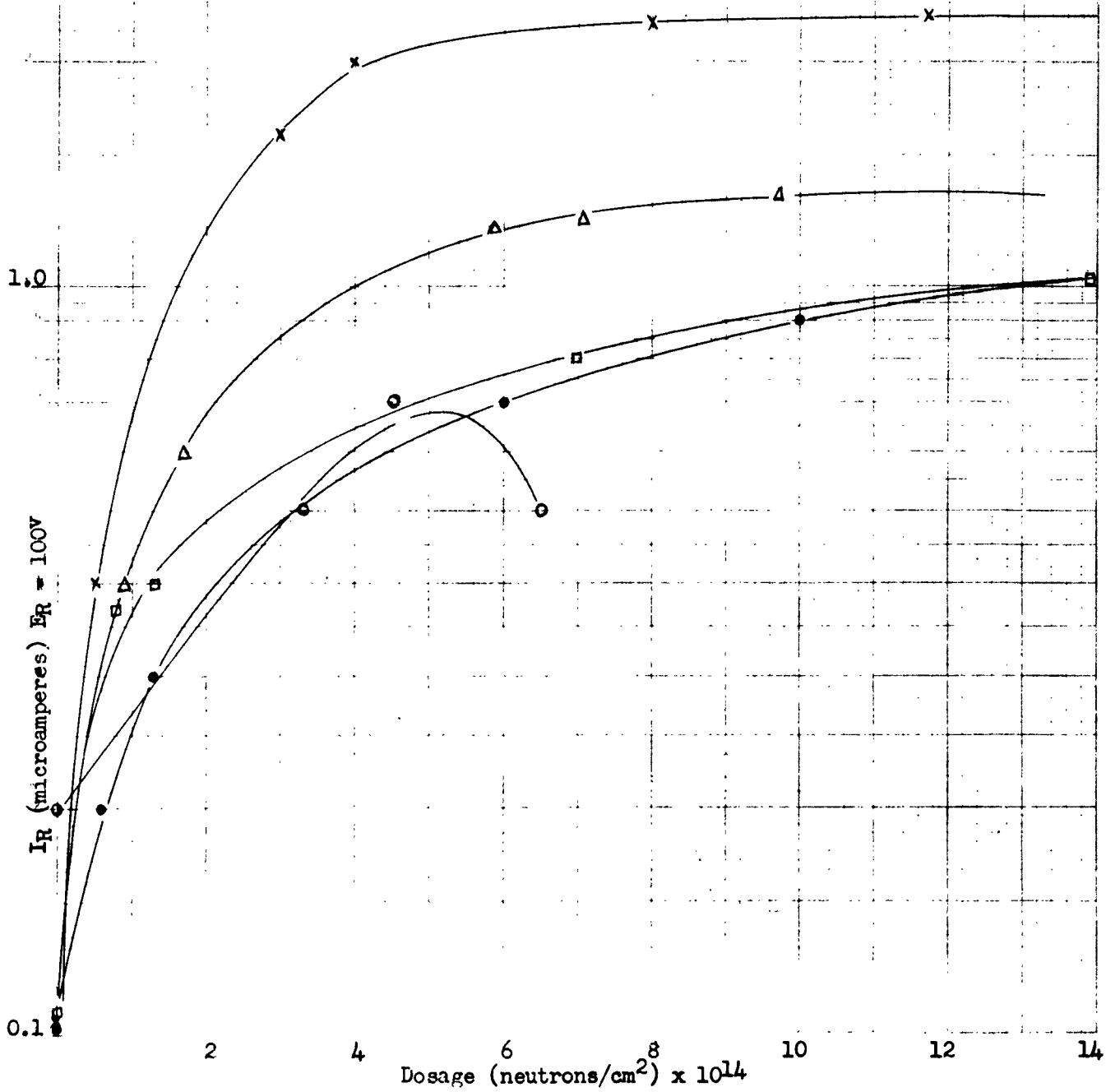
6

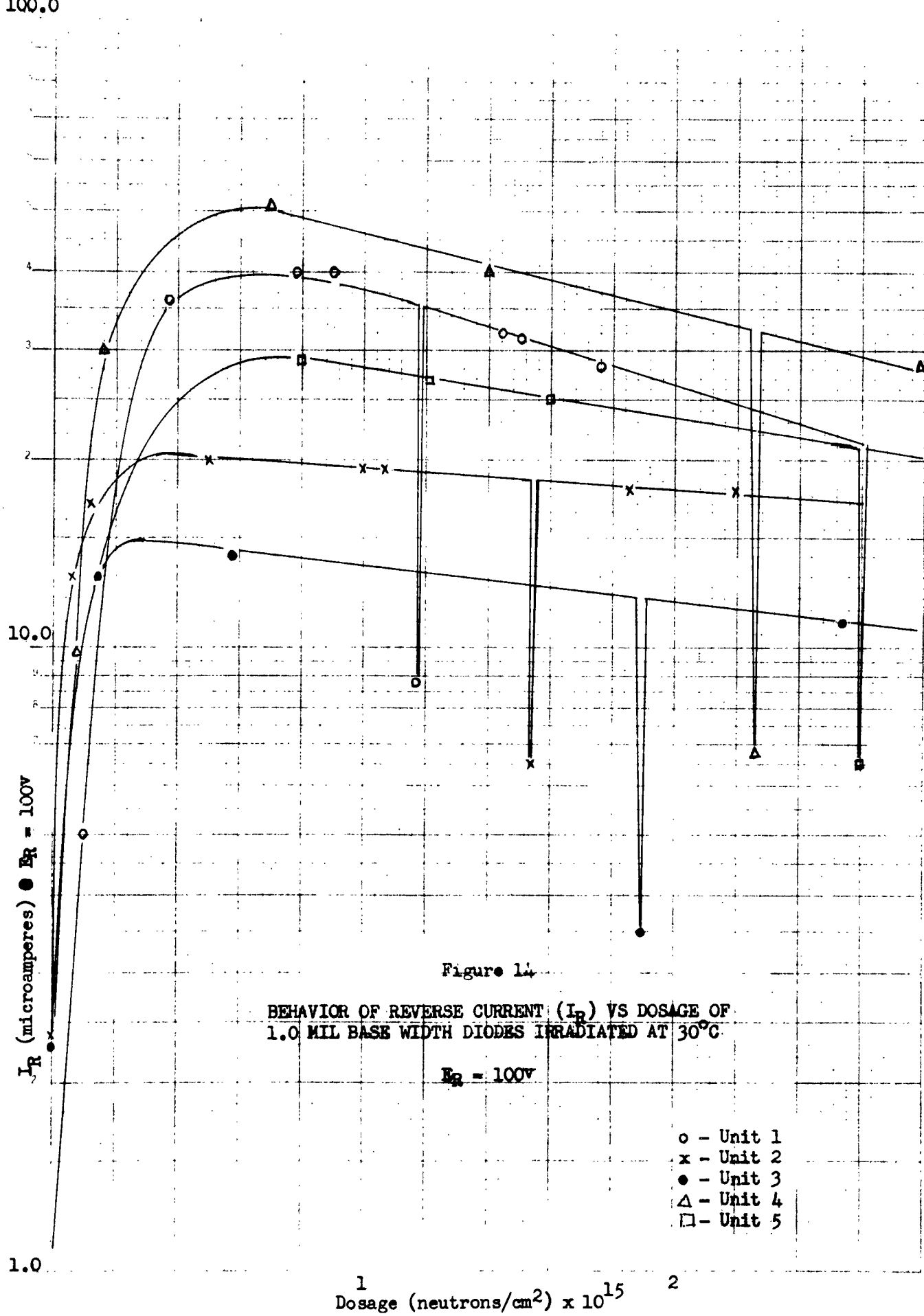
8

10

12

14

Dosage (neutrons/cm²) x 10¹⁴



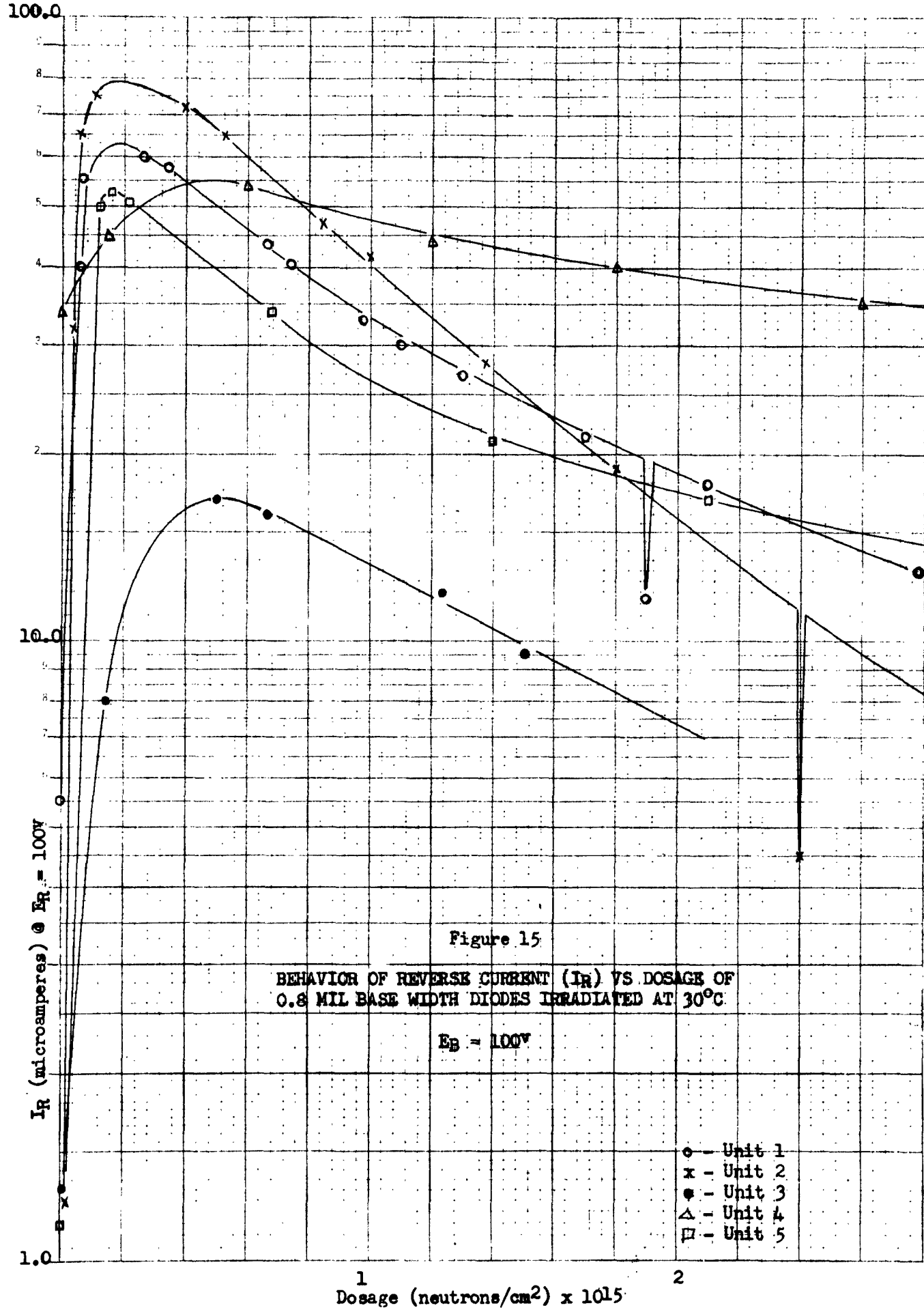
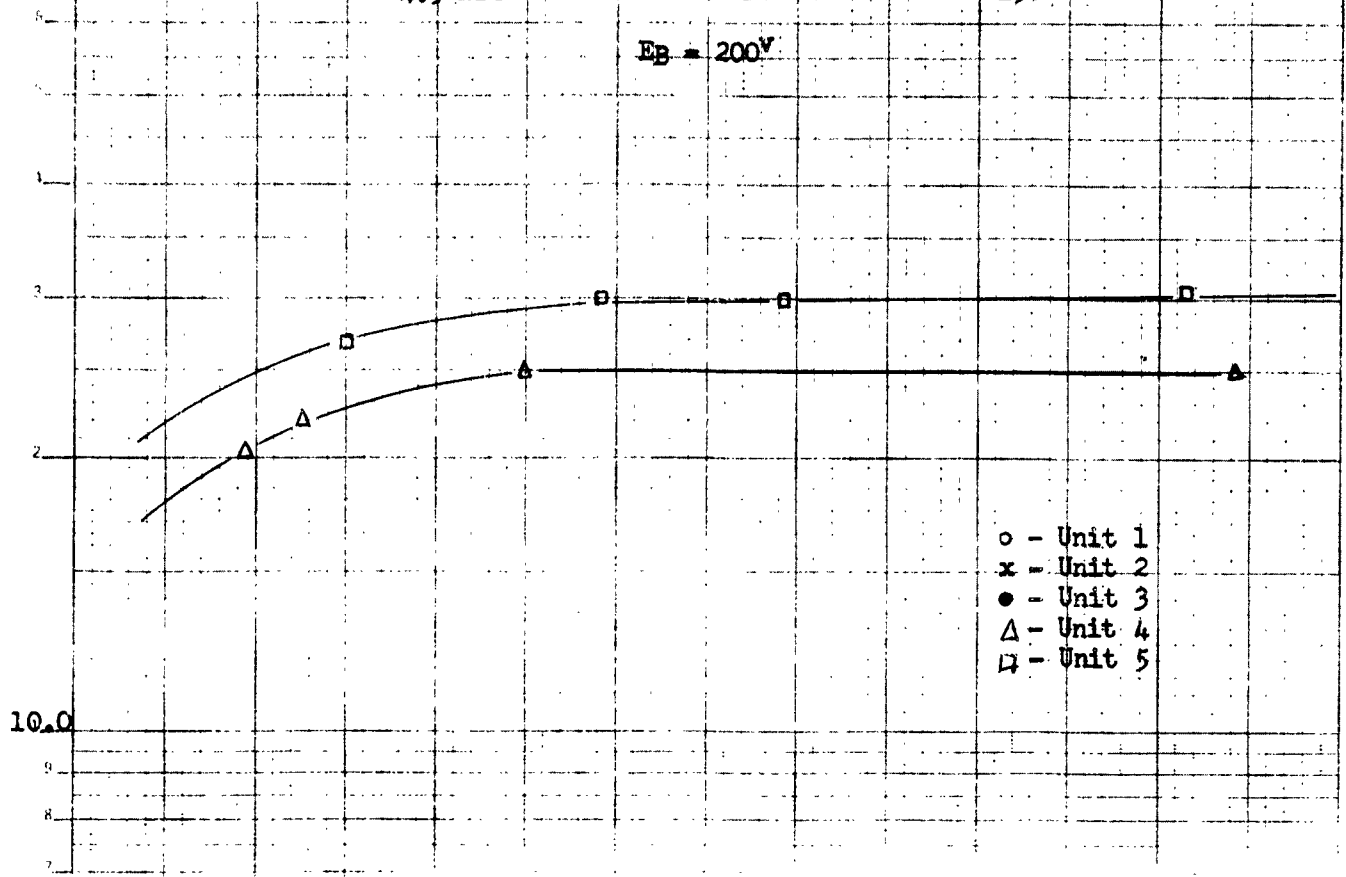


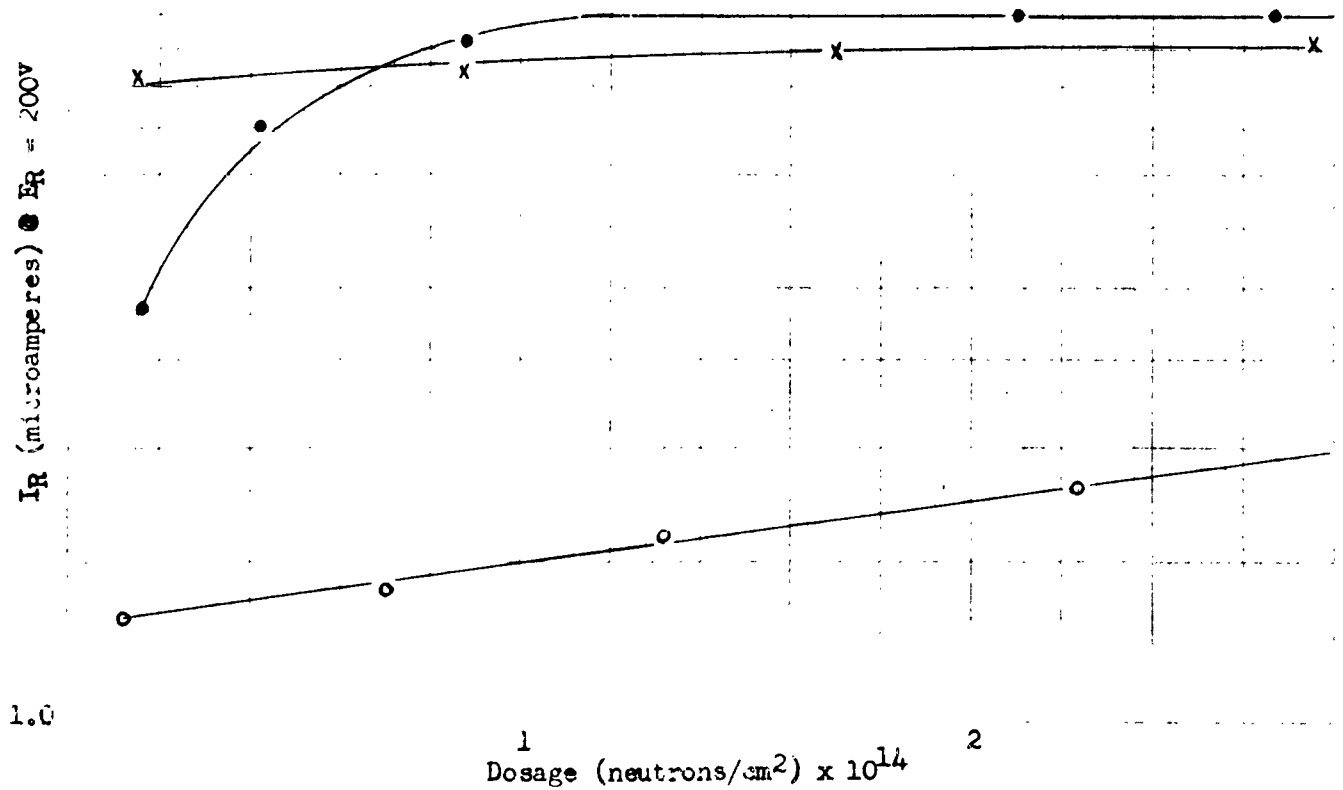
Figure 16

BEHAVIOR OF REVERSE CURRENT (I_R) VS DOSAGE OF
4.5 MIL BASE WIDTH DIODES IRRADIATED AT 150°C

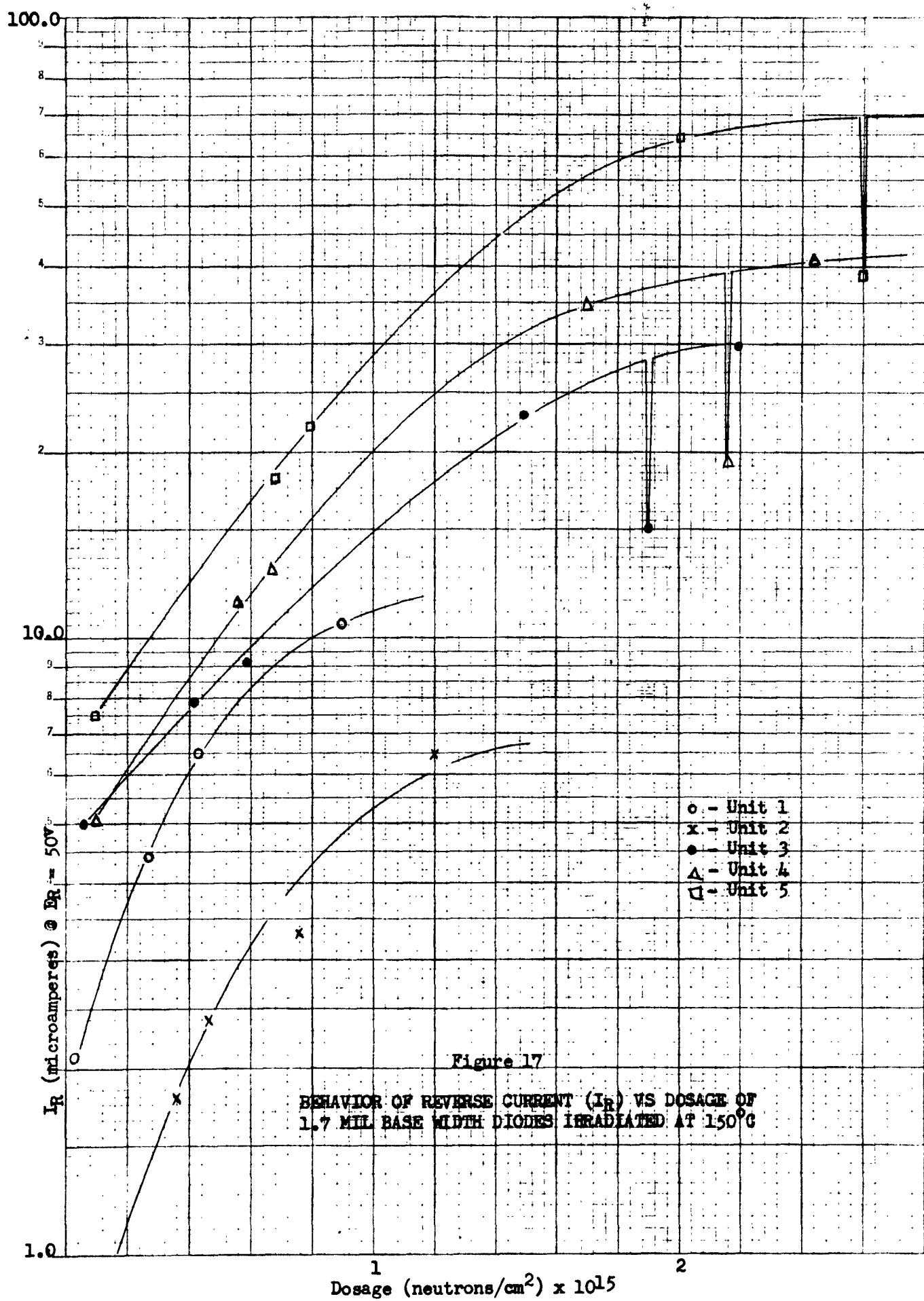
$E_B = 200V$



I_R (microamperes) ● $E_B = 200V$



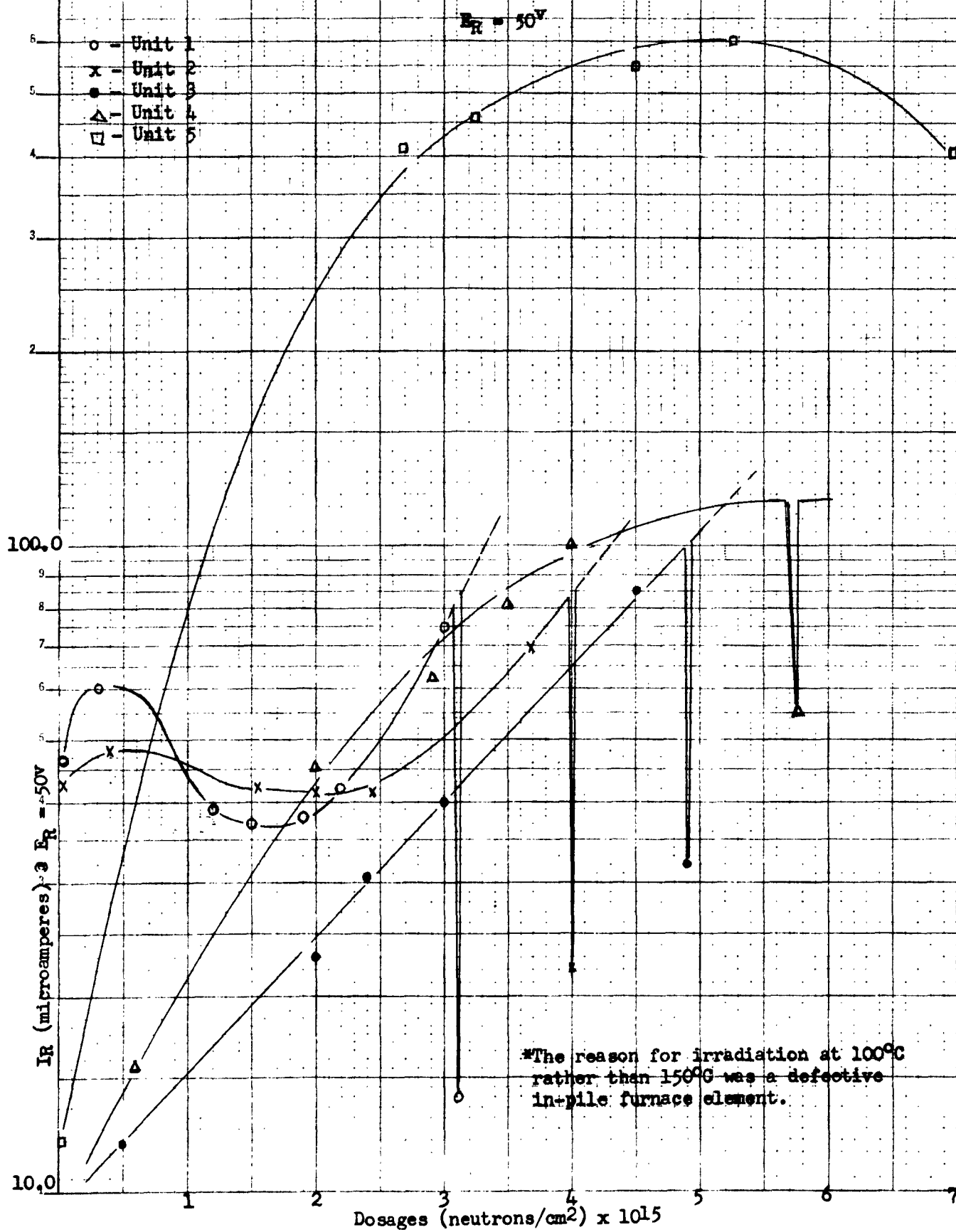
Dosage (neutrons/cm²) $\times 10^{14}$

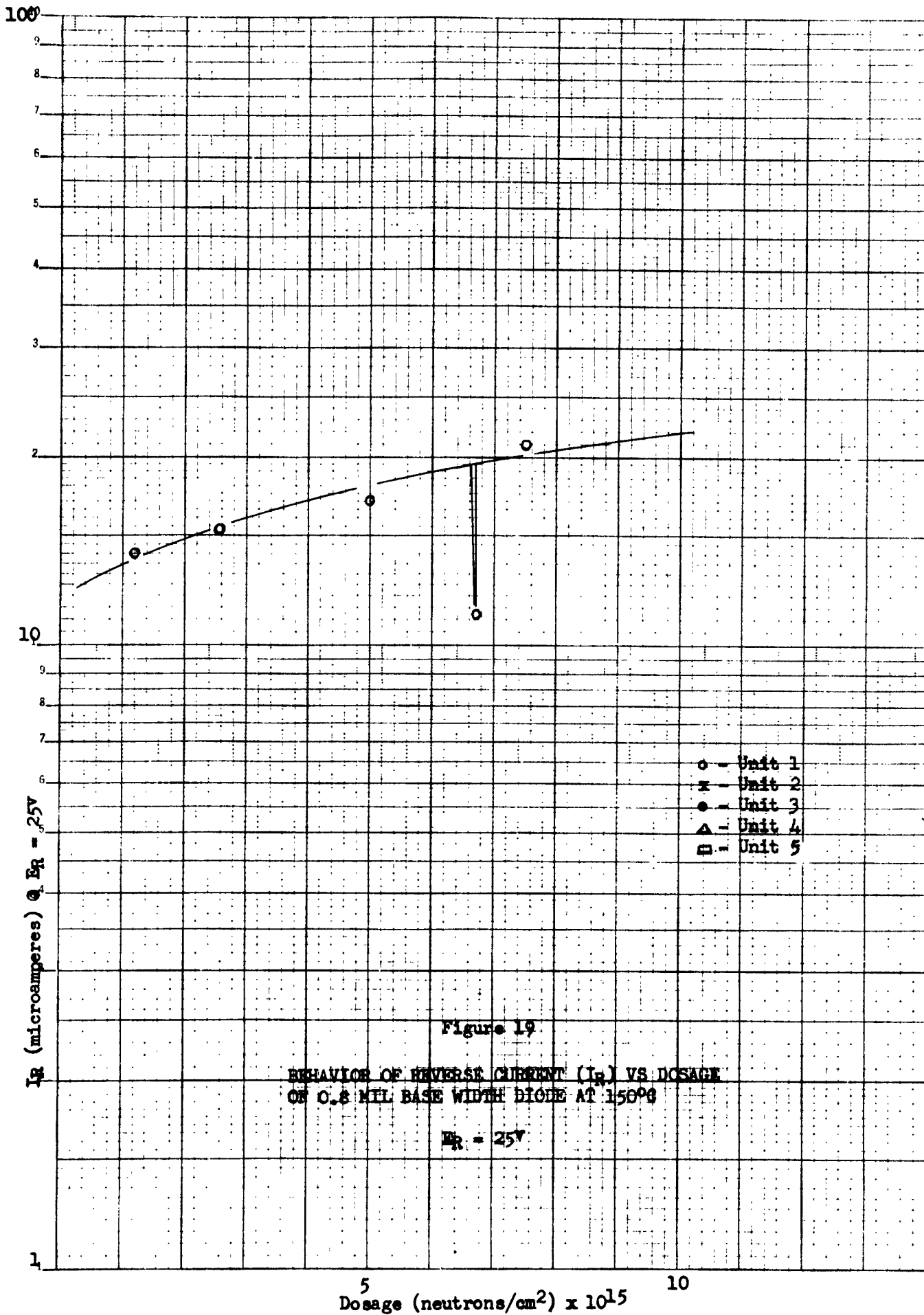


1000.0

Figure 18

BEHAVIOR OF REVERSE CURRENT (I_R) VS DOSAGE OF
1.0 MIL BASE WIDTH DIODES IRRADIATED AT 100°C*





THE EFFECT OF NUCLEAR RADIATION ON COMMERCIAL SILICON DIODES

by

John R. Crittenden

General Electric Company
Aircraft Nuclear Propulsion Department
Cincinnati 15, Ohio

Several types of commercial silicon diodes were irradiated to 10^{16} NVT ($E_n > 0.58$ ev) in the Brookhaven Reactor at 25°C and at 150°C . The forward and reverse characteristics of each diode were photographed periodically from an oscillographic display during the irradiation period. Noise and switching time measurements were also accomplished. The results of this work indicate that electrically similar diodes vary in their response to nuclear radiation and that the response to nuclear radiation is temperature dependent.

INTRODUCTION

The purpose of this paper is to present the results of a study made by the American Nuclear Science Corporation under subcontract to the General Electric Aircraft Nuclear Propulsion Department. The work was performed at the Brookhaven National Laboratory.

The objective of the subcontract was to obtain information about the effects of temperature and nuclear radiation on the performance of various silicon diodes. The diodes were purchased from commercial stock to permit the evaluation of presently available devices for operation in a nuclear environment. Of particular interest was the effect of high temperature and nuclear radiation on the forward and reverse functions of the diode, the switching characteristics, and the noise characteristics.

After initial investigation of the various irradiation facilities in the reactor, a one inch facility (hole W-13) and two four inch facilities (holes W-12 and W-14) were chosen. The position for all experiments was ten feet into the reactor from the shield face. The ambient temperature there was about 25°C . The flux levels and spectra were such that the rates of radiation effects were sufficiently slow to make observation easy and yet fast enough for considerable diode damage to occur within a reasonably short period.

In order to determine the radiation environment a series of neutron flux and gamma-ray measurements were made. The values of neutron flux were obtained by activation of gold, cobalt, and sulfur foils. Gamma-ray intensity was determined by measuring the induced oxidation of ferrous to ferric ions. Sample flux values and the cadmium ratio, as measured at the position for diode irradiation in W-12, are given in Table I for a constant reactor power of 15 Mw. The flux values for the other two holes were comparable and in each hole varied approximately 10% over the length of the experimental assembly.

TABLE I

Thermal neutron flux: 5.1×10^{11} n/cm ² -sec
Resonance (epicadmium) neutron flux ($0.57 \text{ ev} \leq E_n \leq 1 \text{ Mev}$): 2.6×10^{10} n/cm ² -sec
Fast neutron flux ($1 \text{ Mev} \leq E_n \leq 2 \text{ Mev}$): 2.2×10^8 n/cm ² -sec
Fast neutron flux ($E_n > 2 \text{ Mev}$): 3.3×10^8 n/cm ² -sec
Gamma-ray intensity: 2.7×10^4 r/hr
Cadmium ratio: 20

Unless otherwise stated, all neutron flux values (nv) or integrated neutron flux values (nvt) given in this report refer to epicadmium (resonance) neutrons.

In the course of this study eleven types of commercial silicon junction diodes were irradiated. Life tests lasting one thousand hours were performed for five types of diodes. See Table II, page 3.

The diodes to be irradiated were mounted on a suitable material, such as polyethylene or micarta, and enclosed in aluminum containers. For the 150°C experiments the diode assemblies were placed in a furnace equipped with temperature controls. The measurement of forward and reverse characteristics was accomplished by curve tracing circuits which displayed the characteristic curves on an oscilloscope. The characteristic curves of the various diodes being irradiated were displayed and photographed in succession by an automatic switching and recording system.

DISCUSSION

In the interest of brevity, only a few of the some 40,000 data have been selected. Figure I illustrates the change in Forward Voltage Drop of all diodes observed as integrated flux increases. The characteristics shown represent the most rapid change observed.

The Forward Voltage Drop data was taken from curves such as those of Figure II. In this slide four different 1N538 histories are shown, two from experiment number six and two from experiment number seven. Although there is a scale change between the two sets of data, a comparison is possible. The curves labeled "E" in the left hand data are for almost the same integrated flux as the curves labelled "L" in the right hand data. Note the variations in the changes.

In the diode described by the upper left characteristic, there is a region of instability, apparently a discontinuity in the trace. A later slide will illustrate the action of this region. Similar regions were seen in many of the diodes tested, but no correlation was found. The club shaped lines were caused by a hysteresis effect.

The unusually high peak inverse voltage capability of the two 1N538 devices is not fully understood. About six percent of the 1N538's received did not exhibit a knee in the reverse direction to 500 volts applied.

The lower right history is not at all unusual. It is representative of a large number of the diodes tested. Careful observation will reveal that the back characteristic reverses its

direction of change and then loses the knee as integrated flux increases. At the end of irradiation, as shown by the nearly horizontal curve, the device is a resistor.

TABLE II - TYPES AND QUANTITIES OF DIODES IRRADIATED

Manufacturer Type		At 25°C			At 150°C			
		Number Tested	Total Integrated Epicadmium Neutron Flux	Bench Test	Number Tested	Total Integrated Epicadmium Neutron Flux	Bench Test	
General Electric	IN538	3	7.6 × 10 ¹⁵	X	2	2.5 × 10 ¹⁶	X	
		3	1.1 × 10 ¹⁶		2	2.3 × 10 ¹⁶		
	4JA60B	4	2.1 × 10 ¹⁶		2	1.1 × 10 ¹⁶		
Raytheon	IN303A	3	7.6 × 10 ¹⁵	X	2	2.5 × 10 ¹⁶	X	
		3	1.1 × 10 ¹⁶		2	2.3 × 10 ¹⁶		
	CK776	4	2.1 × 10 ¹⁶		2	1.1 × 10 ¹⁶		
Hughes	6006	3	8.6 × 10 ¹⁵	X	2	2.5 × 10 ¹⁶	X	
		2	1.9 × 10 ¹⁶		2	2.3 × 10 ¹⁶		
	6007	3	7.6 × 10 ¹⁵	X	2	2.5 × 10 ¹⁶	X	
		3	1.1 × 10 ¹⁶		2	2.3 × 10 ¹⁶		
Hoffman	IN212	3	8.6 × 10 ¹⁵	X	3	2.5 × 10 ¹⁶	X	
		3	1.9 × 10 ¹⁶		2	2.3 × 10 ¹⁶		
	IN430B	4	2.1 × 10 ¹⁶		2	1.1 × 10 ¹⁶		
Transitron	TJ10A	3	8.6 × 10 ¹⁵		2	2.5 × 10 ¹⁶		
		2	1.9 × 10 ¹⁶		2	2.3 × 10 ¹⁶		
	IN336	6	1.9 × 10 ¹⁶		2	2.5 × 10 ¹⁶		
					2	2.3 × 10 ¹⁶		
	IN339	6	1.9 × 10 ¹⁶		2	2.5 × 10 ¹⁶		
					2	2.3 × 10 ¹⁶		

Figure III shows the characteristics of several IN212 diodes. Again note the variation from unit to unit. This diode is rated for much lower current and inverse voltages than the IN538. It does illustrate the improvement which can be obtained by using the suggested techniques for increasing radiation tolerance such as thin base-width.

Note also the different failure mechanism -- that of falling-over versus that of walking out.

Figure IV illustrates the response at 150°C of both diode types. Careful observation will show that the forward resistance did not increase quite so rapidly as it did at 25°C. In the

IN538 histories there is a scale change as the reverse current readings at high integrated flux levels were made on the same scale as the forward current readings.

Note the normal effect of temperature changes on both diode types as illustrated by the curves "H", "J", and "K". As the temperature was lowered after irradiation, the forward resistance increased and the back current decreased only to return to the same values when the temperature was raised to its original level. There was no noticeable annealing at these temperatures.

To make the data resulting from this study more easily compared with other studies, Figure V shows the Forward Voltage Drop at a constant current for each of several diodes, both IN212 and IN538 types, at 25°C and 150°C. Note the variation from unit to unit, both initial and radiation induced.

Figure VI shows some data on the often neglected reverse current characteristic. The data again illustrates the unit to unit variation although the IN212 reverse characteristic was apparently unchanged at 25°C to 10^{16} nvt and greater.

Noise measurements were made in the 100 cps to 1000 cps band before and after irradiation. The amplification factor was 10^6 and the signal was observed on an oscilloscope. Pre-irradiation experiments could detect no signal from the diode samples. Post-irradiation data are shown in Figure VII.

An investigation of the discontinuity region illustrated in Figure I revealed an oscillatory condition. Figure VIII describes the experiment.

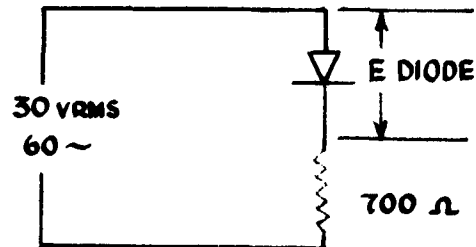
As has been determined by many investigators, and presented here for the sake of completeness, the switching time does decrease as shown in Figure IX.

CONCLUSION

The response of silicon diodes to nuclear irradiation was found to vary greatly among diodes, even those of the same type. A few general observations, however, can be made. The results showed that radiation invariably increased the forward resistance of a diode. This effect was more pronounced at 25°C than at 150°C. The behavior in the reverse direction did not follow any regular pattern. It can be said, though, that at room temperature the reverse current usually increased as a function of integrated neutron flux. In some instances a partial recovery was noted as the integrated flux continued to increase. The normally larger reverse currents at 150°C increased considerably more upon exposure in the reactor. Switching time of diodes invariably decreased with irradiation, and post-irradiation measurement of diode noise indicated that the noise level had increased and varied greatly among diodes, from microvolts to millivolts, irrespective of diode type.

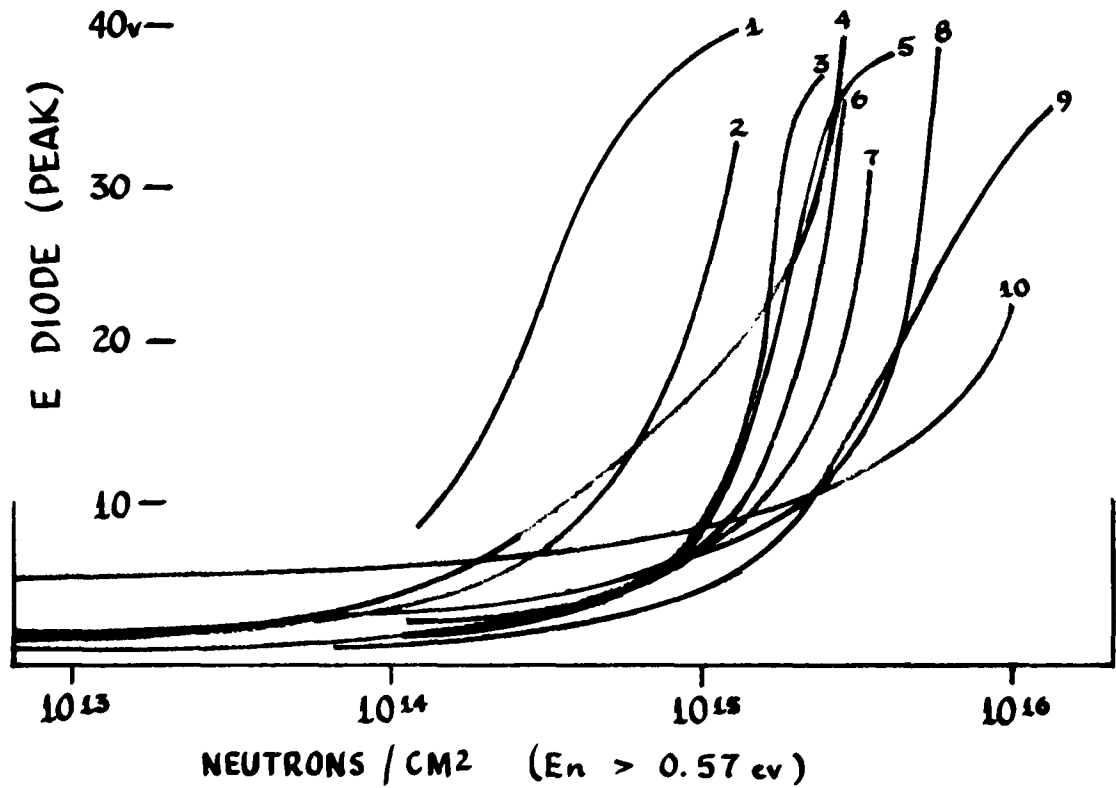
Figure I

FORWARD VOLTAGE DROP VS. NVT



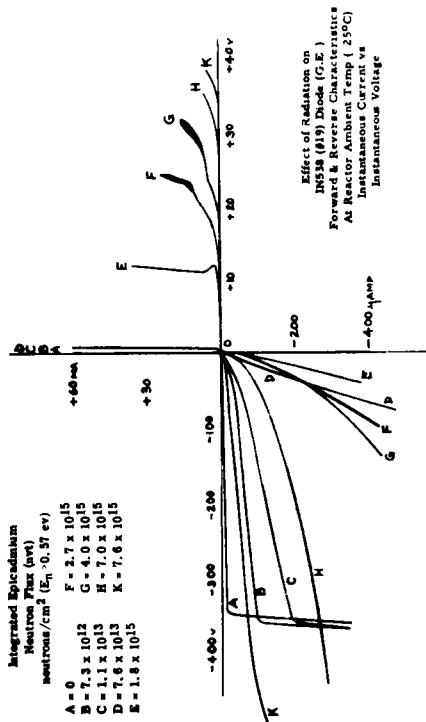
1 ~ IN339
2 ~ TJ10A
3 ~ IN336
4 ~ 6007
5 ~ CK776

6 ~ IN538
7 ~ 6006
8 ~ IN303A
9 ~ 4JA60B
10 ~ IN212



Integrated Episcadum
Neutron Flux (nvt)
neutrons/cm² (E_n = 0.57 ev)

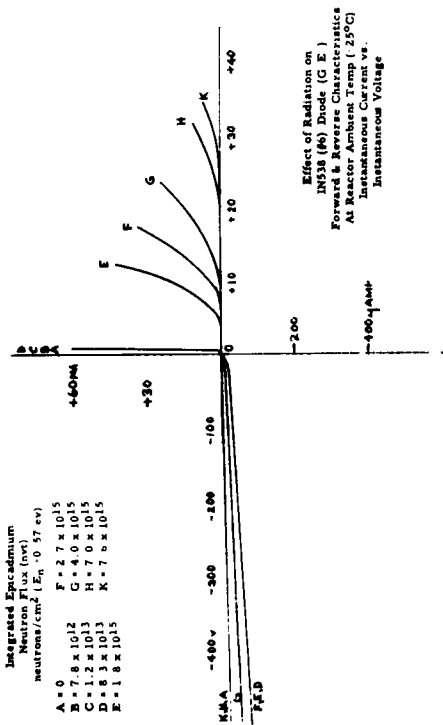
A = 0
B = 7.3 x 10¹²
C = 1.1 x 10¹³
D = 7.6 x 10¹³
E = 1.8 x 10¹⁵
F = 2.7 x 10¹⁵
G = 4.0 x 10¹⁵
H = 7.0 x 10¹⁵
K = 7.6 x 10¹⁵



RADIATION EXPERIMENT #6

Integrated Episcadum
Neutron Flux (nvt)
neutrons/cm² (E_n = 0.57 ev)

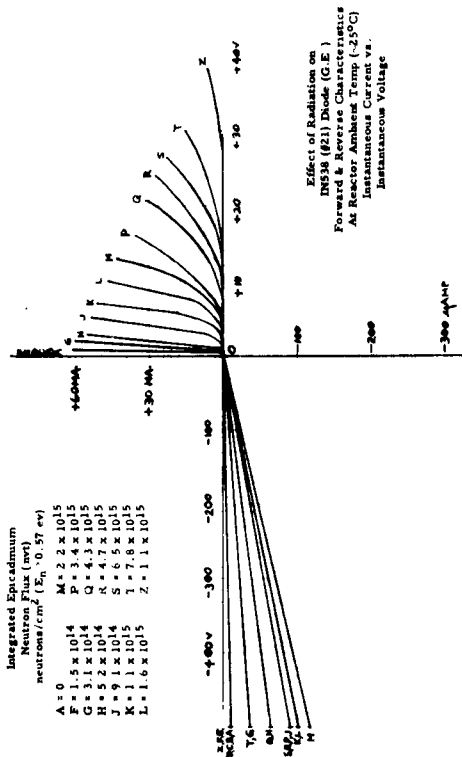
A = 0
B = 7.8 x 10¹²
C = 1.2 x 10¹³
D = 8.5 x 10¹³
E = 1.8 x 10¹⁵
F = 2.7 x 10¹⁵
G = 4.0 x 10¹⁵
H = 7.0 x 10¹⁵
K = 7.6 x 10¹⁵



RADIATION EXPERIMENT #6

Integrated Episcadum
Neutron Flux (nvt)
neutrons/cm² (E_n = 0.57 ev)

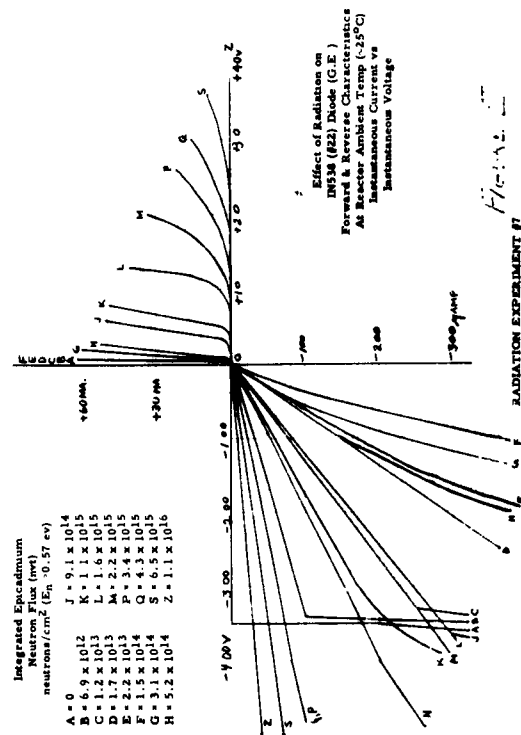
A = 0
B = 1.5 x 10¹⁴
C = 3.1 x 10¹⁴
D = 2.2 x 10¹⁵
E = 1.1 x 10¹⁵
F = 1.6 x 10¹⁵
G = 2.7 x 10¹⁵
H = 7.0 x 10¹⁵
K = 7.6 x 10¹⁵
L = 1.6 x 10¹⁵
M = 2.2 x 10¹⁵
P = 3.4 x 10¹⁵
Q = 4.3 x 10¹⁵
S = 4.7 x 10¹⁵
T = 7.8 x 10¹⁵
Z = 1.1 x 10¹⁶



RADIATION EXPERIMENT #7

Integrated Episcadum
Neutron Flux (nvt)
neutrons/cm² (E_n = 0.57 ev)

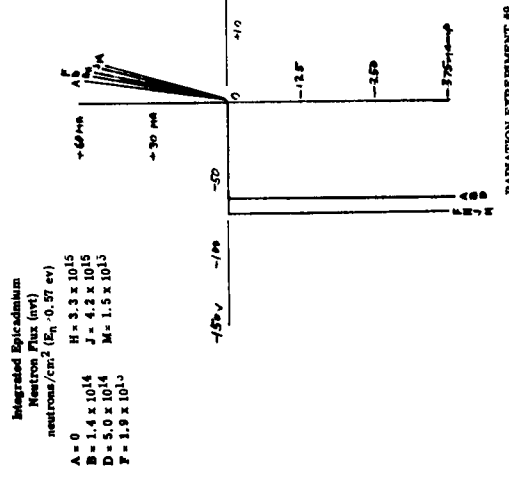
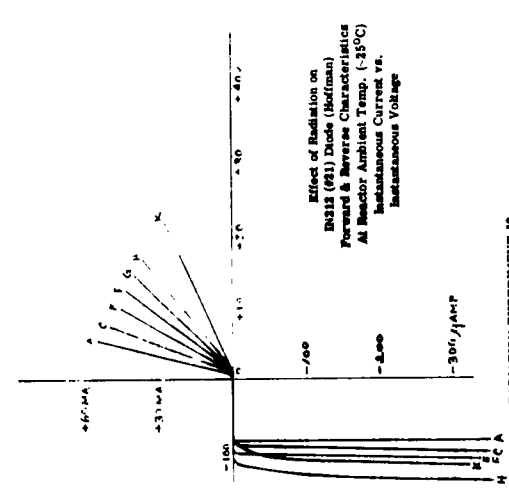
A = 0
B = 6.9 x 10¹²
C = 1.2 x 10¹³
D = 1.7 x 10¹³
E = 2.2 x 10¹³
F = 1.5 x 10¹⁴
G = 3.1 x 10¹⁴
H = 5.2 x 10¹⁴
J = 9.1 x 10¹⁴
K = 1.1 x 10¹⁵
L = 1.6 x 10¹⁵
M = 2.2 x 10¹⁵
P = 3.4 x 10¹⁵
Q = 4.3 x 10¹⁵
S = 6.5 x 10¹⁵
Z = 1.1 x 10¹⁶



RADIATION EXPERIMENT #7

Integrated Episcadanium
Neutron Flux (nvt)
neutrons/cm² (E_n > 0.37 ev)

A = 0
C = 7.3 x 10¹⁴
E = 2.3 x 10¹⁵
F = 3.5 x 10¹⁵
G = 4.7 x 10¹⁵
H = 6.5 x 10¹⁵
K = 8.6 x 10¹⁵



Integrated Episcadanium
Neutron Flux (nvt)
neutrons/cm² (E_n > 0.37 ev)

A = 0
C = 7.3 x 10¹⁴
E = 2.3 x 10¹⁵
F = 3.5 x 10¹⁵
G = 4.7 x 10¹⁵
H = 6.5 x 10¹⁵
K = 8.6 x 10¹⁵

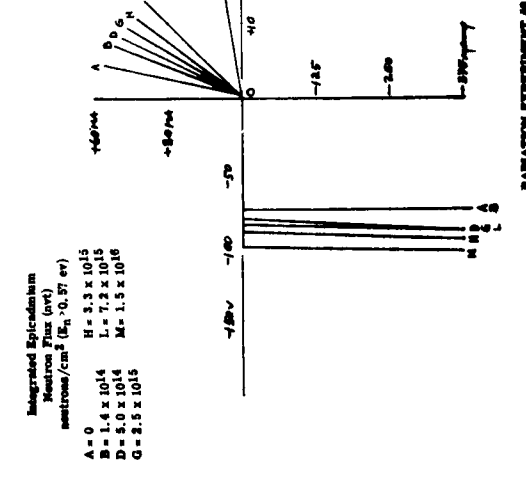
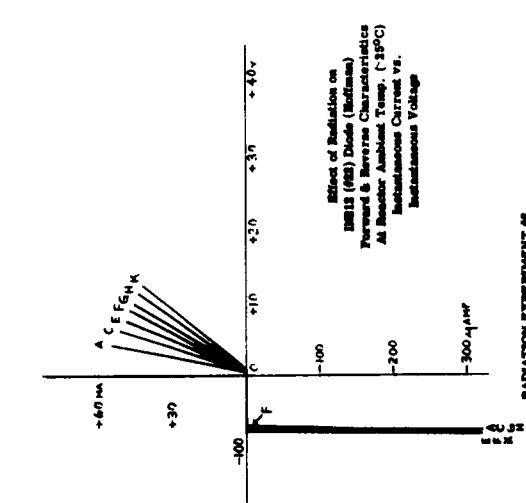
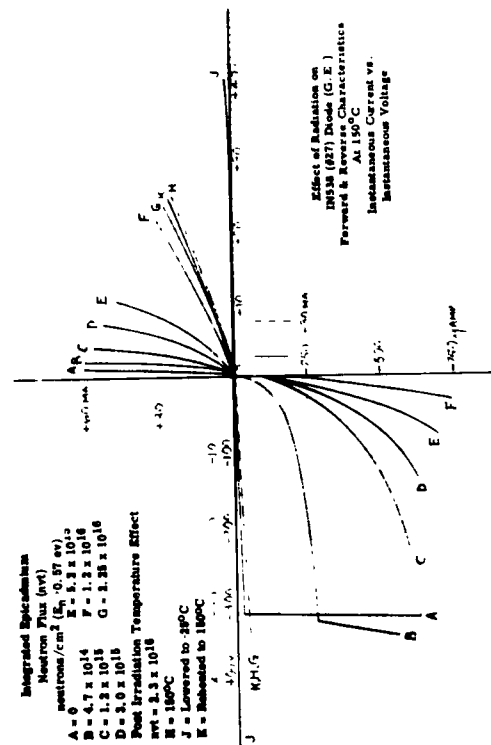
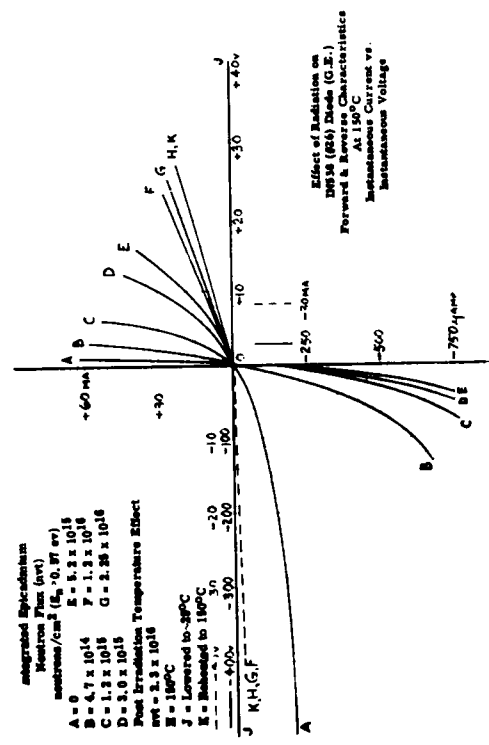


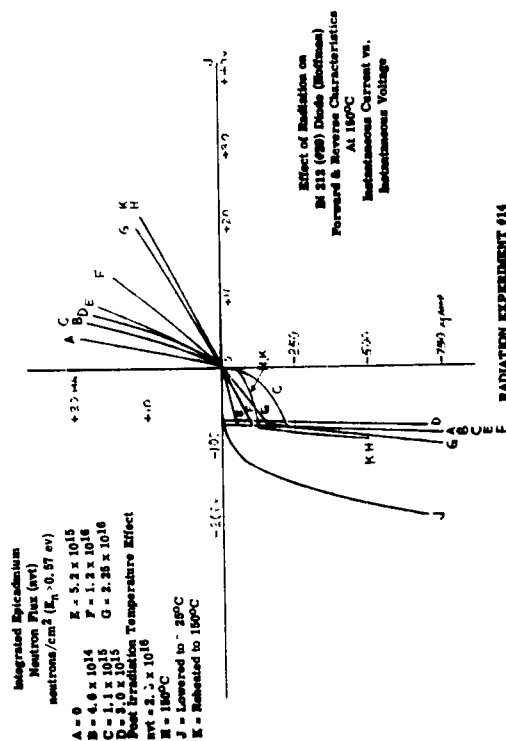
FIGURE III



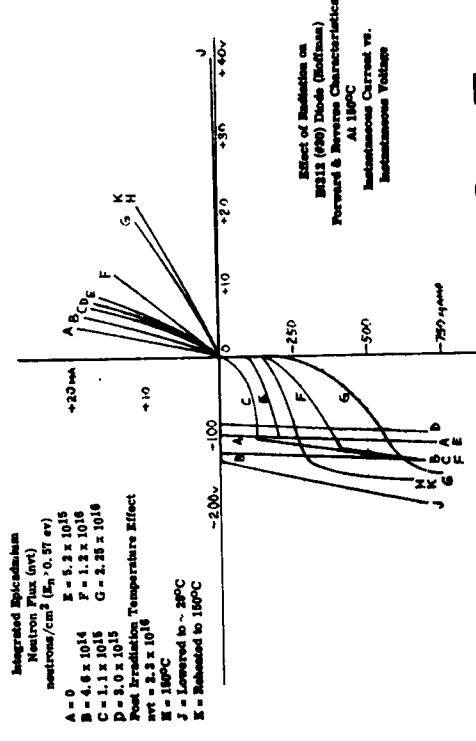
RADIATION EXPERIMENT #14



RADIATION EXPERIMENT #14



RADIATION EXPERIMENT #14



RADIATION EXPERIMENT #14

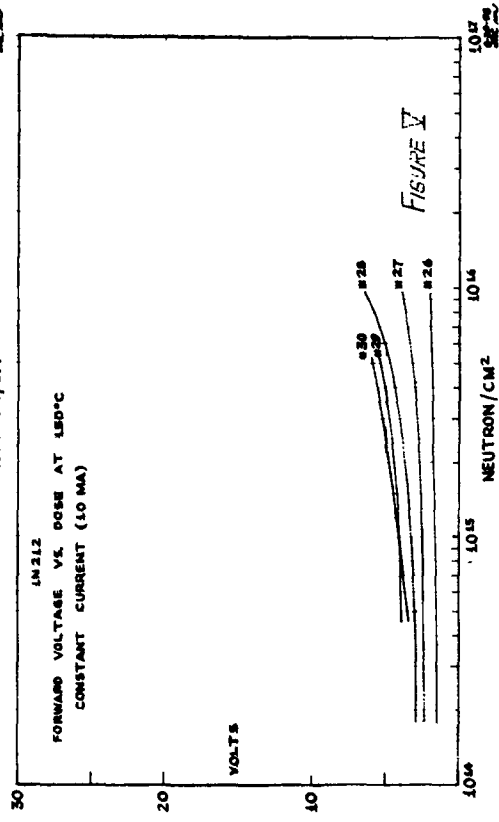
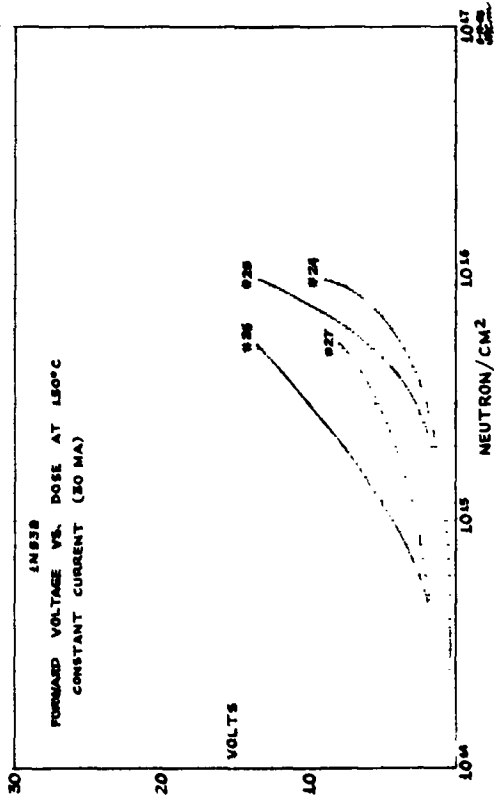
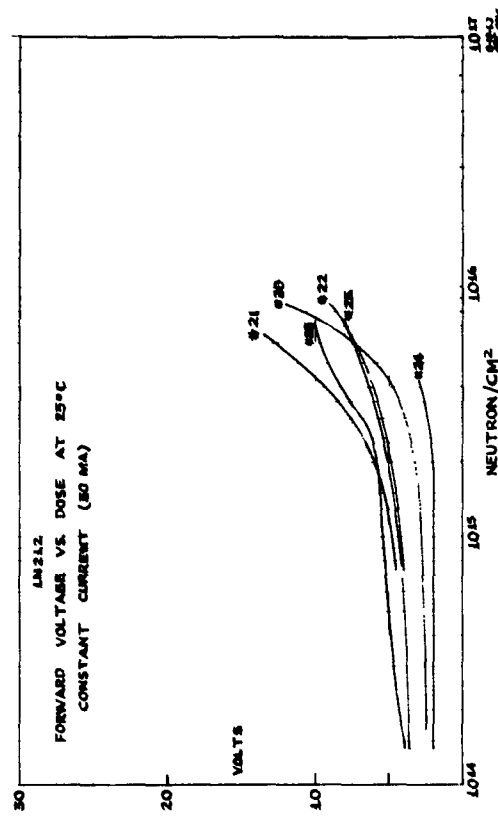
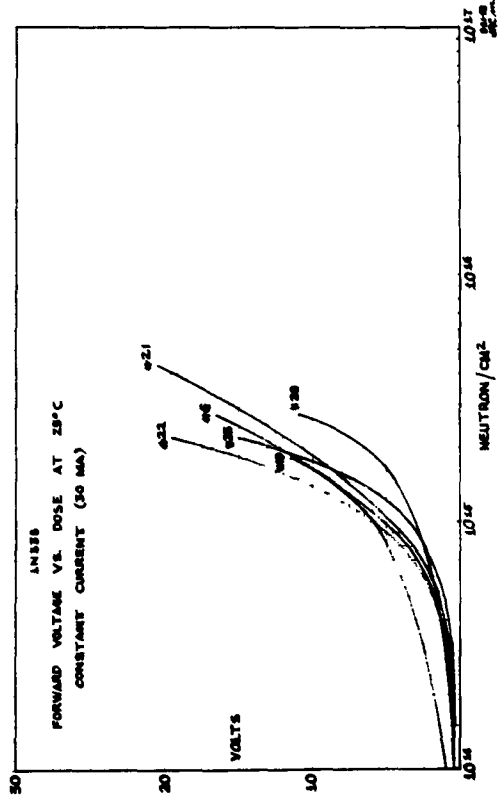
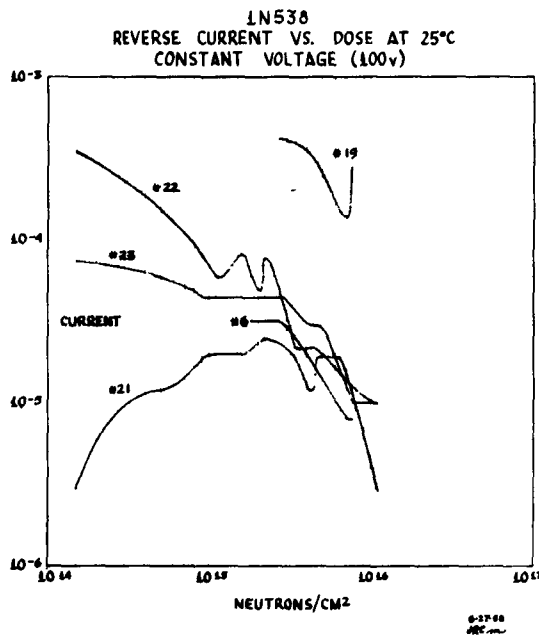
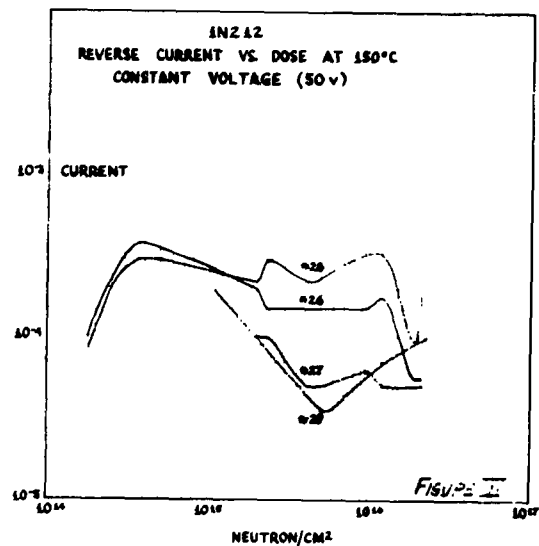
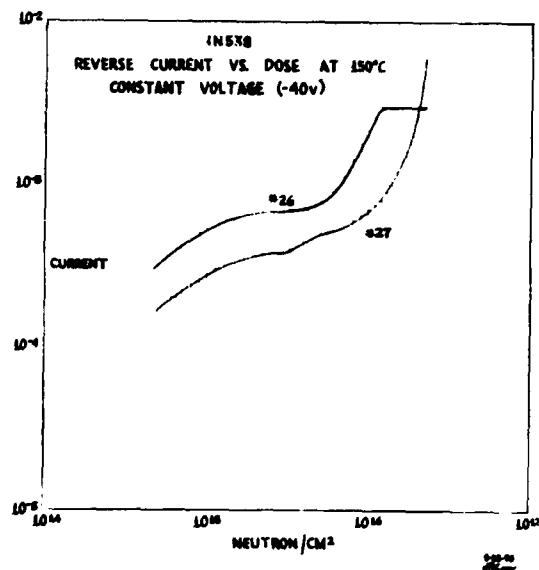


FIGURE V



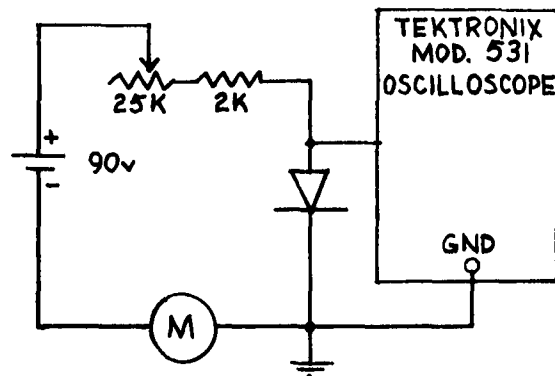
IN212 AT 25°C
NO MEASURED CHANGE IN
THE REVERSE CHARACTERISTIC



**PEAK NOISE VOLTAGES OBSERVED UNDER
VARIOUS ENVIRONMENTAL CONDITIONS**

MANUFACTURER	TYPE	IRRADIATED AT (°C)	RANGE OF PEAK NOISE VOLTAGE OBSERVED	
			Min.	Max.
General Electric	538	25	0.4 mv	1 mv
		150	not observable	0.5 mv
	4JA60B	25	50 μ v	0.5 mv
		150	0.15 mv	0.15 mv
		300	not observable	2 μ v
Raytheon	IN303A	25	40 μ v	0.1 mv
		150	0.4 mv	10 mv
	CK776	25	50 μ v	0.5 mv
		150	0.1 v	0.1 v
Hughes	6006	25	30 μ v	0.1 mv
		150	0.5 mv	7 mv
	6007	25	15 μ v	10 mv
		150	1.5 mv	10 mv
Hoffman	IN212	25	not observable	15 μ v
		150	not observable	1 mv
Transitron	TJ10A	25	50 μ v	1.5 mv
		150	0.3 mv	1.5 mv
	IN336	25	not observable	0.5 mv
		150	20 μ v	2 mv
	IN339	25	20 μ v	0.4 mv
		150	20 μ v	0.2 mv

INVESTIGATION OF THE DISCONTINUITY REGION PRODUCED IN A DIODES' FORWARD CHARACTERISTIC BY NEUTRON IRRADIATION



CIRCUIT USED FOR FIGS. B,C,D,E

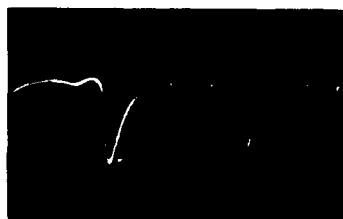
DISCONTINUITY IN THE FORWARD CHARACTERISTIC OF THE DIODE UNDER INVESTIGATION



SCALE
HOR. = 10V/CM
VERT = 5MA/CM

(A)

SCALE
HOR. = 2.4SEC/CM VERT = 2V/CM



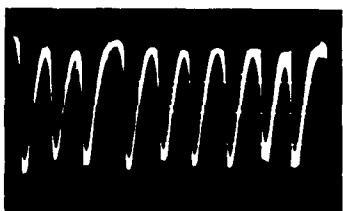
(B)

$I_{\text{FORWARD}} = 2 \text{ MA.}$



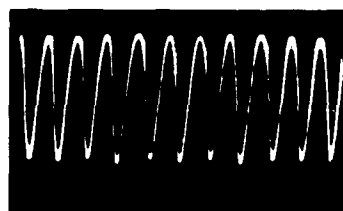
(C)

$I_{\text{FORWARD}} = 3.5 \text{ MA.}$



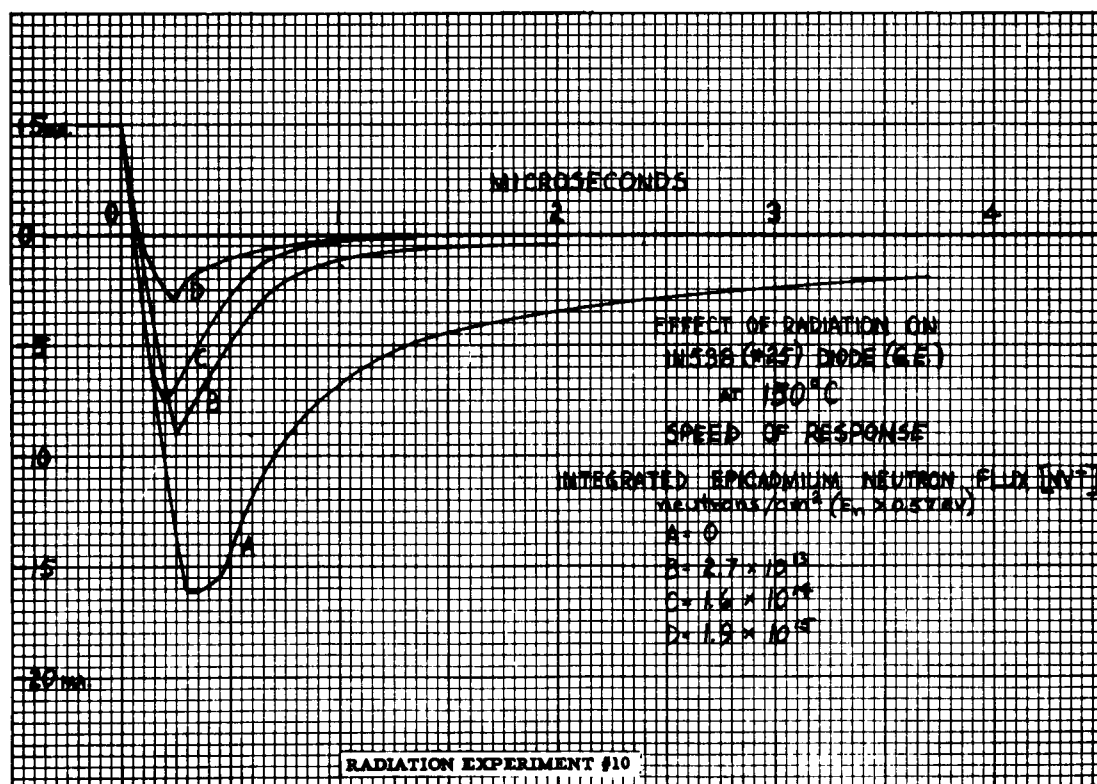
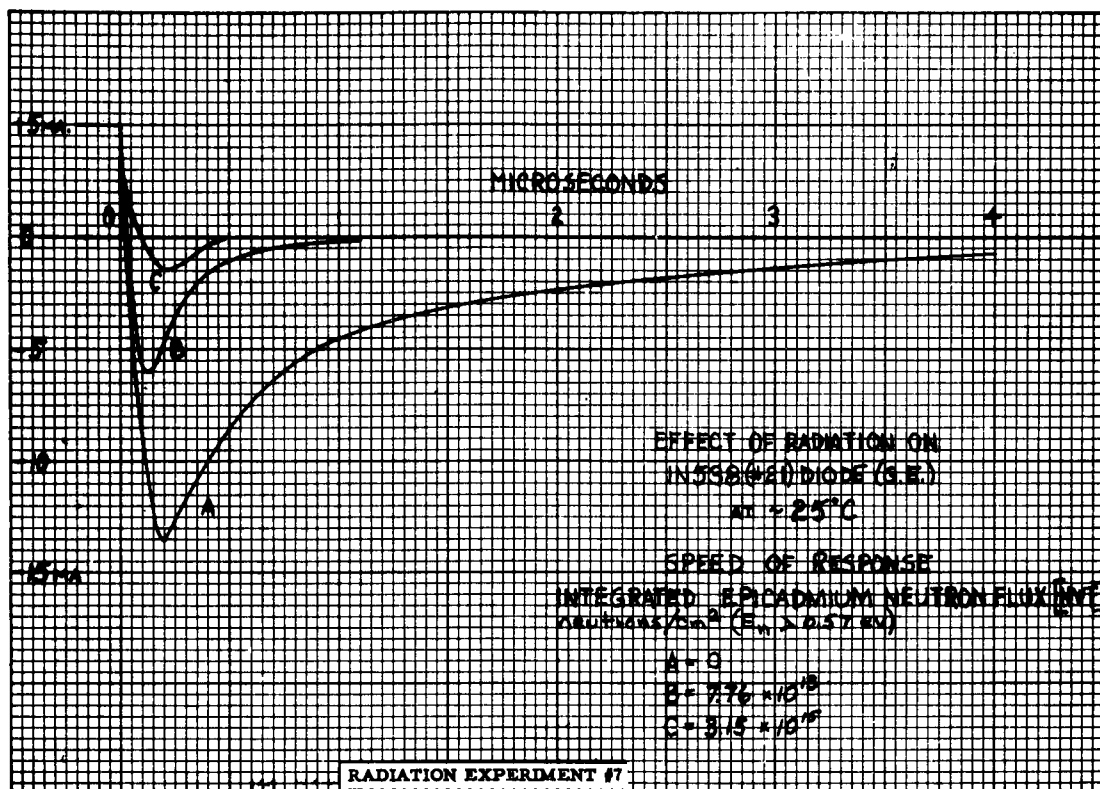
(D)

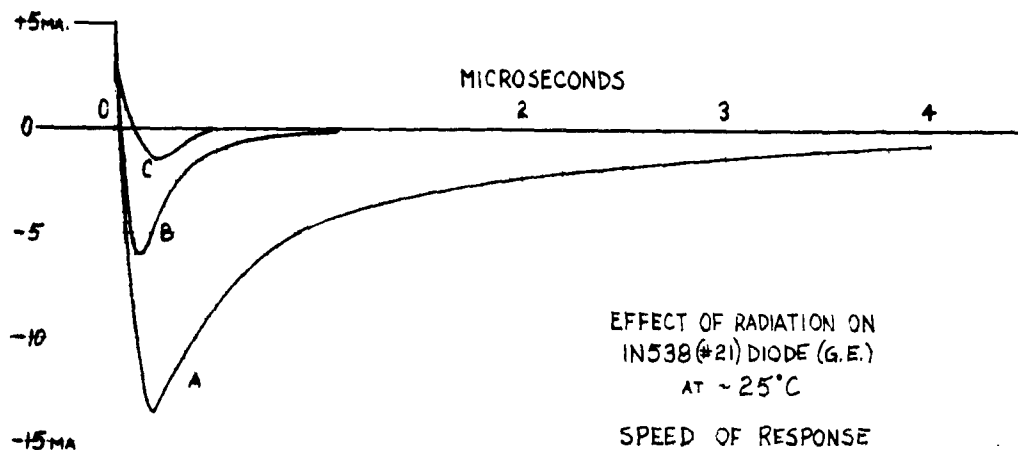
$I_{\text{FORWARD}} = 4 \text{ MA.}$



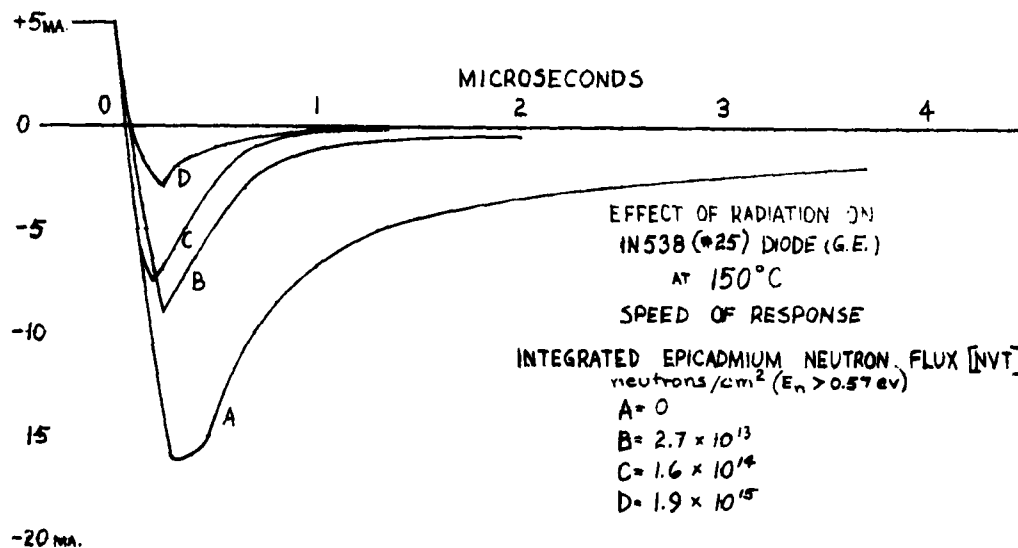
(E)

$I_{\text{FORWARD}} = 5 \text{ MA.}$





RADIATION EXPERIMENT #7



RADIATION EXPERIMENT #10

FIGURE IX

EVALUATION OF SILICON DIODE IRRADIATION RESULTS IN TERMS OF MAGNETIC AMPLIFIER PERFORMANCE

by

Jack A. Russell
General Electric Company
Aircraft Nuclear Propulsion Department
Cincinnati 15, Ohio

Abstract

Three generic types of silicon diode failure under radiation are simulated. The simulation is applied to a full-wave, center-tap magnetic amplifier and a half-bridge, half-wave magnetic amplifier. Conclusions are drawn as to the most suitable basic diode type under radiation. Also discussed are: changes to be expected in magnetic amplifier performance as a result of radiation-induced diode effects; means of reducing some of these effects.

I. PURPOSE

A considerable amount of data has been compiled by various experimenters on the radiation effects on silicon diodes (see References 1, 2, 3, and 4). In the Materials Development Section of ANPD, work has been done to determine the diode design parameters which influence the radiation tolerance of silicon devices. As a result of this work (Reference 2), it is now possible to obtain diodes specifically designed to increase their radiation tolerance by as much as a factor of 100. It is possible to complete development of radiation-tolerant diffused-junction rectifiers or alloy-junction rectifiers in the final phase of this materials development program. It is the purpose of this report to recommend a final development of radiation-tolerant diffused-junction or alloy-junction diode, to reach some conclusions as to the effects of three generic types of diode irradiation produced failures on magnetic amplifier performance and to predict life of magnetic amplifiers exposed to radiation when constructed with these diodes.

II. PROCEDURE

A. Simulation of Radiation Effects on Silicon Diodes

From discussion with Gordon Hall (Reference 4) and G. Huth (Reference 1), it was determined that there were three basic types of semiconductor rectifier radiation failure, as illustrated in Figure 1. Type A, Figure 1, is characterized by "walking out" in the forward region as the dosage increases; that is, the forward voltage to enter the high-conduction region increases as the radiation dosage increases. (This is designated by E_{rf} .) Type B, Figure 1, shows the knee of the forward region remains at its initial value, while the forward conduction decreases as the dosage increases. Type C, Figure 1, exhibits both the "walking out" of the forward conduction knee and the decrease in forward conductivity as the radiation dosage increases.

Four degrees in each of the three types of diode failure were simulated by means of the circuit as shown in Figure 2. The parameters were varied in as realistic a manner as possible, as determined from the various references on diode irradiation (References 1, 2, and 3.) The maximum simulated changes in diode failure characteristics were purposely set beyond where the diode would normally have been considered failed in order to see the greatest possible influence on the magnetic amplifier circuits.

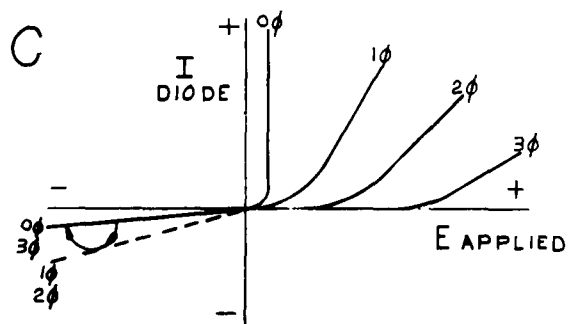
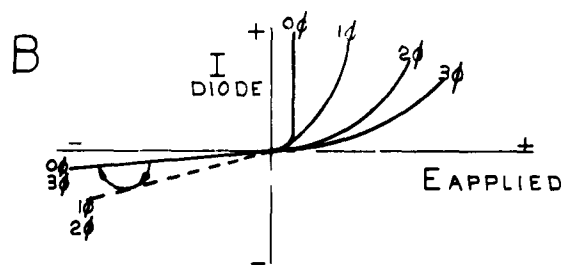
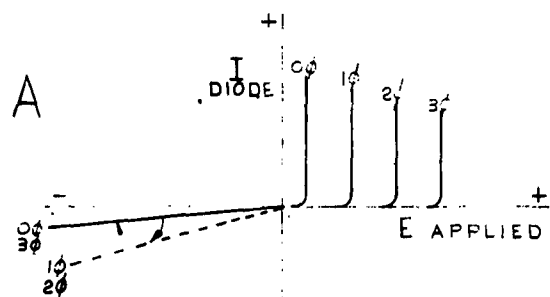
Rather than vary the back resistance with each change in forward resistance or increase in conduction knee, it was decided to set the back resistance shunt at its minimum value and leave it for all but the recordings of unmodified diodes. The shunt resistor is designated by R_{rrs} .

Recorded curves of the four variations of each of the three families of diode failure are shown in Figures 3, 4, and 5. Each of these variations was quadrupled (each circuit requires four diodes) and substituted in the two magnetic amplifier circuits.

To eliminate the variations which might be produced by mismatched diodes, the forward voltage drop of twenty (20) 1N441B diodes were measured at various forward currents and the reverse currents at 100 volts. The four most closely matched units were then used in the simulation. The spread of values was small. Table I contains the results of the matching.

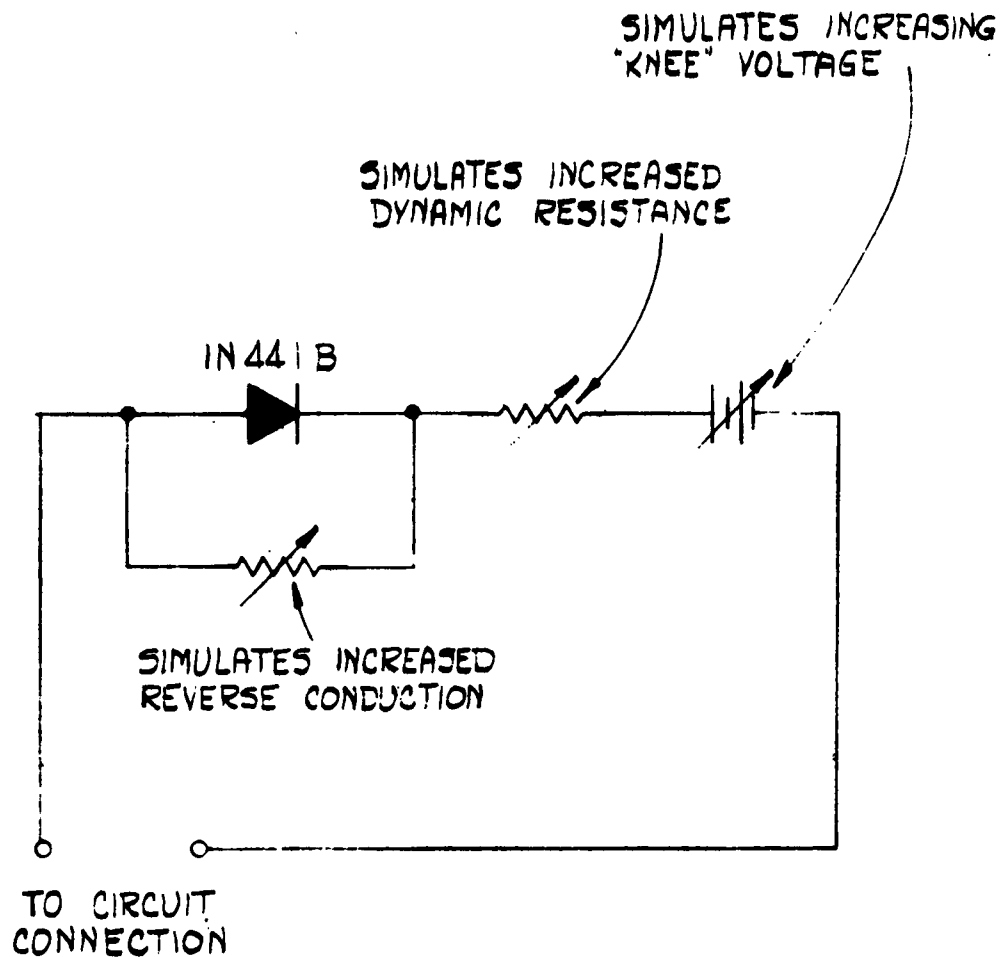
B. Recording of Magnetic Amplifier Static-Gain Curves

A Mosley two-axis recorder with an 8½ x 11-inch bed was used to give good accuracy. Amplifier output was recorded on the horizontal axis while driving current was recorded on the vertical axis. A small rate-controlled motor drive was used to turn a 10-turn helipot supplying both positive and negative drive to the amplifier control windings. This was necessary to insure smoothness of the recordings and saved considerable time in running the curves.



THREE FORMS OF SILICON
DIODE RADIATION INDUCED FAILURE

FIGURE 1 (DRB7C866)

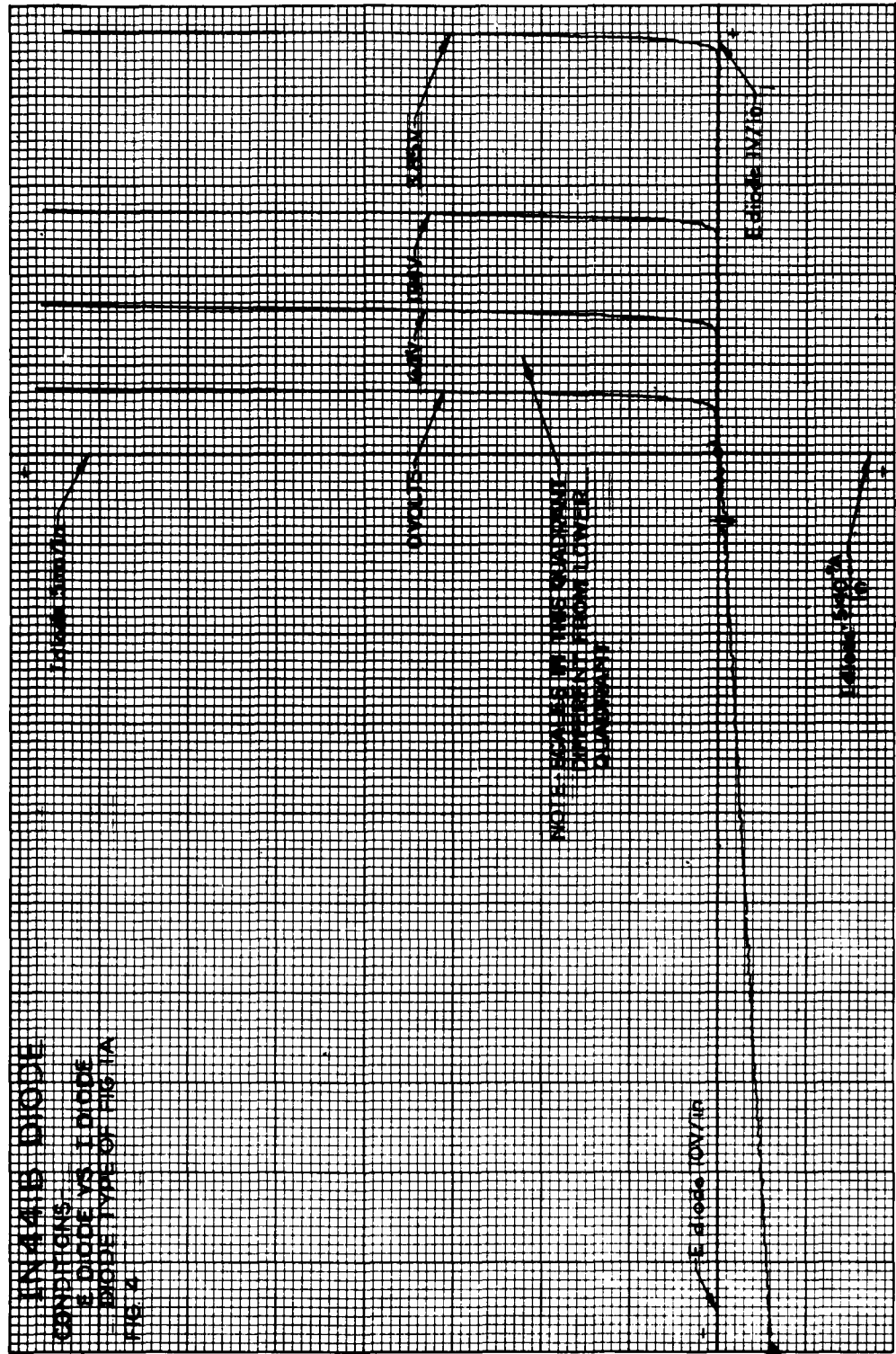


SIMULATION OF DIODE IRRADIATION
INDUCED EFFECTS.

FIG. 2.

-4-

(5K737C873)



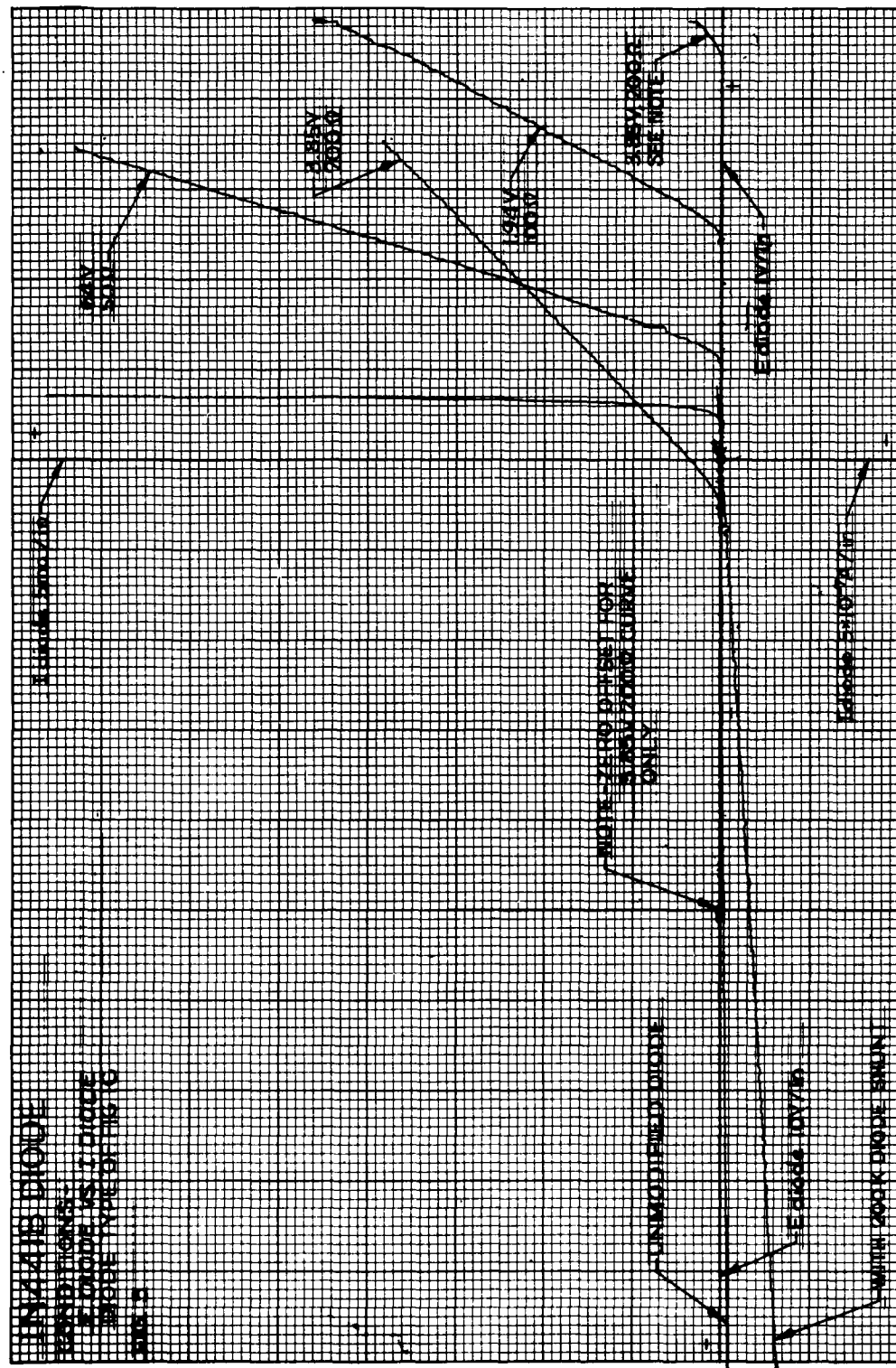


TABLE I
COMPARISON OF 1N441B DIODE
FORWARD AND BACKWARD CURRENTS AT PARTICULAR POINTS

<u>Diode Number</u>	<u>1 Ma IR Drop Across Diode</u>	<u>25 Ma IR Drop Across Diode</u>	<u>50 Ma IR Drop Across Diode</u>	<u>I_{rev.} ● 100 VDC in μ Amps</u>
1	.586	.729	.762	81
2	.586	.735	.776	47
3	.594	.740	.775	97
4	.588	.738	.771	76
5	.592	.744	.783	54
6	.590	.730	.765	50
7	.609	.779	.828	81
8	.585	.746	.791	44
9	.597	.735	.769	65
10	.593	.747	.790	59
11	.596	.749	.788	89
12	.597	.739	.773	66
13	.582	.743	.787	94
14	.588	.750	.797	122
15	.596	.729	.760	33
16	.603	.773	.819	73
17	.595	.740	.778	54
18	.615	.759	.795	112
19	.592	.743	.778	73
20	.592	.748	.785	98

III. RESULTS

A. Full-Wave, Center-Tap Circuit

To fully determine the effects of diode changes on the circuit, it was necessary to remote the 200K shunts which have previously been used across the four rectifiers in this circuit. This, in turn, necessitated redesign of the biasing on this amplifier. The modified circuit is shown in Figure 6. The static-gain curve of this amplifier with no diode modifications is shown in Figure 7.

FULL-WAVE CENTER TAP
MAGNETIC AMPLIFIER

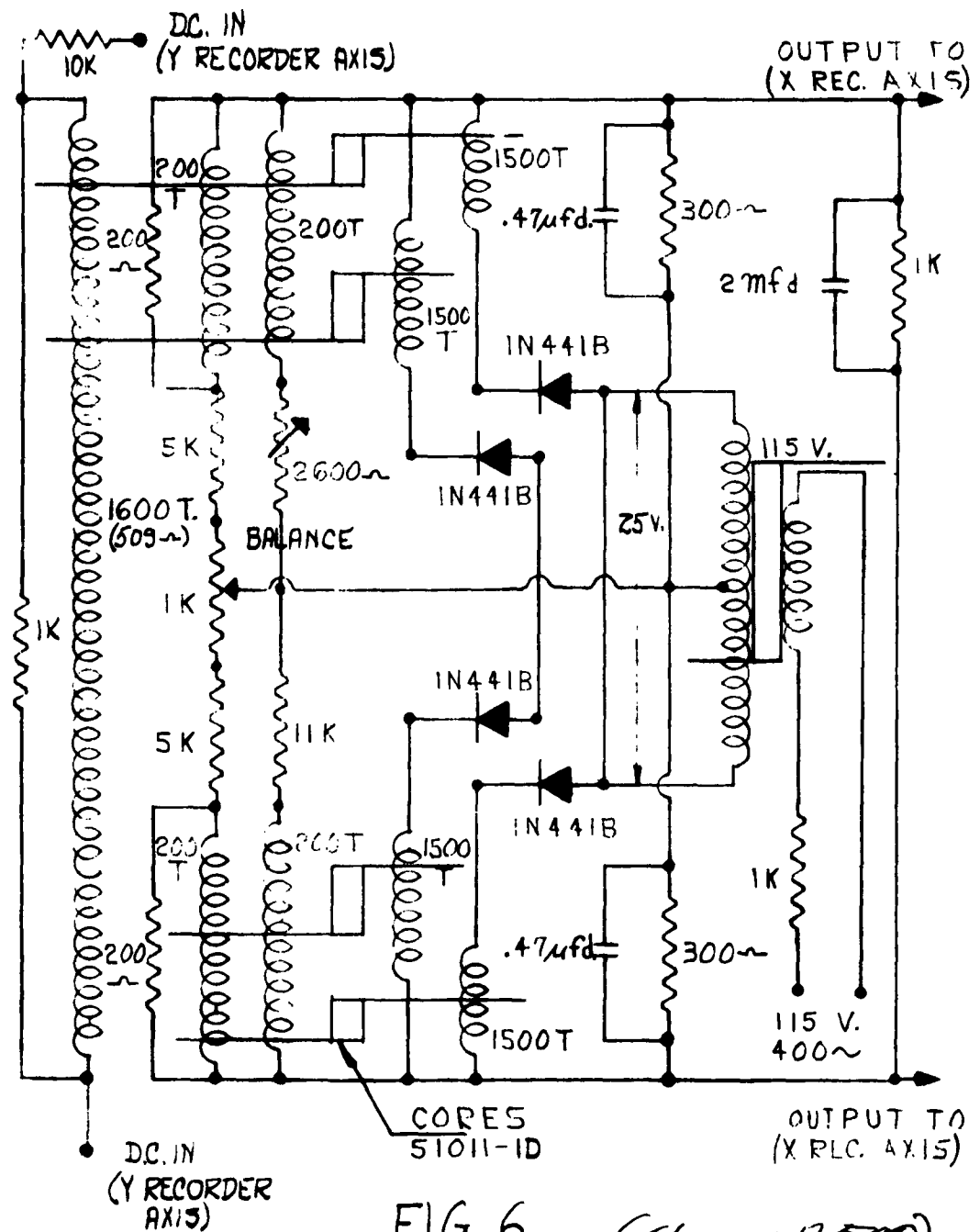


FIG. 6 (5K 664 D 578)

CENTER-TAP FULL-WAVE
RECTIFIER CIRCUIT

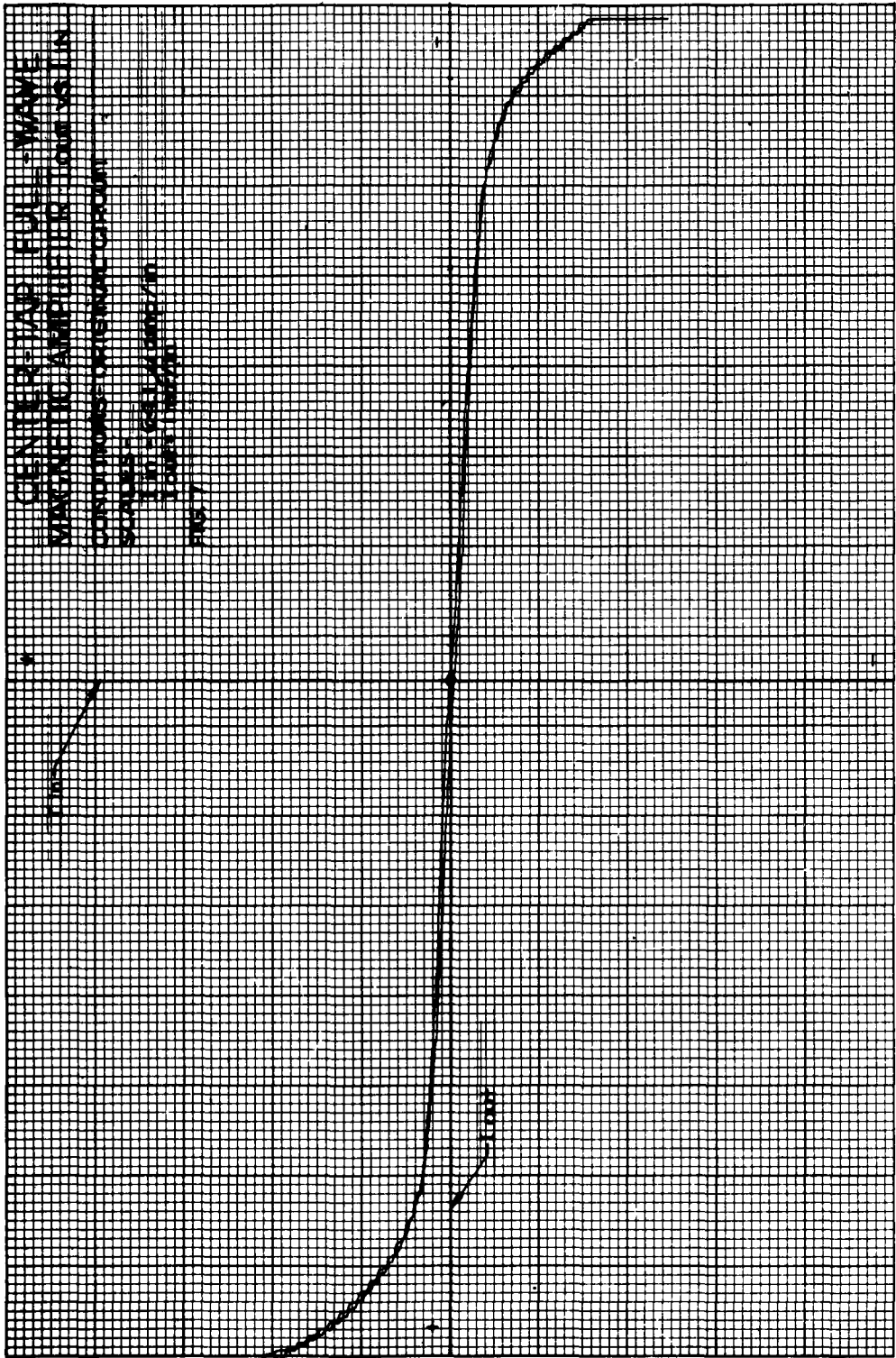
WOLFF

THE

1113	1114	1115	1116	1117	1118	1119	1120	1121	1122	1123	1124	1125	1126	1127	1128	1129	1130	1131	1132	1133	1134	1135	1136	1137	1138	1139	1140	1141	1142	1143	1144	1145	1146	1147	1148	1149	1150	1151	1152	1153	1154	1155	1156	1157	1158	1159	1160	1161	1162	1163	1164	1165	1166	1167	1168	1169	1170	1171	1172	1173	1174	1175	1176	1177	1178	1179	1180	1181	1182	1183	1184	1185	1186	1187	1188	1189	1190	1191	1192	1193	1194	1195	1196	1197	1198	1199	1200
1113	1114	1115	1116	1117	1118	1119	1120	1121	1122	1123	1124	1125	1126	1127	1128	1129	1130	1131	1132	1133	1134	1135	1136	1137	1138	1139	1140	1141	1142	1143	1144	1145	1146	1147	1148	1149	1150	1151	1152	1153	1154	1155	1156	1157	1158	1159	1160	1161	1162	1163	1164	1165	1166	1167	1168	1169	1170	1171	1172	1173	1174	1175	1176	1177	1178	1179	1180	1181	1182	1183	1184	1185	1186	1187	1188	1189	1190	1191	1192	1193	1194	1195	1196	1197	1198	1199	1200

THE UNIVERSITY OF CHICAGO PRESS

2000年12月



Since the radiation-induced changes in diode back resistance were to be simulated by a 200K shunt for all conditions, it was of interest to see the effects of various shunting resistors on the circuit. The results are shown in Figure 8. As would be expected, the reduced diode reverse resistance, when shunted, acts as negative feedback, thereby, reducing the gain. Normal current gain of 225 ma./ma. is reduced to 156 ma./ma. with the 200K diode shunts. The linearity of the 200K curve of Figure 8 is slightly more linear than those of the higher-value shunts. The limits of the linear region are, however, reduced.

1. Effects on This Circuit of the Diode Changes of Figure 1B

The effects on the center-tap, full-wave magnetic amplifier with the diode characteristics of Figure 3 inserted are shown in Figures 9, 10, 11, and 12. The first effect noticed is the bistable action at the extremes of all curves. Since this circuit is operated just at saturation, the increased forward drop caused by the diodes increased forward resistance results in insufficient gate voltage to reach positive saturation when one-half of the unit has been driven into cutoff. Figure 13 displays the two halves of the center-tap magnetic amplifier in such a way that the combined differential output characteristic is shown. It is clearly seen that the cutoff point of first one side, and then the other, are responsible for the bistable portions at each end of the gain curve.

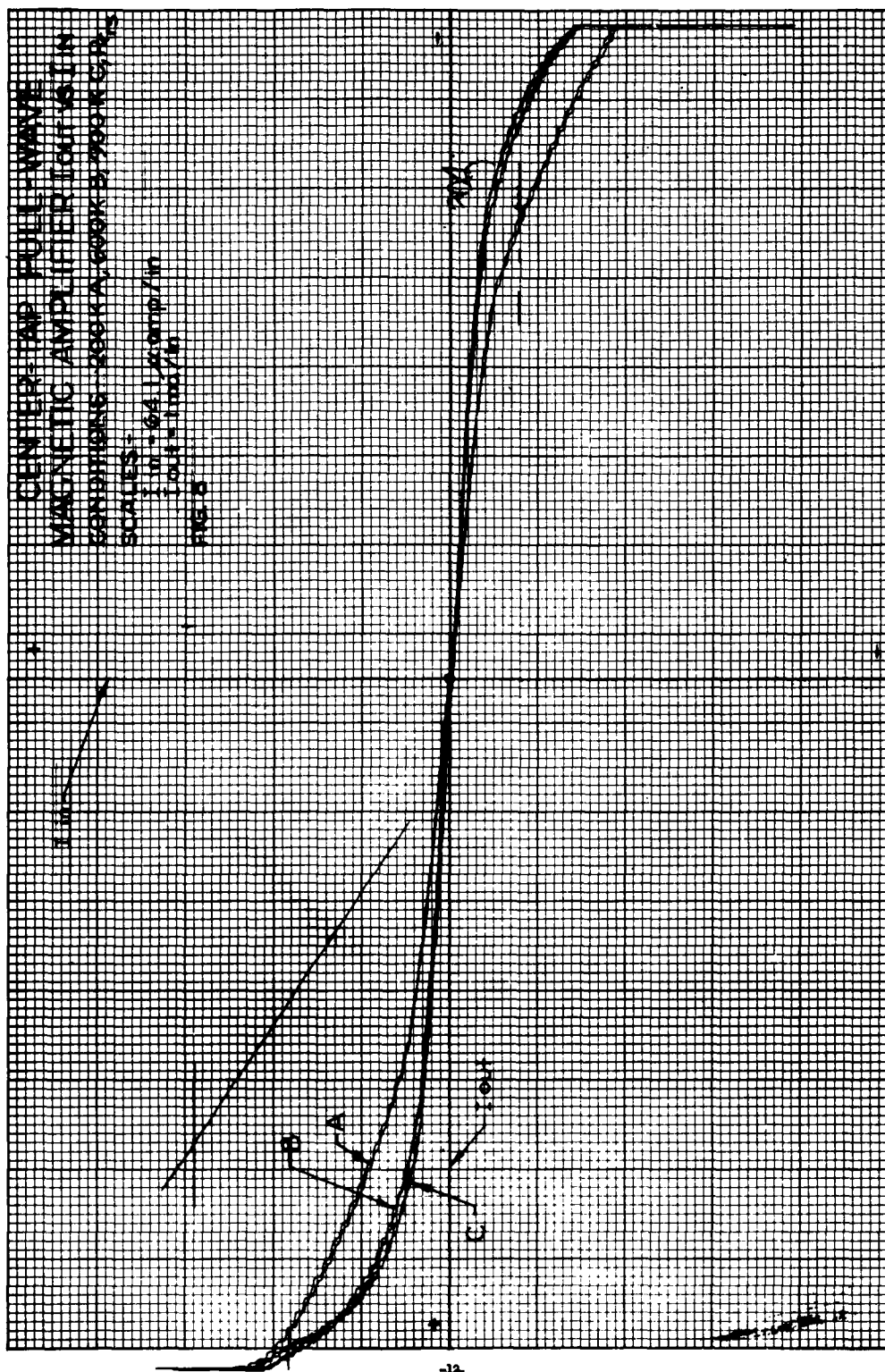
A second effect is the decrease in the saturation level of the gain curve as the diode forward resistance increases. This would be expected, since the output voltage obtained when the core is saturated is divided between the load resistance and the rectifier forward resistance. The rectifier forward resistance is normally low (1 ohm or less) and does not show an appreciable forward voltage drop.

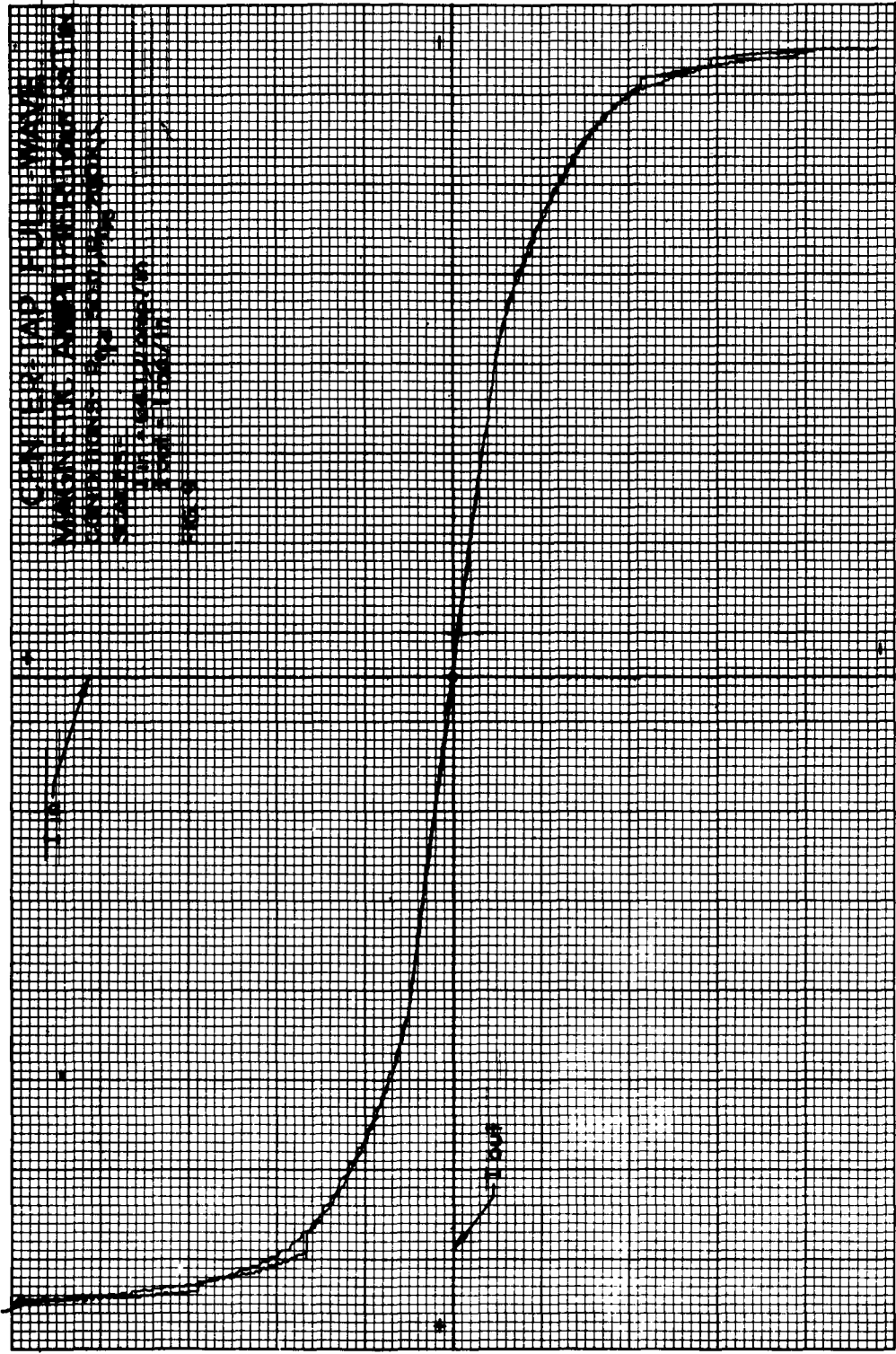
It will also be noticed from Figures 9, 10, 11, and 12 that the amplifier current gain reduces as the diode forward resistance decreases, since the load sees proportionately less of the voltage applied to load and rectifier.

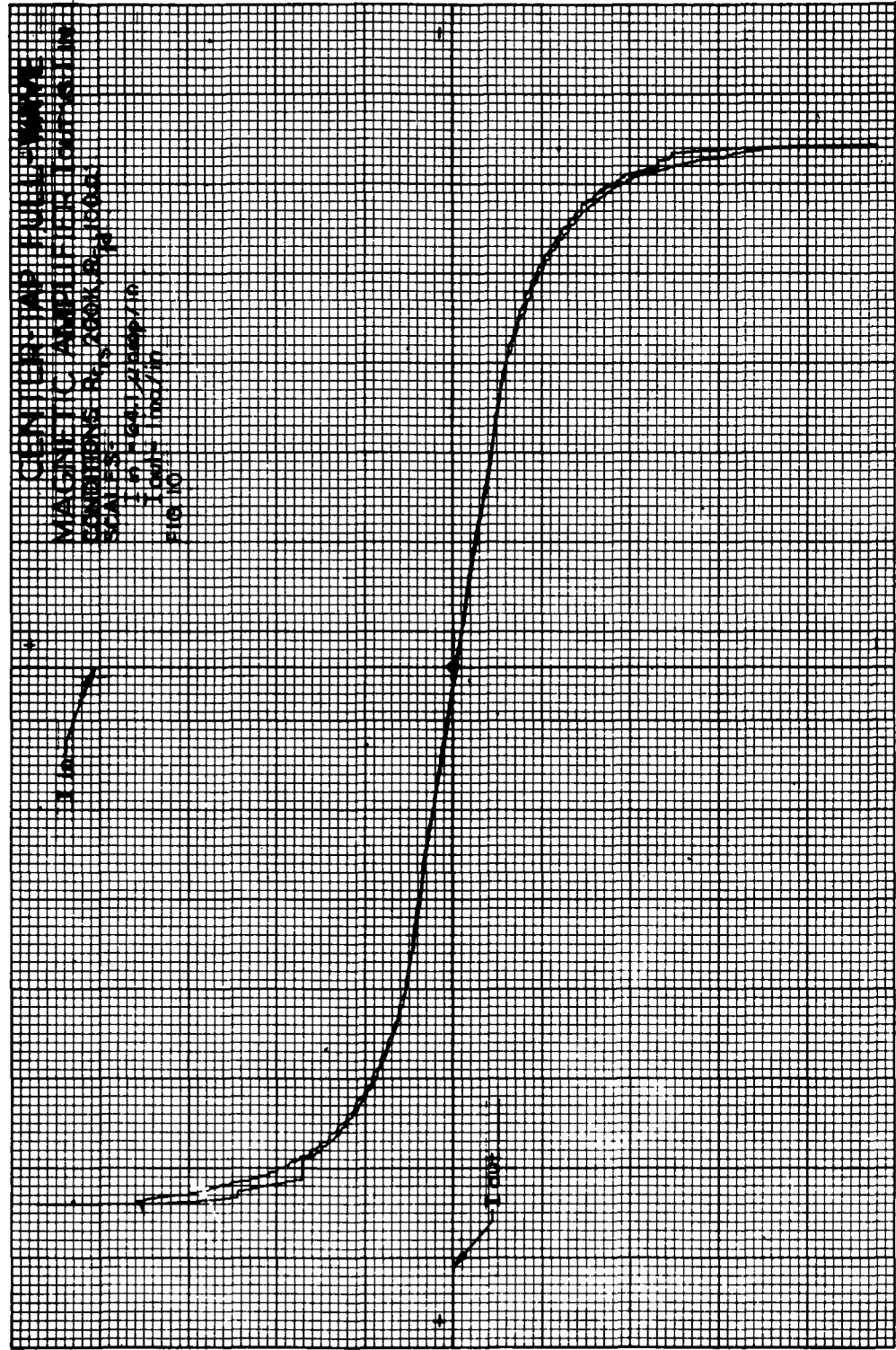
The resistance of the diode in the forward-conduction region is the dynamic resistance as would be give by

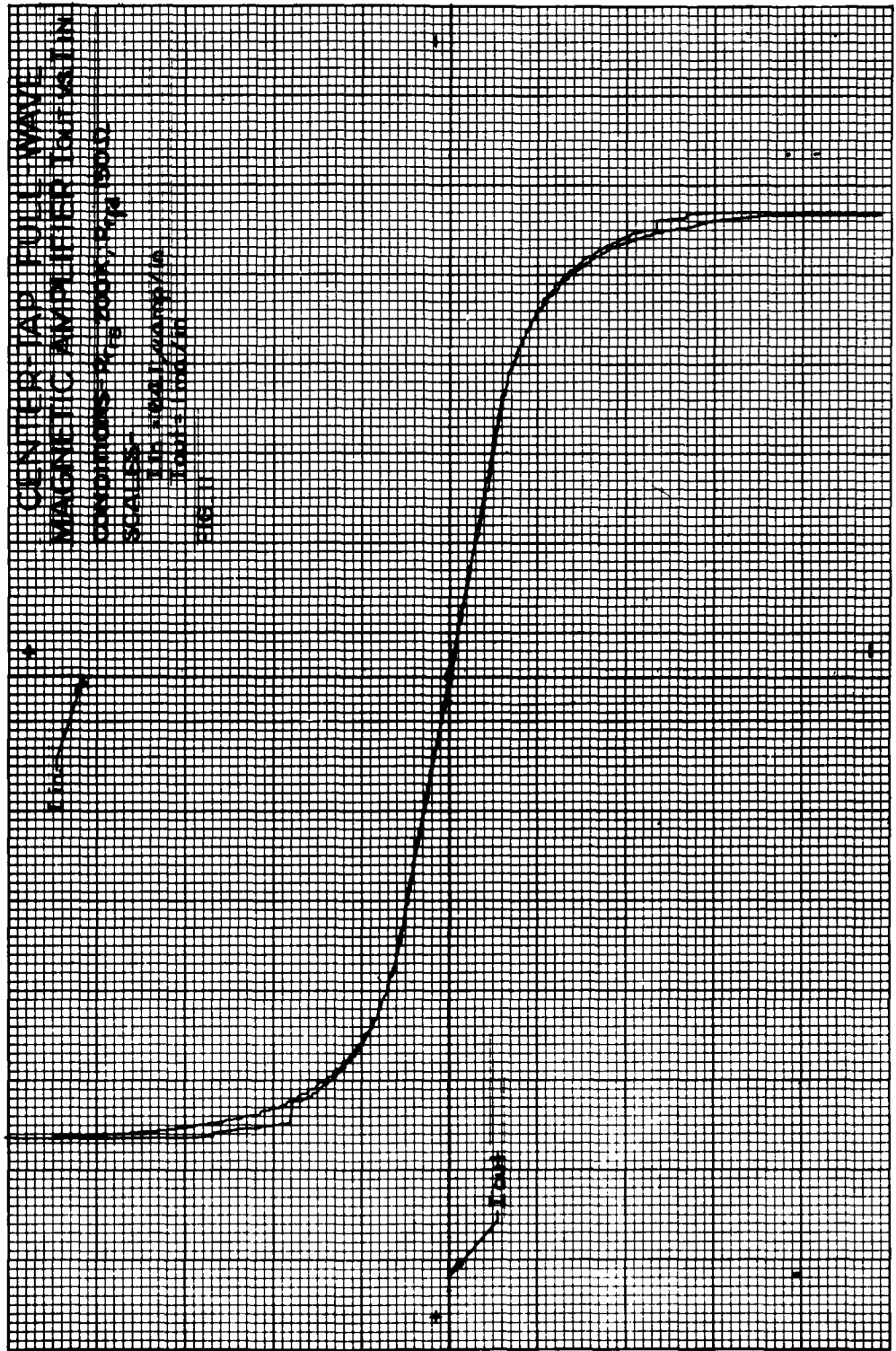
$$\frac{\Delta (I_{\text{diode}})}{\Delta (E_{\text{diode}})} = \frac{\text{Rectifier Forward}}{\text{Dynamic Resistance}} = R_{rfd}$$

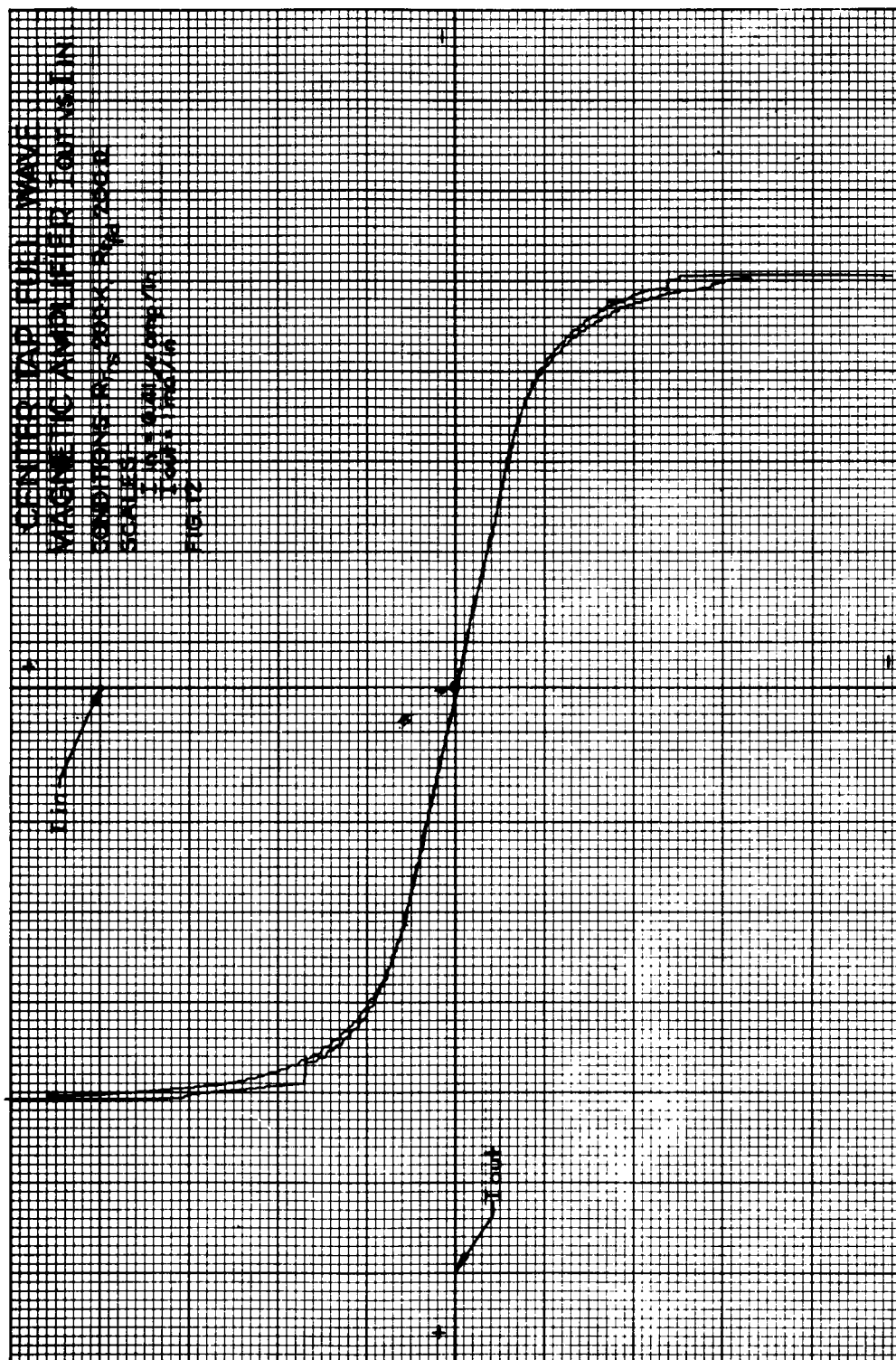
when the diode is definitely beyond the knee of the conduction cone.

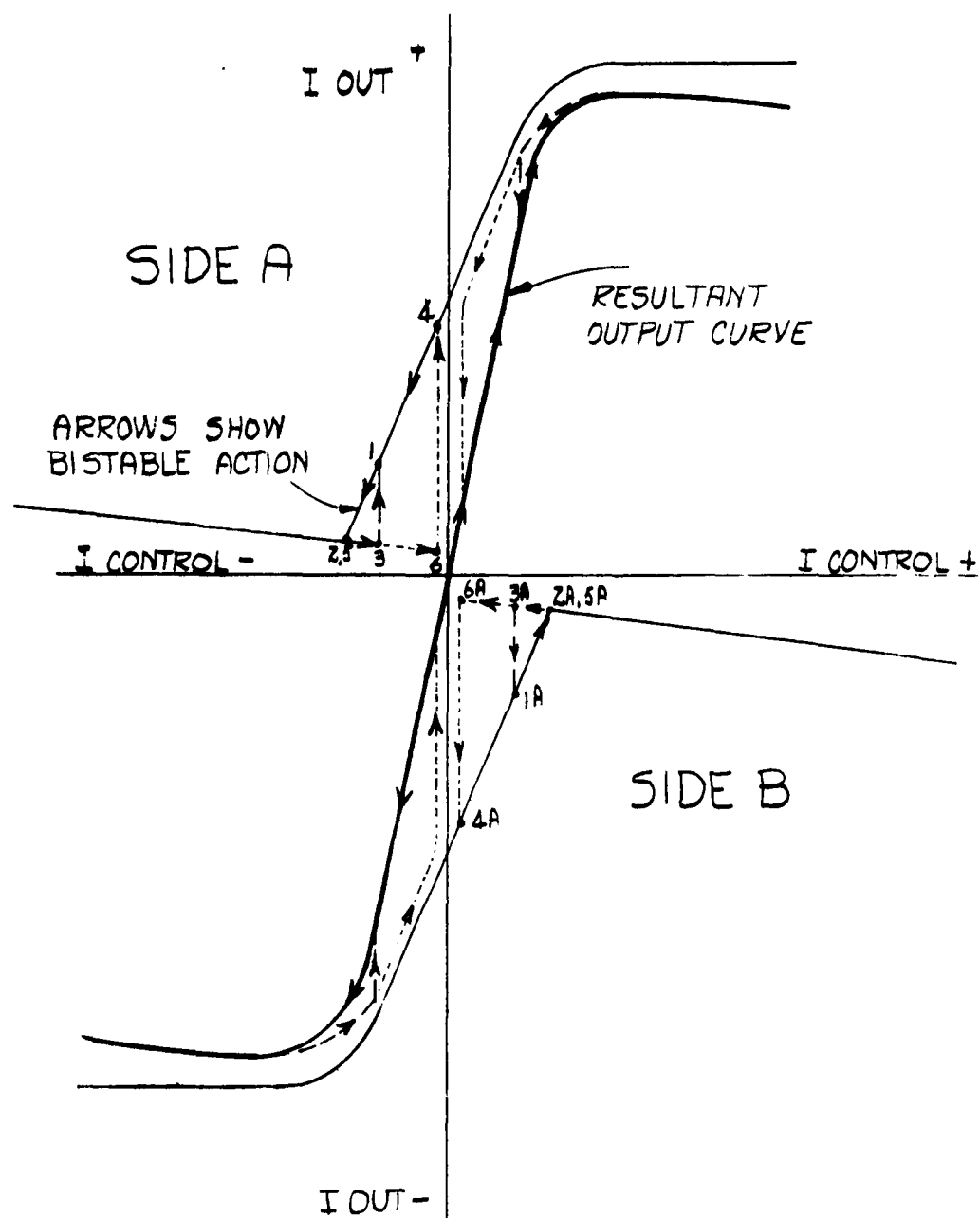












BISTABLE EFFECTS IN FULL WAVE
CENTER TAP MAGNETIC AMPLIFIER

FIG. 13
-17-

(54737C873)

2. Effects on This Circuit of the Diode Changes of Figure 1A

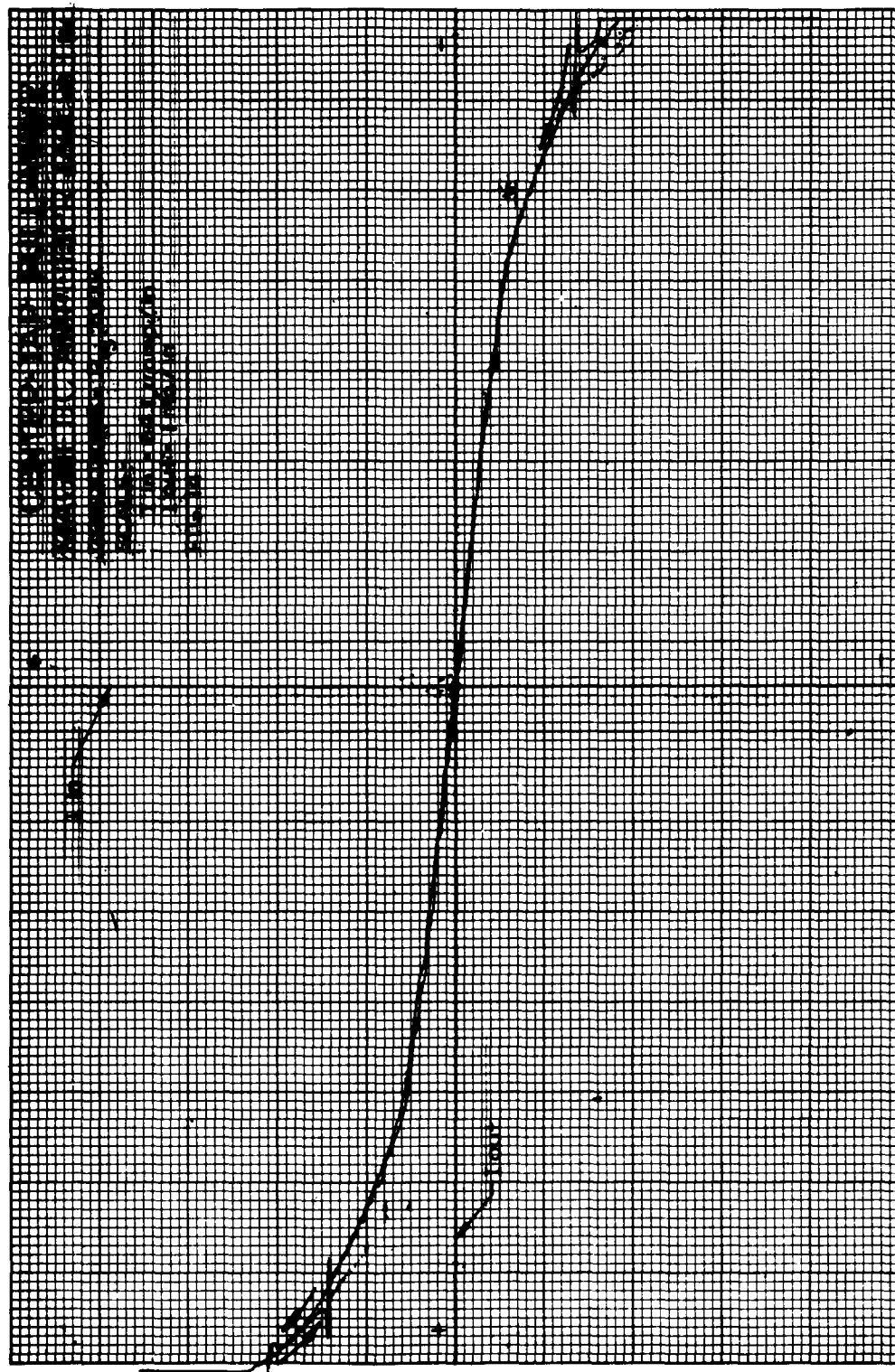
As was shown in Figure 1A, the failure of this type of diode is primarily an increase in voltage of the knee region of the forward-conduction curve as the dosage increases.

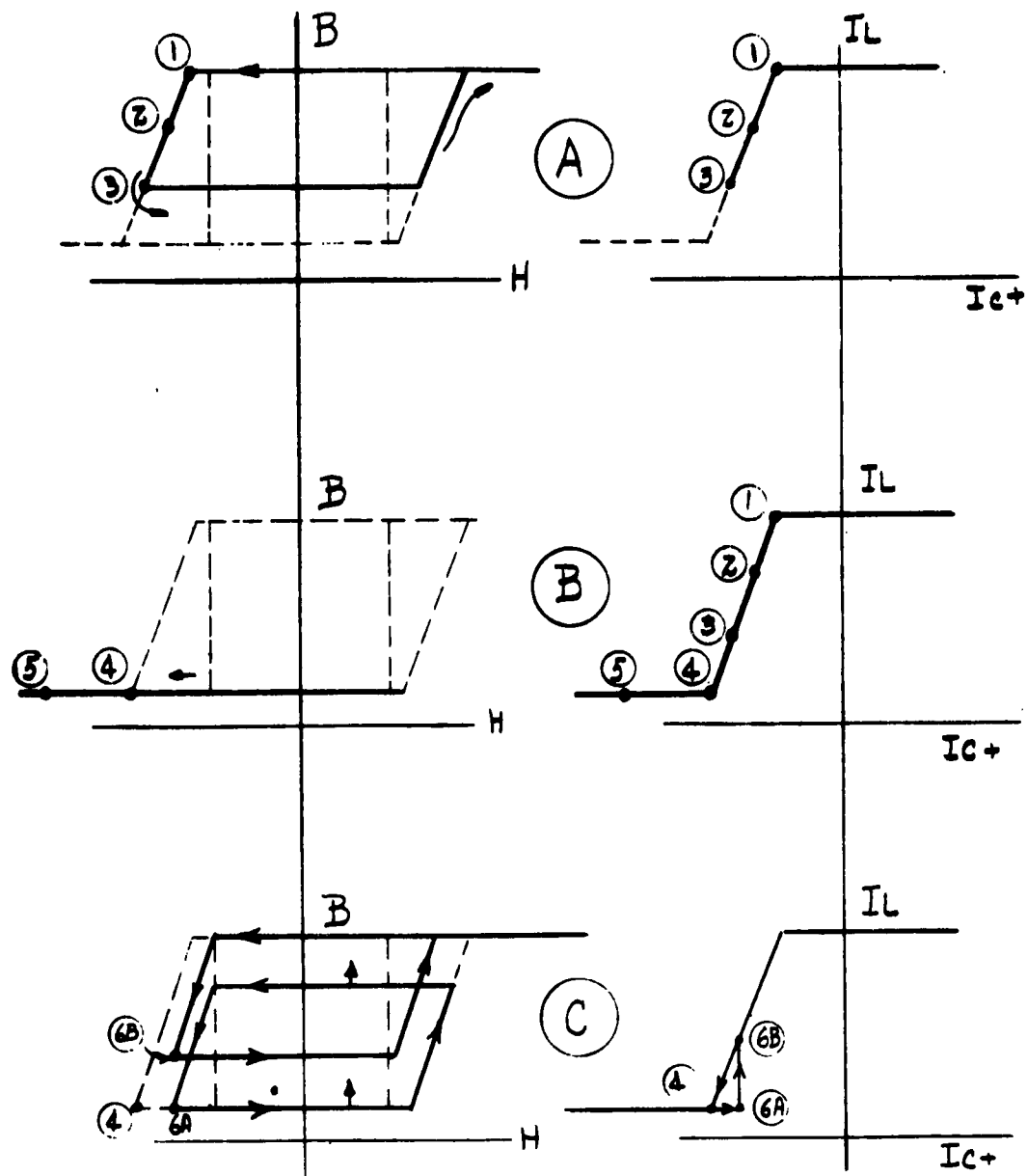
Figure 14 shows the amplifier with only the 200K diode shunt applied to simulate increase in back current of the rectifier under radiation. The same bistable points at the extreme ends of the gain curve occur again when the 200K rectifier shunts are applied as in Figure 10. Note that these points do not occur in the original amplifier gain curve. They are encountered only when the amplifier is driven into cutoff on either end of its transfer characteristic. As the cores are brought back from cutoff (negative saturation) the snap occurs.

Explanation of Triggering Action - Before interpreting any of the amplifier gain curves showing triggering, it is in order to explain the cause of this phenomena.

From Figure 13 it can be seen from the arrow indicators that the triggering, or snap action, takes place only after the core has been driven into cutoff from the action of the control signals. As the core is then leaving the region of cutoff, the control signal increasing, bistable action takes place, jumping from a low value of output current to a higher value.

It has been determined by experiment, Reference 1, that when the core has been driven into negative saturation, also called cutoff, all domain orientations have been aligned in the direction of the applied field. (Only a minute number of the domains will never be orientated with respect of the field. It is thought that these are due to imperfections and discontinuities in the crystal structure of the magnetic material.) Once driven into magnetic saturation, there are no unoriented domains in the direction of the applied field. From experimental evidence and theory it is determined that in this portion of the hysteresis loop the increase in magnetization takes place in the form of domain growth. The domains most nearly aligned with the applied field grow at the expense of their neighbors. Since no domains oriented in the direction of a reverse field will be in existence, after having been aligned 100% in the opposite direction during negative saturation, a larger field must be applied to reverse the magnetization than would be required if the material had not been negatively saturated. This results in the displacement of the left corner of the major loop beyond the locus of the upper left-hand corners of all the minor loops, as shown by the dotted lines in Figures 15 and 16. Further consideration predicts that the locus of the upper left-hand corners of all minor loops will be in a straight vertical line since this represents the lowest coercive force. No magnetization will occur until the field has reached this value of coercive





RELATION OF MINOR LOOPS
TO TRANSFER CHARACTERISTIC

FIG.

16

(5KT37(872))

20-

force. The slope of B/H then, of course, follows the slope (permeability) of the major loop. These precepts are shown in Figure 15.

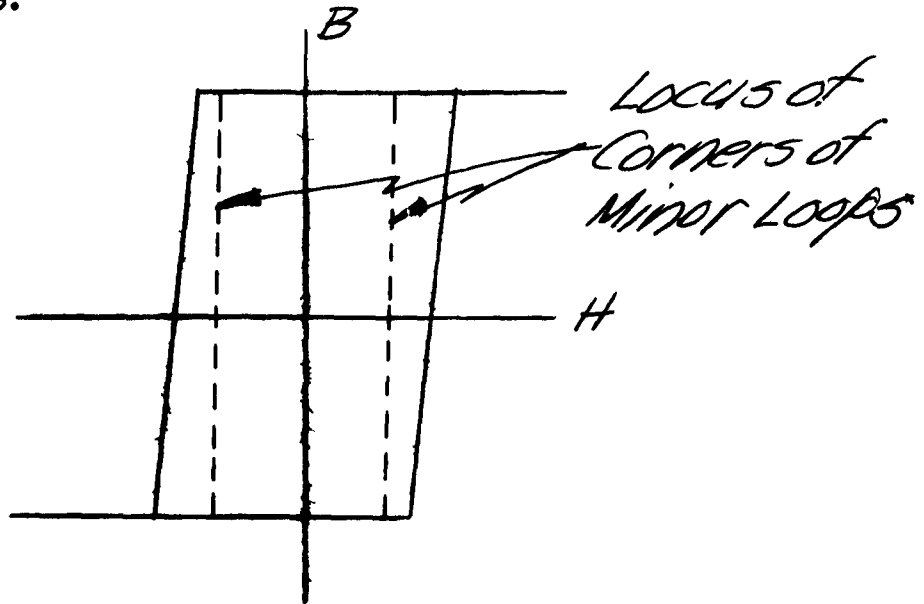


Figure 15

Figure 16 shows the action resulting in triggering. Figure 16A relates the transfer characteristic to the hysteresis loop as the core is driven into negative saturation. It is assumed that the a-c driving voltage on this particular circuit is insufficient to provide a flux excursion from negative to positive saturation every cycle. Figure 16B shows the relation of the minor hysteresis loop to the transfer characteristic after the core has been driven into negative saturation as in Figure 16A. In Figure 16C, the control signal is being returned from values beyond those causing negative saturation into the conduction region once again. No magnetization change will take place until point 6a is reached where sufficient field is being applied to cause domain growth as previously pointed out. At this point a cycling action will take place in which the first minor loop, as the core comes out of negative saturation, will cycle up the major loop towards positive saturation until it reaches saturation finally on one particular gating cycle. This is indicated in Figure 16C by arrows. Since the control signal had to be increased to return the core from negative saturation to point 6a in order to initiate any action, this same amount of control current will determine the firing point on all cycles after that in which the core saturated after completing the ratcheting action.

This will result in continued operation of the core at point 6b on the transfer characteristic and hysteresis loop. For this particular value of control current there are two stable states of output current, depending on the prior history of that core. That is, whether it had been in negative saturation or not. When the control current is reduced from values near positive saturation (full on), the output current can be controlled back and forth around point 6b with no snap as long as negative saturation is never reached. When it is reached, it is necessary to increase the control current to point 6a to obtain any change in output current. It should be noted that there is an associated time delay with this triggering action since several cycles of the applied a-c voltage are required to carry the core from the initial minor loop to the minor loop first achieving saturation. Prior to this time, the core had been able to completely absorb the volt-seconds applied by the a-c driving voltage resulting in the horizontal section in Figure 16C from point 4 to point 6a. On the cycle in which the core reaches saturation, it occurs at a phase angle less than 180 degrees, resulting in the usual sharp change in gate current through its windings and produces the jump which will be seen from 6a to 6b on the transfer curve, Figure 16C. It is at this time that a snap is observed in the amplifier and load using this core.

The cycling or ratcheting, as it is sometimes called, occurs as a result of less gate voltage than that determined by

$$E_g = 4.44 BANF \times 10^{-8} \text{ volts}$$

where B is flux density in Kilogauss
 A is cross-section cm^2
 N number of turns
 F is frequency in cycles/sec.

and unequal positive and negative magnetizing conditions during a cycle of operation. Assuming that the applied bias is less than that required to reach negative saturation, such as point 6a in Figure 16C and that there is a rectifier, in series with the applied gating voltage and the gate winding. The circuit to investigate these conditions is shown in Figure 17.

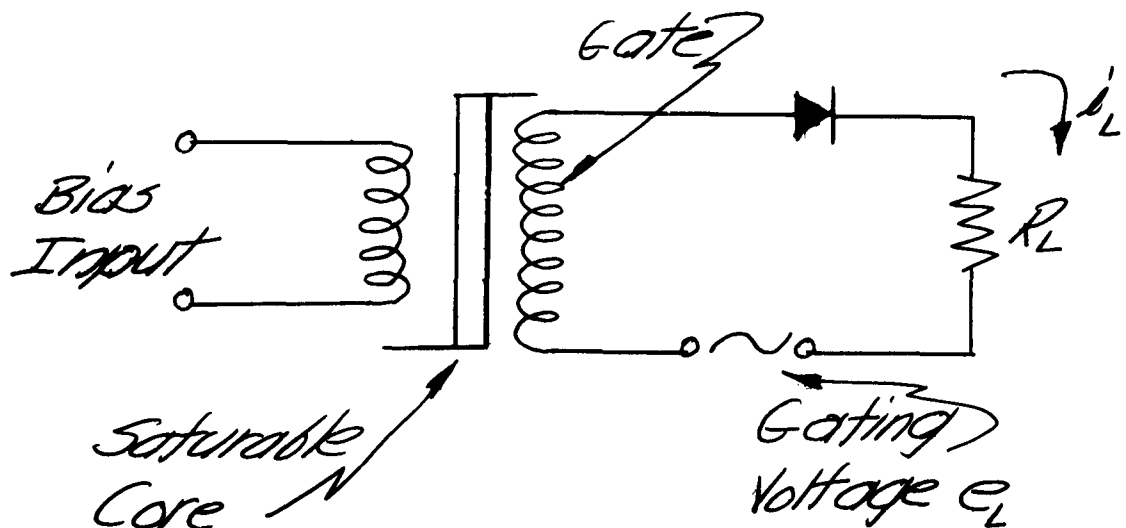


Figure 17

The positive change in flux during the rectifier's conductive time is determined from Faraday's law.

$$(\Delta\phi)^+ = \frac{1}{N} \int_0^{\frac{T}{2}} (e_L - i_L R_L) dt$$

where ϕ is magnetic flux in Maxwells.

Since the rectifier blocks the flow of reverse current in the gate circuit, the resetting or application of negative-going flux is determined primarily by the applied d-c bias. Since this was assumed less than that necessary to carry the core back down the loop to negative saturation the core will be carried negative to a point not yet in negative saturation as determined by the applied d-c bias. The negative change in flux would be identical to the positive change if the rectifier did not block the reverse current flow which would cause negative flux change by the gate circuit.

A net difference in $(\Delta \phi)^+$ and $(\Delta \phi)^-$ occurs

$$\Delta \phi = (\Delta \phi)^+ - (\Delta \phi)^-$$

The number of cycles of ratcheting are determined by

$$n \cong \frac{\phi_s - \phi_c}{\Delta \phi}$$

before reaching positive saturation. This has been observed by several experimenters (Reference 6). The situation is clearly shown in Figure 18.

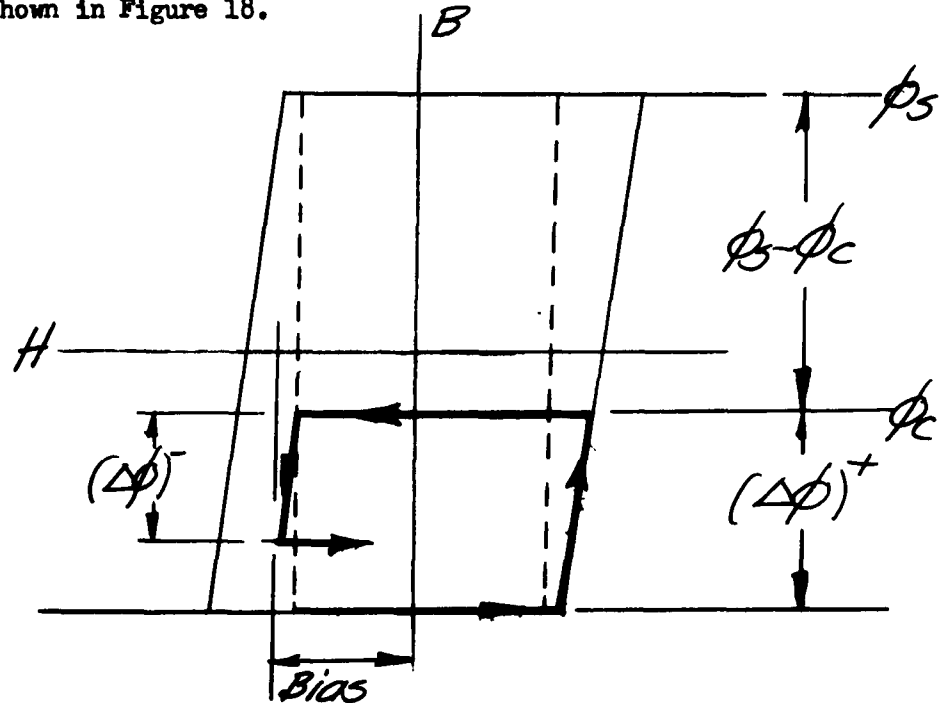


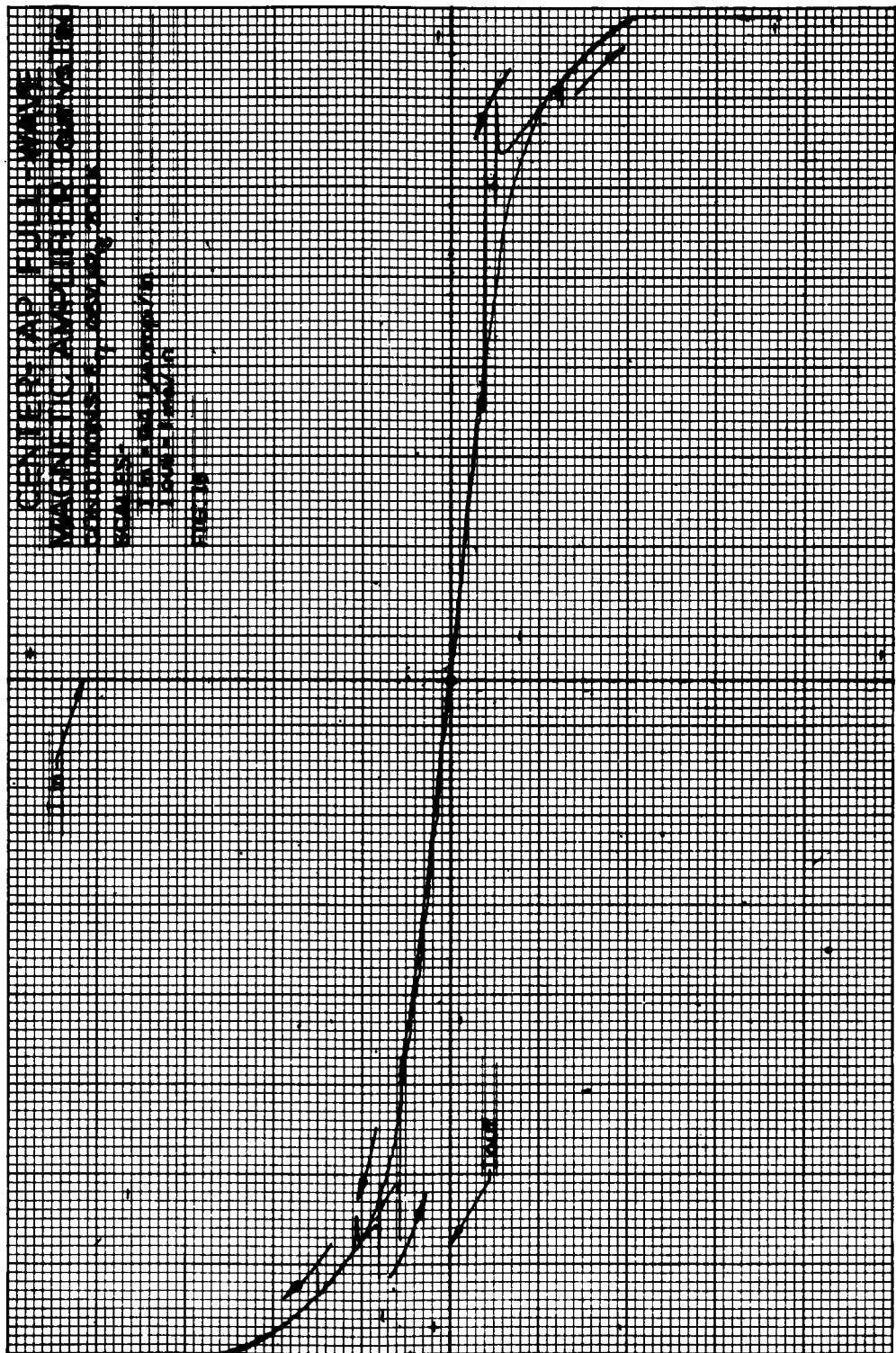
Figure 18

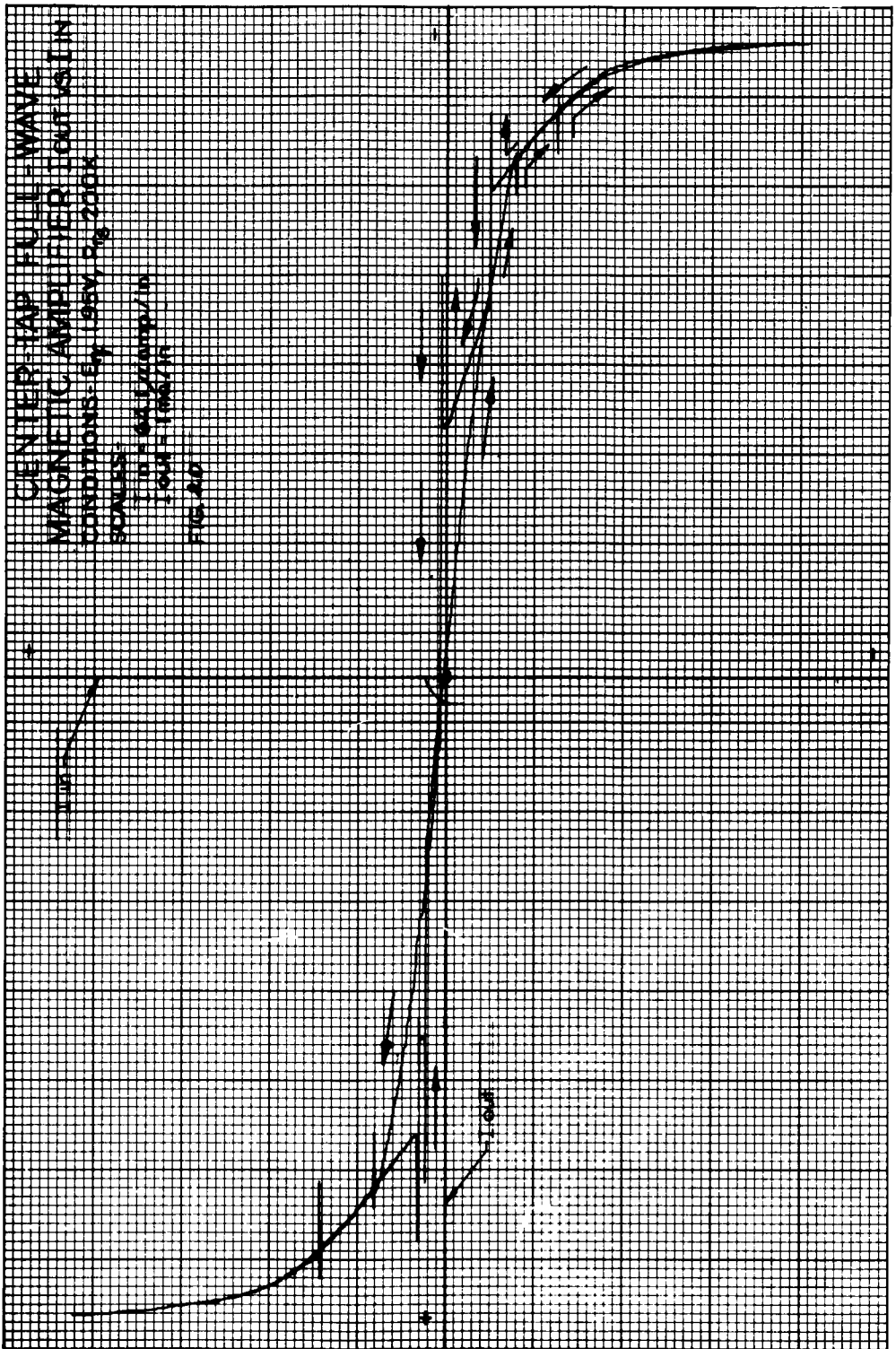
The time in the a-c cycle when the last minor loop reaches saturation is such that a jump in load current will occur for all values of bias less than that required to reach negative saturation, point 4 in Figure 16B.

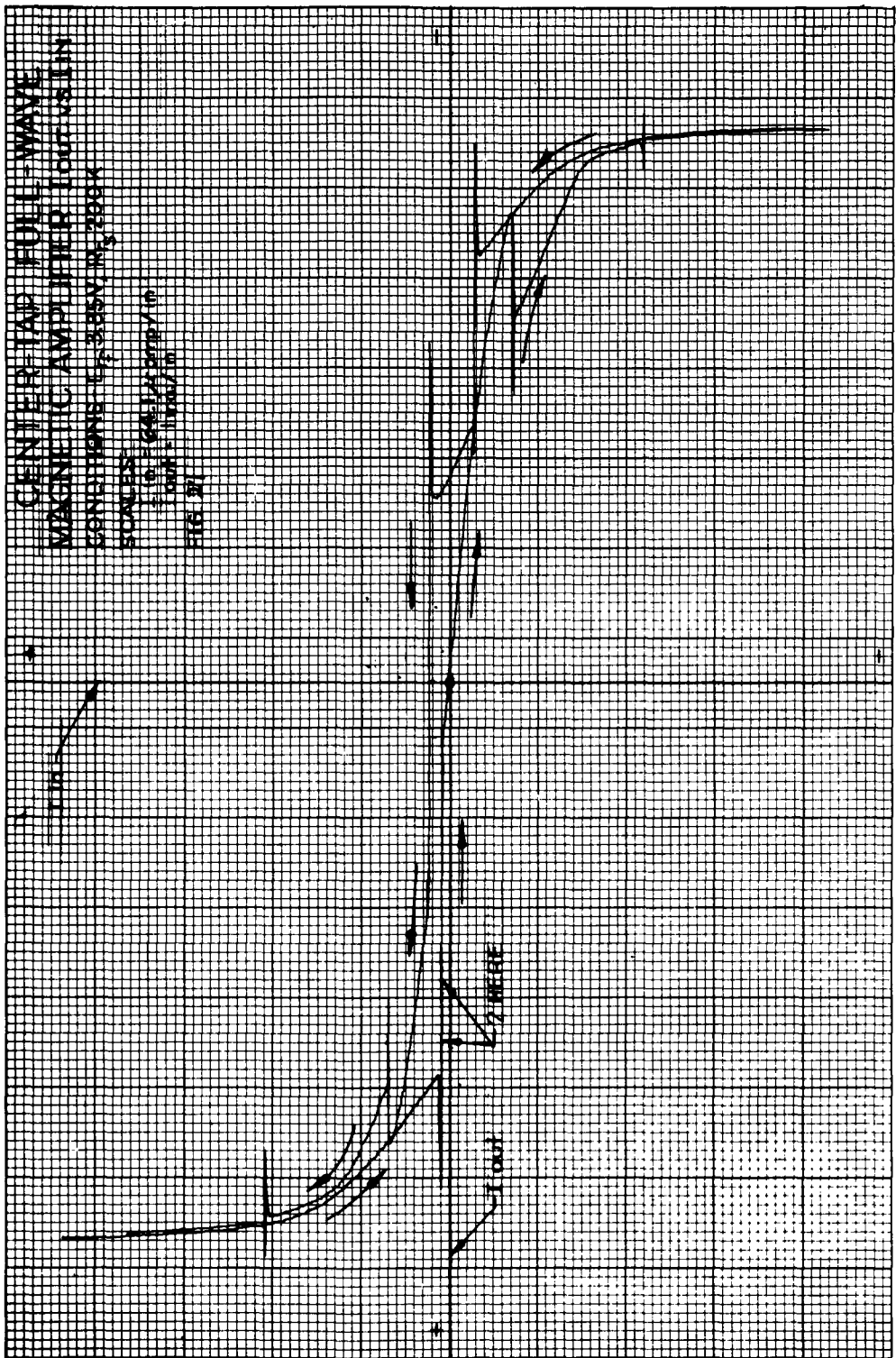
Figure 19 displays the results when 0.65 V forward voltage drop is inserted simulating the increase in the voltage of this diode type under radiation, the bistable regions at each end of the transfer characteristic occur at less control current (I_{in}) and are greater in magnitude (I_{out}). It is felt that variation in components and batteries causes the appearance of 4 separate jumps, probably associated with each of the four cores. As previously pointed out, the jump occurs after having driven out into cutoff (flat regions at each end of the curve). In Figure 20, E_{rf} has been increased to 1.95 V. The bistable regions now cover almost the entire transfer characteristic, rendering the amplifier completely useless. The small jumps are probably caused by induced voltage in the control circuit from the opposite pair of cores which are triggering. Note that the small jumps occur when increasing the control current and are in opposite directions from the larger bistable jumps. The arrows indicate the sequence of events. Figure 21 shows the characteristic with $E_{rf} = 3.85$ V. The transfer characteristic now consists almost entirely of a series of bistable regions. As the E_{rf} has been increasing the bistable regions occur at less and less control current and exhibit large jumps in output current. Since the a-c gating voltage must overcome the knee voltage of the rectifier to cause appreciable conduction, there will be less and less voltage applied to produce $(\Delta \phi)^+$ in the core as the rectifier knee voltage increases. The reduced $(\Delta \phi)^+$ will, of course, cause the core to saturate early in the cycle when the first ratcheting minor loop does reach saturation, resulting in a greater jump in load current. That is, from cutoff, (min. current) to near maximum current. Thus, one could expect the increasing knee voltage to cause more severe triggering. The association of decreased control current to reach the bistable points with increasing E_{rf} can be deduced from Figure 13. Assume control current had been such as to cause $I_{control}$ to be maximum, cutting off side B at point 2a. As the control current is reduced from its maximum value, 2a is reached going in the opposite direction. The rectifier knee voltage has initiated the sequence of events so far described. Triggering would take the place at 3a, the cutout of side B jumping to 1a. The total transfer characteristic is consequently affected, as shown. If the knee voltage continues to increase, triggering will take place at 6a for reasons already explained. Thus, it appears that the triggering takes place at small control currents as the rectifier knee voltage increases with radiation.

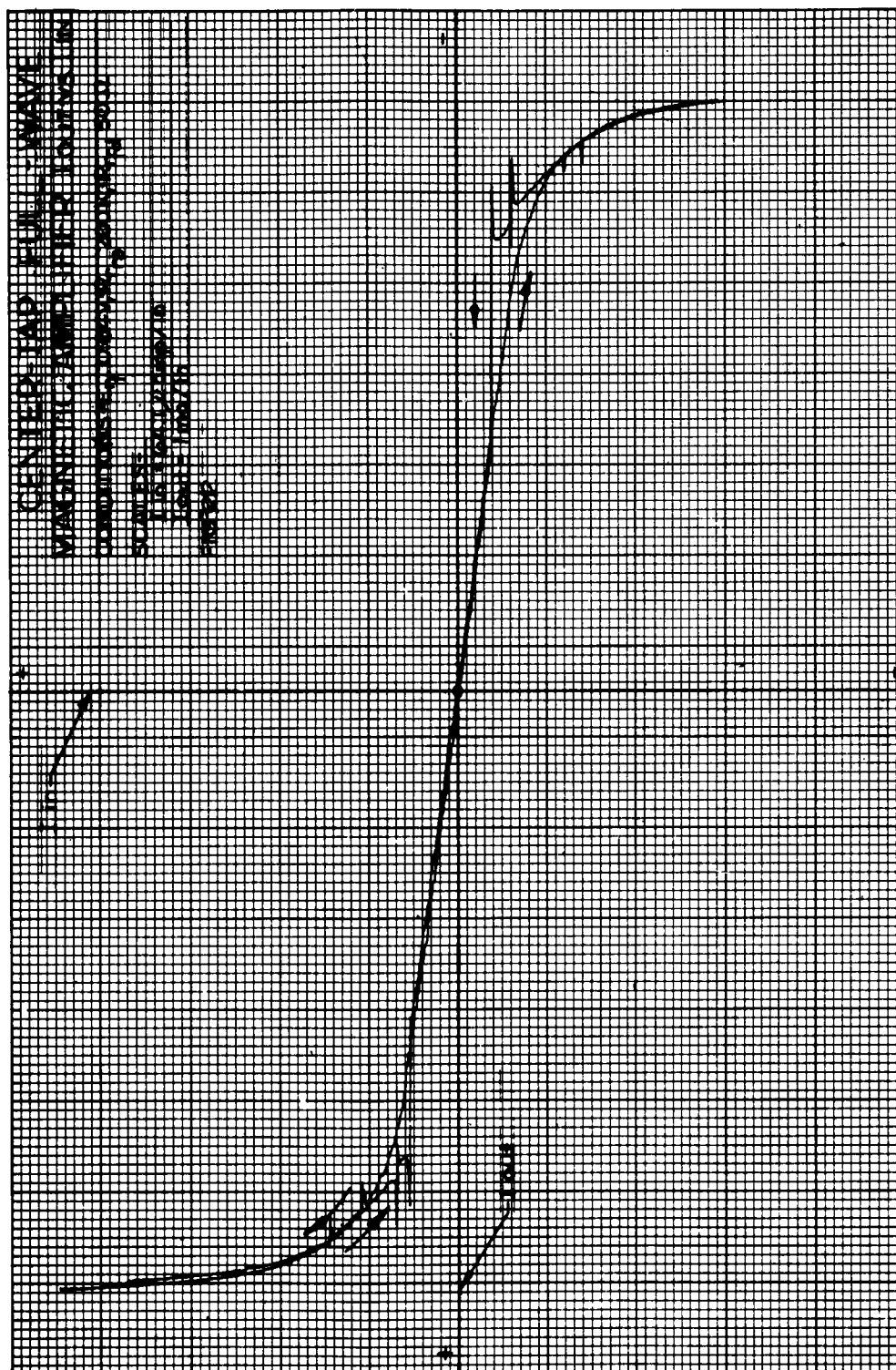
3. Effects on This Circuit of the Diode Changes of Figure 1C

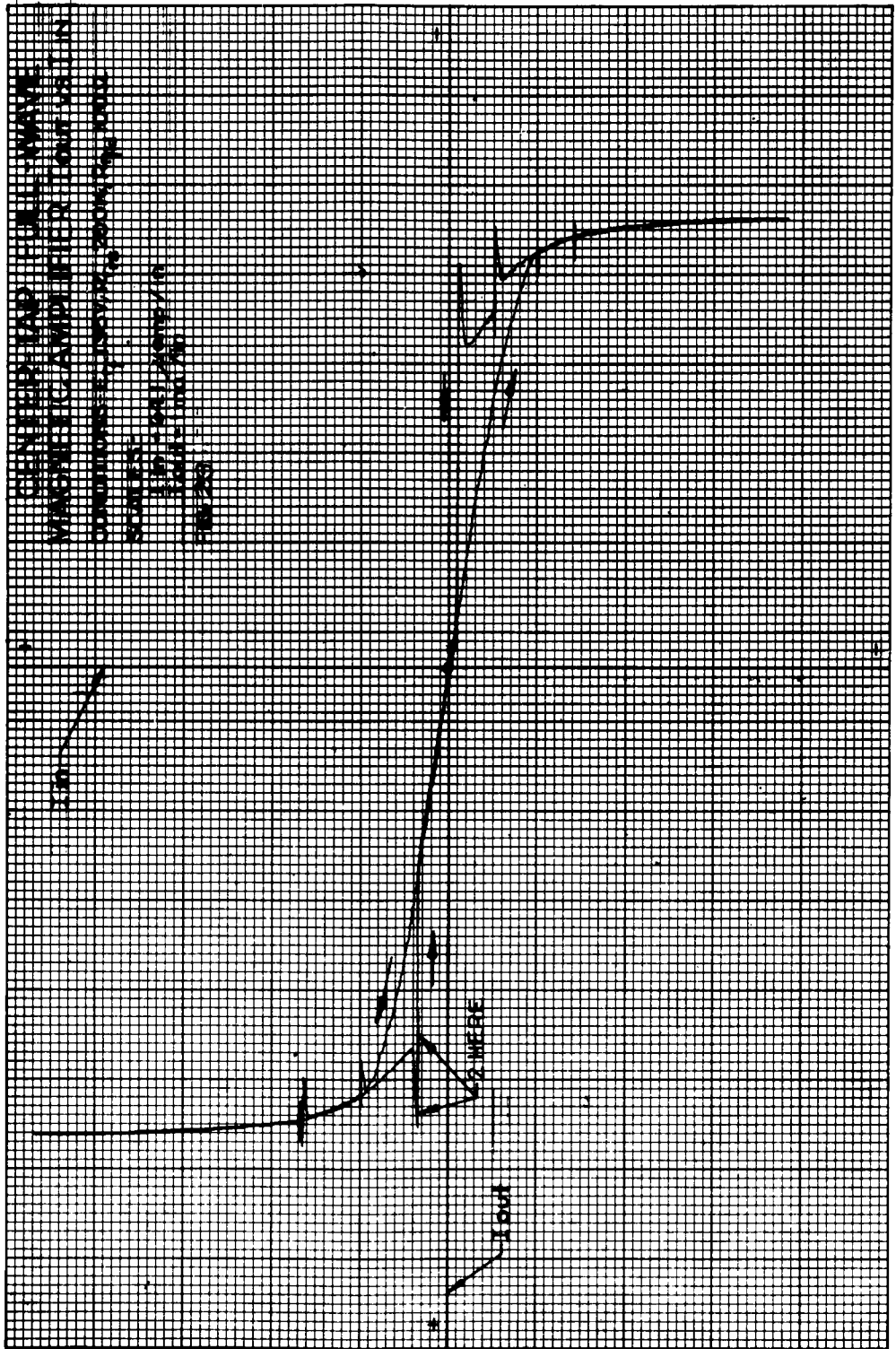
The diode of Figure 1C combines the increasing conduction knee voltage associated with 1a with the decreased forward conduction with the diode at 1b. Results are shown in Figures 22 to 24.

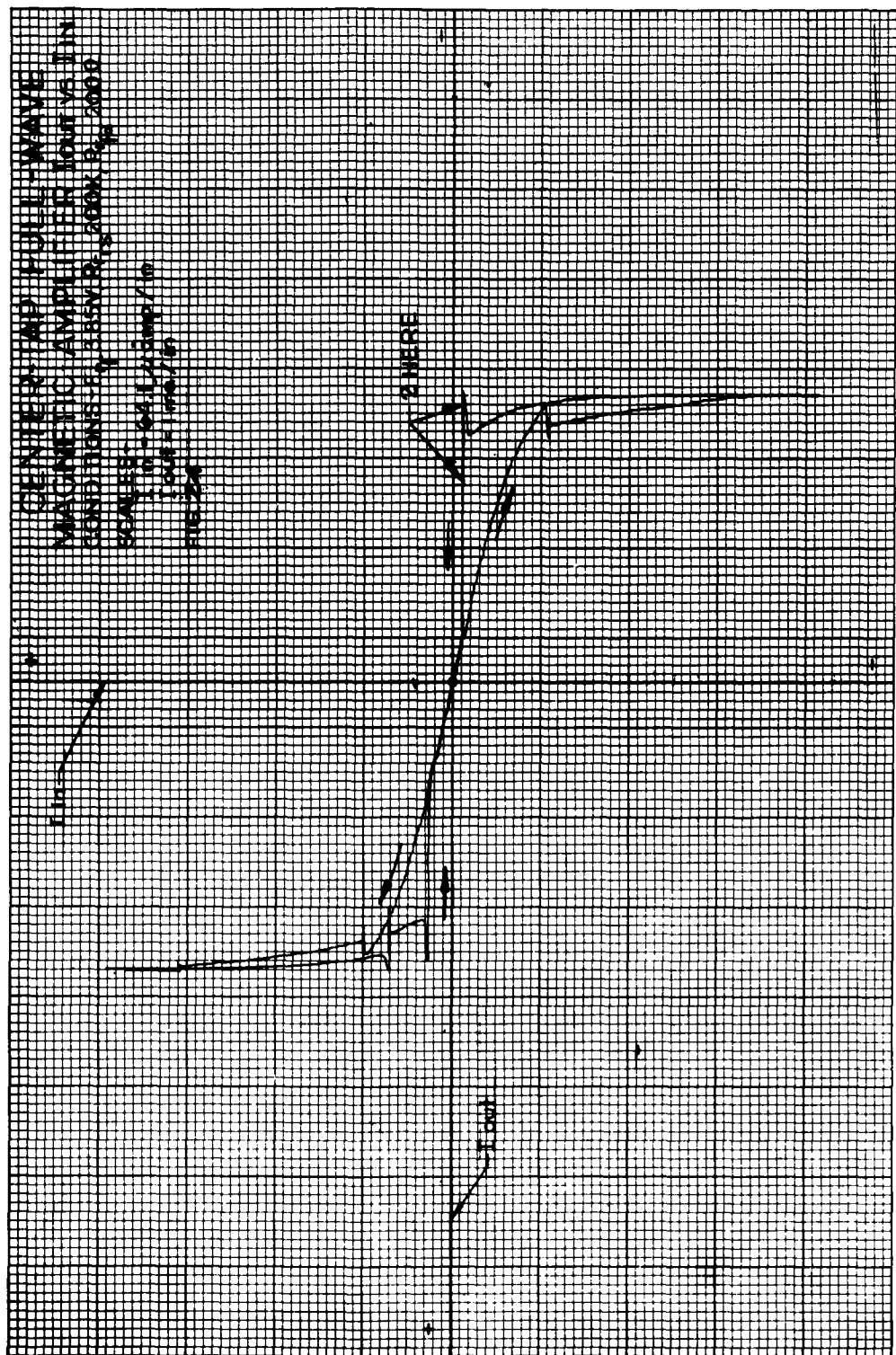












As might be expected, the effect on the magnetic amplifier appears to be superimposition of the effects produced by the two previous diode failure types. The same bistable action is present, increasing in magnitude as the radiation effects increase until little or no proportional region occurs. Because of the decreased forward conductivity of the diode, the maximum output current is less than half for this form of diode failure. The examination of these effects is covered in section III-A-1 and III-A-2.

B. Half-Wave, Half-Bridge Circuit

The circuit of the half-wave half-bridge magnetic amplifier is shown in Figure 25. Again, the circuit effects produced by forward and reverse diode characteristics have been separated for clarity as was done for the full-wave, center-tap circuit.

In Figure 26 the original transfer characteristic of the amplifier is shown for comparison without diode changes.

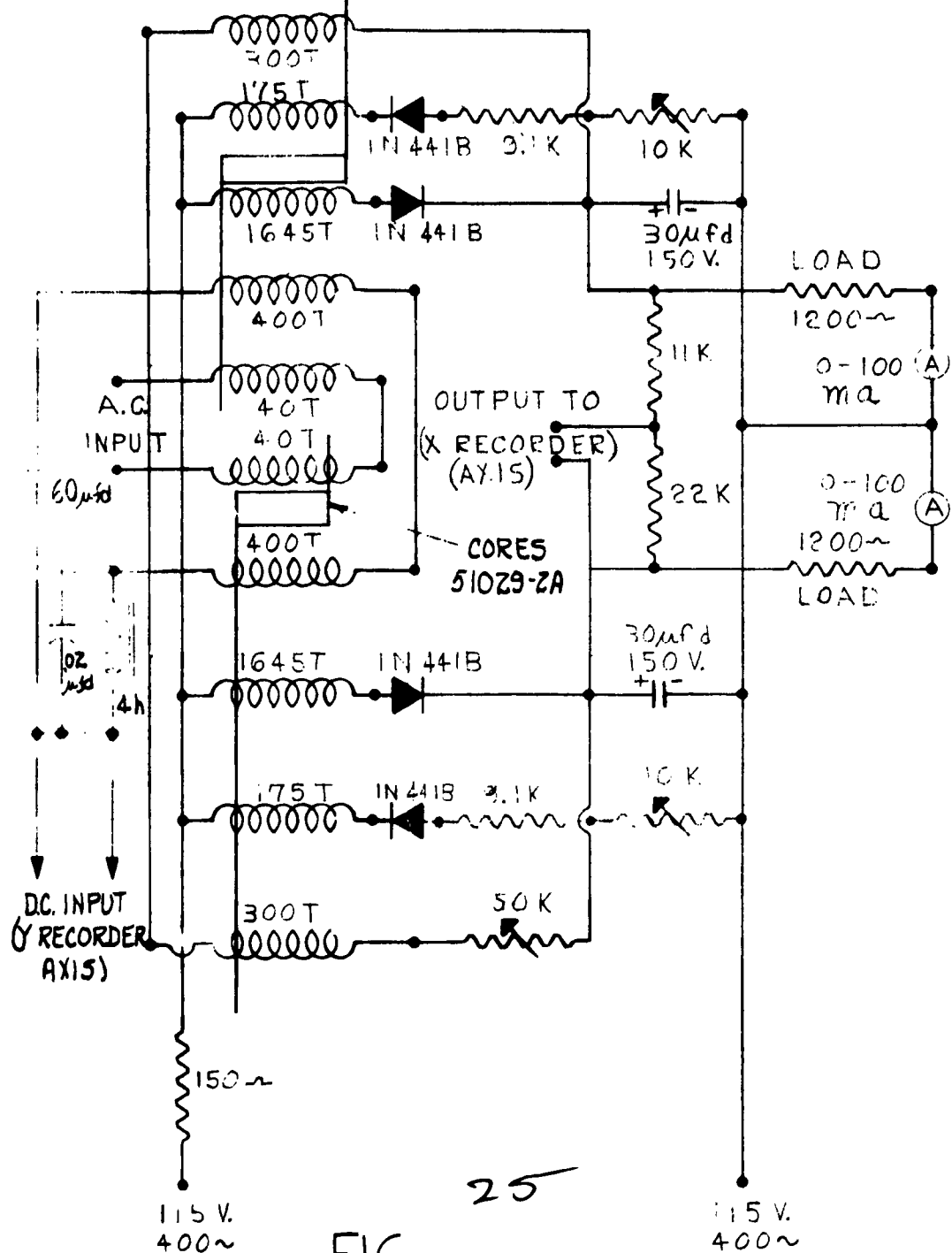
As a matter of interest the reset diodes were shunted independently of the circuit diodes to further separate effects. The results of a 900K and a 200K resistor shunt are shown in Figure 28. No deviation from the original curve of Figure 27 has occurred for either shunt value. The gate diodes were then shunted with the same two values of shunt, leaving the reset diodes unshunted and the effect on the amplifiers transfer characteristic recorded in Figure 27. Figure 27B, 900K shunt, indicated a slight reduction in gain while the 200K shunt produces 27B about a 2-to-1 reduction in gain. This is the only observable effect on the amplifier as a function of diode reverse current increase. As a total effect then, for both gate and reset diodes, one would expect approximately 2-to-1 gain reduction with the worst diode back current condition (200K) due entirely to the gate circuit diodes. The increased resetting produced through the gate turns with the increased diode reverse current, which is of the right phase to cause resetting, is responsible for this reduction. The effect is greater than that produced by shunting the reset diodes because the larger number of gate turns produces a greater NI. (Reset to gate turn ratio is usually 1:10 in this circuit.)

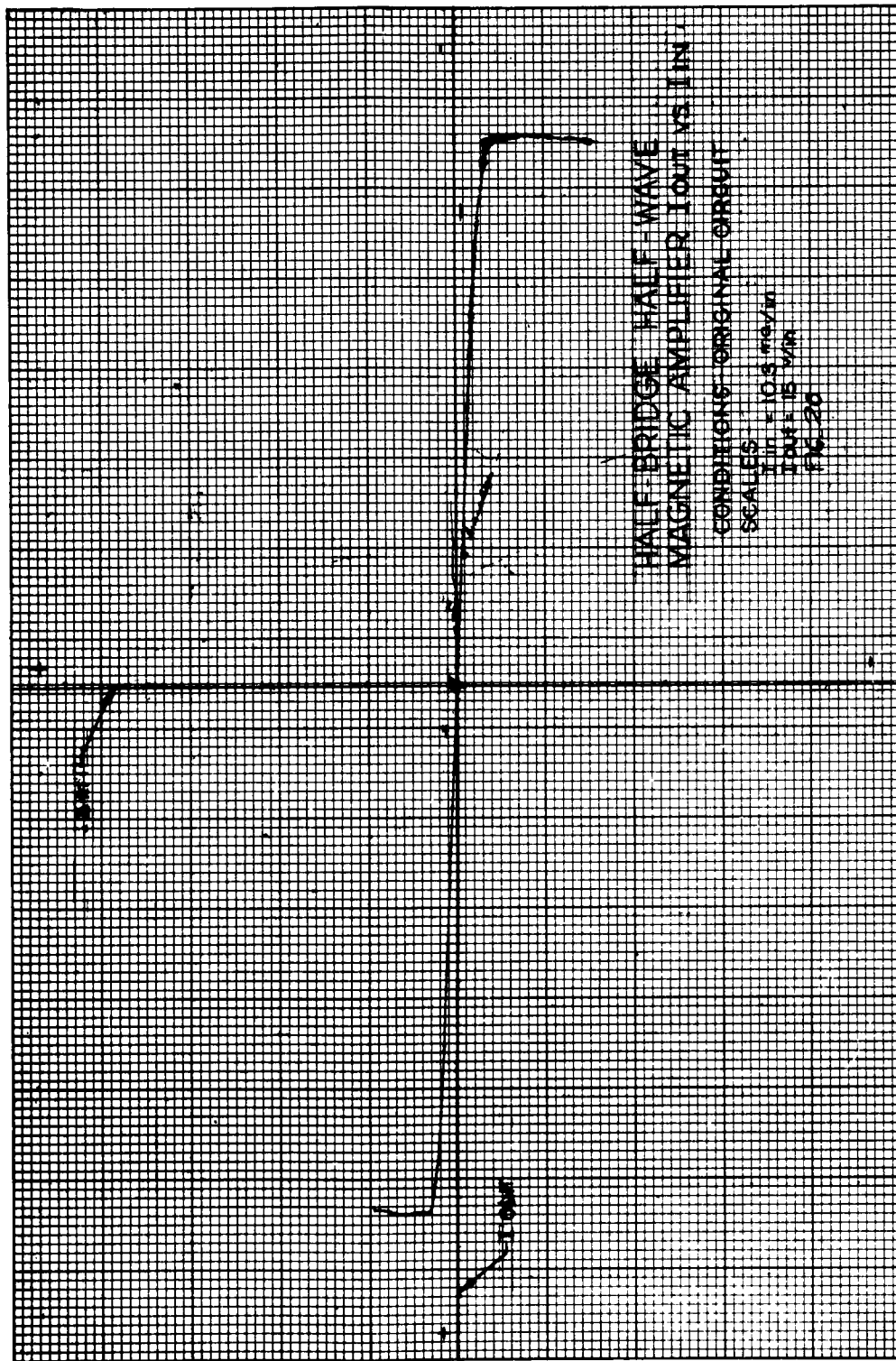
1. Effects on This Circuit of the Diode Changes of Figure 1B

The decreasing forward conductivity of this diode as irradiation progress produces a moderate reduction in gain and a gradually reducing maximum current output. The reasons for this behavior are identical with those of section III-A-1. Results are displayed in Figures 29 and 30.

The shape of the transfer characteristic is not altered and no discontinuities are produced as was found in the full-wave, center-tap circuit. This is a result of operating with greater than saturation voltage in the gate circuit. That is,

HALF-WAVE HALF-BRIDGE MAGNETIC AMPLIFIER





HALF-BRIDGE HALF-WAVE
MAGNETIC AMPLIFIER I_{out} VS. I_{in}

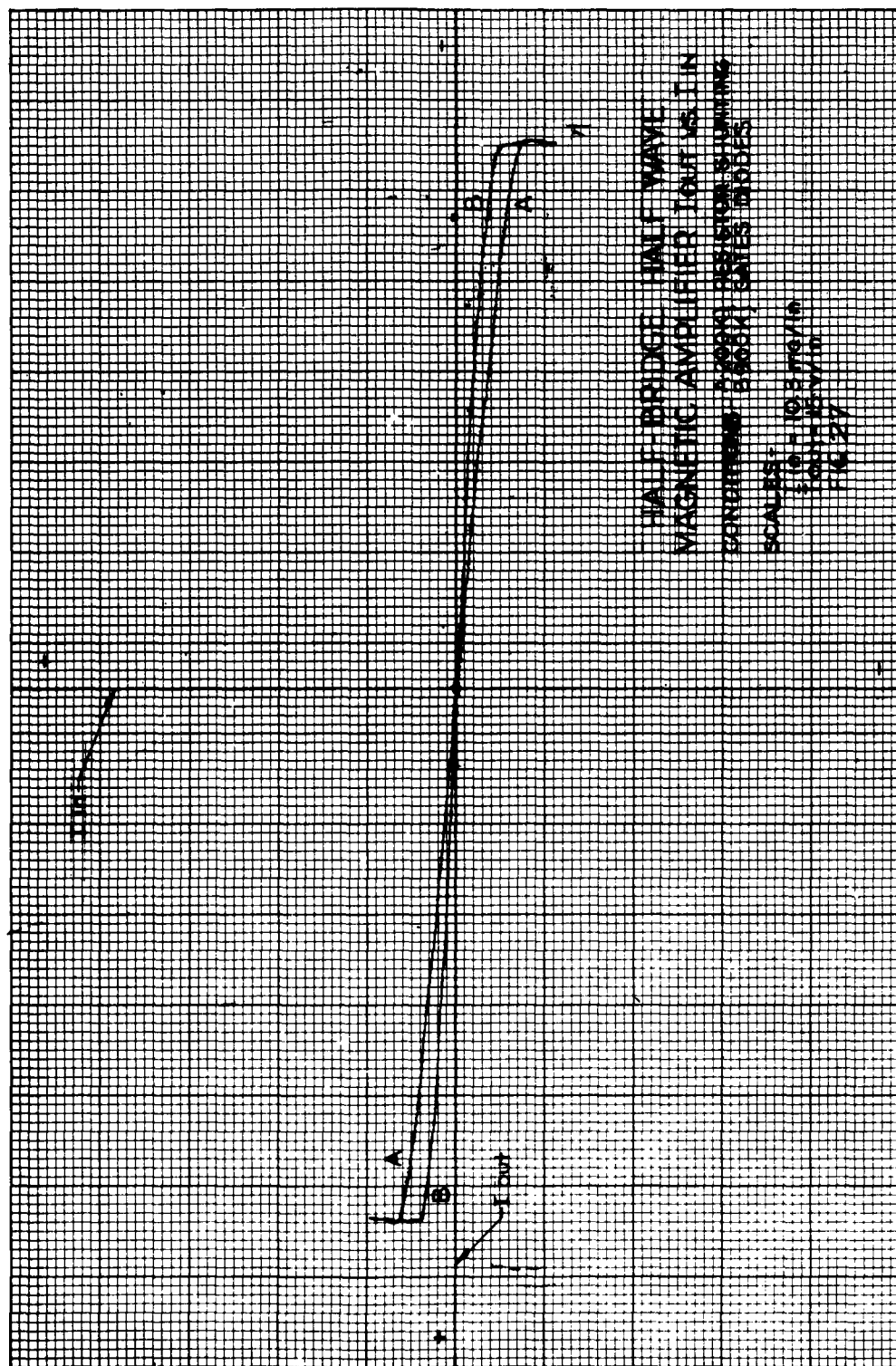
CONDITIONS: ORIGINAL CIRCUIT

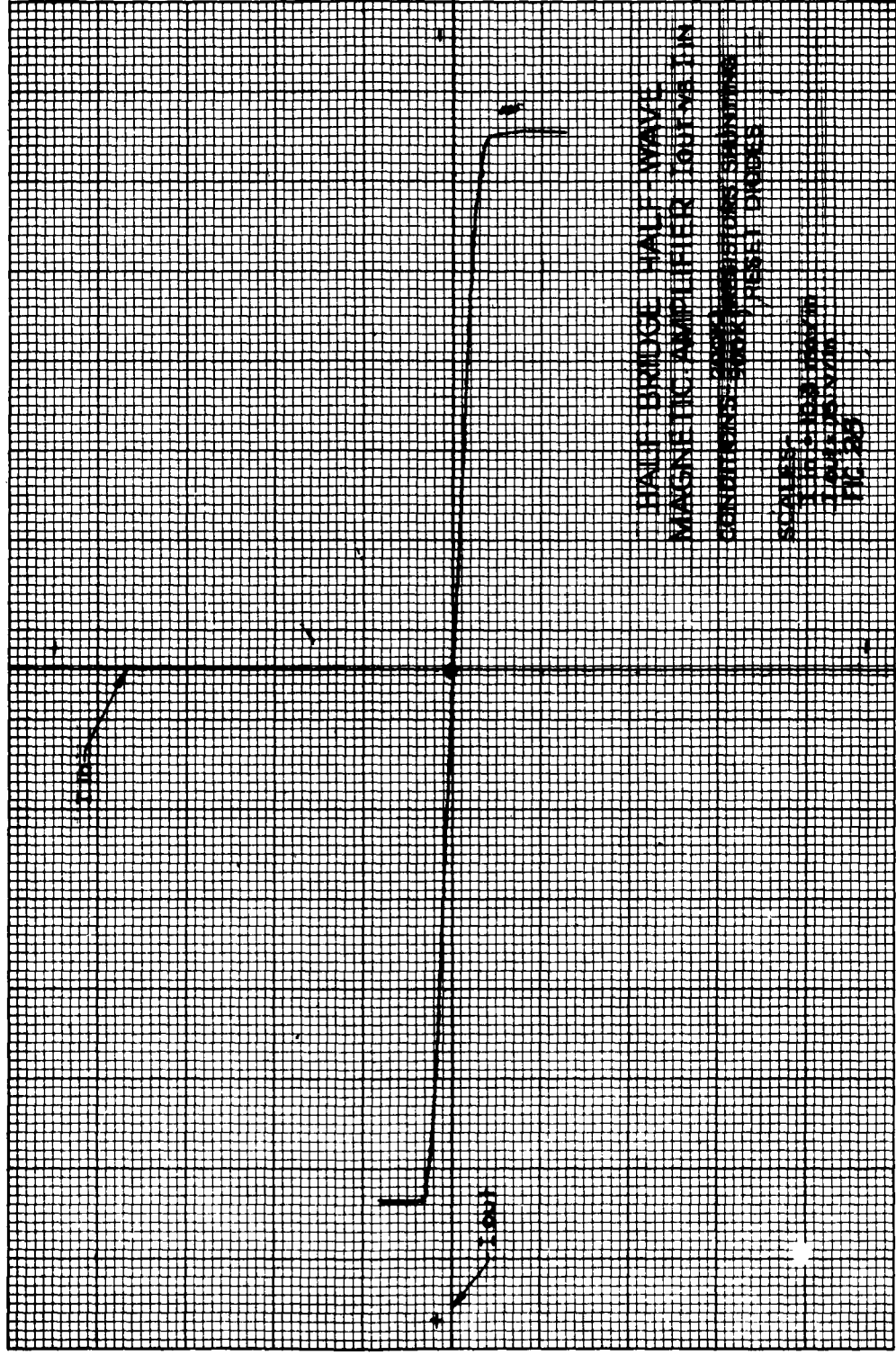
SCALES:

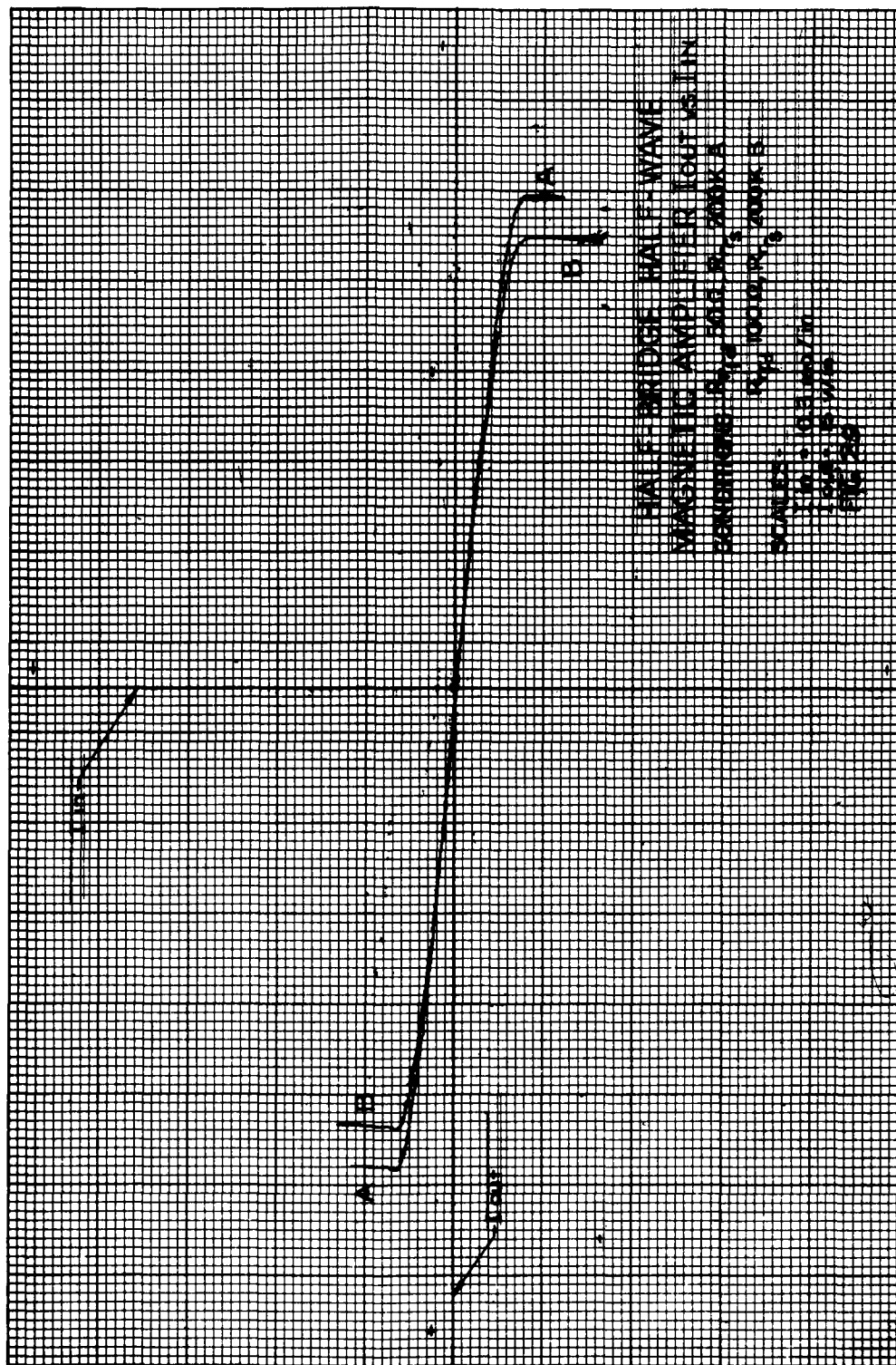
$I_{in} = 10.8 \text{ mA/in}$

$I_{out} = 15 \text{ mA/in}$

FIG. 20







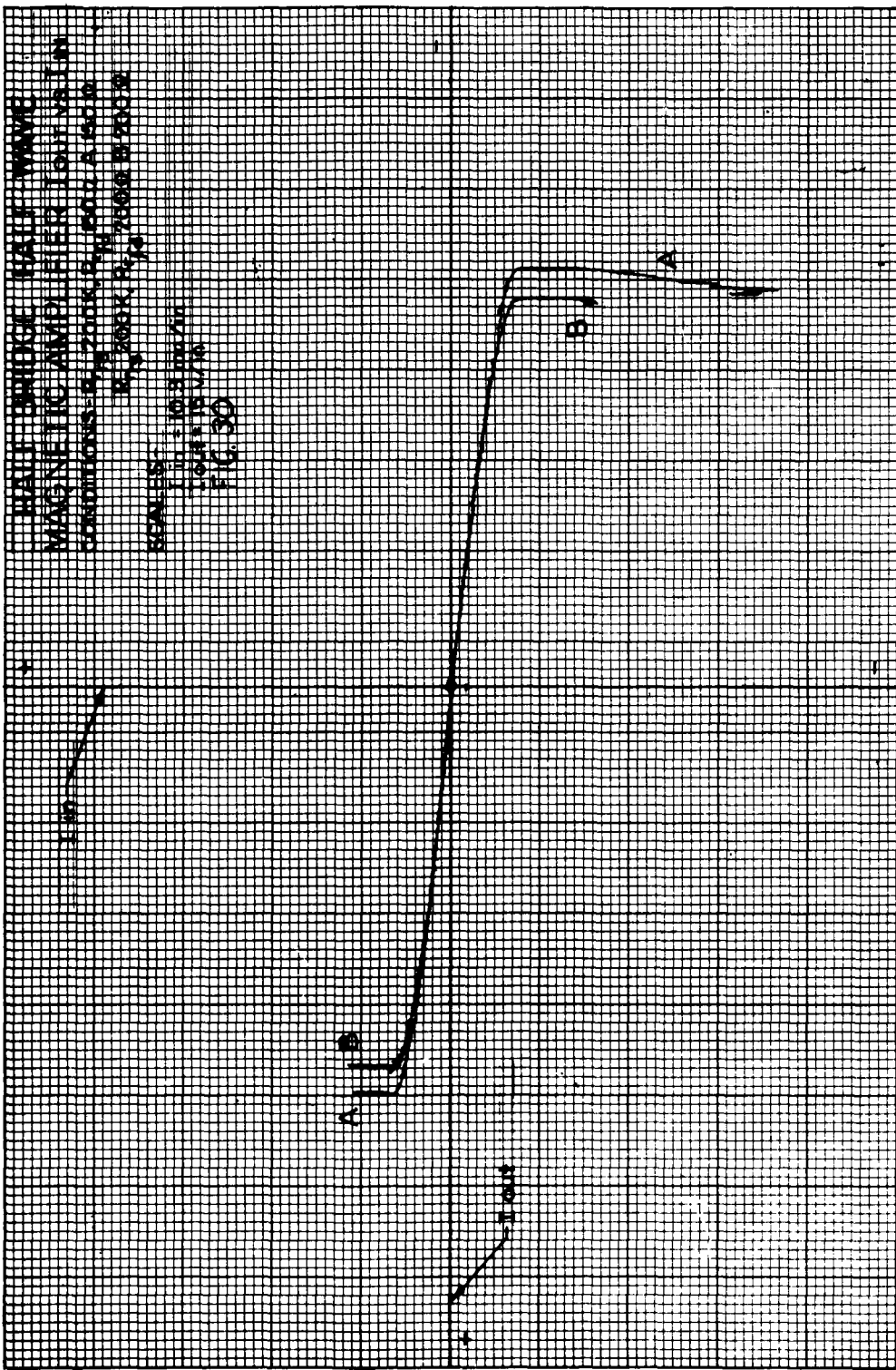
HALF BRIDGE HALF-WAVE
MAGNETIC AND FETTER LOG-5-TIN
ZEROTHONE 548.0. 200K A

SCALES: 100 1000 2000 5

100 1000 2000 5

100 1000 2000 5

100 1000 2000 5



$$E_{line} = 4.44 \text{ BANF} \times 10^{-8} \text{ volts.}$$

The triggering and ratcheting do not occur when the core is carried well into saturation by the gate voltage alone. In addition, this circuit uses a 115-volt gate driving voltage whereas the full-wave center-tap circuit used only 12 volts. The higher voltage will, of course, mask the relatively small diode knee voltage effects and the cores are still cycled completely into position saturation by the gate voltage, regardless of the knee voltage drop. It should be mentioned again that for all forward conditions the reset and gate diodes are shunted by 200K ohms to simulate maximum effect of reverse diode current change due to radiation. The curves are the total effect, as was previously pointed out.

2. Effects on This Circuit of the Diode Changes of Figure 1A

The effect of all four degrees of the diode of Figure 1A are recorded in Figure 31, since no large charges are involved to confuse the multiple plot. There is an extraneous curve on this figure which should be ignored. The right-hand end of the set shows clearly the effects of increasing diode knee voltage. That is, a slight reduction in maximum output current as the knee voltage increases. This is merely subtraction of the diode knee voltage from the total voltage applied to the series combination of diode and load. No change in gain has occurred.

3. Effects on This Circuit of the Diode Changes of Figure 1C

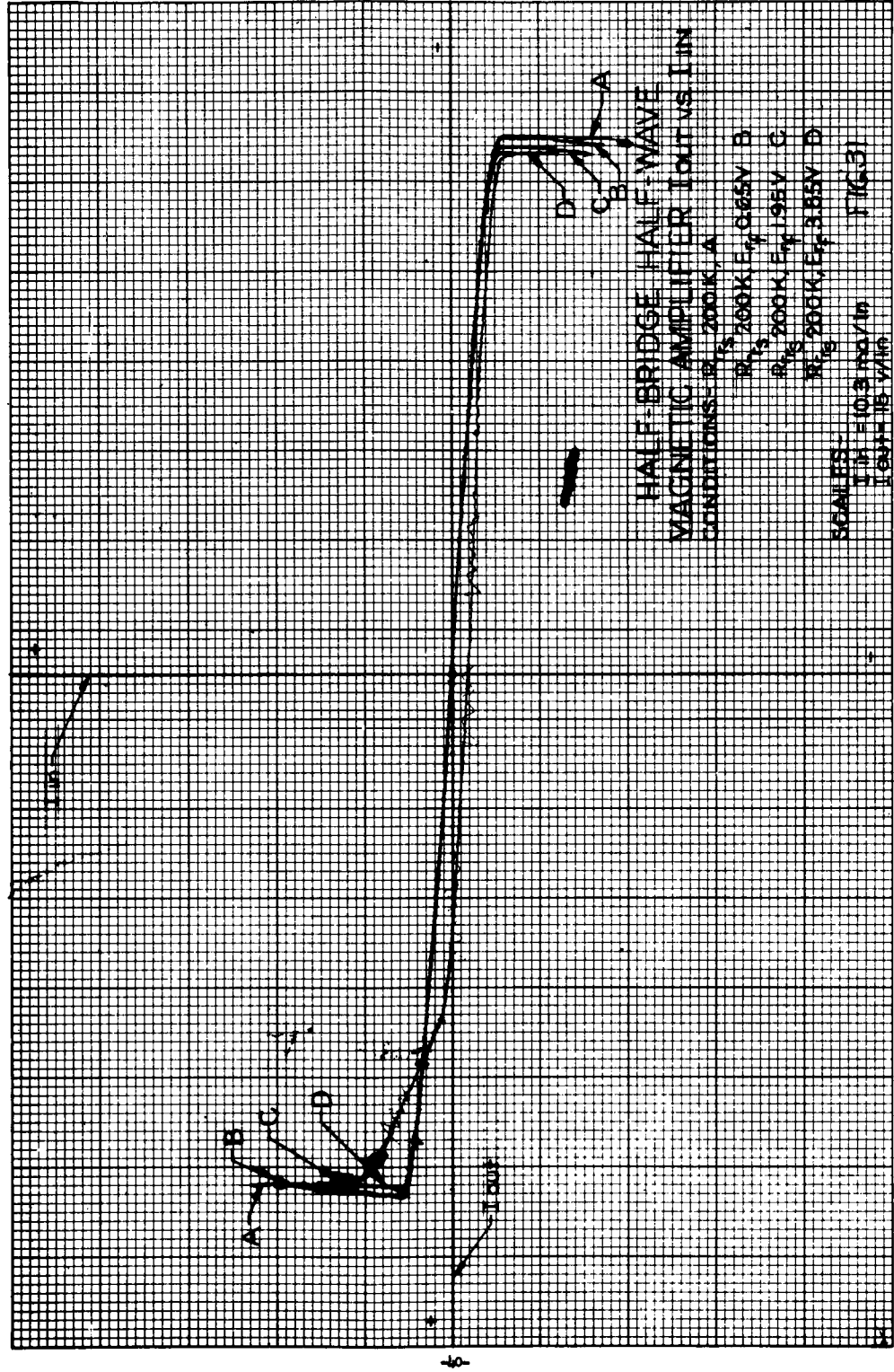
Again, this diode type combines the increasing conduction - voltage knee and decreased forward conductivity as radiation dosage increases. As before, the diode-produced effects can be superimposed. That is, the effects produced by decreasing forward conductivity can be clearly identified in a combination recording involving both knee and conductivity changes in the diode. In Figure 32 the results are displayed of combined knee and conduction changes in the diodes of this circuit.

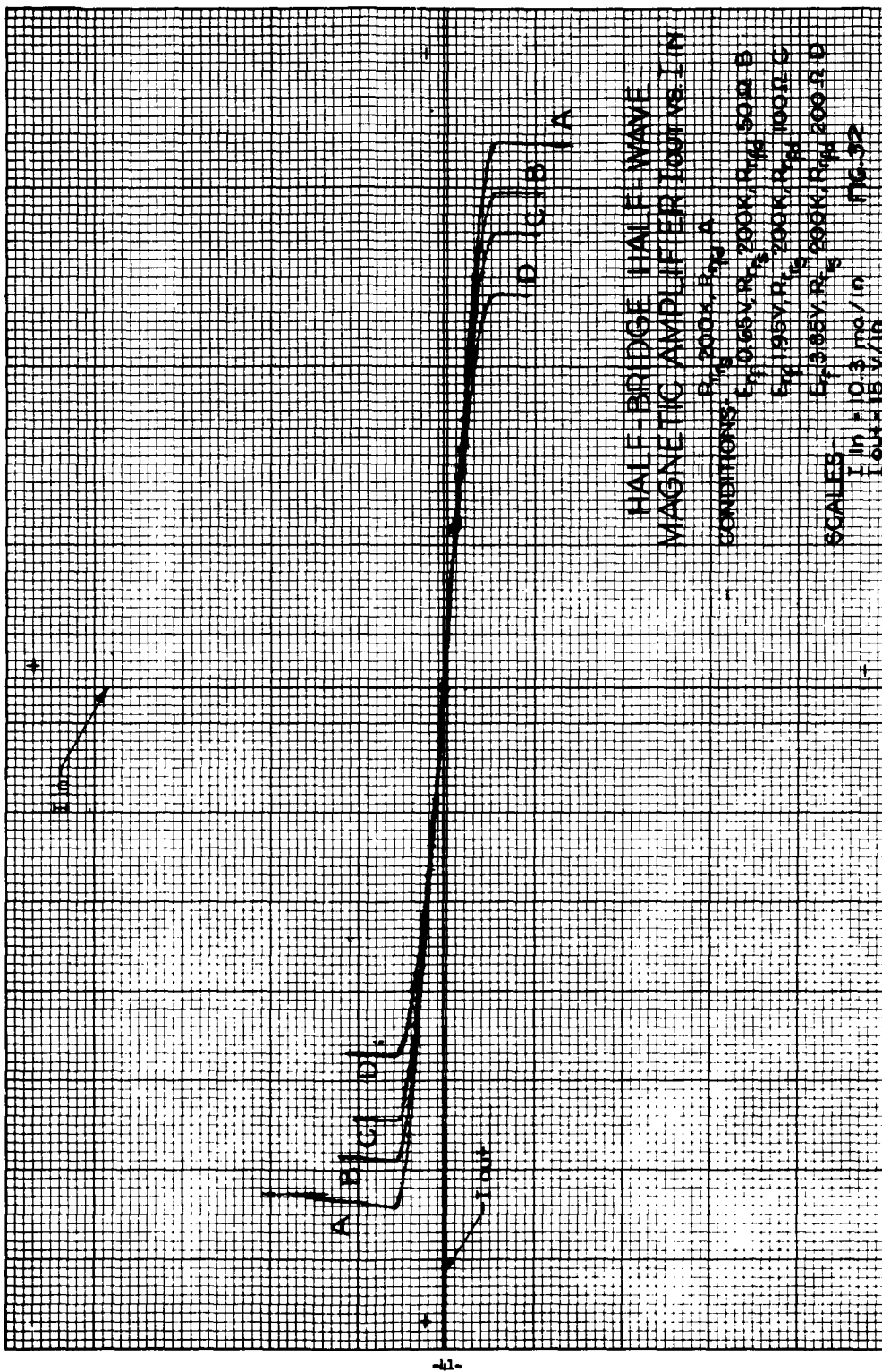
The major effects are produced by the increased forward diode resistance reducing maximum output and gain. The slight reduction in gain due to the knee voltage is added to the larger effect produced by the increased diode forward resistance.

IV. CONCLUSIONS

A. Diodes

The major effects on the magnetic amplifier circuitry are produced by changes in the forward characteristics of the diodes. The most serious forward effect is the increased dynamic forward resistance, since it was found that the effects of increased diode forward knee voltage





could be eliminated, but the effects of an increase in diode forward dynamic resistance cannot.

Reduction in diode reverse resistance, at least down to 200,000 ohms, produces minor reductions in gain which can be compensated for by:

- (1) diode shunts
- (2) increased negative feedback
- (3) Positive feedback through reversed diode to increase gain as diode back resistance reduces.

The choice of 200,000 ohms as a minimum reverse resistance is more than adequate (see 1N538 curves, Reference 2).

From these considerations the diode type of Figure 1A is the most desirable since its irradiation-produced conditions can be compensated for. This form of failure should be characteristic of a diffused-junction rectifier according to References 4 and 5. Recent evidence may contradict this assumption.

Second choice would be the diode of the type of Figure 1B which is supposed to be characteristic of a true alloy-junction device. The total output voltage lost across the diode will be less if the knee voltage does not increase as the forward dynamic resistance increases. Type 1c would be the least desirable choice of the three types considered for reasons detailed already.

B. Circuits

The present design of the full-wave, center-tap magnetic amplifier circuit is unsuitable. All the most serious effects can be traced to a reduction in applied gate voltage below saturation level with resultant ratcheting and triggering. Modification of this circuit can give greatly improved operation in the face of large diode changes with no evidence of bistable triggering. Details of this modification and display of results are contained in the Appendix. The essence of the change is to operate the cores at

$$E_{line} = 2 (4.44 \text{ BANF} \times 10^{-8}) \text{ volts.}$$

This modification allows full use of the diodes simulated here to the maximum forward changes shown and beyond, thereby increasing the radiation life of the magnetic amplifier. High gate voltage is desirable to reduce the effects of diode knee voltage and forward dynamic resistance changes as was shown in section III-B. Higher gate voltages will allow use of the diodes long after they have exceeded changes shown in this report.

Gate voltage in excess of the saturation voltage of the wound core is essential to prevent triggering. When the gate voltages are low but in excess of saturation voltage, it will be necessary to use a large amount of negative feedback to stabilize the gain as considerable gain

change (one-half initial gain) is involved as illustrated in the Appendix. Other means of gain compensation can be devised, as mentioned.

The half-wave amplifier was least affected because of the relatively high gate voltage employed. Charges simulated here produced a reduction in gain of about 2:1. Negative feedback will again be required to stabilize the gain.

Although it is not possible to generalize the radiation-induced effects on several samples of a single diode type from Reference 2, it is of interest to predict the useful life of a magnetic amplifier constructed with 1N538 diodes by comparison with the simulated diodes. A 1N538 plot from Reference 2 was chosen which did not have any unusual effects. By calculation of dynamic forward resistance and knee voltage, it was possible to correlate Figure 5 (curve $E_{rf} = 3.85$ V, $R_{rs} = 200$ K, $R_{fd} = 200$ ohms) with the 2×10^{15} nvt dosage plot of this diode. One may thus predict that the half-wave amplifier would operate satisfactorily to this dosage with minor changes when constructed with 1N538 diodes. The modified center-tap amplifier described in the Appendix would likewise be useful to this dose. Both would require some gain compensation. Further predictions can be made in the same manner.

APPENDIX

Modification of Original Full-Wave, Center-Tap Magnetic Amplifier to Eliminate Triggering

The extreme amount of triggering displayed in some of the previous recordings would, of course, be disastrous in a reactor control or other systems employing this amplifier. Assume for a moment an error amplifier application. The amplifier would receive a large, unbalanced input when a perturbation was introduced. The amplifier would be driven into cutoff on one side. As the servo system acted to reduce the error to null, the side of the amplifier which had been cut off would receive increasing turn-on control current. It is at this point that the multiple triggering would take place. The output would suddenly jump to a new lower output current. The system would try to correct for this by causing a fast reduction in the controlled variable and, consequently, the feedback signal. This, in the case of a large inertia load, would be hard on bearings and actuator and, in the case of a nuclear reactor control, could cause a jump in flux level and possibly initiate safety action.

At any rate, this action continued would certainly be detrimental to the actuators. If the bistable jump were such as to change polarity of the output without changing polarity of the input, the system would enter a limit cycle oscillation. Such a jump can be seen in Figure 21.

At this particular amplifier is to be used in a nuclear reactor control the triggering cannot be tolerated. An investigation was made of the effects of increasing the gate voltage on this amplifier. The increasing severity of triggering as radiation progresses and the clean operation of the higher voltage half-wave amplifier lead to the possibility of eliminating triggering in this particular set of conditions. The applied a-c driving voltage was increased from 13.5 volts (just at saturation) to 27 volts (twice saturation voltage). Saturation voltage is determined by

$$E_s = 4.44 \text{ BANF} \times 10^{-8} \text{ RMS volts}$$

for a sinusoidal driving voltage waveform. It was necessary to alter the bias circuit values and the saturating-regulating transformer with its attendant large power dissipating resistor was no longer found to be necessary. The results are recorded in Figures 33 to 38. The transfer characteristics for the original and modified amplifier for each of three forms of diode radiation-induced failure are shown. The most severe effect in each case is used. The initial transfer characteristics without diode modification are shown superimposed on the recordings of the diode-produced changes.

In Figure 33 the effect of a knee voltage increase of 3.85 volts (diode type A, Figure 1) on the original circuit is recorded for comparison. The results are easily compared with the original transfer characteristic included on the same recording. The characteristic of the modified

ORIGINAL CENTER-AP PULL-PAUSE
MAGNETIC AMPLIFIER CHARACTERISTICS

CONDITIONS

1. MAGNETIC AMPLIFIER OPERATING POINTS

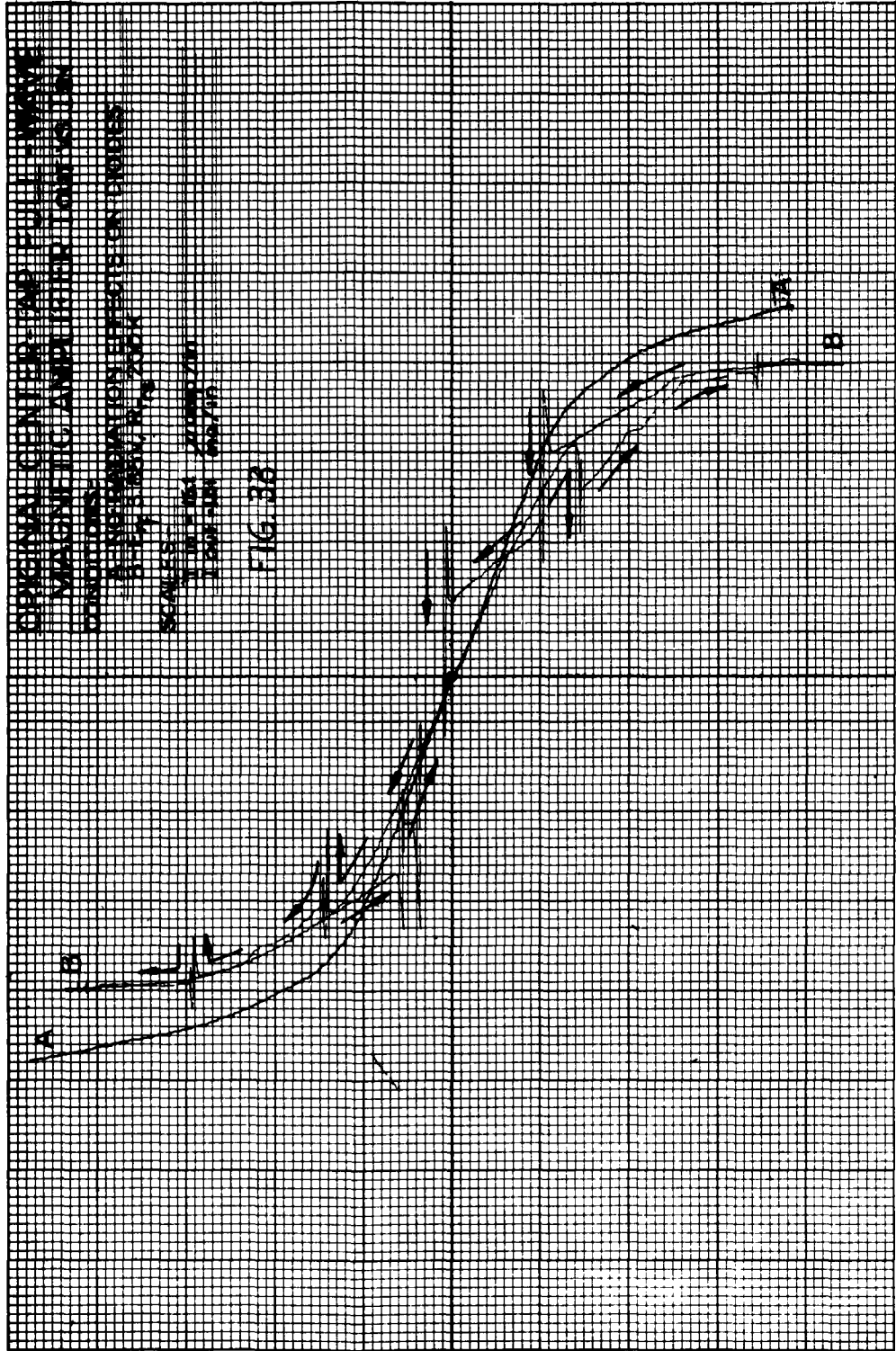
2. 100% 100% 100%

SCALES

1. 100% 100% 100%

2. 100% 100% 100%

FIG. 33



amplifier, incorporating the same diode changes, is shown in Figure 34. The change is striking. No evidence of any bistable action is apparent. Notice that the maximum output of Figure 34-A is twice that of Figure 33-A, an attendant advantage of the higher voltage operation. These curves are all recorded to the same scale. The zero offset has not yet been explained, but could be due to differences in battery voltages. The gain is reduced by the subtraction of the knee voltage of 3.85 volts from the after-saturation voltage. As before, a slight reduction in gain occurs with the 200K diode shunting resistors applied. In Figure 35 the effect on this circuit of the most severe change of the diode of Figure 1-C is recorded with the original unmodified transfer characteristic. The 200-ohm series resistors have reduced the maximum output current and gain over Figure 33 as previously explained. Figure 36B records the same diode conditions in the modified circuit. The gain and maximum are reduced over that in Figure 34B, but no bistable action exists.

Only the series 200-ohm resistors are incorporated in the circuit for Figures 37 and 38, representing the most severe case of the diode failure type in Figure 1B. Here only a slight amount of triggering is noticeable in Figure 37B, the original circuit, none in Figure 38B. By comparison of Figures 36B and 38B, it is easily seen that the major effects are produced by the incorporation of a series resistor representing a gross change in diode forward conductivity. This was previously concluded. It is apparent that by using sufficient negative feedback to stabilize the gain, the modified amplifier can be made to operate satisfactorily well beyond the radiation dosage which had previously rendered the amplifier completely useless. This modification should be incorporated in all future designs.

RESEARCH CENTER FOR ENVIRONMENTAL
MAGNETIC AMPLIFIER 105-0512

2010年12月17日

STATIONARY STATE SOLUTION

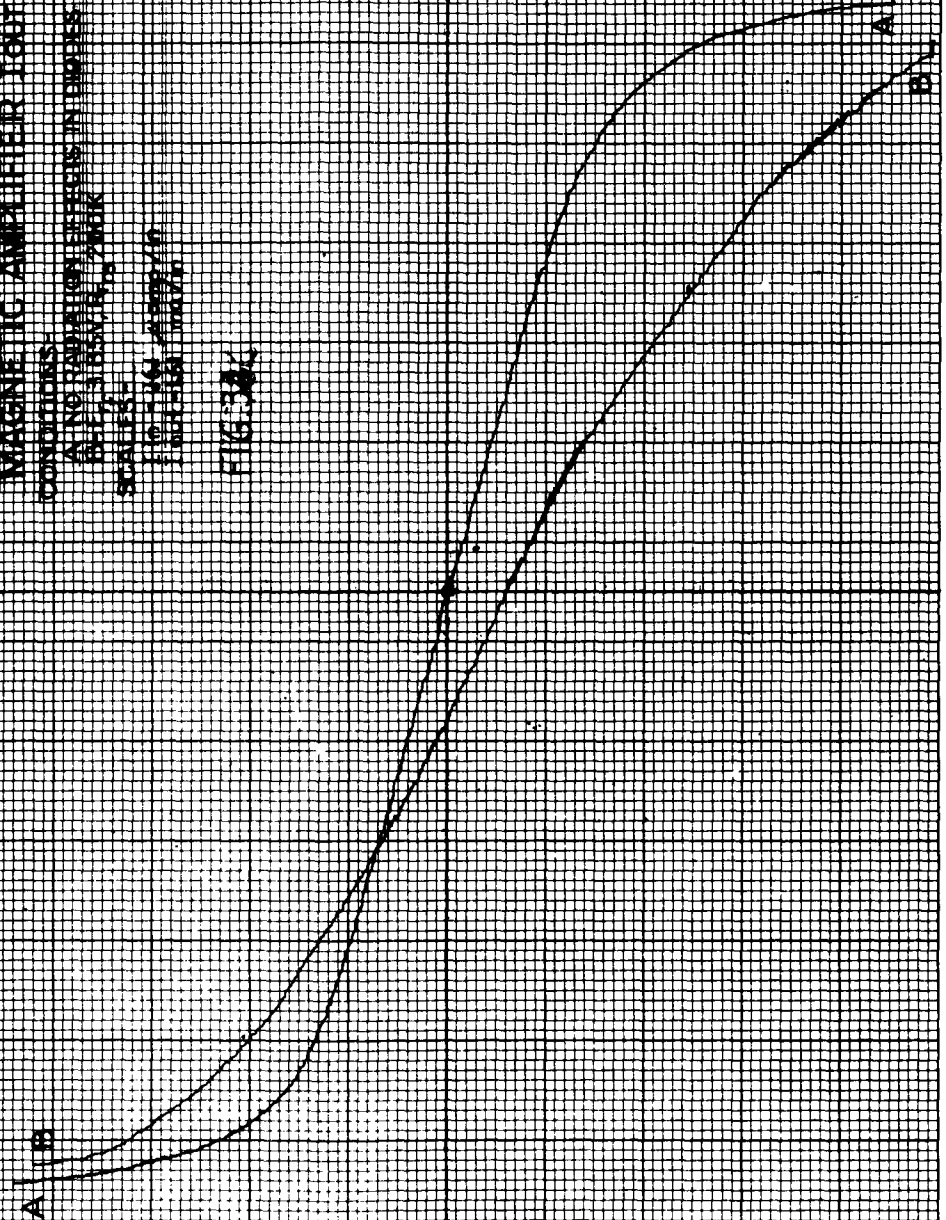
THE UNIVERSITY OF CHICAGO

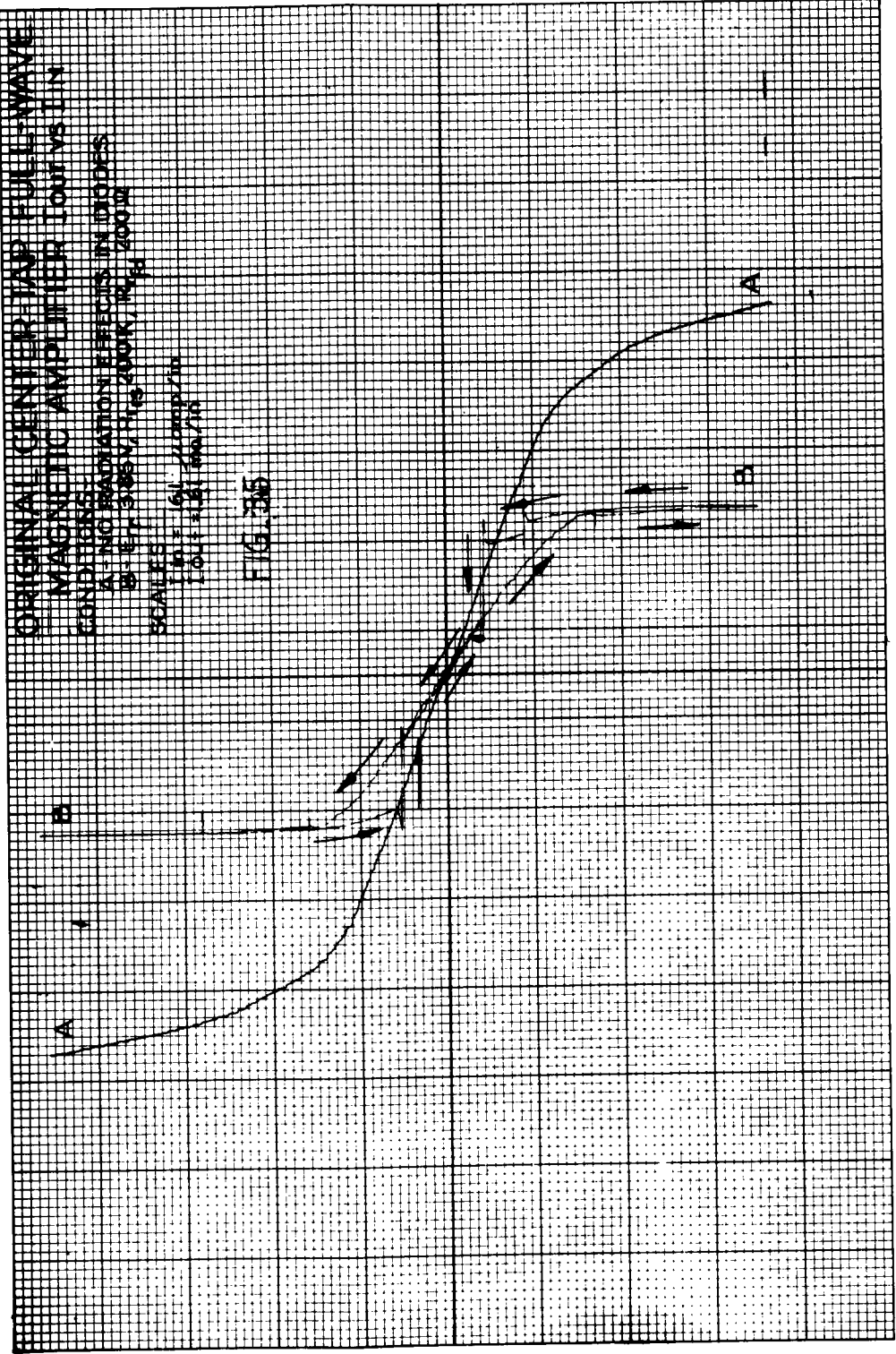
THE
NEW
YORK
PUBLIC
LIBRARY

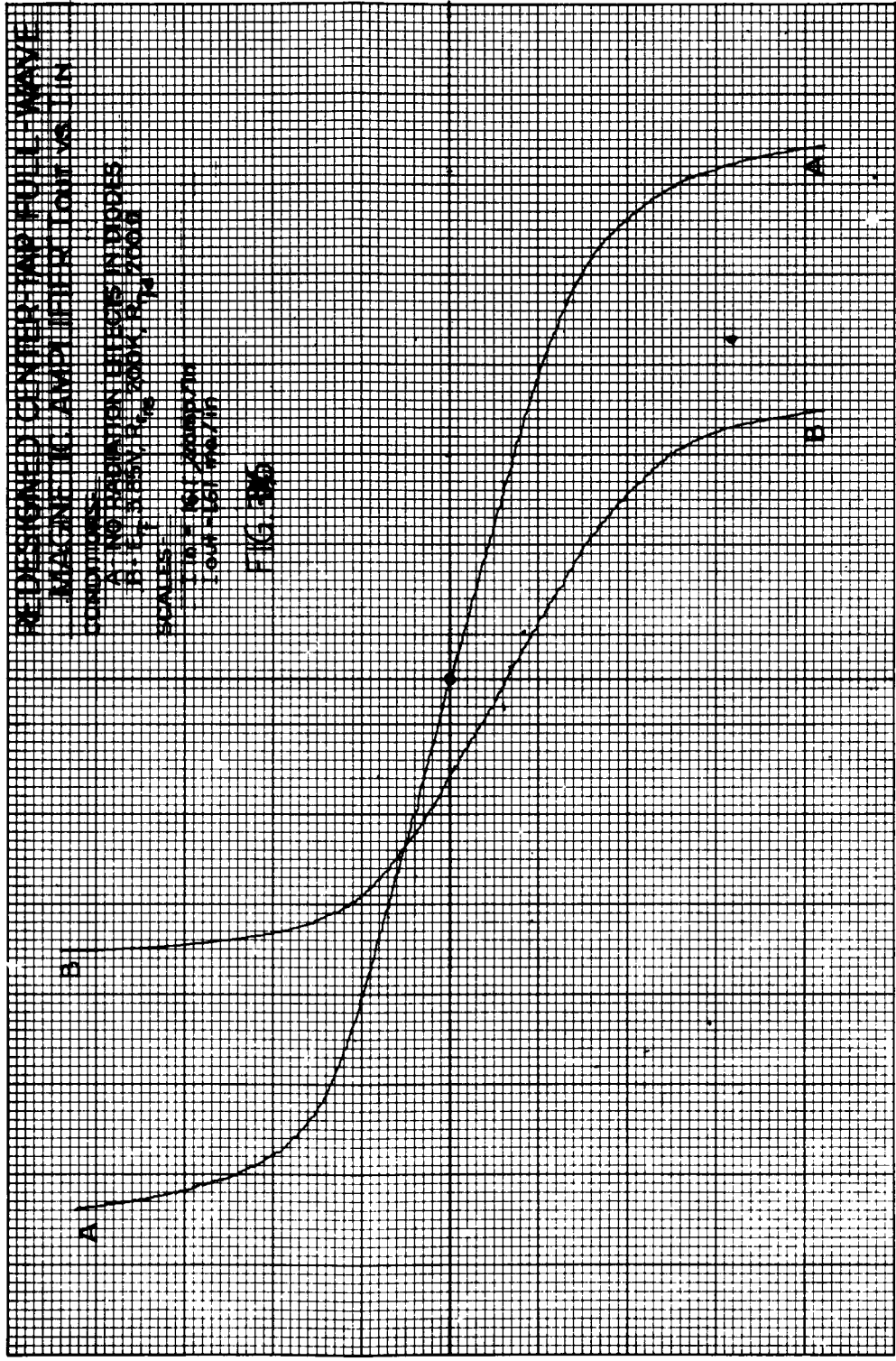
[illegible]

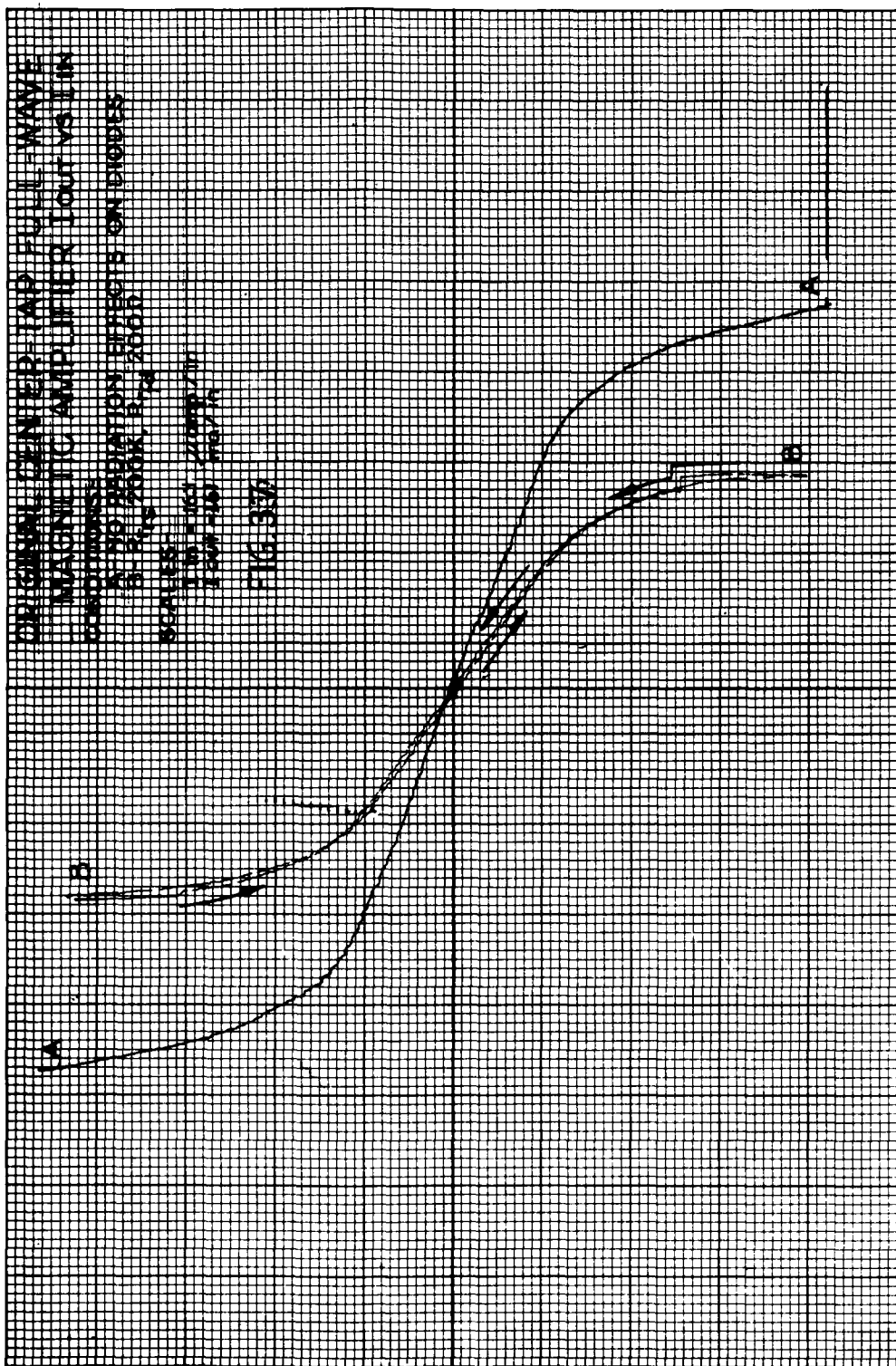
THE NEW YORK PUBLIC LIBRARY

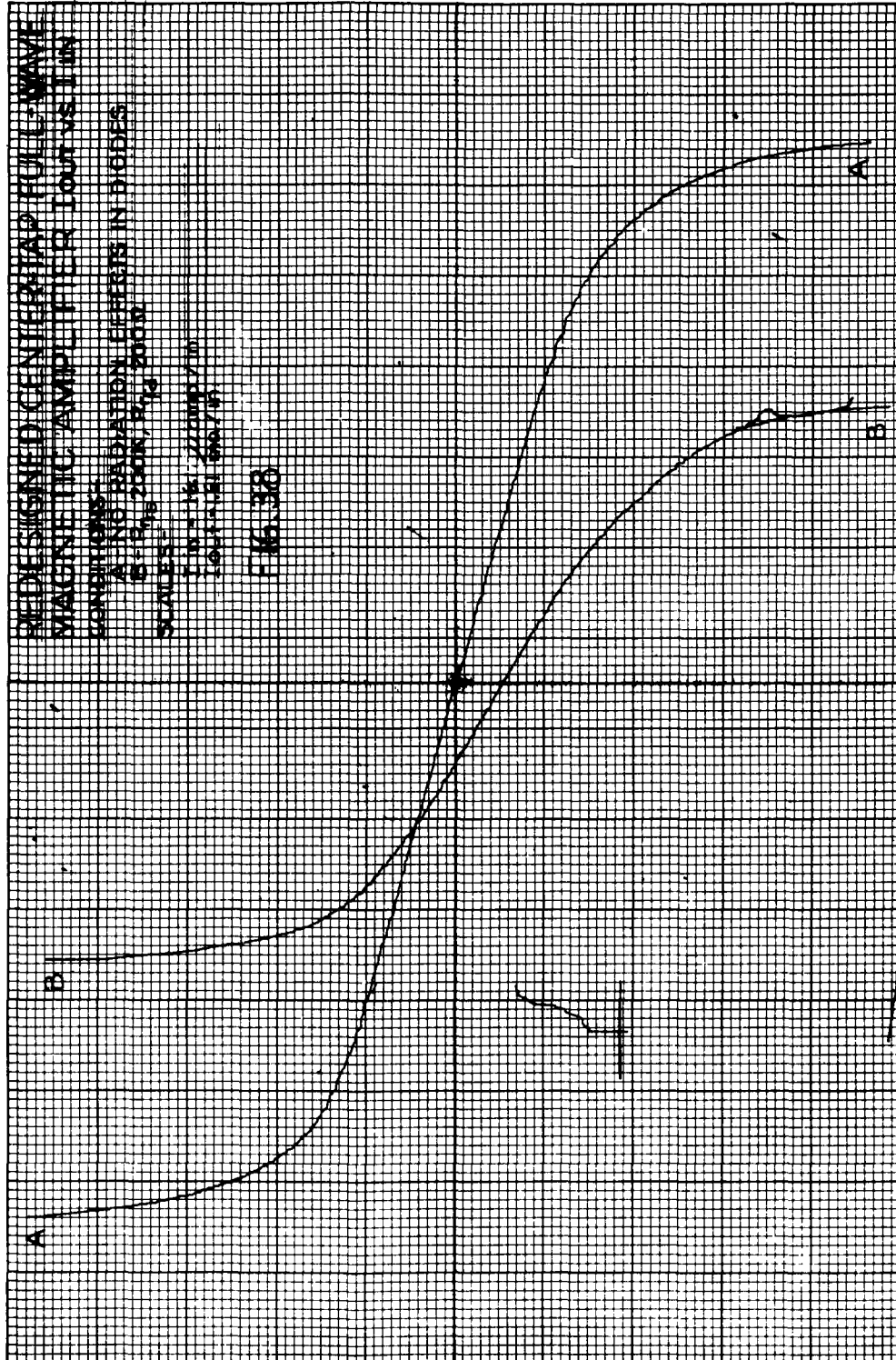
THE











REFERENCES

1. Batdorf, S. B. and Johnson, W. N., "An Instability of Self-Saturating Magnetic Amplifier Using Rectangular Loop Core Material," AIEE Trans. Vol. 72, Part I, pp. 223-27.
2. Crittenden, J. R., General Electric Company, Aircraft Nuclear Propulsion Department, Cincinnati 15, Ohio, and the Americal Nuclear Science Corporation.
3. Friedlaender, F. J., "Flux Reversal in Magnetic Cores," AIEE Trans. Vol. 75, Part I, pp. 268-77.
4. Hall, G. N., General Electric Company, Semiconductor Products Department, Clyde, New York. (Personal Contact.)
5. Huth, G. C., General Electric Company, Aircraft Nuclear Propulsion Department, Cincinnati 15, Ohio.
6. Morgan, R. E., "Reactions of Bistable B-H Loops on Magnetic Amplifiers," General Electric Company, General Engineering Laboratory, Schenectady New York.
7. Russell, J. A., General Electric Company, Aircraft Nuclear Propulsion Department, Cincinnati 15, Ohio, Radiation Experiment performed July 1955.

GAMMA RADIATION EFFECTS IN SILICON SOLAR CELLS

by

G. Enslow, F. Junga, W. W. Happ

Lockheed Aircraft Corporation
Missile Systems Division

Ten silicon solar cells were irradiated by a 100-curie Co^{60} gamma ray source to a dose of 10^7 r. In-situ measurements of the open-circuit voltage and short-circuit current were obtained. Calculations to predict the performance of silicon solar cells under irradiation were made on the basis of known properties of silicon and on the basis of models of radiation damage in solids. Calculated and experimental results were compared. The electrical characteristics of the solar cells were measured as a function of temperature before and after irradiation. The performance of a silicon solar cell power supply in radiation fields is discussed.

1. INTRODUCTION

1.1 SILICON SOLAR CELLS - The silicon solar cell converts visible and infrared radiation into electrical energy by means of the photovoltaic effect in a p-n junction. The device consists of a wafer of n-type silicon, typically of dimensions 1 cm x 2 cm x .05 cm. A p-type impurity, usually boron, is diffused into this wafer to a depth of about 1 micron, producing a p-n junction parallel to the surface. The boron concentration at the surface is of the order of 10^{18} atoms/cm³, but may account for as much as 30 percent of the material at the surface. The impurity concentration in the n-type material, usually arsenic, is of the order of 10^{15} atoms/cm³.

1.2 PHOTOEFFECT IN A P-N JUNCTION - When a p-n junction is illuminated over an area considerably wider than the junction itself, a one hole-electron

pair may be generated for each absorbed quantum if the quantum energy of the light is larger than the energy gap between the valence band and the conduction band. The theory underlying these effects and the resultant circuit performance are summarized by A. van der Ziel (1957), Hunter (1956) and others. For the convenience of the worker interested primarily in radiation damage problems, the terminology and performance characteristics of solar cells will now be briefly reviewed.

Fig. 1-1 shows a schematic diagram of a p-n junction. In this figure w is the width of the transition region from p-type to n-type silicon surrounding the junction. The extent of diffusion of minority carriers from the p-n junction is L_p and L_n .

The effective width of the photosensitive region surrounding the junction can be shown to be the sum of w , L_p and L_n ; hence, the photocurrent I_p will be:

$$I_p = e n (w + L_p + L_n) \quad (1-1)$$

where:

e = the electronic charge

n = the number of hole-electron pairs generated per unit length per unit time.

This device may be used in either of two ways:

- a. The junction may be biased in the reverse direction so that the whole current I_p is collected and the cell may then be used as a photoelectric cell or photodiode.
- b. The junction may be left unbiased so that a photovoltage is developed across the open-circuited terminals. This photovoltaic effect is the one used in the solar cell.

The junction in a solar cell is parallel to the surface, and is usually obtained by gaseous diffusion of impurities which provides an excellent control of surface concentration. Therefore, the effective incident light is that travelling normal to the surface.

Since I_p is proportional to the effective surface area, it is advantageous to employ light beams of large cross sections. It is also desirable to have

light of sufficient intensity and appropriate wave length to match the spectral response of the cell as discussed by Browne, Francis, and Enslow (1958).

Consider now the characteristics of the p-n junction under the influence of light. Application of a bias voltage V_{bb} to the device through a load resistance R , results in the appearance of a voltage V across the cell. The characteristic of the device in the absence of light is then:

$$I = - I_0 \left[\exp (V/V_T) - 1 \right] \quad (1-2)$$

where:

I = the current in the load

I_0 = the current traversing the junction

$V_T = kT/e$ (about 25 millivolts at room temperature)

T = the absolute temperature

k = Boltzmann's constant

e = the electronic charge

When the cell is illuminated, we have:

$$I = I_p - I_0 \left[\exp (V/V_T) - 1 \right] \quad (1-3)$$

where I_p is proportional to the light intensity.

1.3 PHOTOVOLTAIC EFFECT - When the cell is used as a photovoltaic cell, the open circuit voltage V_{oc} follows from the condition $I = 0$, thus:

$$I_0 \exp (V_{oc}/V_T) = I_0 + I_p \quad (1-4)$$

or

$$V_{oc} = V_T \ln (1 + I_p/I_0) \quad (1-5)$$

For sunlight (where the light intensity is sufficiently large), $I_p \gg I_0$, and the open circuit voltage then becomes:

$$V_{oc} = V_T \ln (I_p/I_0) \quad (1-6)$$

The temperature dependence of I_o calculated under the assumption that all the current is carried by holes is given by van der Ziel (1957) as:

$$I_o = K_1 T^3 \exp(-E_o/V_T) = K_2 V_T^3 \exp(-E_o/V_T) \quad (1-7)$$

where:

E_o = gap width between the filled band and the conduction band in electron volts

$V_T = kT/e$ is proportional to the absolute temperature (about 25 millivolts at room temperature)

$$K_1 = 4 \left(\frac{2\pi mk}{h^2} \right)^3 \left(\frac{m_n^* m_p^*}{m^2} \right)^{3/2} e^2 \mu_n \rho_n A \left(\frac{D_p}{\tau_p} \right)^{1/2}$$

$$K_2 = K_1 e^3/k^3$$

m = electron rest mass

m_n^* = effective mass of electrons

m_p^* = effective mass of holes

μ_n = electron mobility

ρ_n = resistivity of the n region

A = area of cell

D_p = diffusion constant of holes in the n region

τ_p = lifetime of holes in the n region

k = Boltzmann's constant, and

h = Planck's constant

K_1 depends on temperature in a way predictable from the temperature variation of the quantities ρ_n , τ_p , and D_p .

1.4 SOLAR CELL CHARACTERISTICS - Equation (1-6) describes the solar cell as a photovoltaic cell operated at high light intensities. The voltage current characteristic shown in Fig. 1-2 follows from Equation (1-3) and clearly shows the non-linear response of this device. Note that if the voltage V across the cell is zero, then the short circuit current I_{sc} is equal to the photocurrent I_p ; that is, when $V = 0$

$$I_{sc} = I_p \quad (1-8)$$

Further, from Equation (1-6) and (1-7) the temperature dependence of V_{oc} can be shown to be:

$$V_{oc} = E_o - (kT/e) \ln(I_{sc}/K_1 T^3) = E_o + V_T \ln(I_{sc}/K_2 V_T^3) \quad (1-9)$$

This expression shows that the open circuit voltage varies with temperature.

A typical loadline OB for a given value of R is shown in Fig. 1-2. The operating point B($I = I_B$, $V = V_B$) is chosen so that the power $I_B V_B$ delivered to the load is a maximum. This maximum is called the maximum available power P_{max} of the device.

$$P_{max} = (I_B V_B)_{max} \quad (1-10)$$

If the solar cell were an "ideal" p-n junction diode with the characteristics horizontal for $V < V_{oc}$ and vertical for $V = V_{oc}$ (dashed lines), then the loadline for optimum power would be the "ideal" loadline OA and the maximum available power would be

$$P_{max} = I_p V_{oc} = I_{sc} V_{oc} = J_p V_{oc} A \quad (1-11)$$

Where A is the junction area and J_p is the short-circuit emission current density (i.e., $J_p = I_p/A$).

The above equations show that the characteristics of the solar cell depend strongly on the minority carrier lifetimes as pointed out by Cummrow (1954).

1.5 RADIATION EFFECTS ON DEVICE PERFORMANCE - As explained in Section 1.3, any change in the minority carrier lifetime affects the open-circuit voltage V_{oc} and the short-circuit current I_{sc} generated by the solar cell. Theoretical calculations indicate that the performance of the device is affected by a dose of the order of 10^6 roentgens for 1.2 Mev gamma rays.

Radiation damage studies on silicon solar energy converters were undertaken by Lofersky and Rappaport (1956). A review of this work by Ziegler (1957) estimates the lifetime of silicon solar cells for various components of cosmic ray flux as follows:

Type of Radiation	Estimated Lifetime in Years
Protons	3.6×10^4
Alpha particles	1.4×10^5
Electrons	10^8
Ultraviolet radiation	85
X-rays	6.7

The above report gives us no data for damage to solar cells due to gamma radiation and fast (epicadmium) or slow (thermal) neutrons.

Photovoltaic effects induced by radiation are discussed by Rappaport (1954) and Keister and Stewart (1957).

The approximate gamma doses at which various devices (including solar cells) are affected are shown in the flux-dose plot given in Fig. 1-3. If gamma flux is plotted versus dose, then lines which are inclined at a constant angle denote time intervals. The figure shows the gamma dosages required to cause 50 percent derating of the solar cell at various fluxes. Steele (1956) points out that fluxes in excess of 10^3 r/hr are required to produce damage in transistors. This should also apply to solar cells. The upward trend of the 50 percent derating curve for solar cells at high fluxes is explained in Section 2.2.

1.6 SCOPE AND LIMITATIONS OF PRESENT INVESTIGATION - Damage studies due to neutron radiation and X-rays are not considered in this investigation. However, the effect of neutron bombardment on the boron layer of a solar cell is likely to be of importance because of the large neutron cross section of boron and the ensuing dislocations in the vicinity of the junction.

This study is directed toward the experimental determination of the range of gamma ray doses at which the operation of silicon solar cells is affected. A theoretical estimate of the flux required to influence the operation of the device by ionization is also made.

In the experiments, the open circuit voltage V_{oc} and short-circuit current I_{sc} for a number of commercially available silicon solar cells were measured while the cells were being irradiated with a gamma flux from a 100 curie Co^{60} radioisotope source. The facilities available permitted doses of 10^5 roentgens per hour. The same electrical characteristics V_{oc} and I_{sc} of the solar cells were measured as a function of temperature before and after irradiation and the results compared.

This study being of an exploratory nature, a sample consisting of 10 cells was considered adequate. This corresponds to an estimated overall accuracy of 20 percent, due to the production spreads in solar cells and the sample size.

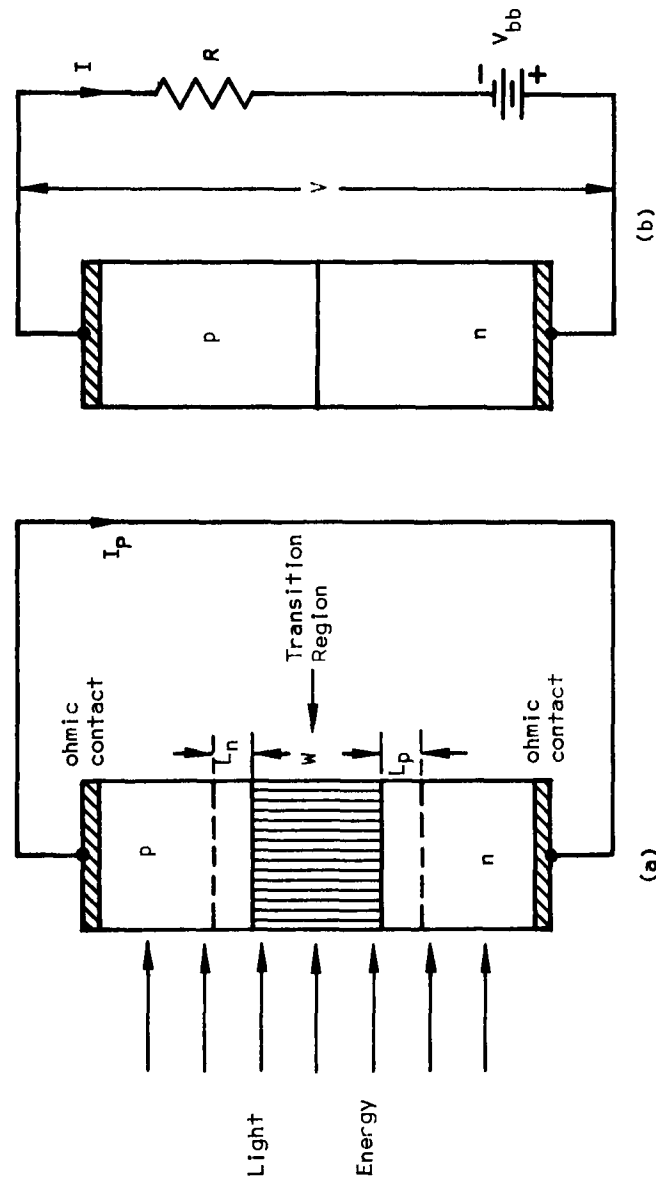


Fig. 1-1 Schematic Diagram of a P-N Junction
 (a) an illuminated p-n junction with the output short-circuited
 (b) an illuminated p-n junction with a load resistance R across the output. Note that V_{bb} is zero when the device is used as a photovoltaic cell and is negative when used as a photoelectric cell.

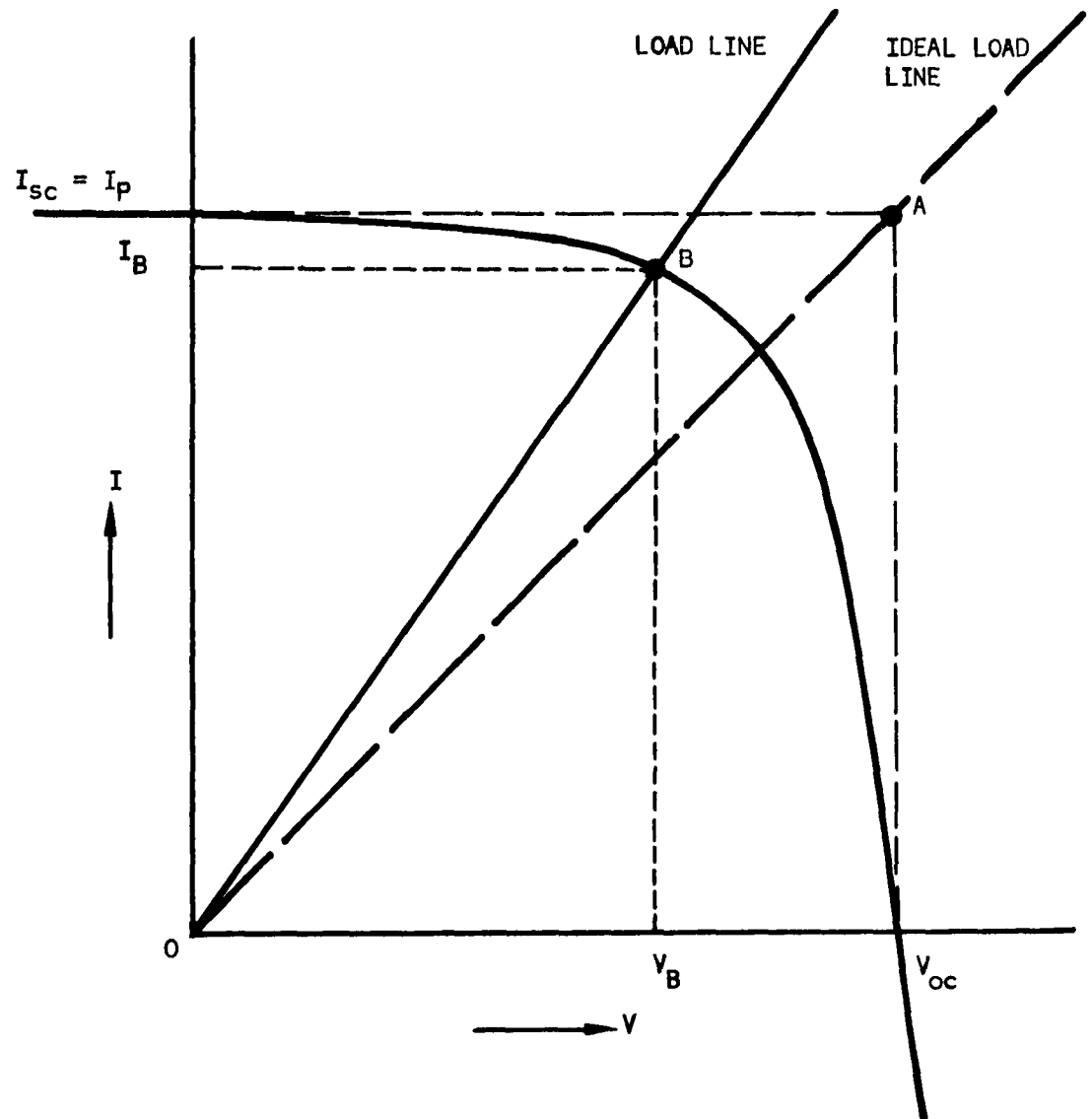


Fig. 1-2 I-V Characteristic of a Solar Cell
or Photovoltaic Cell

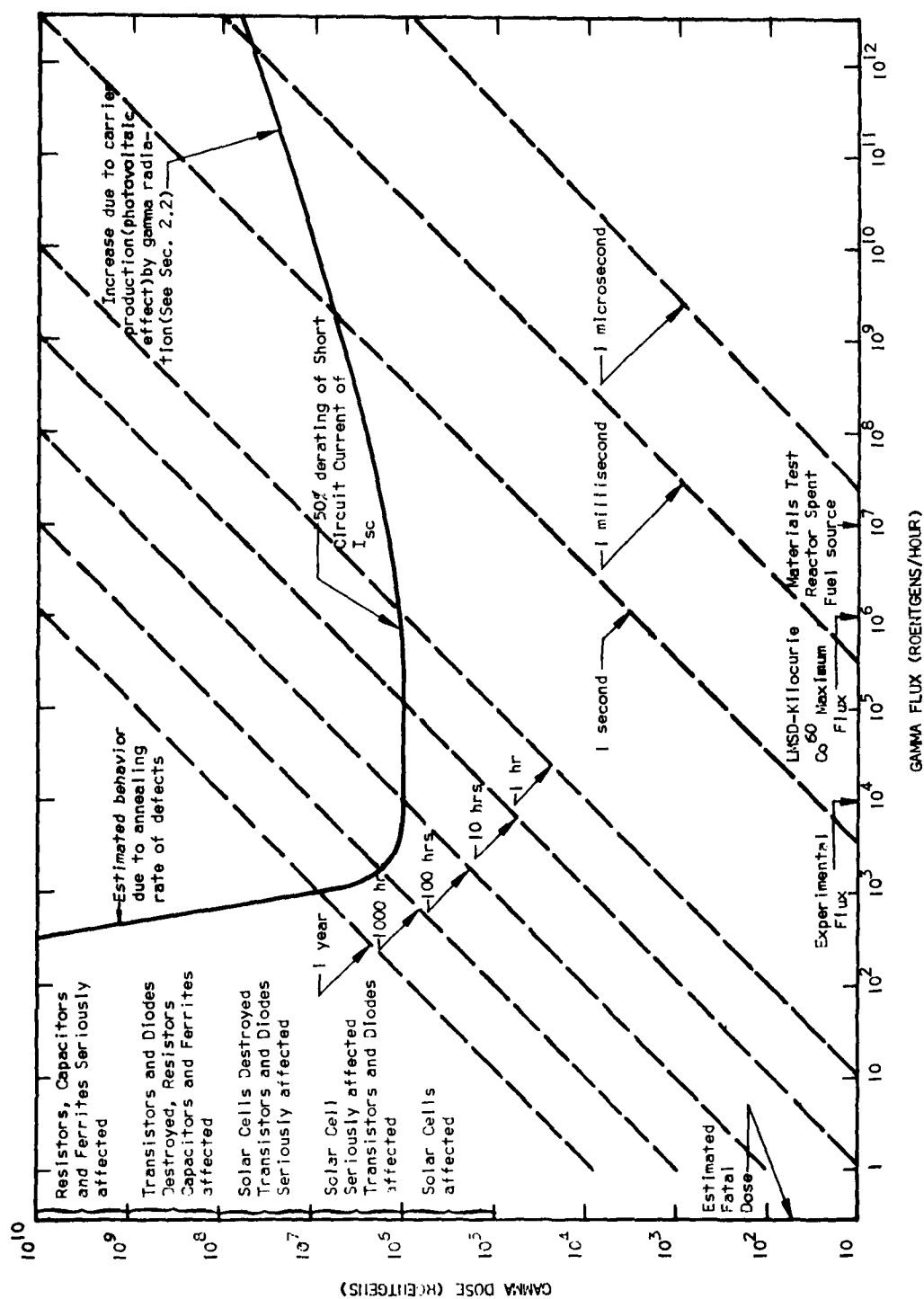


Fig. 1-3 Flux-Dose Plot for Silicon Solar Cells Under Gamma Irradiations

2. THEORETICAL CONSIDERATIONS FOR GAMMA IRRADIATION OF SILICON SOLAR CELLS

2.1 INTRODUCTION - The passage of high-energy photons through matter produces electrons and secondary photons in the material. Most electrons are produced as a result of the Compton effect, (Evans, 1955) and the electrons are called Compton electrons. The other processes are negligible in the range of photon energies with which we are concerned here as Evans (1955) points out. Many of the Compton electrons collide with atoms in the lattice. Those electrons with sufficient energy (about .3 Mev) may displace atoms from their normal lattice sites. An atom so displaced constitutes a defect (Dienes and Vineyard, 1957) and can affect many properties of the material. Rappaport (1954) has shown that the minority carrier lifetime in semiconductors is a very sensitive indication of such damage.

Cummerow (1954) points out that the performance of a photovoltaic device is strongly dependent on the minority carrier lifetime in the n and p regions of the device. One would then expect the performance of a silicon solar cell to change under irradiation. Since the minority carrier lifetime decreases under irradiation, a reduction in the output of the device can be anticipated.

2.2 ESTIMATES OF THE LIMITS OF OPERATION - To estimate the limit of operation, the number of displacements produced during irradiation must be determined. Only order of magnitude computations, with a view to estimate the number of dislocations, will be presented here.

The gamma rays from the LMSD Co⁶⁰ source have an average energy of 1.25 Mev. The maximum energy transferrable to an electron from a 1.25 Mev photon in a Compton interaction is 1.04 Mev, while the average energy transferred to all electrons in a Compton interaction is .97 Mev (Evans, 1955).

Seitz and Koehler (1956) have given an integrated form of the electron-atom displacement cross-section σ_d

$$\sigma_d = \pi Z^2 \left(\frac{e^2}{mc^2} \right)^2 \frac{1}{\beta^4 \gamma^2} \left[\left(\frac{T_m}{E_d} - 1 \right) - \beta^2 \ln \frac{T_m}{E_d} + \pi \alpha \beta \left\{ 2 \left[\left(\frac{T_m}{E_d} \right)^{\frac{1}{2}} - 1 \right] - \ln \frac{T_m}{E_d} \right\} \right] \quad (2-1)$$

where $\beta = \frac{v}{c}$ is the ratio of the electron velocity to the speed of light,

$\gamma = \frac{1}{\sqrt{1 - \beta^2}}$, $\alpha = \frac{Z}{137}$ and Z is the atomic number of the target material.

T_m is the maximum energy transferrable to an atom by an electron of given energy and E_d is the minimum energy which must be imparted to an atom to displace it from its normal position. E_d is about 30 ev for silicon.

Thus, for silicon, calculations show $\sigma_d = 21 \times 10^{-24} \text{ cm}^2$ when σ_d is computed on the basis that all electrons have the maximum energy available to Compton electrons, and $\sigma_d = 20 \times 10^{-24} \text{ cm}^2$ when σ_d is computed on the basis that all electrons have the average Compton electron energy. The total number of displacements per second R is

$$R = \phi_\gamma n Z \sigma_d \quad (2-2)$$

where ϕ_γ is the gamma flux in photons/cm²/sec, and n is the molecular density of the target material. Thus, for a 100 Curie Co⁶⁰ source, R is in the range of 1×10^{10} to 1.5×10^{10} displacements/sec. Using the Shockley-Read (1952) recombination statistics, the minority carrier lifetime τ_p is related to the number of displacements N , by

$$\tau_p = A(1 - KN) \quad (2-3)$$

where A and K are constants depending on the properties of the material, and the nature of the defects. A simplification of Cumberow's (1954) formulae give the following predictions for the output of a solar cell

$$I_{sc} = eg_0 (D_p \tau_p)^{1/2} \quad (2-4)$$

$$V_{oc} = \frac{kT}{e} \ln \left[g_0 L_\lambda \left(\frac{\tau_p}{D_p} \right)^{1/2} \right] \quad (2-5)$$

where g_0 , L_λ , D_p are constants of the material which are negligibly affected by irradiation, while k is Boltzmann's constant, T is the absolute temperature and e is the electronic charge. All quantities are expressed in c.g.s. units. Thus, we see that

$$I_{sc} = eg_0 D_p^{1/2} \left[A(1 - KN) \right]^{1/2} \quad (2-6)$$

$$V_{oc} = V_T \ln \left\{ \frac{g_0 L_\lambda}{D_p^{1/2}} \left[A(1 - KN) \right]^{1/2} \right\} \quad (2-7)$$

where t is the number of seconds under irradiation and $V_T = kT/e$. It is often useful to write these equations in terms of dosage rather than time under irradiation. Since R is the number of displacements per second, and t the irradiation time expressed in seconds, then Rt is the total number of displacements N. The dose received, Φ , is

$$\Phi_\gamma = \Phi t \quad (2-8)$$

Thus, since

$$N = Rt \quad (2-9)$$

it follows that

$$N = \sigma_d n Z \phi_\gamma t = \sigma_d n Z \Phi \quad (2-10)$$

If δ is defined as $\sigma_d n Z$

$$I_{sc} = e g_o D_p^{1/2} \left[A(1 - K\delta\Phi) \right]^{1/2} \quad (2-11)$$

$$V_{oc} = V_T \ln \left\{ \frac{g_o L_A}{D_p^{1/2} \left[A(1 - K\delta\Phi) \right]^{1/2}} \right\} \quad (2-12)$$

Since gamma rays and light are both electromagnetic radiations, both will produce carriers in the material. However, the number of carriers produced by sunlight is far in excess of the number produced by the gamma rays in LMSD facilities, and the effects of the latter may safely be neglected. (See Fig. 2-1.)

The rate effect, or effect due to high-flux densities, can be calculated from the following formula for the relative value of the short circuit,

$$\langle I_{sc} \rangle : \quad \langle I_{sc} \rangle = \left(1 + \frac{\eta \phi_\gamma}{g_o} \right) \sqrt{1 - K \sigma_d n Z \phi_\gamma t} \quad (2-13)$$

where η is the number of free carriers produced per gamma ray (approximately 1). This accounts for the increase in $\langle I_{sc} \rangle$ along the 1 millisecond curve in Fig. 2-1, and the upward bend in the curve at high-flux densities in Fig. 1-3.

2.3 COMPUTATION OF PERFORMANCE CURVES - Using data appropriate to silicon solar cells and in a radiation flux of 10^4 r/hr, we can predict the results of exposure to radiation.

$$I_{sc} = 2.0 \times 10^7 \sqrt{1 - 10^{-5} t} \quad (2-14)$$

$$V_{oc} = 4.0 \times 10^{14} \ln \left\{ 10^6 \sqrt{1 - 10^{-5} t} \right\} \quad (2-15)$$

Thus, one can expect I_{sc} to be reduced by 50 percent at a dose of about 3×10^4 r and V_{oc} to be reduced by 50 percent at about 2.4×10^5 r (See Fig. 2-2 and 2-3). It must be pointed out, however, that this evaluation does not take into account annealing effects, which will prolong the life of the cells. If annealing is taken into account then

$$\frac{dN}{dt} = R - SN^2 \quad (2-16)$$

where S is a constant related to the annealing rate in silicon.

The data (see Fig. 2-2) suggests that this is not a negligible effect. The calculations taking annealing into consideration, however, have only reached the qualitative stage. An interesting result is that, when annealing is taken into account, the curves of I_{sc} and V_{oc} vs. Φ can be approximated by a straight line at sufficiently high doses. Using this approximation to extrapolate the experimental data to higher doses, one can predict that I_{sc} will decrease to zero in 10^8 seconds, or at a dose of about 5×10^9 roentgens.

2.4 PLANNING THE EXPERIMENT - It was decided that in-situ measurements of V_{oc} and I_{sc} would be taken. These parameters were chosen since they are of general interest and can easily be compared with the theoretical work.

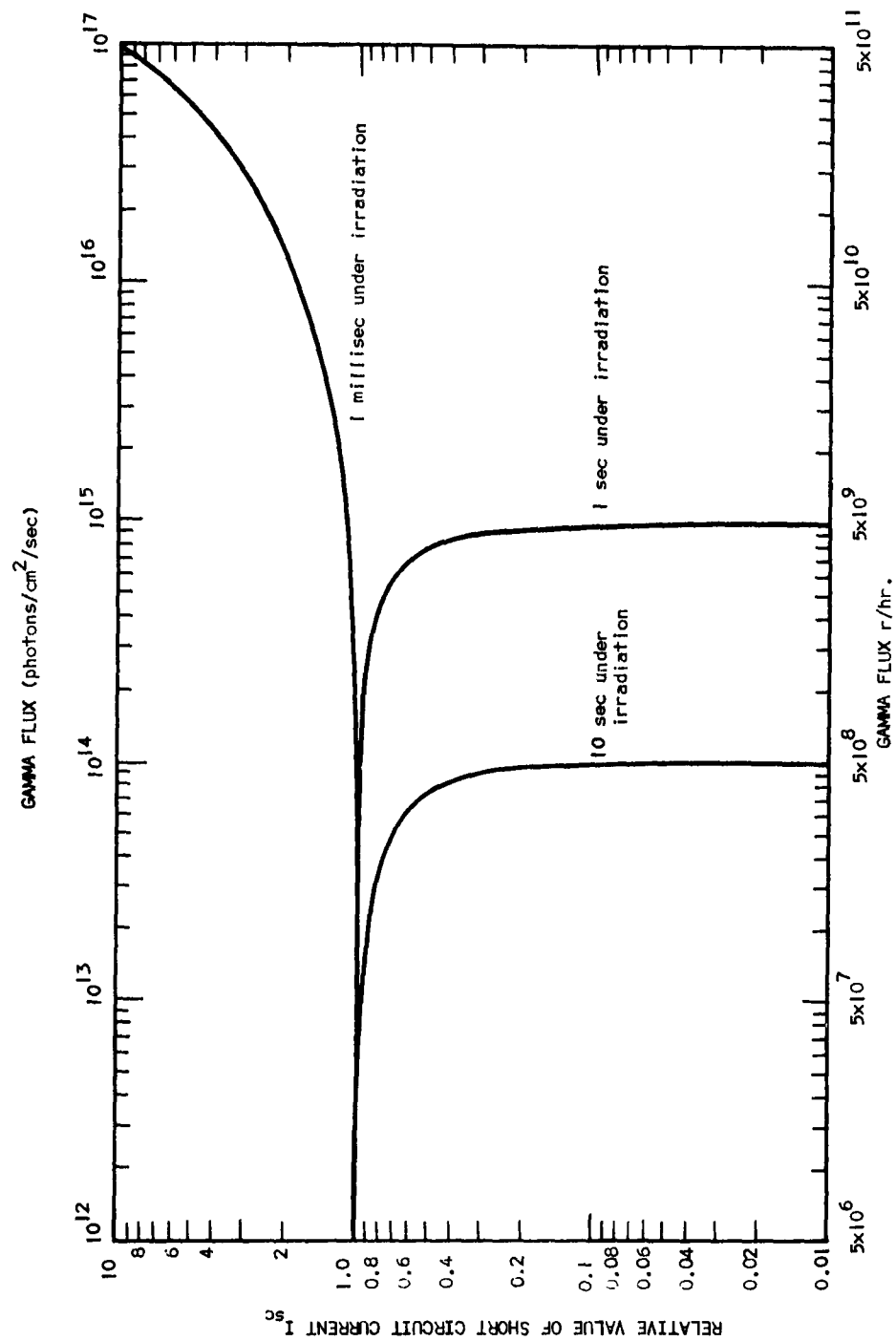


Fig. 2-1 Relative Values of Short Circuit Current I_{sc} for Various Gamma Fluxes Showing Rate Effect (Note: LMSD Facilities Operate at About 3×10^5 r/hr Maximum)

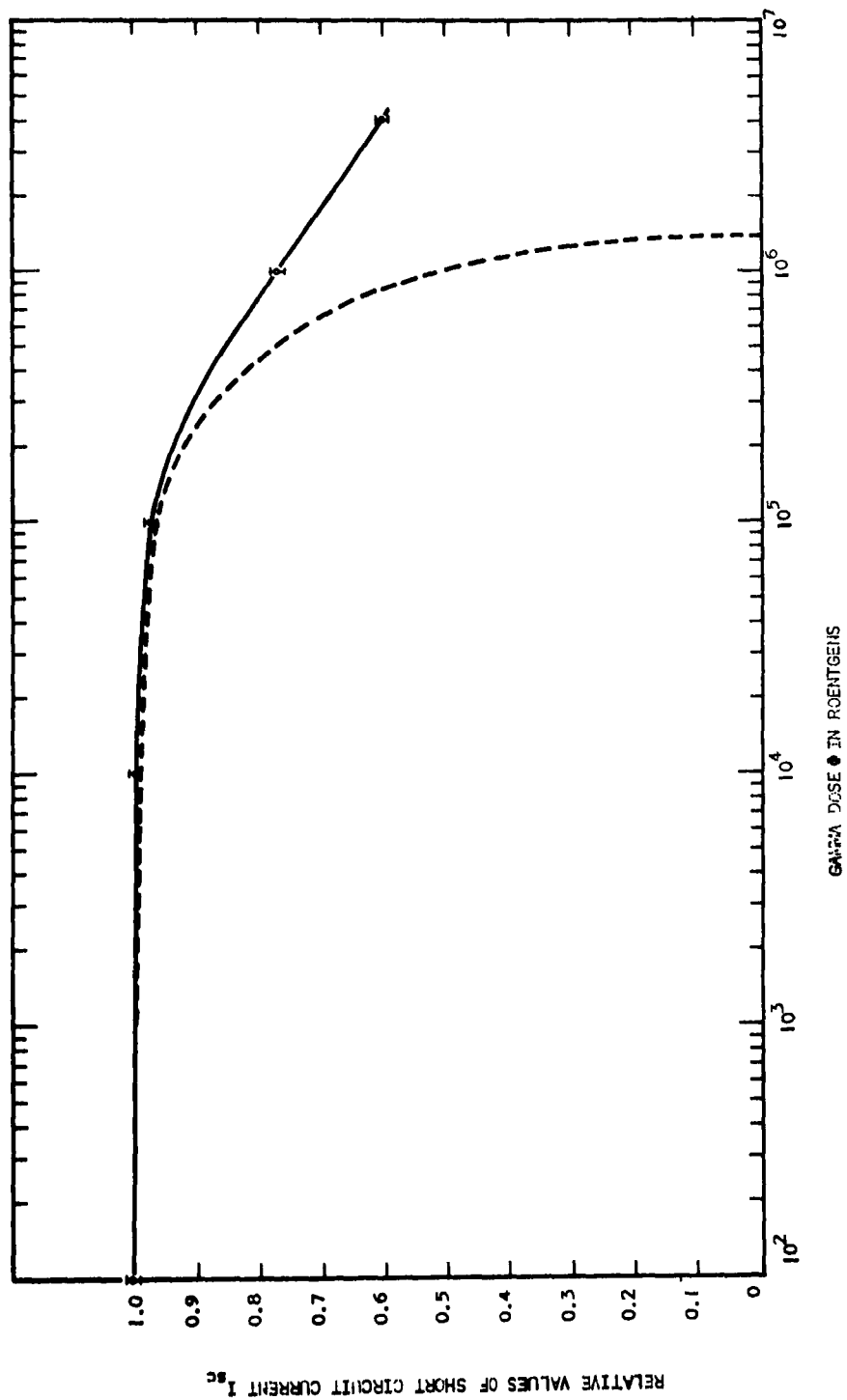


Fig. 2-2 Relative Values of Short Circuit Current I_{sc} Under Gamma Irradiation
 Typical Experimental Curve: Solid Line
 Theoretical Curve: Broken Line

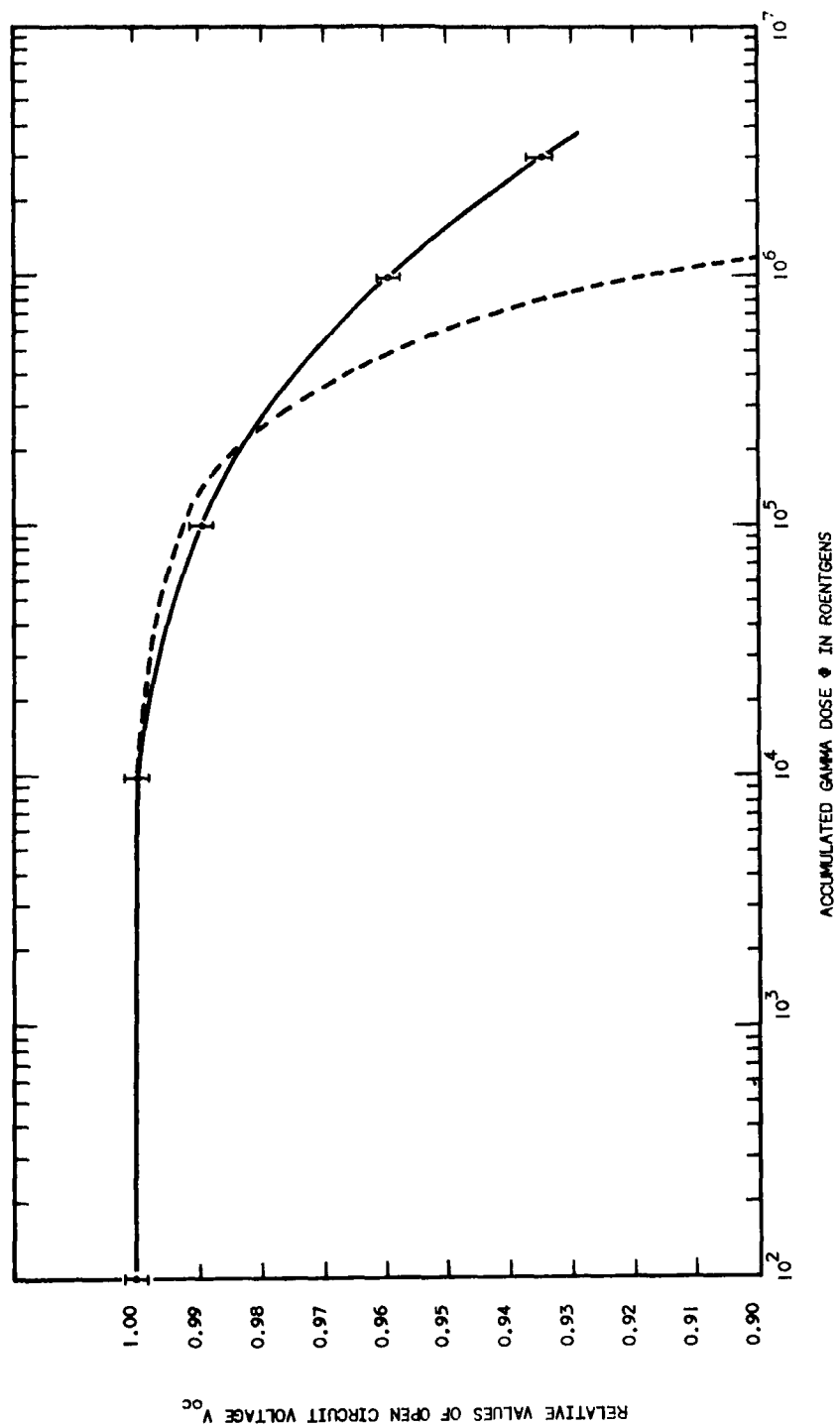


Fig. 2-3 Relative Values of Open Circuit Voltage V_{oc} Under Irradiation
 Typical Experimental Curve: Solid Line
 Theoretical Curve: Broken Line

3. EXPERIMENTAL RESULTS AND INTERPRETATION

3.1 IRRADIATION FACILITIES AND AUXILIARY APPARATUS - The gamma irradiation facilities at Lockheed Missile Systems Division include a radiation chamber with a 100-curie Co^{60} gamma ray source. The radiation chamber is a shielded room approximately 10 feet by 20 feet. A special radiation-safe optical window is provided in one side of the room with various manipulators and their associated controls. An opening which can be filled with lead bricks to any required extent is used to enable test leads to be introduced into the radiation chamber.

When originally installed about two years ago, the source had an estimated strength of 100 curies. When last calibrated immediately after this experiment the equivalent point source strength was 98 curies for points along the lower cylinder axis.

Other apparatus used included a mobile test stand designed for use in evaluation studies of solar cells. This test stand includes a Leads and Northrup Type K-3 Universal Potentiometer, a Minneapolis-Honeywell Model 104WIG Null Indicator, a Rubicon Decade Resistance Box, a Leads and Northrup Model 8662 thermocouple potentiometer, a Sorensen Model 1000S voltage regulator, a Sola Model 30809 voltage regulator, and the various reostats and meters required for the operation and monitoring of a light source and temperature test chamber.

A temperature test chamber was constructed in the laboratory some time ago for use in solar cell studies and consists of a 7 in. x 7 in. x 8 in. box, of 1/2 in. transite, with heater coils mounted inside. A 4 in. x 5 in. x 6 in. steel chassis box is recessed behind the front opening. A blower was mounted in the back of the chamber so that a uniform temperature distribution could be maintained. A phosphor-bronze spring clip holds each cell in place on a micarta board. This spring clip also presses an iron-constantan thermocouple against the front electrode of the solar cell. Pressure contacts to the solar cell electrodes were found to introduce too much resistance and fine wires were therefore soldered to the solar cell electrodes for the purpose of the experiments.

3.2 EXPERIMENTAL PROCEDURE - A sample of ten commercially available silicon solar cells (Hoffman Electronics Corporation Type 120c, efficiency 10 percent) was selected at random for this study.

Measurements of the open circuit voltage, V_{oc} , and short circuit current, I_{sc} , were taken during the period of irradiation at various dosages. I_{sc} was obtained by reading the voltage across a one ohm load and using Ohms' Law (i.e. $I = V/R$).

The ten cells were mounted on a piece of 1/8 in. aluminum by a solder connection from the back electrode to a piece of thin wire which was stretched across the aluminum plate, and which also served as an electrical connection. The plate, with the cells grouped symmetrically in the center, was illuminated by two 500-watt light bulbs within the irradiation chamber, and a blower was installed to help maintain constant temperature. Lead bricks were used to shield the lamps from the radioactive source, as many glasses tend to discolor under irradiation. (See Shaw and Krogstad, 1958.)

No attempt was made to calibrate the light source used for these measurements or to obtain an even distribution of intensity across the ten solar cells. This was considered to be unnecessary since only the relative values of the open circuit voltage, V_{oc} , and the short circuit current, I_{sc} , at various dosages were of interest.

The 100-curie Co^{60} source was placed approximately 8 cm from the center of the group of ten solar cells. This gave a flux of 10^4 roentgens/hr in the vicinity of the cells.

Before being subjected to gamma radiation, these cells were placed in the temperature test chamber. The light source consisted of four 500-watt reflector-type light bulbs. A 2-1/2 in. thick water filter was mounted between the source and the temperature test chamber for the purpose of absorbing most of the infrared. This gave a light spectrum similar to that of the sun in the sensitive region of the solar cells.

This equipment was mounted on a standard laboratory optical bench. A block diagram of the measuring apparatus is shown in Fig. 3-1.

The light source intensity was adjusted so that the effective incident power falling on the cells was approximately the same as the incident power of open sunlight ($87.3 \text{ milliwatts/cm}^2$) at the location of this laboratory in Palo Alto, California.

This calibration was accomplished by using a silicon solar cell in the following manner. Through a series of experiments conducted on a silicon solar cell in open sunlight, the electrical characteristics as a function of temperature of this particular solar cell were obtained within an accuracy of ± 3 percent. The light source and water filter were then adjusted to give similar results, for this particular solar cell, as were obtained in open sunlight.

The electrical characteristics of the ten silicon solar cells were measured by this technique as a function of temperature from 30°C to 130°C . The parameters measured were the following:

V_{oc} = open circuit voltage of the cell

I_{sc} = short circuit current obtained by reading the voltage across a one-ohm load and calculating V/R

After irradiation, the solar cells were remounted in the same positions in the measuring apparatus. The electrical characteristics of the solar cells were then measured in the same manner as before irradiation.

3.3 EXPERIMENTAL PERFORMANCE CHARACTERISTICS - Experimental curves for the short circuit current I_{sc} versus gamma dose for 10 cells are shown in Fig. 3-2. These curves show that damage had occurred at doses of 10^5 r . However, some cells were affected at doses as low as 10^4 r . On the average, I_{sc} decreased by approximately 25 percent of its original value at 10^6 r , and 50 percent at 10^7 r . The open circuit voltage, V_{oc} , is plotted, in Fig. 3-3, versus gamma dose. These curves show that V_{oc} is definitely affected at 10^5 r and on the average had decreased approximately 10 percent at $5 \times 10^6 \text{ r}$.

Measurements of the short circuit current I_{sc} of the ten solar cells before and after Co^{60} gamma radiation were taken as a function of temperature, and fall within the shaded areas of Fig. 3-4. A "typical" cell gives experimental data for the representative sample used. Note that the spread of the

measurements increases under radiation. A small increase in spread could be expected since the gamma ray flux received by the solar cells varied on account of the position of each cell with respect to the Co^{60} source. However, the actual spread is larger than expected from dosimetry effects alone. The short circuit current versus temperature curve is affected by radiation as shown by the curve for a "typical" cell. Some cells showed a more radical change than the "typical" cell.

Similar measurements of the open circuit voltage V_{oc} versus temperature of the cells fall within the shaded areas of Fig. 3-5; measurements before and after irradiation are given. The data show a linear dependence as illustrated by the "typical" cell, which incidentally is the same "typical" cell used in the I_{sc} versus temperature graph in Fig. 3-4. For the "typical" cell used, the open circuit voltage V_{oc} is a linear function of temperature with a slope - 2.2 mv/ $^{\circ}\text{C}$ before irradiation and remained a linear function of temperature after irradiation with a slope of - 2.1 mv/ $^{\circ}\text{C}$.

It follows from Fig. 3-5 that the V_{oc} characteristics of a solar cell exposed to a gamma radiation dose of up to 10^7 roentgens remains a linear function of temperature with practically the same slope.

Irradiation somewhat increased the spread of V_{oc} measurements for our sample. This increase is adequately explained by the slight variance in dosage received by the individual cell due to varying proximity to the Co^{60} source.

3.4 DERATING AND RELIABILITY - Derating as used in this report is the fraction by which the voltage and current parameters are reduced from their initial values as a result of exposure to gamma radiation. Reliability is used to indicate the expected percentage of survival, i.e. ability to meet or exceed the derated parameters within a typical group of cells.

The derating of the short circuit current, I_{sc} , for each cell was obtained from the experimental short circuit current curves for various gamma radiation dosages. The percentage derating for each cell was computed for each dosage used and the data plotted on probability paper. This gave a

family of dosage curves from 10^4 roentgens to 5×10^6 roentgens showing the percentage of cells possessing a given derating Δ , for a given dosage Φ . Figure 3-6 shows this family of dosage curves for the short circuit current, I_{sc} .

The set of reliability curves for I_{sc} is shown in Fig. 3-7. These curves were obtained from the derating curves by plotting the percentage derating of the short circuit current, ΔI_{sc} , as a function of various dosages, Φ , for a given percentage of silicon solar cells. The curves are, therefore, lines of constant survival ratios for various values of derating and gamma radiation dose.

To illustrate the use of these curves, consider first the dosage curves in Fig. 3-6. If we allow a 10 percent derating in the short circuit current of the solar cells to occur in a specific case, we can read the percentage of cells that will survive or fail for the various dosages as follows:

Dosage in Roentgen	% Survive	% Fail
5×10^4	89	11
1×10^5	70	30
2×10^5	34	66

The short circuit current reliability curves in Fig. 3-7 show the dosages for 1 percent, 10 percent, 50 percent and 99 percent survival. For an allowable 10 percent derating the following fraction of cells would fail - or survive:

% Fail	% Survive	Dosage in Roentgen
1	99	2.1×10^4
10	90	4.8×10^4
50	50	1.5×10^5
90	10	3.3×10^5
99	1	5.1×10^5

From Fig. 3-7 one can read the derating required at a specific dosage for the given percentage of cells to fail or survive. For example, an expected dosage of 10^6 roentgens postulates the following deratings and survivals:

% Survive	% Fail	% Derating
1	99	16.3
10	90	21.2
50	50	28.0
90	10	37.5
99	1	46.0

Similar dosage curves for the open circuit voltage are shown in Fig. 3-8.

Fig. 3-9 shows a set of open circuit voltage reliability curves. These curves were obtained from the data of Fig. 3-8 in the same manner as for the short circuit current.

The derating and reliability curves for the open circuit voltage are read in a similar manner as the short circuit current curves.

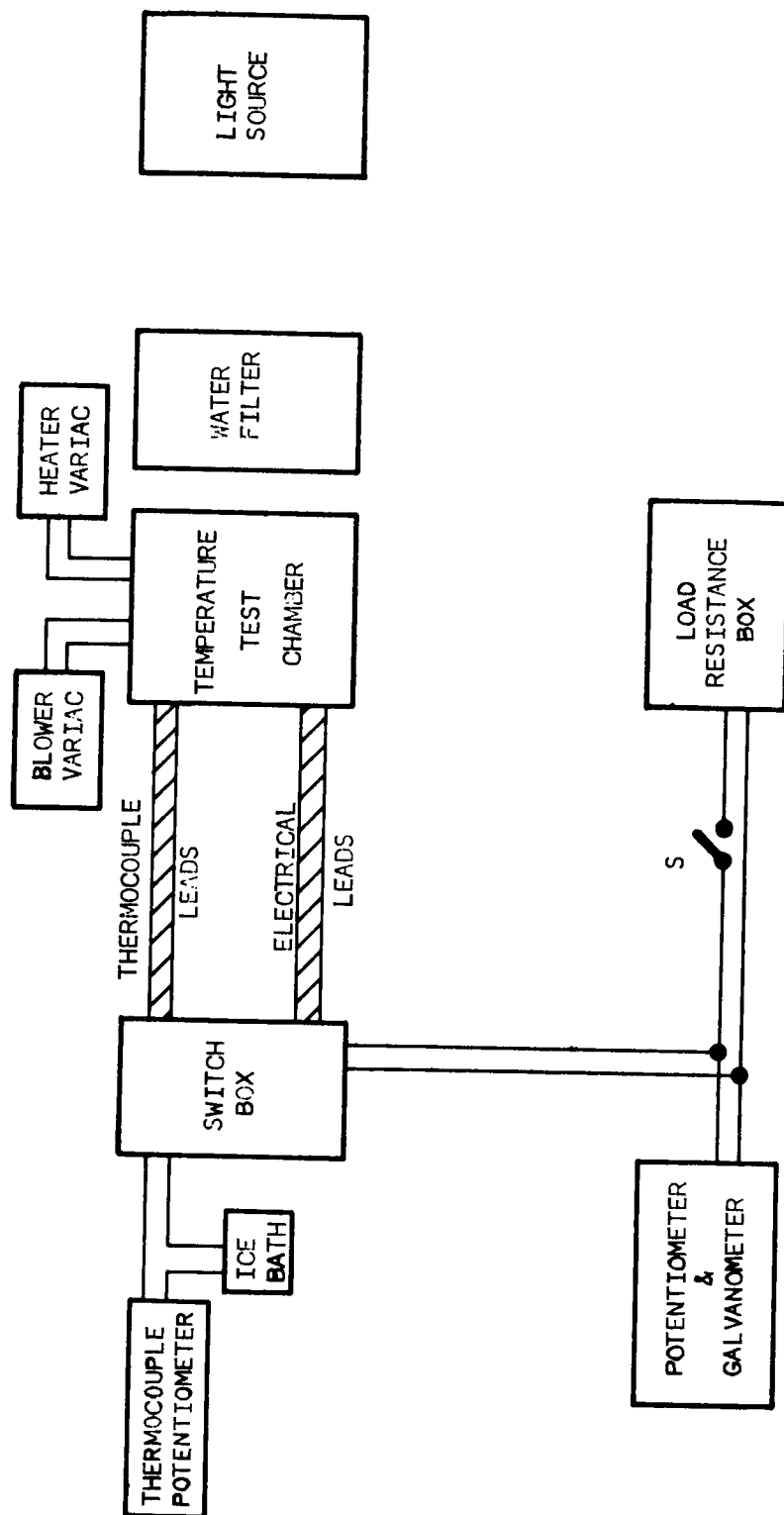


Fig. 3-1 Block Diagram of Measuring Apparatus

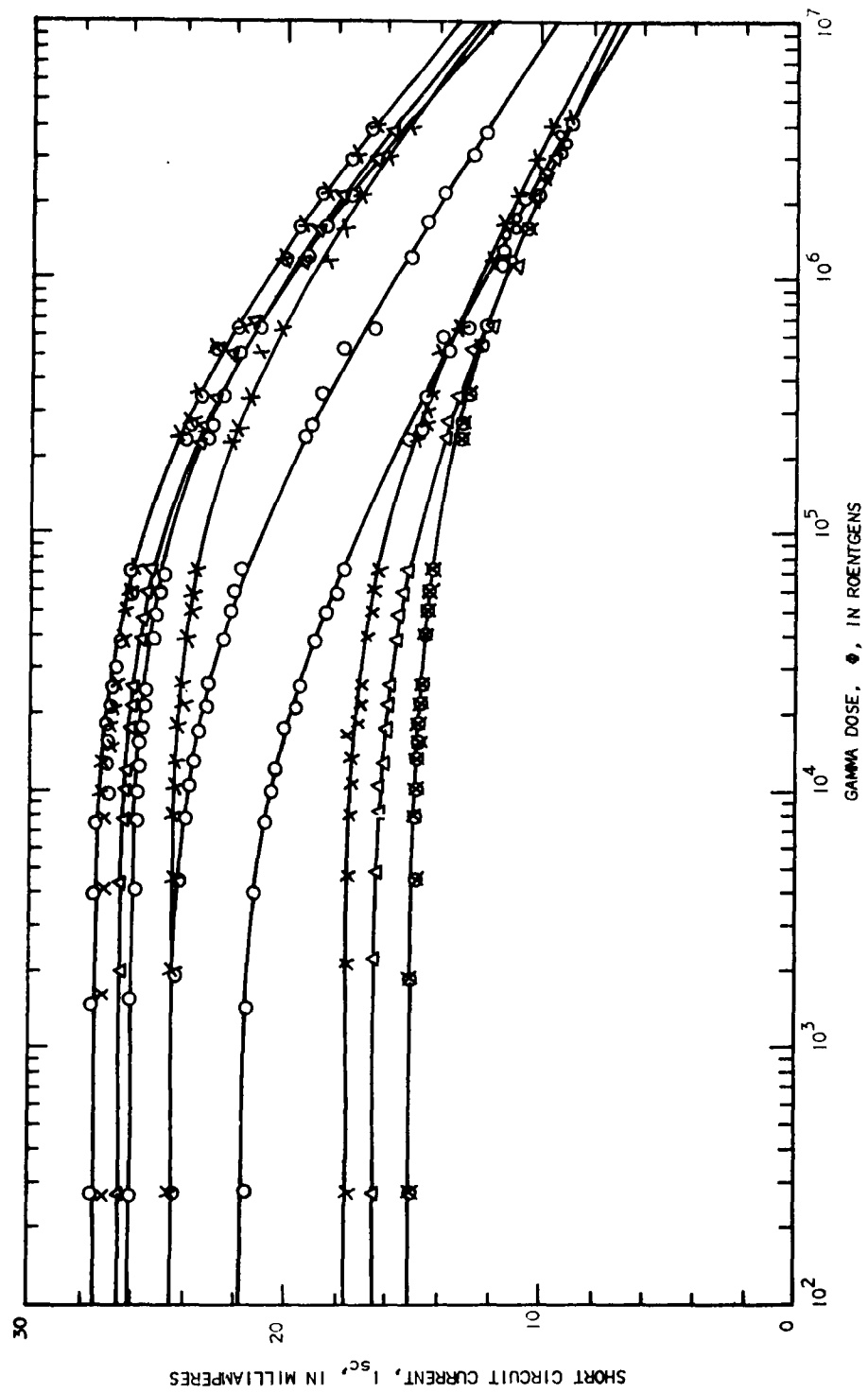


Fig. 3-2 Short Circuit Current I_{sc} of Silicon Solar Cells Under Gamma Irradiation

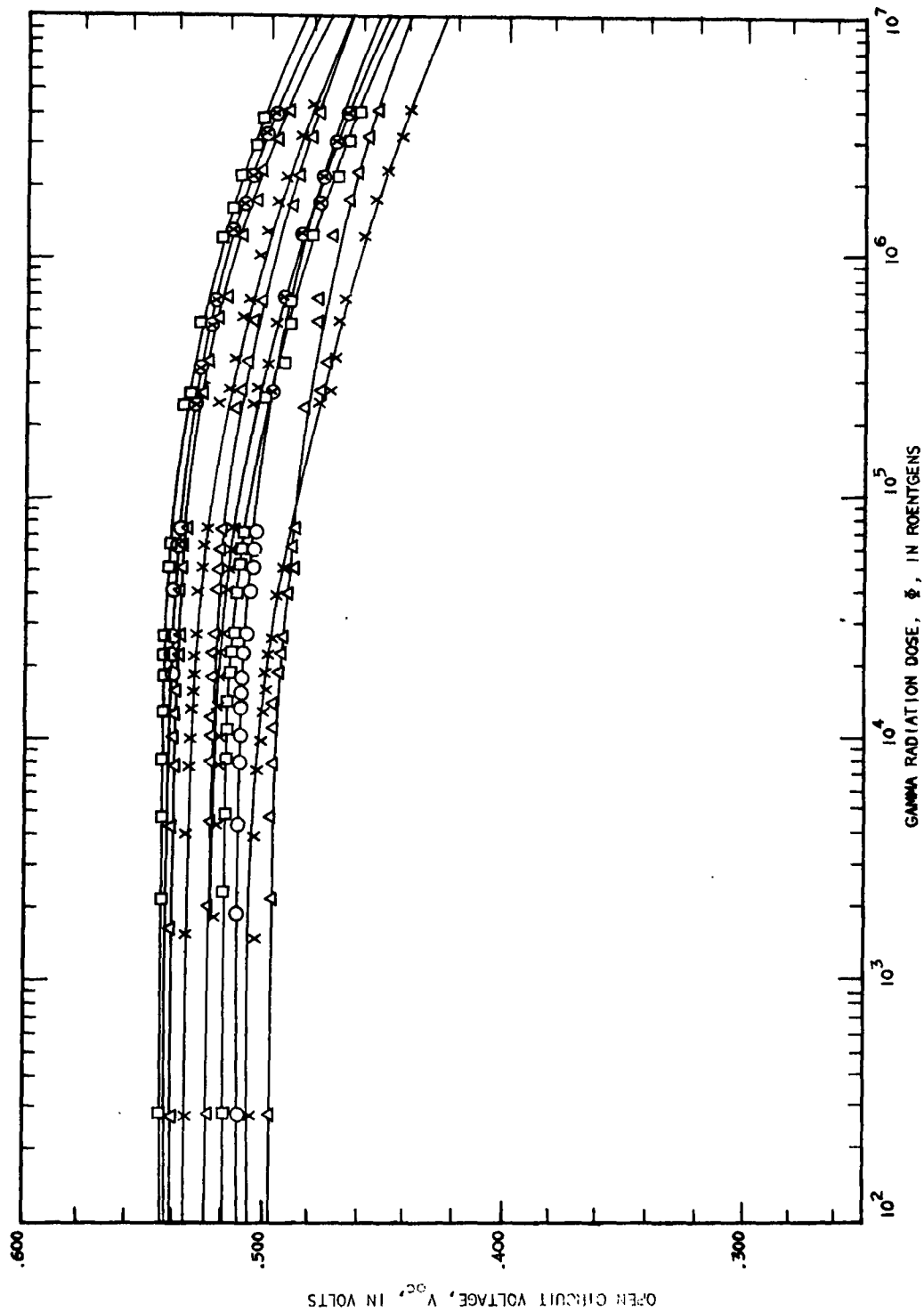


Fig. 3-3 Open Circuit Voltage V_{oc} of Silicon Solar Cells Under Gamma Irradiation

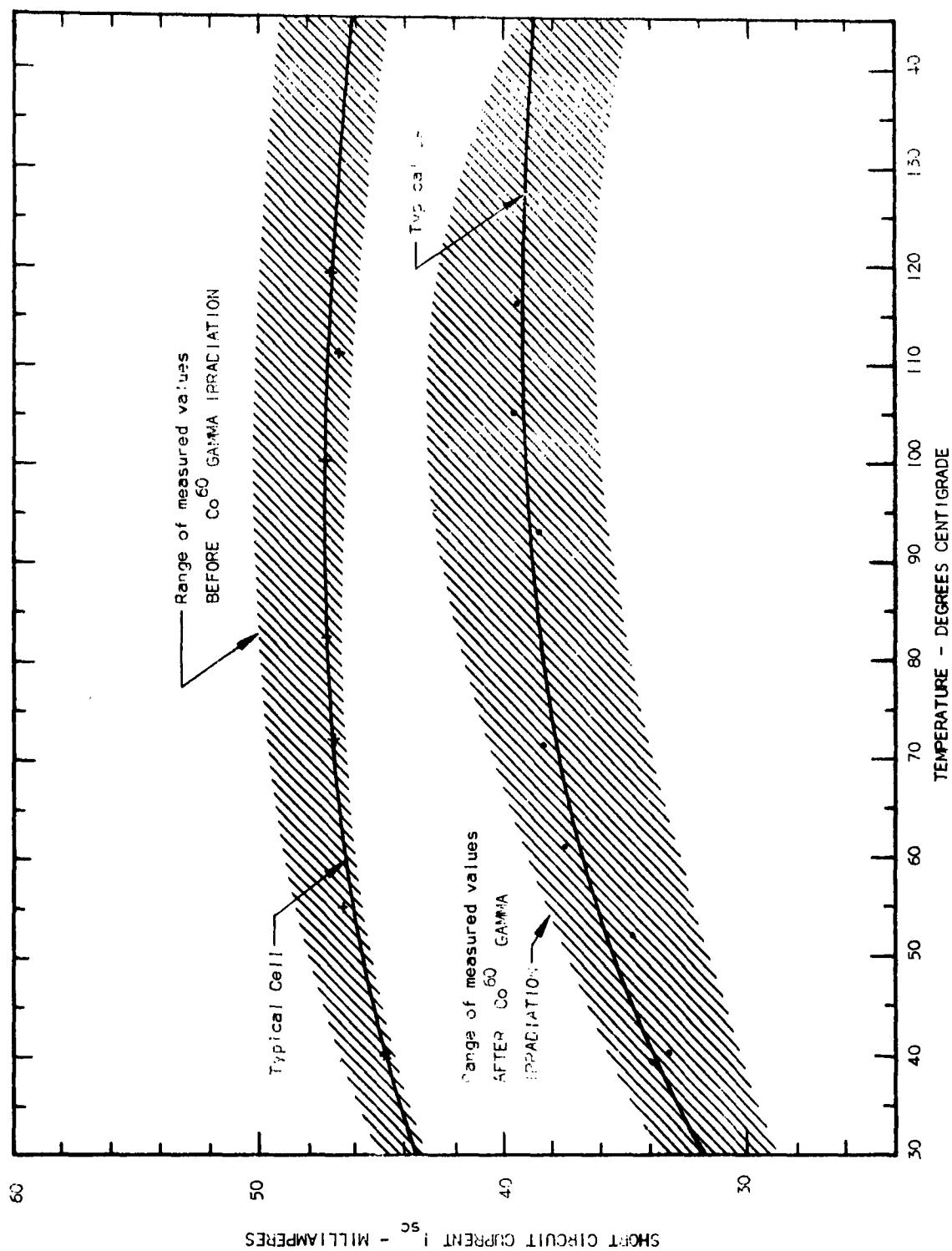
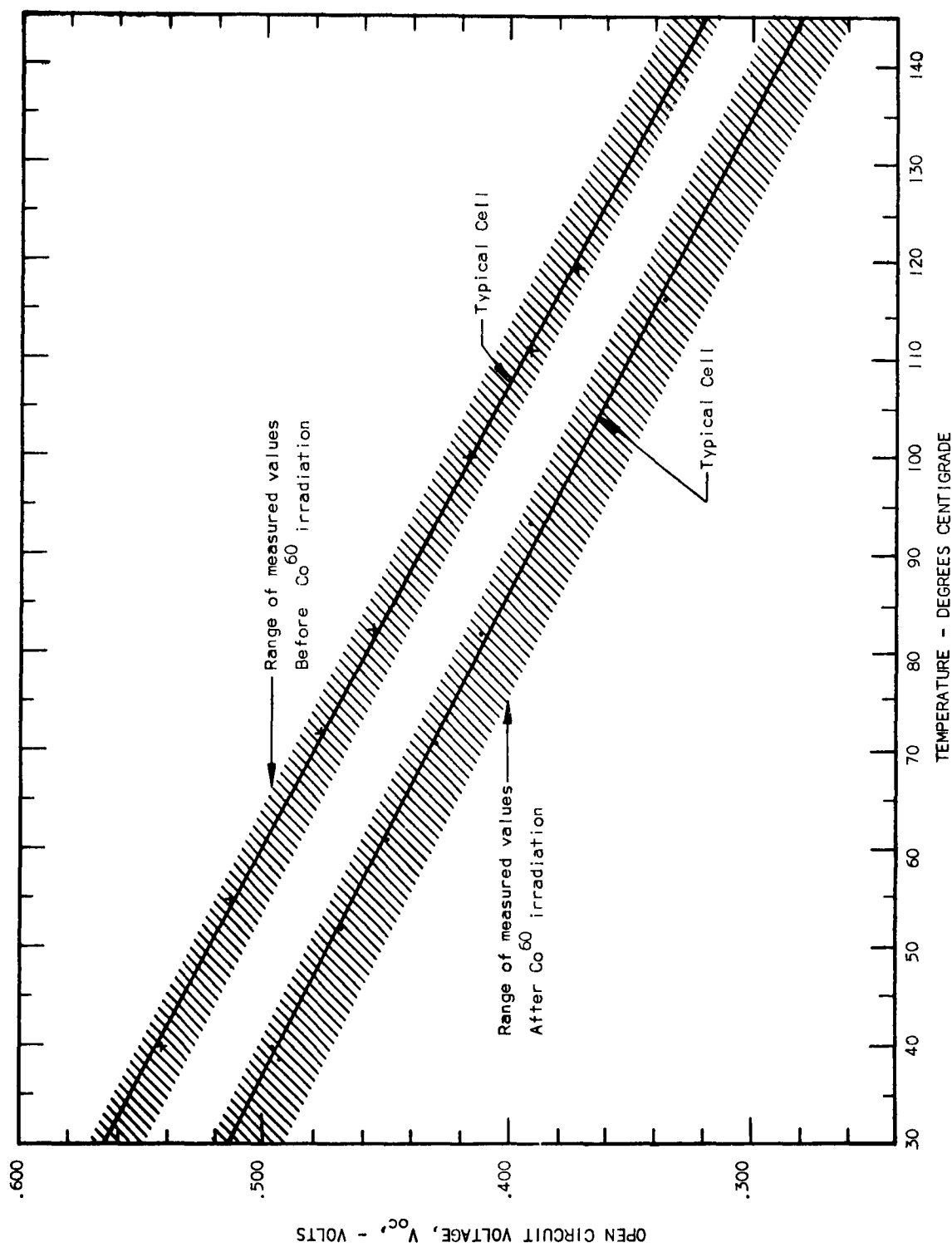


Fig. 3-4 Short Circuit Current I_{sc} as a Function of Temperature

Fig. 3-5 Open Circuit Voltage V_{OC} as a Function of Temperature

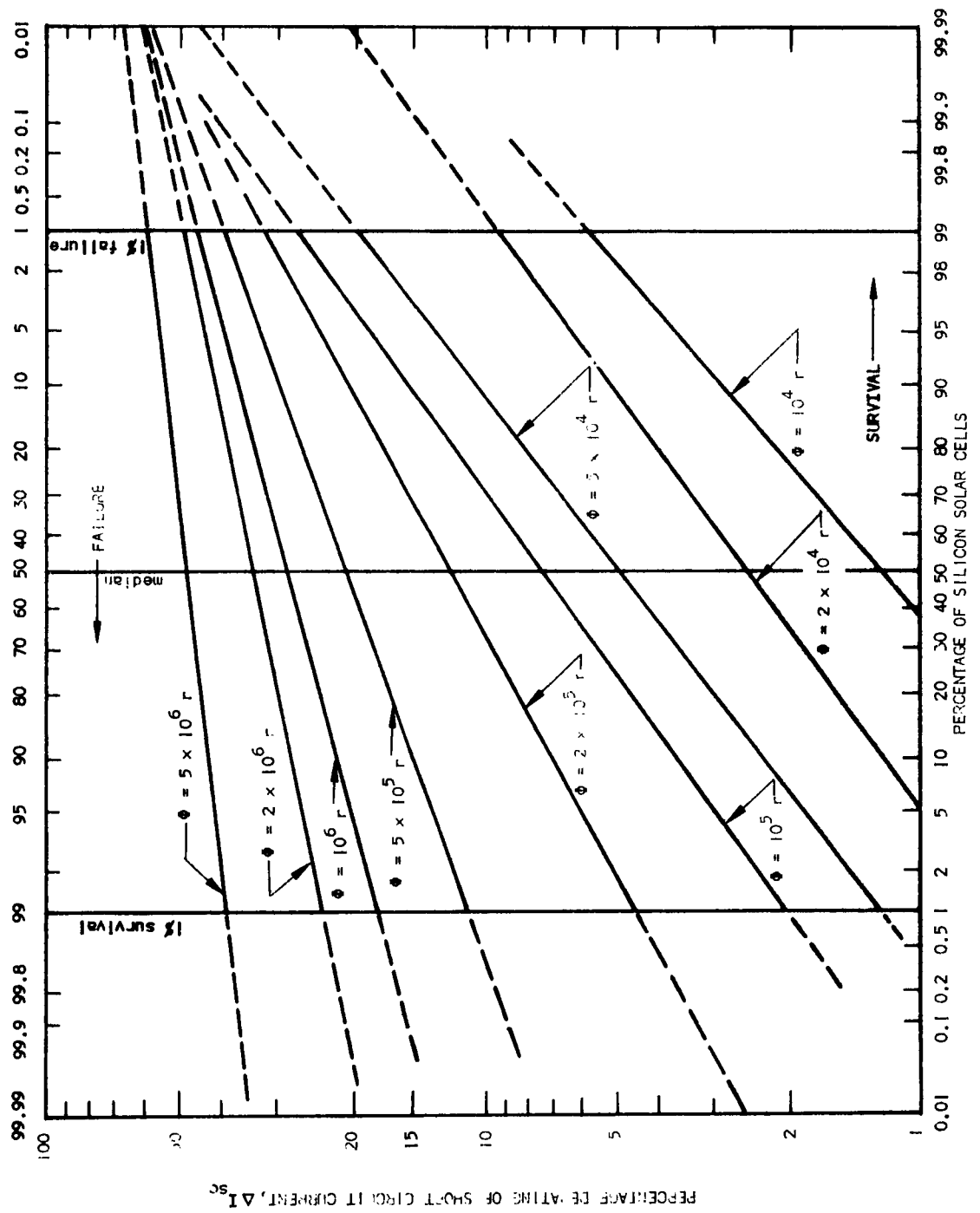


Fig. 3-6 Percentage of Silicon Solar Cells That Have a Short Circuit Current Derating ΔI_{sc} at a Dose ϕ

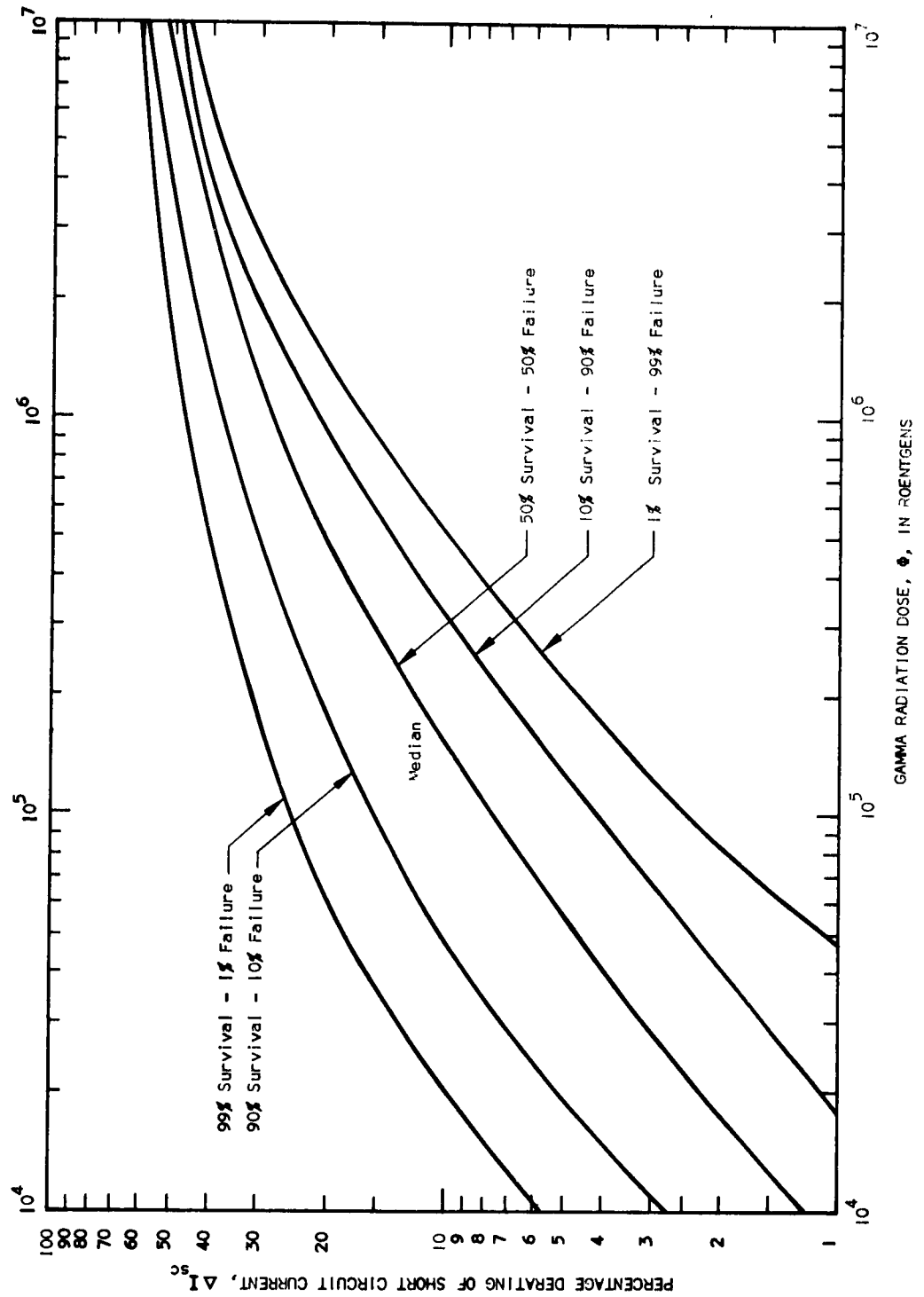


Fig. 3-7 Short Circuit Current Reliability Curves

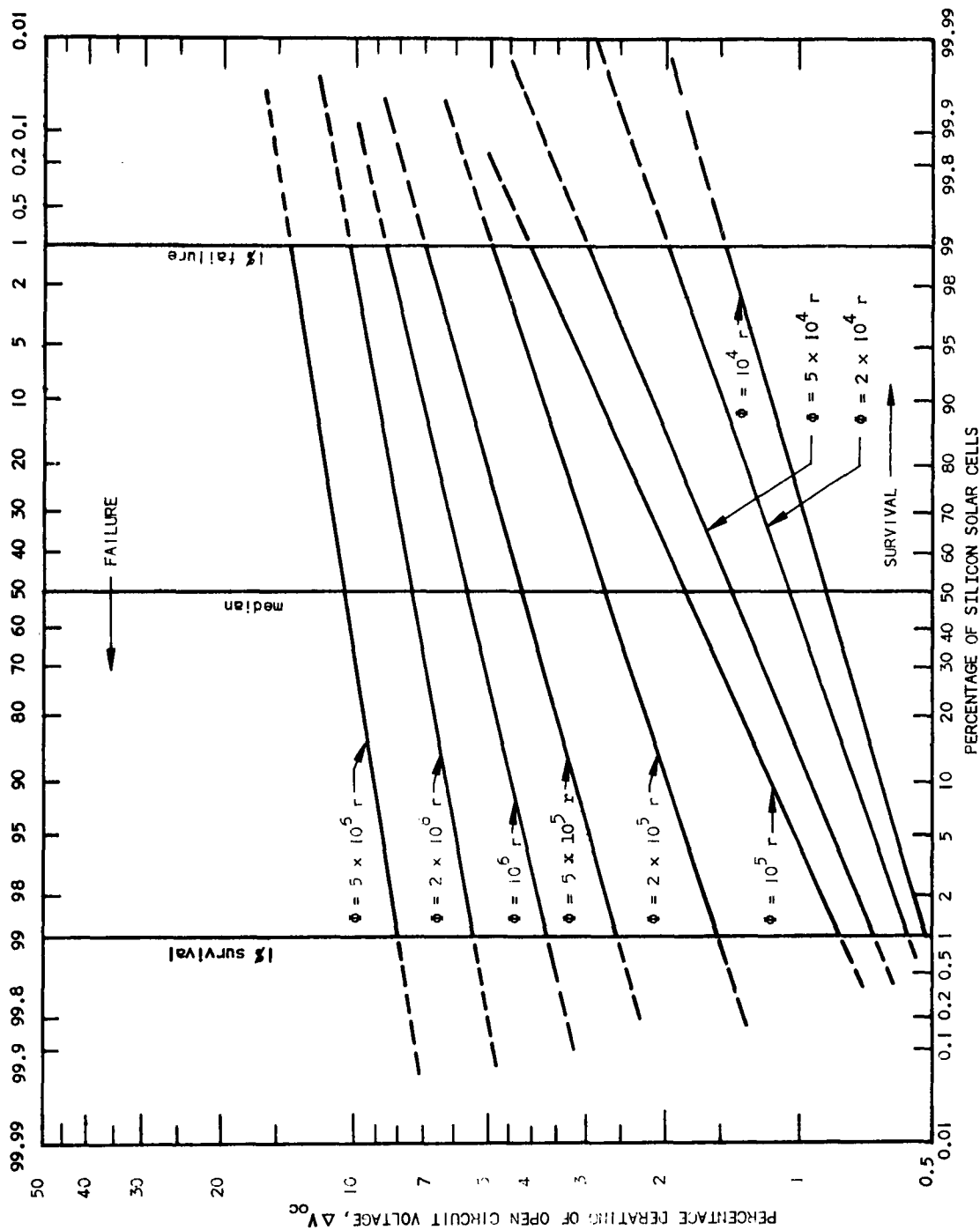


Fig. 3-8 Percentage of Silicon Solar Cells That Have an Open Circuit Voltage Derating ΔV_{oc} at a Dose Φ

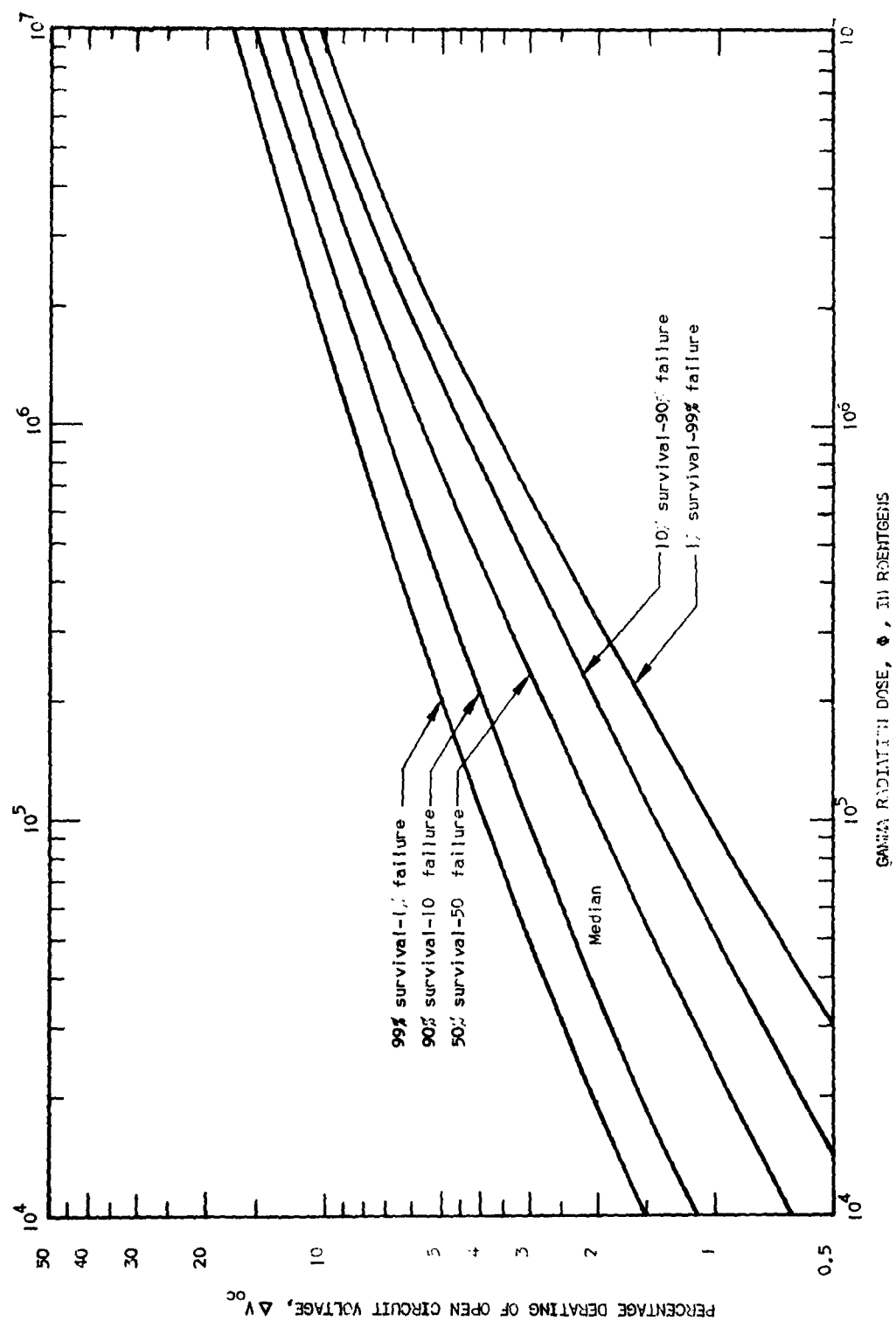


Fig. 3-9 Open Circuit Voltage Reliability Curves

4. DISCUSSION

This study has shown that the silicon solar cell is affected by gamma radiation beginning at an integrated dosage of the order of 10^5 roentgens. The short circuit current I_{sc} was found to be affected more radically than the open circuit voltage V_{oc} . After an integrated dose of the order of 10^7 roentgens the short circuit current I_{sc} was down to 50 percent of its initial value and the open circuit voltage was down to 90 percent of its initial value.

It can easily be seen from Equation (1-11) and the above data that after an integrated gamma dosage of 10^7 roentgens a silicon solar cell will have an "ideal" available power of only 45 percent of its "ideal" available power before gamma irradiation. The actual available power can reasonably be expected to have decreased by a similar amount.

The temperature dependence of the short circuit current I_{sc} was changed after the solar cell was exposed to gamma radiation. The open circuit voltage temperature dependence, however, remained unchanged. Due to the short circuit current I_{sc} vs. temperature curvature it is indicated that the optimum temperature of operation may be higher than that of non-irradiated samples; further work is required to ascertain this. One must bear in mind, however, that the available power at any temperature is reduced after irradiation as stated above.

Certain effects on a silicon solar cell power supply or array in a gamma radiation field can be predicted. The output power from such a solar power supply would decrease after an integrated dosage of 10^5 roentgens. After the total dose reached 10^7 roentgens the output power would be reduced to approximately 50 percent of its initial value, possibly more.

The current that could be drawn from such a power supply would decrease more rapidly, as the total dosage increased, than the voltage output up to dosages of 10^7 roentgens. Therefore, a silicon solar cell power supply operating in a gamma radiation field, where the total dosage accumulated by the power supply would be 10^5 roentgens or greater, would be seriously affected. Not only would its usable lifetime be shortened greatly, but the available power from such a supply would be greatly reduced.

This study was limited to the effects of gamma radiation in silicon solar cells; an investigation of the effects of neutron, cosmic, and x-ray radiation is planned by this laboratory.

BIBLIOGRAPHY

- 1952 Shockley, W. and W. T. Read, Jr., "Statistics of the Recombination of Holes and Electrons," Phys. Rev., 87, 835
- 1954 Cummertow, R. L., "Photovoltaic Effect in p-n Junctions," Phys. Rev., 95, 16
- 1954 Rappaport, P., "The Electron - Voltaic Effects in p-n Junction Induced by β -Particle Bombardment," Phys. Rev., 93, 246
- 1954 Rappaport, P., "Minority Carrier Lifetime in Semiconductors as a Sensitive Indication of Radiation Damage," Phys. Rev., 94, 1407
- 1955 Evans, R. D., "The Atomic Nucleus," McGraw Hill Book Co., Inc., Chapters 23 and 25
- 1956 Hunter, L. P., "Handbook of Semiconductor Electronics," McGraw Hill Book Co., Inc.
- 1956 Loferski and Rappaport, "Radiation Damage Study on Silicon Solar Energy Converters," U. S. Army Signal Corps Contract with RCA Labs, Princeton, N.J., Contract No. DA-36-039-SC-64643
- 1956 Seitz, F. and J. S., Koehler, "Displacement of Atoms During Irradiation," Solid State Physics, Vol. II, Seitz and Turnbull, Editors, Academic Press, Inc., N. Y.
- 1956 Steele, H. L. Jr., "Effects of Gamma Radiation on Transistor Parameters," Proc. Transistor Reliability Symposium, p. 96, New York University Press
- 1957 Dreves, G. J. and G. H. Vineyard, "Radiation Effects in Solids," Interscience Publishers, Inc., N. Y.
- 1957 Curtis, O. L., J. W. Cleland, J. H. Crawford, J. C. Pigg, "The Effect of Irradiation on the Hole Lifetime of n-type Germanium," J. Appl. Phys. 28, 1161
- 1957 Keisler, G. L. and H. V. Stewart, "The Effect of Nuclear Radiation on Selected Semiconductor Devices," Proc. of the IRE, 45, 931
- 1957 van der Ziel, A., "Solid State Physical Electronics," Prentice-Hall, Inc. Englewood Cliffs, N. J.

- 1957 Ziegler, H. K., "Solar Power Sources for Satellite Applications,"
(U. S. Army Signal Eng. Labs., Ft. Monmouth, N. J.) CSAGI Rocket
and Satellite Conference 30 Sep. - 5 Oct., 1957, Washington, D. C.
- 1958 Browne, M. E., A. B. Francis, and G. M. Enslow, "Study and Evaluation
of Silicon Solar Cells," LMSD-5021, June, 1958
- 1958 Shaw, C. and R. S. Krogstad, "Effects of Gamma Radiation on Infrared
Transmitting Materials and Filters," LMSD Report No. 5014, June, 1958

THE EFFECTS OF NUCLEAR RADIATION ON POWER TRANSISTORS

by

Frederick Gordon Jr.
U. S. Army Signal Research and Development Laboratory
Fort Monmouth, New Jersey

This paper presents the results of nuclear radiation experiments performed at Brookhaven National Laboratory to determine the effects of this radiation on power transistors of various types. A brief analysis of device parameter changes, and of the evaluation of the results is presented. In addition, there is a short discussion of the interrelation between the minimizing of the effects of nuclear radiation on transistors and the specific application of the devices.

The device types that were exposed were homogeneous-base germanium power transistors. The device parameters that were monitored were small-signal and large-signal grounded-emitter current gain, as well as the reverse collector current. The techniques of measurement included multiple point measurements and curve tracer techniques. The results show fair agreement between experimental results and calculated values.

INTRODUCTION

Experiments were performed to determine the effect of a nuclear radiation environment (primarily neutrons) upon germanium power transistors. This type device is now being used in military equipment which may be exposed to similar radiation fields. The devices exposed were conventional types of germanium power transistors (2N297 and 2N236B).

The objectives of the experiment were twofold; first, to determine the extent of damage in these devices so that radiation limitations in current devices might be set and, secondly, to utilize this information in designing transistors that will have a greater resistance to radiation.

The interesting device characteristics from the standpoint of their susceptibility to radiation damage as well as their importance to the device designer and user, are those associated with gain and reverse collector current. The actual parameters that were measured were I_{CR} , H_{FE} , and I_{CBO} , the reverse collector current, d-c (or average) grounded-

emitter current gain, and small-signal grounded-emitter current gain respectively. In addition, photographs were taken of the grounded-emitter collector characteristics (V_c vs. I_c).

These experiments were performed at the bulk shielding facility of the reactor at the Brookhaven National Laboratory, Upton, New York. The experimental procedures and results are described herein.

EXPERIMENTAL PROCEDURE

Analysis of Problem

Experiments on nuclear radiation effects on semiconductor materials by various groups^{1,2,3} have shown that the bulk material parameters that are affected by neutron bombardment are primarily minority carrier lifetime, τ , conductivity, σ , and mobility, μ . There are also surface effects, but these are not easily analyzed. All three of the bulk parameters measured affect the performance of the transistor. The lifetime and conductivity are changed much more radically than the mobility and, for the purpose of this analysis, only the τ and σ changes will be considered.

The transistors chosen for these experiments were alloy junction types with homogeneous base regions.

The small-signal common-emitter current gain for these devices can be expressed by equation (1).

$$\frac{\partial I_c}{\partial I_B} \bigg|_{V_c=K=\alpha_{ob}} = \left[\frac{\sigma_{nbo} W_o (1 + \frac{M}{2})}{\sigma_{peo} \sqrt{D_{ne}} \tau_{no}} + \frac{A_s SW_o (1 + \frac{M}{2})}{A_c \mu_{pb} (1 + M)} + \frac{W_o^2}{2D_{pb} \tau_{po}} - \frac{n_{pco} \mu_{nco}}{p_{co} \mu_{pco}} \right]^{-1} \quad (1)$$

$$M = \frac{W_o I_e b q}{k T A_e \sigma_{nbo}} \quad (2)$$

The first term in brackets is the emitter injection efficiency term; the second, the surface recombination term; the third, the minority carrier transport term; and the fourth is the collector multiplication factor. If typical material parameter values are used, the fourth term is insignificant. It may be seen that all three significant terms have parameters which are affected by radiation (σ , μ , τ). The radiation sensitive conductivity for the surface factor appears in the M-term, and there is a probability that "S" is also nuclear radiation sensitive.

Loferksi⁴ and Messenger⁵ have reported equation for damage effects for the minority lifetime. Equation (3) is the Messenger version of the equation,

$$\tau_p = \left(\frac{1}{\tau_{po}} + \frac{\phi}{K} \right)^{-1} \quad \tau_{po} = \text{initial minority carrier lifetime} \quad (3)$$

K = lifetime reduction constant
(Neutron-sec-cm²)

Equation (4) for conductivity change permits the utilization of the carrier removal constant (Q) for electrons in N-type germanium given by Cleland and Crawford².

$$\sigma_{nb} = \sigma_{nbo} \left(1 - \frac{Q\Phi}{n_{nbo}} \right) \quad (4)$$

Q = carriers/cm³ removed per incident neutron/cm²

n_{nbo} = initial majority carrier concentration

Φ = total neutron flux, neutrons/cm²

σ_{nb} = majority conductivity of base region

σ_{nbo} = majority conductivity of base region initially.

Equations (3) and (4) can be put into equations (1) and (2), yielding (5) and (6):

$$\alpha_{cb} = \left[\frac{\sigma_{nbo} \left(1 - \frac{Q\Phi}{n_{nbo}} \right) W_o \left(1 + \frac{M'}{2} \right)}{\sigma_{peo} \left(1 - \frac{Q'\Phi}{p_{peo}} \right) \sqrt{D_{ne} \left(\frac{1}{\tau_{no}} + \frac{\Phi}{K} \right)}^{-1}} + \frac{A_e}{A_c} \frac{SW_o \left(1 + \frac{M'}{2} \right)}{\mu_{pb} \left(1 + M' \right)} + \frac{W_o^2}{2D_{pb} \left(\frac{1}{\tau_{pc}} + \frac{\Phi}{K} \right)}^{-1} \right]^{-1} \quad (5)$$

$$M' = \frac{W_o I_e b_q}{kT A_e \sigma_{nbo} \left(1 - \frac{Q\Phi}{n_{nbo}} \right)} \quad (6)$$

If values for the parameters in equations (5) and (6) that are representative of the P-N-P power transistors used in this experiment are inserted in these equations, a calculated expected change in α_{cb} with radiation can be plotted. The resistivity of the emitter, base, and collector regions is known within a factor of two. The minority carrier lifetime is not as well known for the devices under test. There are indications from preliminary tests that the Lederhandler-Giocoletto⁶ effective minority carrier lifetime may be quite useful in evaluation of radiation damage in these devices, but this test was not performed for this experiment. Figure 1 shows the plot of α_{cb} vs. Φ using equation (5) and values of the parameters chosen to be representative of the 2N297 power transistor. The τ_{po} was selected to give an initial α_{cb} that is close to the measured values. Several damage constants (K) were used to determine which values would result in a curve fall-off close to the actual experimental curves shown in Figure 2 for a representative 2N297. There is fair agreement in magnitude and shape of curve 2 of Figure 1 and curve 2 of Figure 2. The actual magnitude difference of these curves is easily within the results that may be expected because of the difference between the values of some of the parameters

chosen for equation (5) and the actual values of transistor #35. This experimental curve shows the damage constant (K) to be about 6×10^7 nvt-sec which is in fair agreement with Messenger's value (5×10^7 nvt-sec).

The experimental curve of d-c common emitter current gain (H_{FE}) vs. Φ is also shown for a typical 2N297. The theoretical basis for this particular parameter is not as well established as the α_{cb} , although Huang and Chang⁷ have developed an equation for H_{FE} that is very similar to equation (1). No theoretical plot is made for H_{FE} at this time. The H_{FE} is always larger than α_{cb} for a given set of bias currents (I_b, I_c), and the ratio of H_{FE} to α_{cb} tends to increase with increasing currents. This ratio seems to generally decrease slightly at low currents after the units have been irradiated and, at high currents, to generally increase. The trends shown in the experiment are not definite enough to be conclusive.

Figure 3 shows calculated curves for α_{cb} vs. Φ with τ_{po} as the family parameter. It may be seen that the lower initial minority carrier life-time (τ_{po}) (curve 2) while having a lower resultant initial α_{cb} has a much lower relative change with radiation than the higher α_{cb} (higher τ_{po}) unit. If the radiation damage point for α_{cb} is taken at the point where it falls to one-half of its initial value, this occurs at about 5×10^{11} nvt for the $\tau_{po} = 10^{-4}$ sec unit, and 4×10^{11} nvt for the $\tau_{po} = 10^{-6}$ sec unit. There will probably be applications where this method of obtaining radiation resistance is acceptable.

Another important device parameter that is affected quite radically by nuclear radiation is the reverse collector current with the emitter open. This current has two principal parts as shown in equation (7).

$$I_{cr} = I_{co} + I_L \quad (7)$$

I_{co} is that portion of the reverse current which is due to the bulk characteristic of the semiconductor material (in this case, germanium), and the I_L is the leakage current due to surface phenomena. I_{co} may be represented by equation (8). In alloy type transistors such as the 2N297, which have a collector region with a much higher conductivity than the base,

$$I_{co} = \frac{\mu_p n_1^2 \sqrt{\mu_n k T q^3}}{\sigma_{pco} \sqrt{\tau_{no}}} + \frac{\mu_n n_1^2 \sqrt{\mu_p k T q^3}}{\sigma_{nbo} \sqrt{\tau_{po}}} T \sinh \left[\frac{2W_o}{\sqrt{D_{pb} \tau_{po}}} \right] \quad (8)$$

Equation (8) reduces to equation (9) under most circumstances. This is primarily because $\sigma_{pco} \gg \sigma_{nbo}$.

$$I_{co} = \frac{\mu_n n_1^2 \sqrt{\mu_p k T q^3}}{\sigma_{nbo} \sqrt{\tau_{po}}} T \sinh \left[\frac{2W_o}{\sqrt{D_{pb} \tau_{po}}} \right] \quad (9)$$

This simplification generally holds true even after the devices are irradiated because the low conductivity material of the base region will convert from "N" to "P" type before the conductivity of the collector region would approach that of the base region. Thus, the transistor would cease to be before the approximation became invalid.

By examining equation (9), it may be seen that I_{co} is a function of both the conductivity and the minority carrier lifetime in the base region. As in the case of α_{cb} , one can substitute for τ_{po} and σ_{nbo} their radiation sensitive equivalents as shown in equations (3) and (4).

$$I_{co} = \frac{\mu_n n_1^2 \sqrt{\mu_p k T q^3} \beta}{\sigma_{nbo} \left(1 - \frac{Q\phi}{n_{bo}}\right) \sqrt{\left(\frac{1}{\tau_{po}} + \frac{\phi}{K}\right)} - 1} T \sinh \left(\frac{2W_0}{D_{pb} \left(\frac{1}{\tau_{po}} + \frac{\phi}{K}\right)} - 1 \right) \quad (10)$$

To show which of these factors (σ_{nbo} or τ_p) contributes the greater change with radiation, Figure 5 is a plot of I_{co} vs. ϕ with τ_{po} as the family parameter. For all of the curves, the initial conductivity is the same ($.5 \text{ ohm}^{-1} \text{ cm}^{-1}$). There are three values of initial minority lifetime ($\tau_{po} = 10, 100, 1000 \text{ } \mu\text{sec}$). Curve 1 is a plot of I_{co} vs. ϕ ($\tau_{po} = 10 \text{ } \mu\text{sec}$) with only τ_p changing with radiation. Curve 2 is the same transistor with only σ_{nb} changing. Curves 3 and 4 and curves 5 and 6 are similarly paired with $\tau_{po} = 100 \text{ } \mu\text{sec}$ for 3 and 4, and $\tau_{po} = 1000 \text{ } \mu\text{sec}$ for 5 and 6. Two principal factors may be noted from these curves. First, that the change in minority carrier lifetime is far more important to I_{co} changes than the conductivity change with radiation, and that the lower initial lifetime material is subject to less change for a given level of neutron flux. Material with a minority carrier lifetime of $10 \text{ } \mu\text{sec}$ has only trebled in I_{co} at 10^{13} nvt , while $100 \text{ } \mu\text{sec}$ material has increased by a factor of 20 at this radiation level. It must be noted, however, that the initial I_{co} is an order of magnitude higher for the lower lifetime material. This smaller percentage change of I_{co} with lower lifetime is very much like the effect determined above for α_{cb} . More will be said about this later.

Experimental Procedure

As mentioned in the introduction, the actual experiment was performed at the Brookhaven nuclear reactor's bulk shielding facility. A cross-sectional diagram of the facility is shown in Figure 6. This facility is on top of the reactor. The fast neutrons issue forth from the converter (fission) plate which has thermal neutrons from the reactor fuel elements incident on it from the under side. A tank of water is set down on this plate in lieu of the heavy shielding material that is elsewhere on the top of the reactor. There is about 12 feet of water in the tank. About three feet up from the bottom of the tank is a lead shield in which there are holes through which the equipment to be irradiated can be lowered. The hole used in this experiment was ten inches in diameter. The nature of the experimental setup necessitates the use of water-tight containers and

connector cables for the transistors. The fast neutron flux inside the aluminum container holding the transistors was estimated to be about 1.13×10^9 neutron/cm² sec. This figure was arrived at by the Nucleonics Section, Applied Physics Division, USASRD after evaluation of the dosimetry wafers of sulfur and gold that were placed in the container.

The transistors were connected to the test equipment through water-tight shielded cables. The test equipment permitted selection of a transistor and the test to be performed upon that transistor by means of two banks of rotary switches. The test conditions were fixed for any given test position. As mentioned previously, the device parameters monitored were α_{cb} at two values of collector current, H_{FE} at the same two values of collector current, and I_{CR} at two voltages. In addition, the collector characteristics in the common emitter, as presented on a Tektronix curve tracer were photographed.

The water-tight container was an aluminum cylinder eight inches high with an inside diameter of six inches. The can was lined with a one-sixteenth inch thick sheet of cadmium to minimize the ratio of thermal to epi-cadmium neutrons.

The measurements were made at various lengths of radiation exposure time. Due to the fact that the tests were manually monitored and, therefore, took about ten to 20 minutes to perform per set, the cylinder was pulled up through the lead shield to effectively suspend irradiation during the individual test periods.

Two sets of transistors were tested; the first Olevite 2N297 units, and the second Bendix 2N236B units. Both are alloy type P-N-P germanium power transistors. The 2N297 units were exposed for a total of 120 minutes to the flux which was equivalent to a total flux of about 8×10^{12} nvt fast neutrons. The 2N236B units were exposed to 660 minutes of radiation. The tests performed were not identical for both types.

For the 2N297 transistors, I_{CR} was measured at -2 volts and -30 volts, I_c ($V_c = 2$ to 4 volts), with I_b equal to six and 48 milliamps, α_{cb} at the same points (with a base a-c signal of 10 microamps), and the V_c-I_c characteristics were photographed. For the 2N236B transistors, I_{CR} was measured at -2 volts and -20 volts, and the V_c-I_c and I_c-I_b characteristics photographed. This modification was due to equipment difficulties at the time of the 2N236B measurement. The lower value of upper voltage measurement of reverse collector current (I_{CR}) is due to the low collector breakdown voltage of the Bendix units.

Experimental Results

The experimental results showed that device parameters performed about as indicated in the theoretical calculations. The agreement between the experimental and calculated curves was within the error that might be expected from the spread of actual material and geometric factors of the devices as manufactured. Figures 7 and 8 show actual experimental V_c-I_c

common-emitter curves of representative 2N297 and 2N236B transistors as they appeared at zero radiation as indicated. Unfortunately, due to malfunctioning of the temperature-indicating apparatus, these curves are not corrected for any temperature difference, but inasmuch as there was very little change in ambient and the individual measurements were made as quickly as possible, it is felt that this lack of temperature indication does not distort the picture very much.

The reverse saturation current, I_{CR} , was measured at two voltages. The lower voltage was chosen so that a measurement would be made that would give a fair indication of the bulk saturation current ($I_{CR} \approx I_{co}$). Actually, the two volts bias brings the current into the leakage current region somewhat, but it was a convenient value of voltage to use for this test. The higher voltage gives a value of I_{CR} that includes the leakage component as shown in equation (7). The higher voltage was chosen low enough so that it was felt that no appreciable breakdown or collector carrier multiplication takes place, and that the slope between the two voltage points would be an indication of the leakage current. Inasmuch as I_L is basically a surface phenomenon, it was hoped that an indication would be given of surface changes due to radiation effects as well as the bulk material effects. Figure 9 shows a plot of I_{CR} vs. V_c on some of the transistors that were used in the experiments. The I_{CR} is drawn as a straight line between the two measured points. Subsequent photographs of the swept V_c - I_{CR} curve taken at the laboratory after the experiment show that this straight line approximation is not too far off in most cases.

Table I shows the I_{co} and I_L of the ten 2N297 transistors before being irradiated and after 120 minutes of exposure to radiation ($\sim 8 \times 10^{12}$ nvt). The units are listed from top to bottom in Table I in order of increasing low-voltage I_{CR} ($I_{CR} \approx I_{co1}$). The spread in I_{co1} is small, well within lifetime, resistivity, and geometry fabrication variations. The change in I_{co} with radiation for the 120 minutes of exposure for all cases is about an order of magnitude. Actually, the range in $\frac{\Delta I_{co}}{I_{co1}}$ is from 8.09

to 10.8. The relatively small spread in $\frac{\Delta I_{co}}{I_{co1}}$ serves to indicate that there is a predictable pattern to the bulk saturation current as expected. Figure 10 shows theoretical curves plotted for equation (10), and the values indicated on the Figure and the plot of one of the 2N297 transistors that was irradiated during the course of the experiment. The curves show the initial magnitude of I_{co} of the experimental curve to be such that the initial lifetime (τ_{po}) would be somewhere between 10^{-4} and 10^{-6} sec. This is in general agreement with the α_{cb} results (see Figures 1 and 2) and the value chosen for τ_{po} (5×10^{-6} sec in Figure 1). There is fair agreement between the shape of the experimental curve (#5) and that of curve #3 ($\tau_{po} = 10^{-4}$ sec) although it has a somewhat sharper slope as would be expected for a unit with lower τ_{po} . There are a number of possible causes of any discrepancy, assuming the theory is correct. In order to have a direct comparison with the calculated curves, which are in terms of current densities, and the experimental curves, the latter must also be in terms of

current density. However, the measurements are made in total current, and must be converted to densities. In order to do this, it is assumed that the collector diameter is 150 mils. This diameter may be slightly different from the actual value and, therefore, the calculated current density may be slightly different. In addition to this geometric factor, the experimental curves are not normalized to 300°K, but are about 300°K \pm 1.5°K which would also change the curve shape slightly. In the case of the theoretical calculations, W_0 and σ_{nbo} , the base width and base conductivity respectively, have assumed values of three mils and 0.33 ohm⁻¹ cm. In the actual transistor, these may be different by factors great enough to account for the difference in current density magnitude. The damage constants used in the calculations are about what might be expected from comparison of Figures 1 and 2. Another possibility of variation is the actual exposure value. The dosimetry check point was that of neutrons with energies greater than 2.5 Mev. This information was supplied by sulfur pellet evaluation. The actual dose rate is dependent upon the spectrum assumed. Because of the utilization of a fission plate for conversion of slow neutrons into fast, a fission spectrum similar to Godiva was assumed. The actual sulfur count showed a total flux (neutron energies > 2.5 Mev) of 10¹³ nvt, which was extrapolated to 1.13 x 10¹⁴ neutrons per cm² per sec for the entire spectrum (Godiva).

The leakage current, I_L , is defined as that part of the reverse collector current that is due to surface leakage across the collector junction. It seems to be essentially a linear function of voltage in the region of observation, i.e. between two and 32 volts. This is essentially the region above the bulk saturation current, and below which any breakdown is perceptible. Because of the linearity of the voltage-current relationship in this region, we assume a leakage resistance (R_L) for the surface that is defined as:

$$R_L = \frac{\Delta V}{\Delta I} = \frac{30}{I_{CR}(32V) - I_{CR}(2V)} \quad (11)$$

In Table I, R_{L1} is the leakage resistance at zero radiation, and R_{L2} the leakage resistance after 120 minutes of exposure ($\sim 8 \times 10^{12}$ nvt). The variation in this initial leakage resistance (R_{L1}) is quite large, ranging from 175 kilohms to 3750 kilohms (a factor of better than 20). After the radiation exposure, all the surface resistances are considerably lower showing much higher leakage currents. The variation in leakage resistance after exposure ranges from 41 kilohms to 69 kilohms (a factor of less than two).

Figures 11 and 12 show the variation of leakage current with exposure, and the resultant leakage resistance with exposure respectively. These seem to indicate that the leakage tends toward a radiation saturation value almost independent of initial value. The higher initial leakage surfaces thus have the smaller percentage change in leakage current.

CONCLUSIONS

The general results of this experiment are in good agreement with the theoretical calculations for the germanium homogeneous base region power transistors. If one takes the arbitrary damage end points for the reverse collector current, I_{co} , and grounded emitter current gain, α_{cb} , of an increase of an order of magnitude and a decrease by a factor of two respectively, the experimental results show that for the former this occurs about $5-8 \times 10^{12}$ nvt, and for the latter at about $0.9-1 \times 10^{12}$ nvt. Inasmuch as the latter is, for many applications, usually the most important device parameter, we may see that use of these devices (i.e. the germanium homogeneous base alloy type power transistor as represented by the 2N297) is not recommended in neutron fluxes greater than 10^{12} nvt. This refers only to the permanent damage caused by fast neutrons, and does not refer to any transient and or rate effects that may occur as a result of gamma radiation or any other associated phenomena.

The major damage, as far as the device performance is concerned, in the alloy type homogeneous base type power transistor, results from the deterioration of the minority carrier lifetime. With respect to I_{co} , this relative importance of the change of τ_{po} and σ_n with radiation was shown clearly in Figure 5. This decrease in minority carrier lifetime results

in an increase in the ratio $\frac{W_o}{\sqrt{D_p \tau_p}}$. It is the increase in this ratio that results in the degradation of the device parameters, I_{co} and α_{cb} . This effect can be minimized by decreasing W_o , the effective base region, so

that even though $\frac{W_o}{L_p} (L_p = \frac{1}{\sqrt{D_p \tau_p}})$ increases, this ratio is small enough so

that reasonable gain and reverse collector current can be maintained. In high-frequency, low-power devices, this is a somewhat practical solution; however, in the fabrication of power devices, W_o cannot be practically reduced to any value that would really be effective against the deleterious effect of nuclear radiation. This is not only because of the limitations of fabrication techniques, but due to voltage punch-through considerations. It is, therefore, advisable to go to device designs other than the homogeneous base, e.g., graded base (see report titled "A Preliminary Analysis of the Effect of Nuclear Radiation on Graded-Base Power Transistors").

Another feature of the radiation effect upon power transistors is that devices that have low initial minority carrier lifetime with the resultant lower α_{cb} and higher I_{co} are less affected by radiation than the higher gain, low I_{co} unit (see Figures 3, 10). For some applications, the devices with poorer initial performance might be utilized to benefit from the greater radiation resistant qualities of these devices. For example, in Figure 3, a homogeneous based device with an initial α_{cb} equal to about 85 drops to one-half of this value at about 5×10^{11} , whereas the unit with an initial α_{cb} of 10.5 has dropped to only about 9.5 at this point, and α_{cb} does not reach the half value until about 5×10^{12} . Of course, this

is not the ultimate solution to the transistor radiation problem, but it is a partial solution. Utilization of this facet of device performance under radiation conditions is, of course, dependent upon the needs of the particular application.

Still another important feature is the effect of the radiation upon the surface as reflected in the leakage currents. This phenomenon is not as easy to analyze as the bulk properties; however, here again it is noted that the poorer surfaces, i.e. those with higher leakage, have a smaller percentage change with radiation. It might be possible to design devices that have fairly high "S" values (see equation 1), but have good α_{cb} and acceptable I_{GR} values. This surface problem with respect to leakage current will exist in all designs, but possibly can be minimized. It may be noted that by making $A_s \approx 0$ (as for example, in grown junction units) the "S" factor drops out of the given equation, but these units are more prone to other surface conditions such as channelling. In any case, more work must be done to investigate the effect of neutron bombardment on the surface of transistors before any valid conclusions can be drawn and concrete recommendations made.

In conclusion, it must be repeated that if one is to have power transistors that have and will retain good device characteristics in high neutron fields ($>10^{18}$ nvt), designs other than those of the type investigated in this experiment will have to be utilized. Ultimately, when the development of compound semiconductors is sufficiently advanced to permit fabrication of reliable devices, then transistors that utilize some of these materials will solve a number of the problems associated with the effects of nuclear radiation on germanium and silicon semiconductor devices.

REFERENCES

1. Rappaport, P., Loferski, J., Phys. Rev. 98, 1861 (1955)
2. Cleland, Crawford, Pigg, Phys. Rev. 98, 1742 (1955)
3. Cleland, Crawford, Pigg, Phys. Rev. 99, 1170 (1955)
4. Loferski, J., J. Appl. Phys., 29, 35 (1958)
5. Messenger, G. C., Philco Corporation (Private Communication)
6. Lederhandler, S. R., Giacoletto, L. J., Proc. I.R.E., re, 477 (1955)
7. C. Huang, C. H. Chang, IPS Final Report, Sylvania Electric Products, Inc., 3 May 1957, Contract DA 36-039 so-54661

ACKNOWLEDGMENT

The author wishes to acknowledge the assistance given by H. Wannemacher, M. Levy, and J. R. Anderson of the Solid State Devices Branch, in making the measurements; R. Loveland of Techniques Branch for obtaining the radiation facilities; and H. Murphy of Nucleonics Section, Applied Physics Division in making the dosimetry measurements and calculations.

TABLE I
(μ amps)

<u>Unit #</u>	<u>I_{co1}</u>	<u>I_{co2}</u>	<u>I_{co}</u>	<u>$\frac{I_L}{I_{co}}$</u>
35	39	460	421	1.32
43	42	410	368	1.13
38	44	500	456	1.12
39	46	475	419	1.10
44	47	470	423	1.04
39	49	550	501	0.954
36	51	485	434	1.01
45	51	560	509	0.96
40	54	490	436	1.36
37	56	560	504	1.12

<u>Unit #</u>	<u>$\frac{I_{co}}{I_{co1}}$</u>	<u>R_{L1} x 10⁶</u>	<u>R_{L2} x 10⁶</u>	<u>$\frac{R_L}{R_{L1}}$</u>
35	10.80	.897	.050	.92
43	8.76	2.14	.069	.96
38	10.35	3.75	.057	.98
39	9.10	2.0	.063	.968
44	8.98	3.75	.067	.982
34	10.25	1.0	.059	.941
36	8.50	0.254	.054	.787
45	9.97	0.175	.045	.743
40	8.09	0.221	.041	.814
37	9.00	1.30	.051	.961

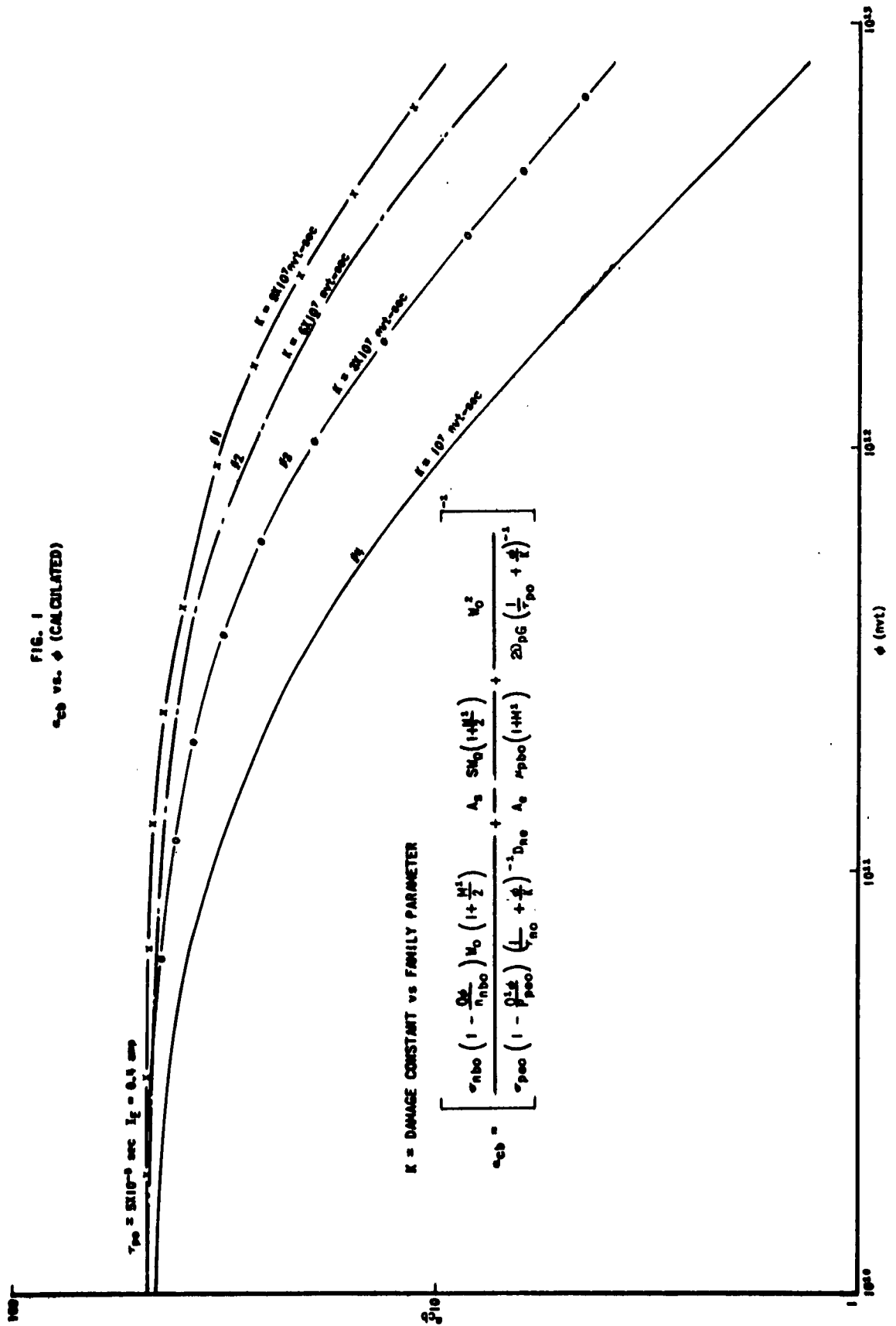
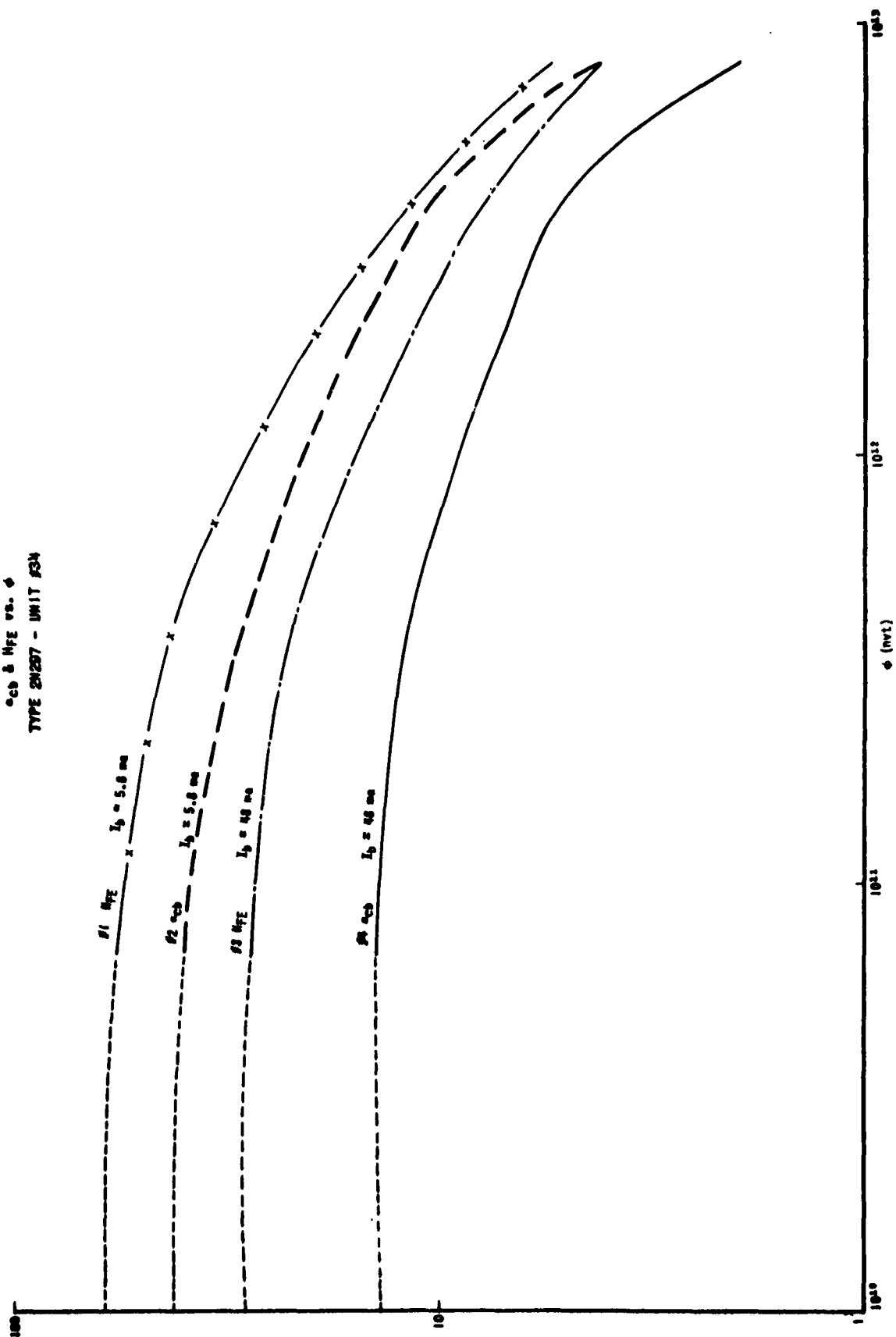
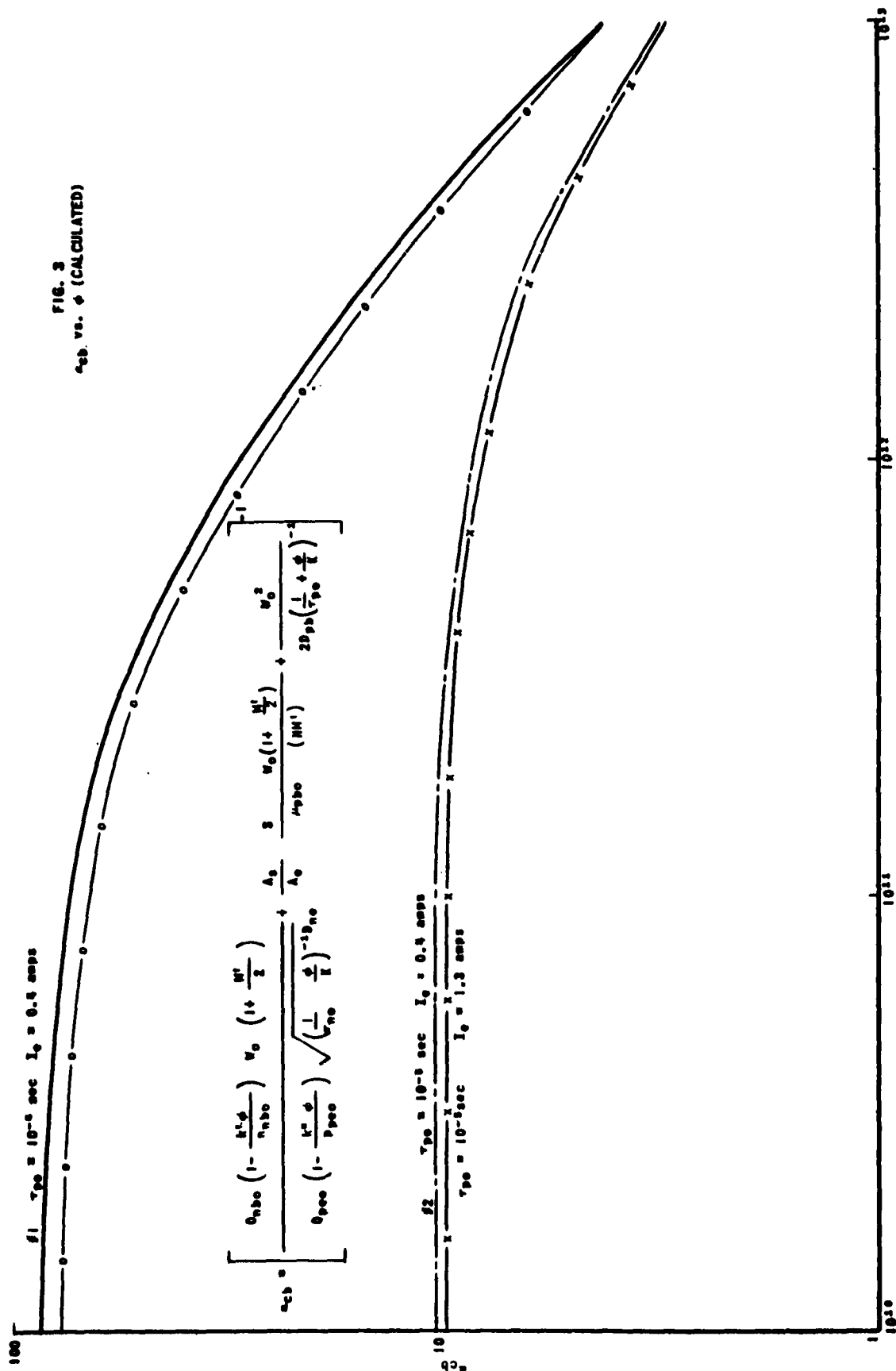
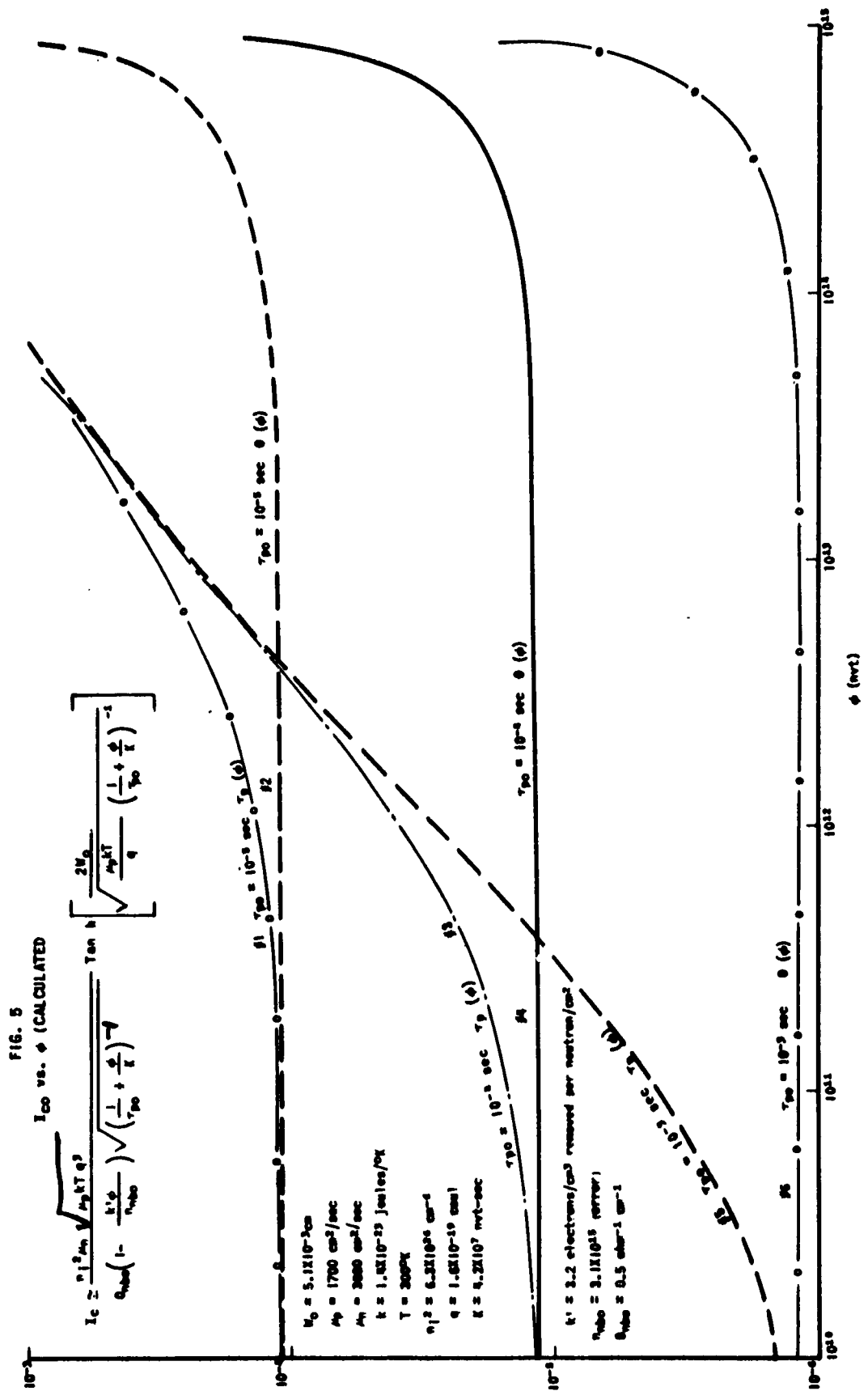


FIG. 2
 α_{cb} & η_{FE} vs. ϕ
 TYPE 24227 - UNIT 234







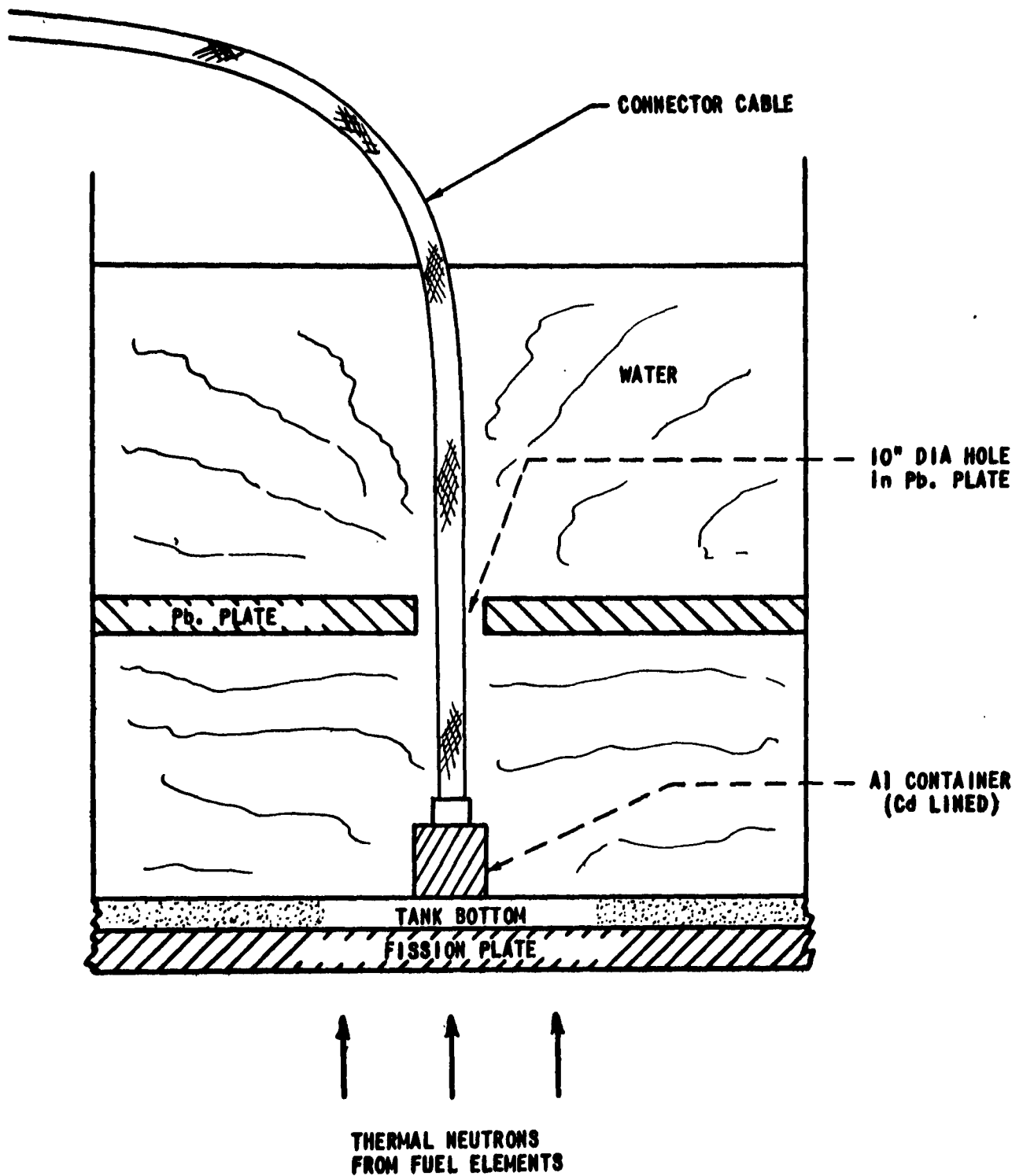
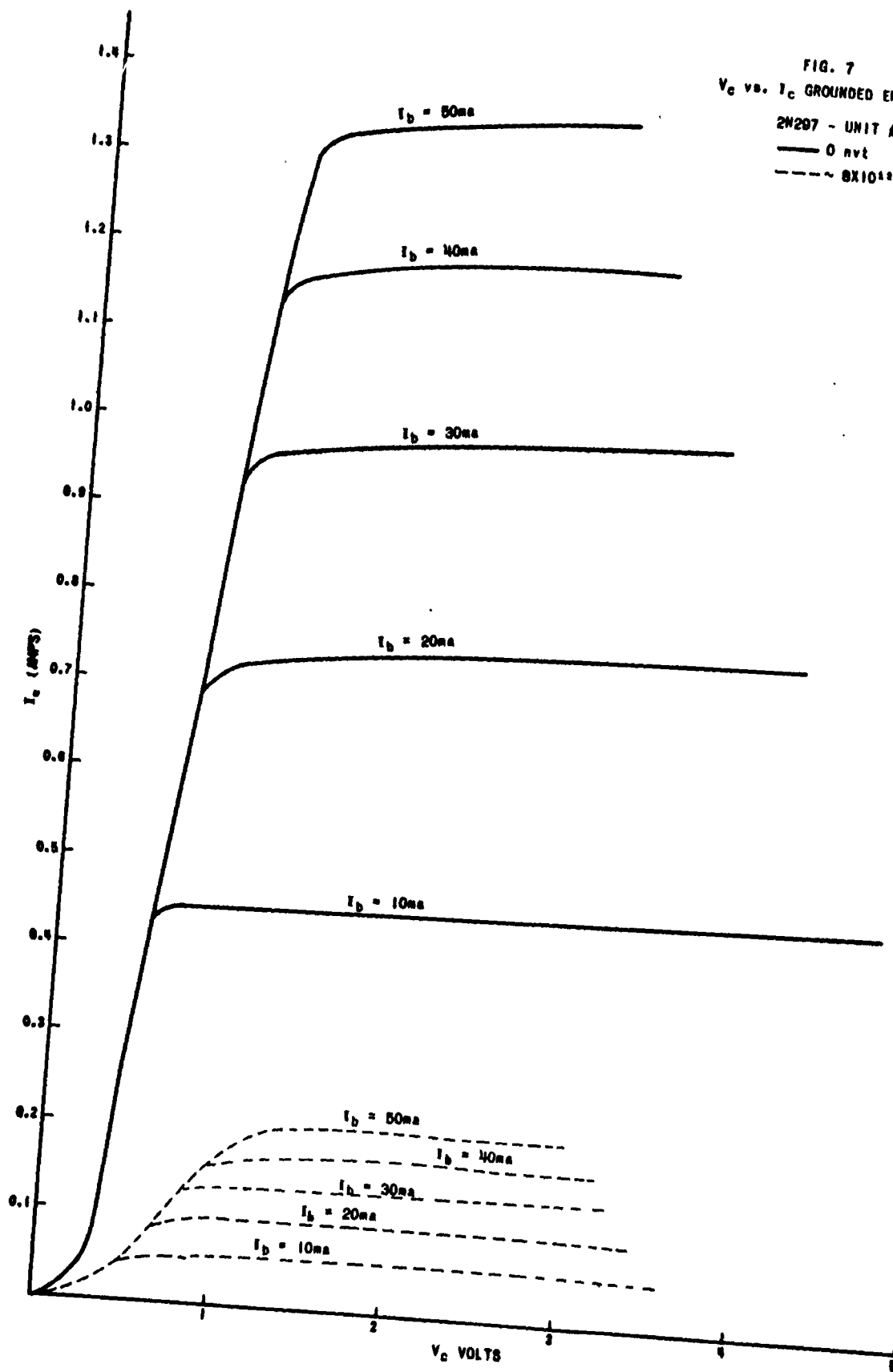


FIG. 6

FIG. 7
 V_C vs. I_C GROUNDED EMITTER
 2N207 - UNIT #35
 — 0 nvt
 --- $\sim 8 \times 10^{12}$ nvt



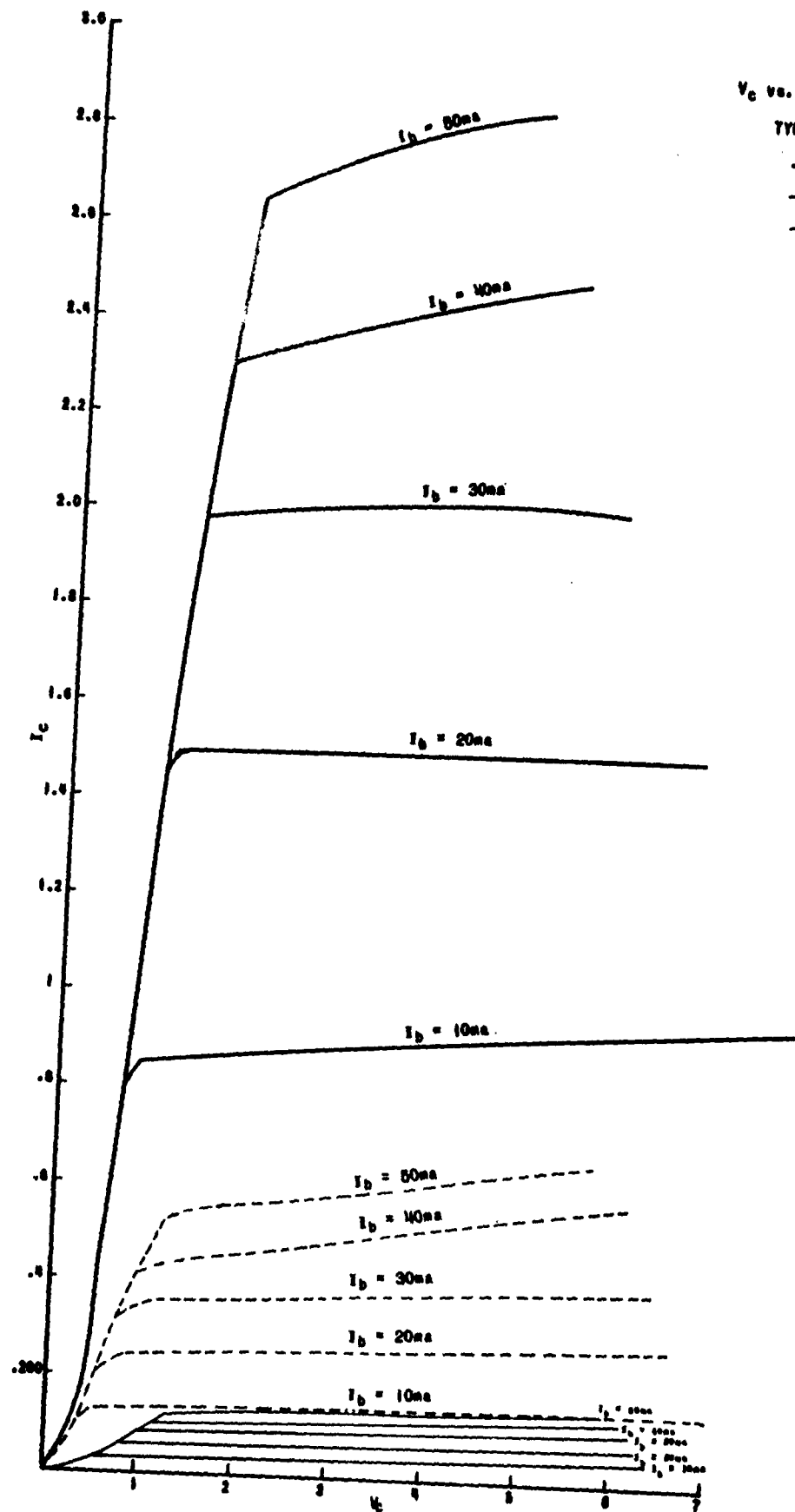


FIG. 8
 V_c vs. I_c GROUNDING EMITTER
 TYPE 2N2308 - UNIT #1

FIG. 9
 I_{cr} vs. V_c
 TYPE 2N257

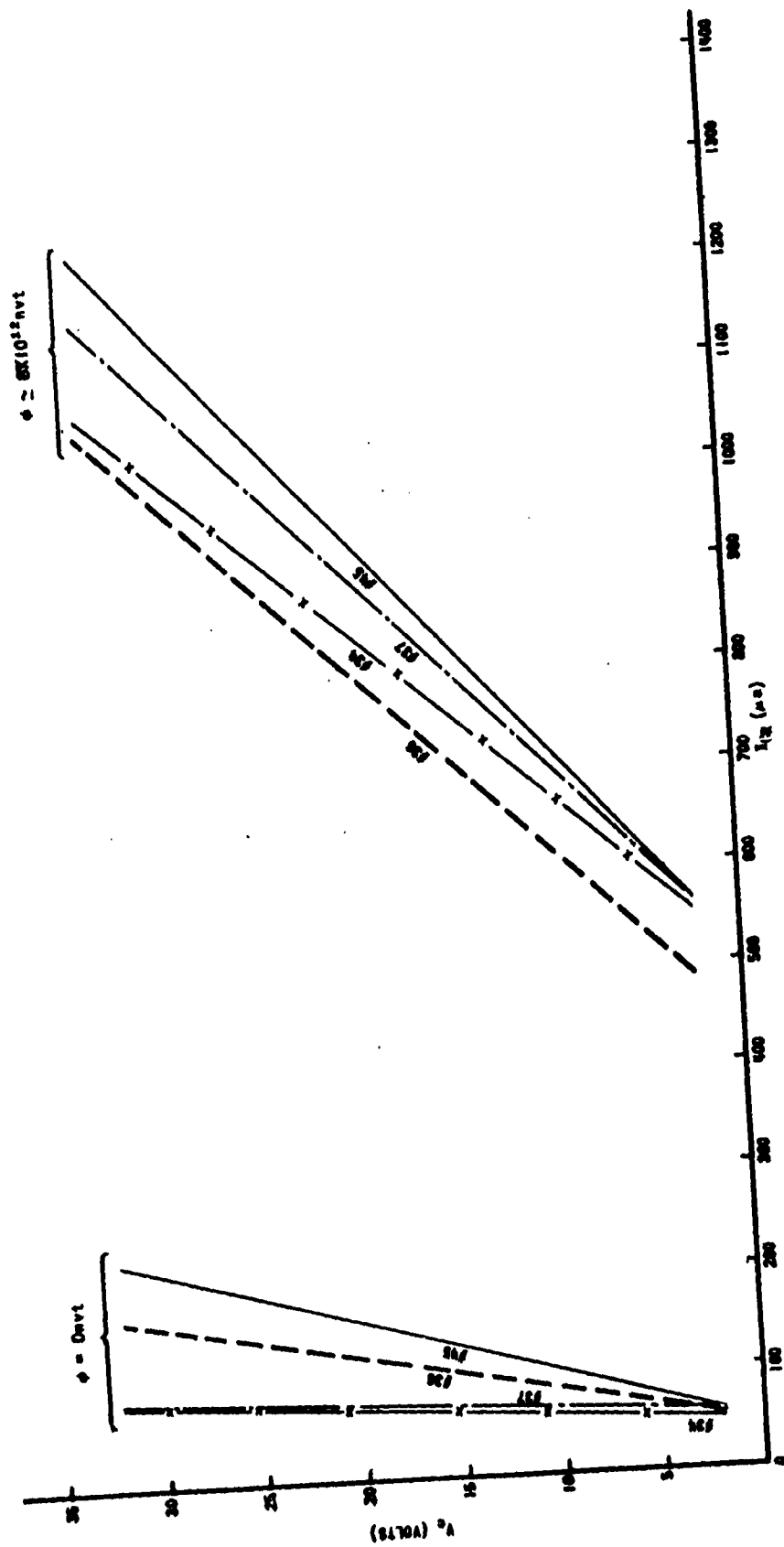
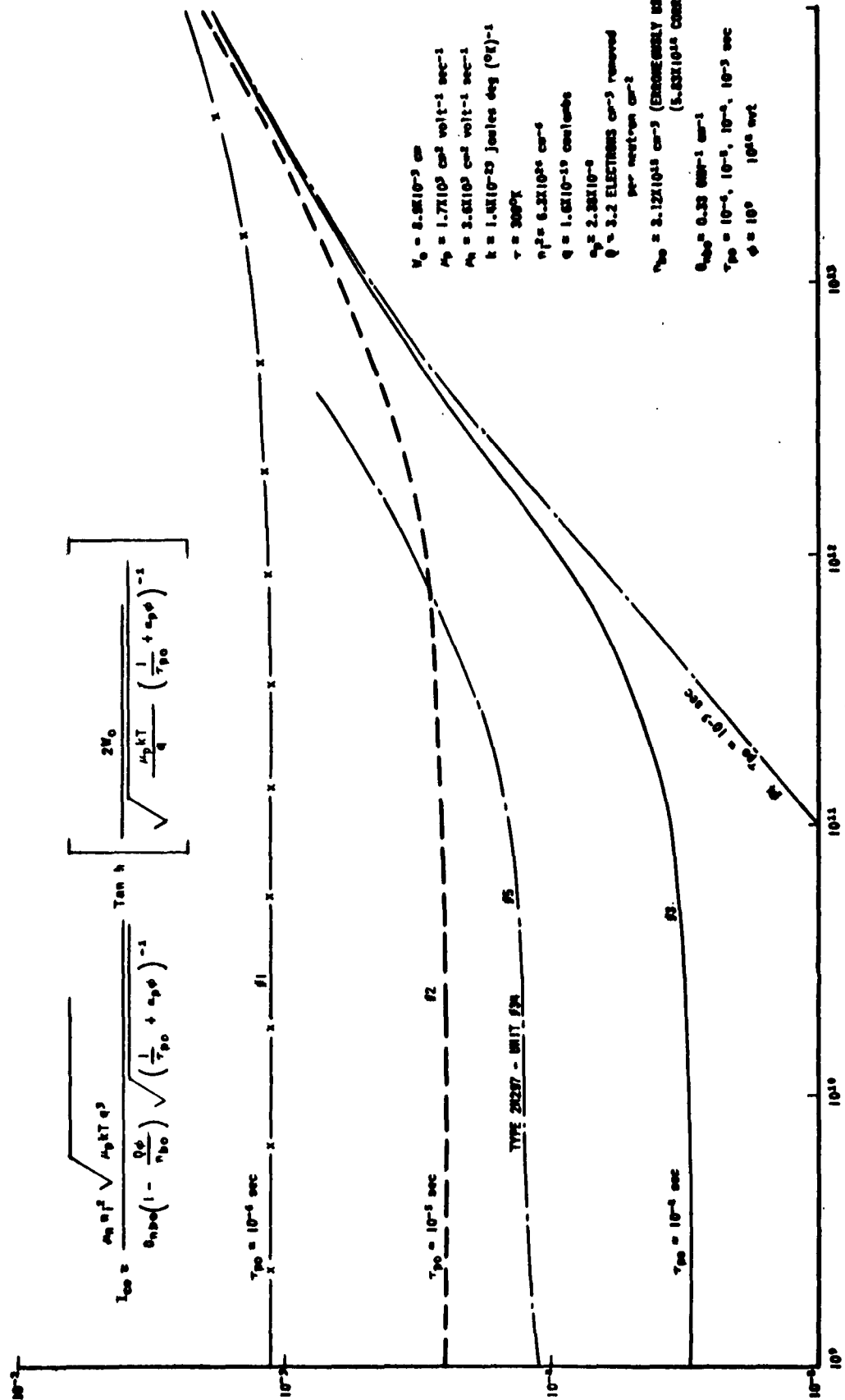


FIG. 10
 I_{co} vs. ϕ



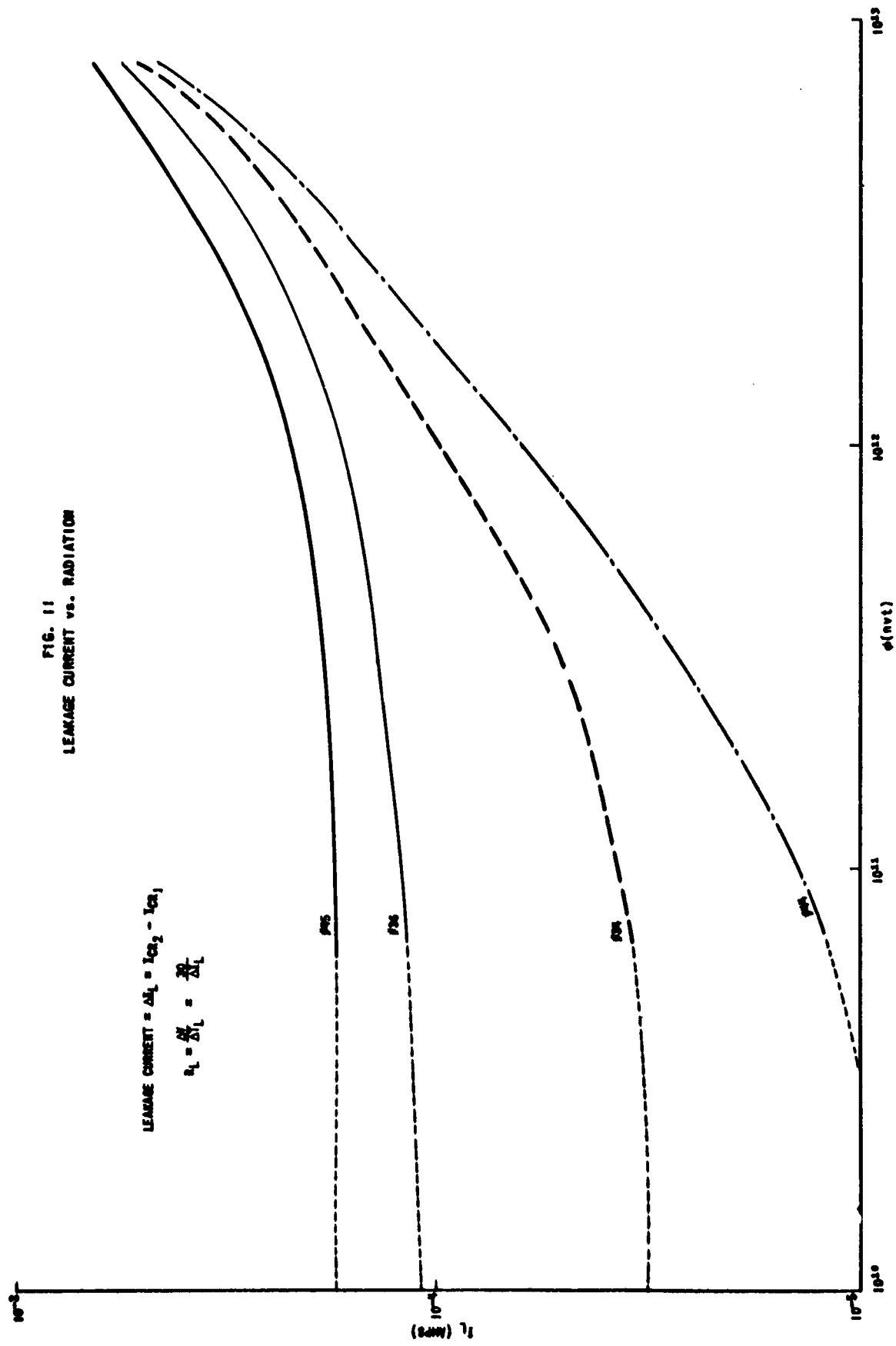
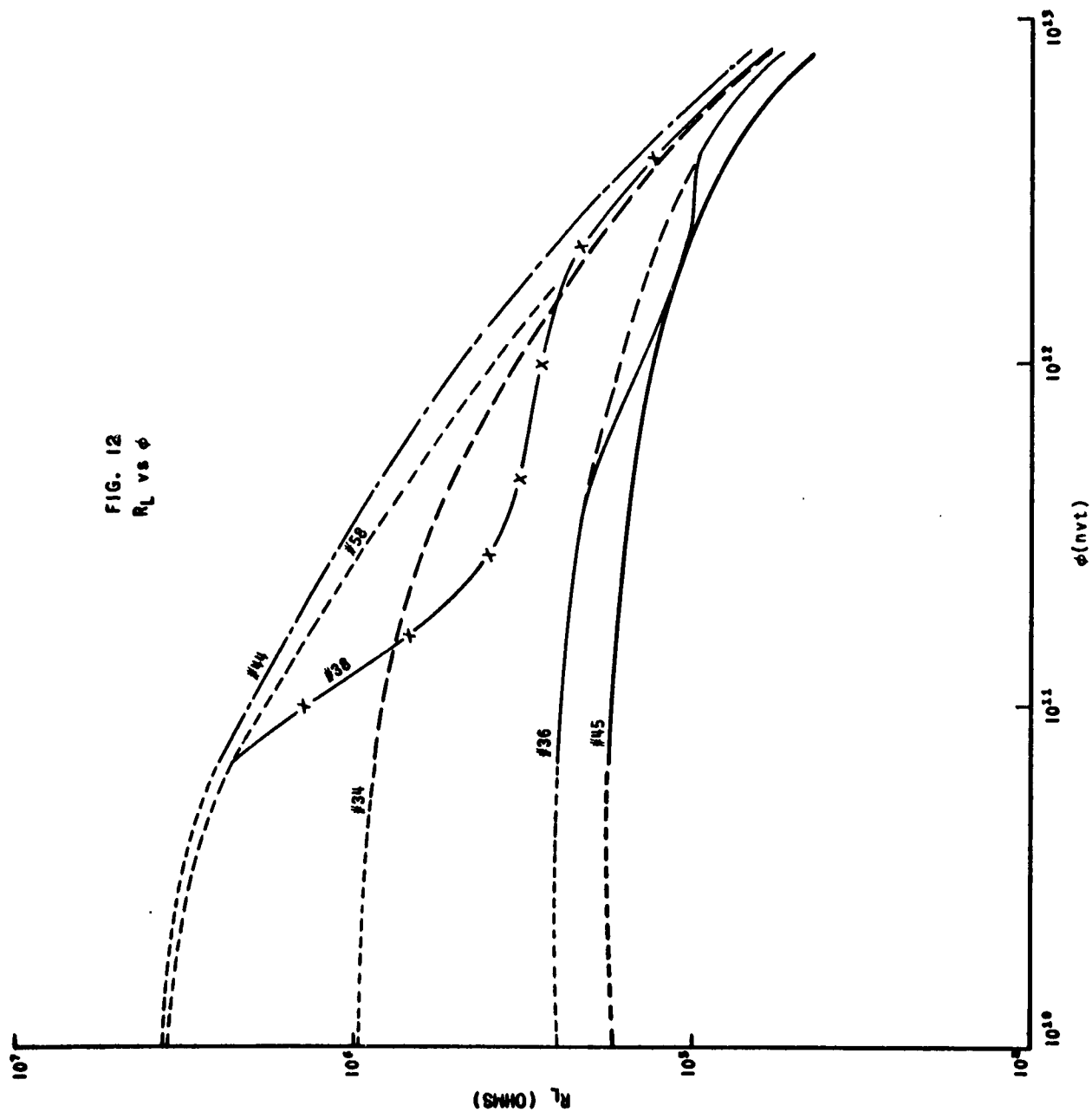


FIG. 11
LEAKAGE CURRENT vs. RADIATION



THE PERFORMANCE OF SOME ZENER REFERENCE ELEMENTS DURING EXPOSURE TO NUCLEAR RADIATION

by

M. A. Xavier

Cook Research Laboratories Division
Cook Electric Company
Morton Grove, Illinois

Sixteen type 1N429 and sixteen type 1N430B Zener Reference elements were exposed to the radiation field of a nuclear reactor. This paper describes the measurement techniques and the corrections made to insure accurate results required in dealing with the voltage reference elements. Irradiations were performed at epicaadmium neutron flux levels of the order of 10^{11} nv_e until doses of up to $10^{15} \text{ nv}_e \text{ t}$ were reached. The corresponding gamma dose rate was 2.1×10^6 roentgens per hour.

Detailed results are presented in the paper and possible mechanisms of damage are described. The reference voltages of all the devices tested showed permanent decreases of up to 2.9 per cent although the average of the changes were in the order of 1-1/4 per cent. The temporary damage was generally about 1/3 per cent. The case temperature was monitored for one sample in each of the four irradiations.

During the past two years, there has been considerable activity in determining the effects of nuclear radiation on semiconductor electronic components. The emphasis has, however, been placed on transistors and little information is available on other devices. This paper deals with the behavior of two types of Zener reference elements, which have found wide application as reference voltage sources because of their relative stability with temperature, small physical size, and mechanical ruggedness. At the time of the experiments, two types (1N429 and 1N430B by Hoffman Semiconductor) were generally considered as the best commercially available, so the irradiations were performed on these types.

EXPERIMENTAL PROCEDURE

1. Irradiation Technique

Sixteen samples of each type were irradiated at the Bulk Shielding Reactor facility of the Pennsylvania State University, using the technique described previously¹ and depicted in Figure 1. The watertight aluminum tube, 3 inches in diameter, is supported vertically by a weighted tripod. A stop in the tube permits centering of the test samples with the center-line of the reactor core assembly. The distance between the core and the tube is variable allowing considerable flexibility in neutron flux levels and spectrum if desired. The semiconductor devices are mounted on polyethylene boards, and the leads are brought out through the top of the tube to the electrical instrumentation. The lead wire used was 300 ohm polyethylene insulated twin-lead. The leakage current of the twin lead was considerably below the currents encountered in these tests.

2. Instrumentation

All voltages were measured semiautomatically with the simple tester shown in Figure 2. The meter used was an Electro-Instrument Type 1050P, which has an accuracy of ± 1 digit in the last digit of a four digit reading. The diode voltage is recorded on a Clary printer actuated by the voltmeter. The voltage across the diode includes the voltage drop across the resistance of the cable between the samples being irradiated and the power supply and instrumentation, and the Zener voltage is determined by subtracting the line voltage drop from the total voltage. The lead resistances were measured to three significant figures using an impedance bridge and the required corrections were made.

The ambient temperature and the case temperatures of several units were recorded using a set of iron-constantin thermocouples and an Illinois Testing Laboratories' temperature meter calibrated for 40 foot long thermocouple leads.

The neutron dosimetry was provided by the staff at Pennsylvania State University.

TEST RESULTS

1. 1N429 Reference Element

The 1N429 Reference Element has a maximum change in reference voltage of ± 0.05 volt from its value at 7.5 ma (5.9 to 6.5 volts) and 25°C over a temperature range of -55°C to +100°C. The devices were irradiated in two sets of eight units. The results of the tests are

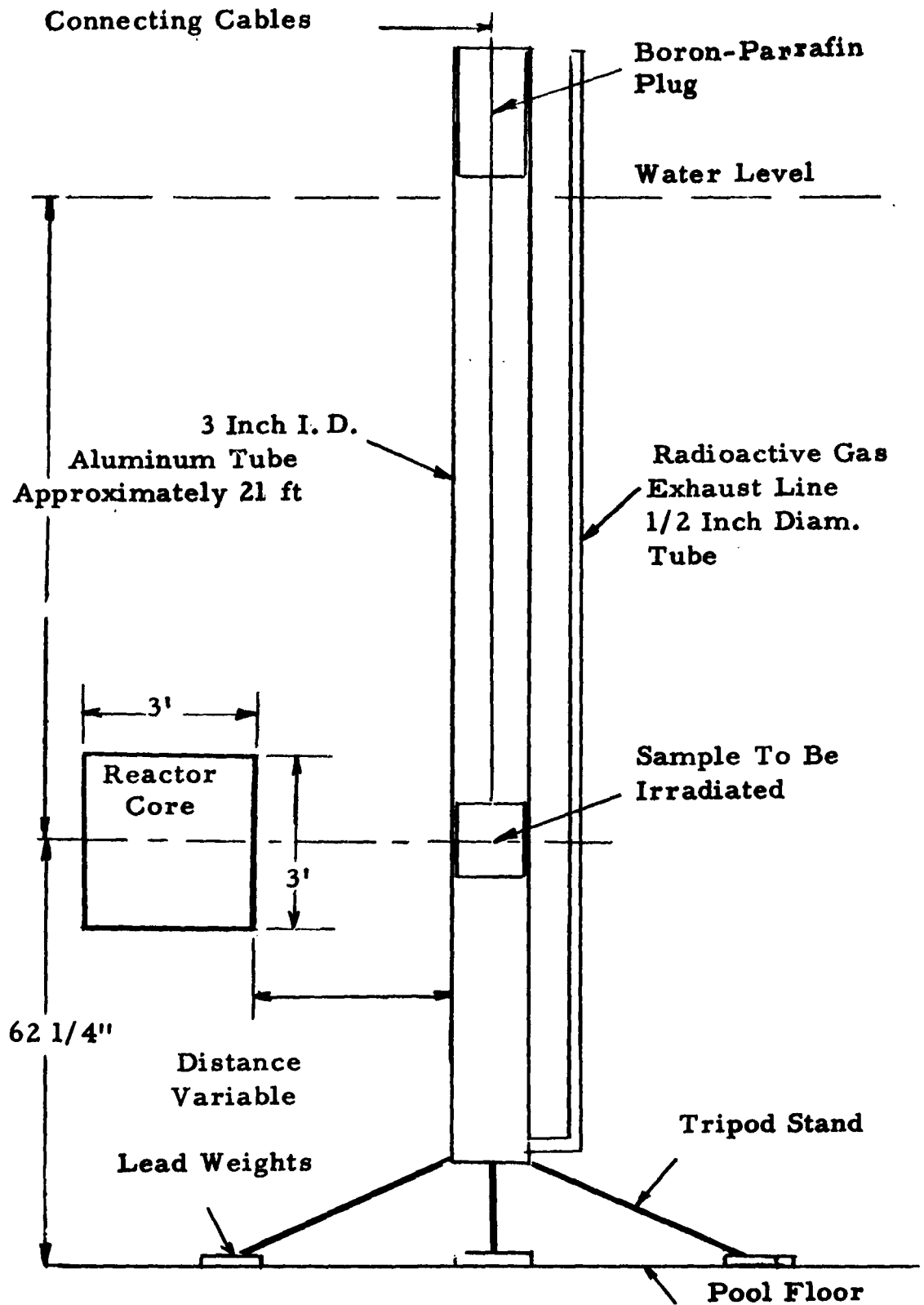
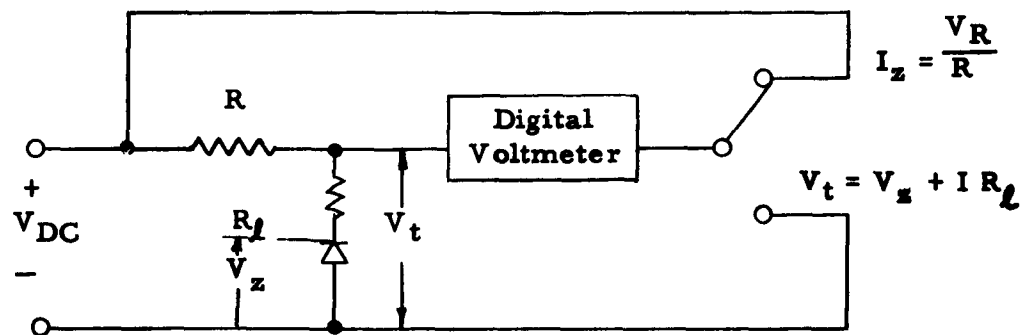


Figure 1. Method of Reactor Irradiation



Basic Current Zener Diode Tester

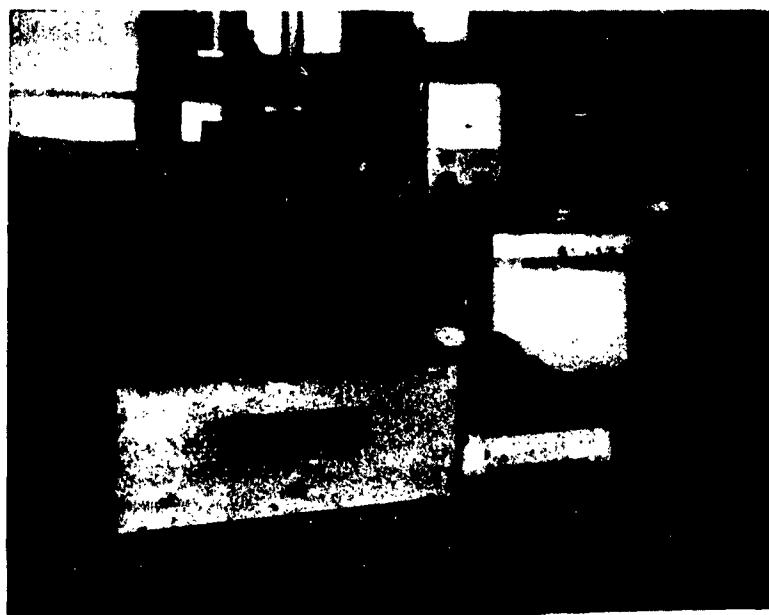


Figure 2. The Semiautomatic Zener Reference Element Test Set

typified by the curves of Figures 3 and 4, which show one unit of each irradiation. It is seen that the trends are the same in both units. The reference voltages decrease with increasing epicadmium neutron doses. The reference element voltage decreases consistently with increasing neutron dose as shown in both Figures 3 and 4. In Figure 4, it is seen that the reference voltage recovers partially upon removal of the devices from the radiation field.

A summary of the behavior of the 16 Type 1N429 devices during irradiation is given in Tables 1 and 2. The reference voltages at approximately the rated Zener current of 7.5 ma are given as a function of integrated epicadmium neutron flux in order to provide a quick quantitative view of voltage changes during irradiation. It is to be noted that the voltage variations shortly after insertion into the radiation field are often larger than the variations observed during the remainder of irradiation.

For the 16 units irradiated, after a dose of approximately $0.4 \times 10^{15} \text{ nv}_e \text{ t}$ was reached, the reference voltages had decreased by 0.32 to 1.16 per cent with a mean value $\frac{\sum_{16} \Delta V}{16}$ of 0.90 per cent

change. Fourteen of the 16 units showed changes of 0.76 or greater. After $10^{15} \text{ nv}_e \text{ t}$, the changes were from 0.34 to 1.79 per cent with a mean value of 1.11 per cent. At this dose, 14 of the 16 units had suffered reference voltage decreases of 0.84 per cent or more. Thirteen units showed better than 0.94 per cent variation. Temperature changes due to gamma-ray absorption in the case material were found to be between 3°C and 6°C .

2. Hoffman Type 1N430B Reference Element

This type of reference element is rated by its manufacturer to have a change in voltage drop (from its value at a current of 10 ma and at 25°C) of less than ± 0.001 per cent per degree Centigrade over a temperature range of -55°C to $+150^\circ\text{C}$.

The results of the two irradiations are summarized in Tables 3 and 4. Figures 5 and 6 show the complete characteristics of two typical units during the irradiation. The reference voltages suffer a relatively large incremental decrease before low doses are reached ($\sim 10^{13} \text{ nv}_e \text{ t}$), followed by gradual drops of the reference voltage as the doses are increased to greater than $t \times 10^{14} \text{ nv}_e \text{ t}$. At approximately $10^{14} \text{ nv}_e \text{ t}$, the reference voltages of the 16 units changed from 0.14 to 2.33 per cent with a mean change of 1.23 per cent. At $5 \times 10^{14} \text{ nv}_e \text{ t}$, the decreases in

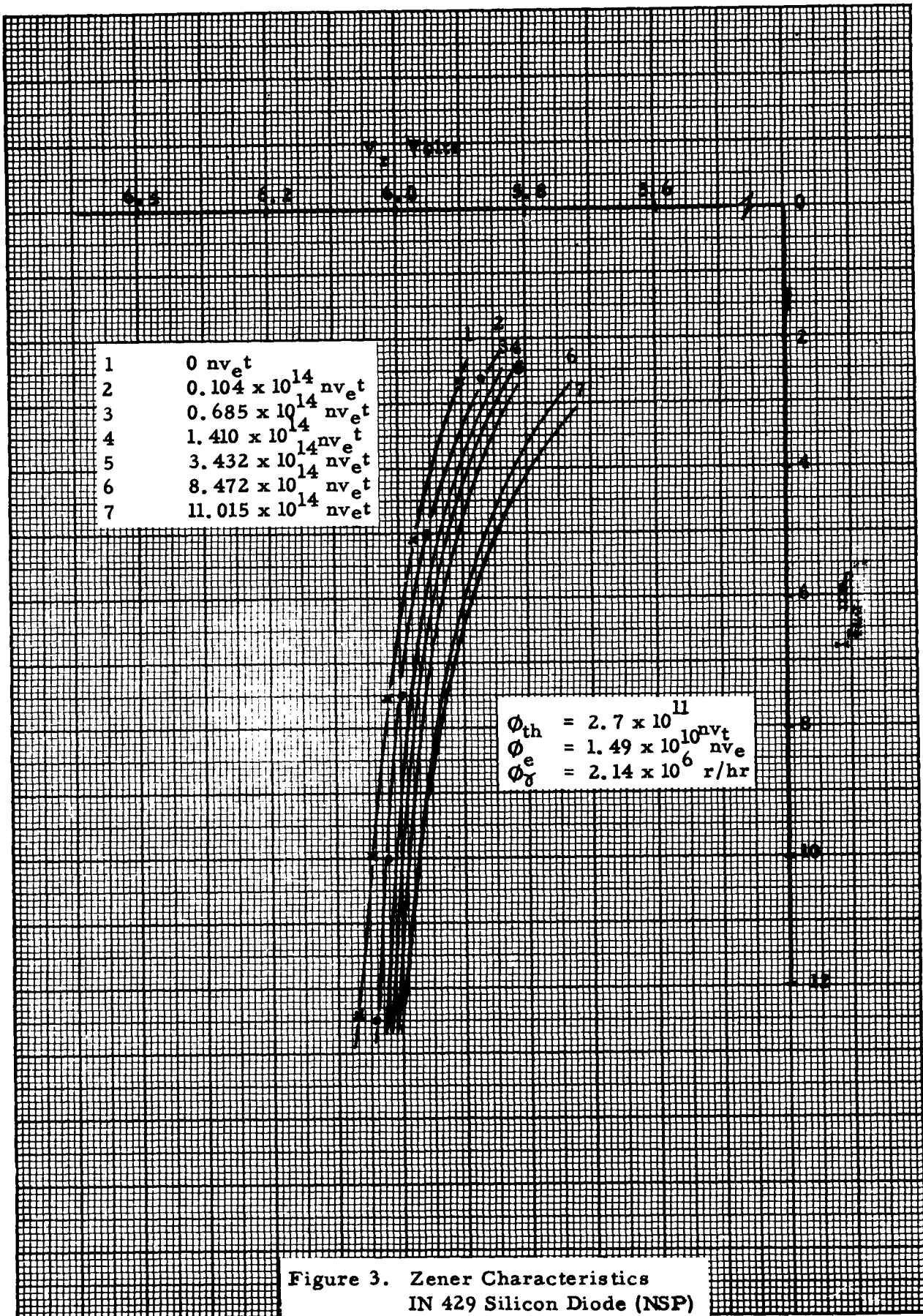


Figure 3. Zener Characteristics
IN 429 Silicon Diode (NSP)
Reactor Irradiation PD 481

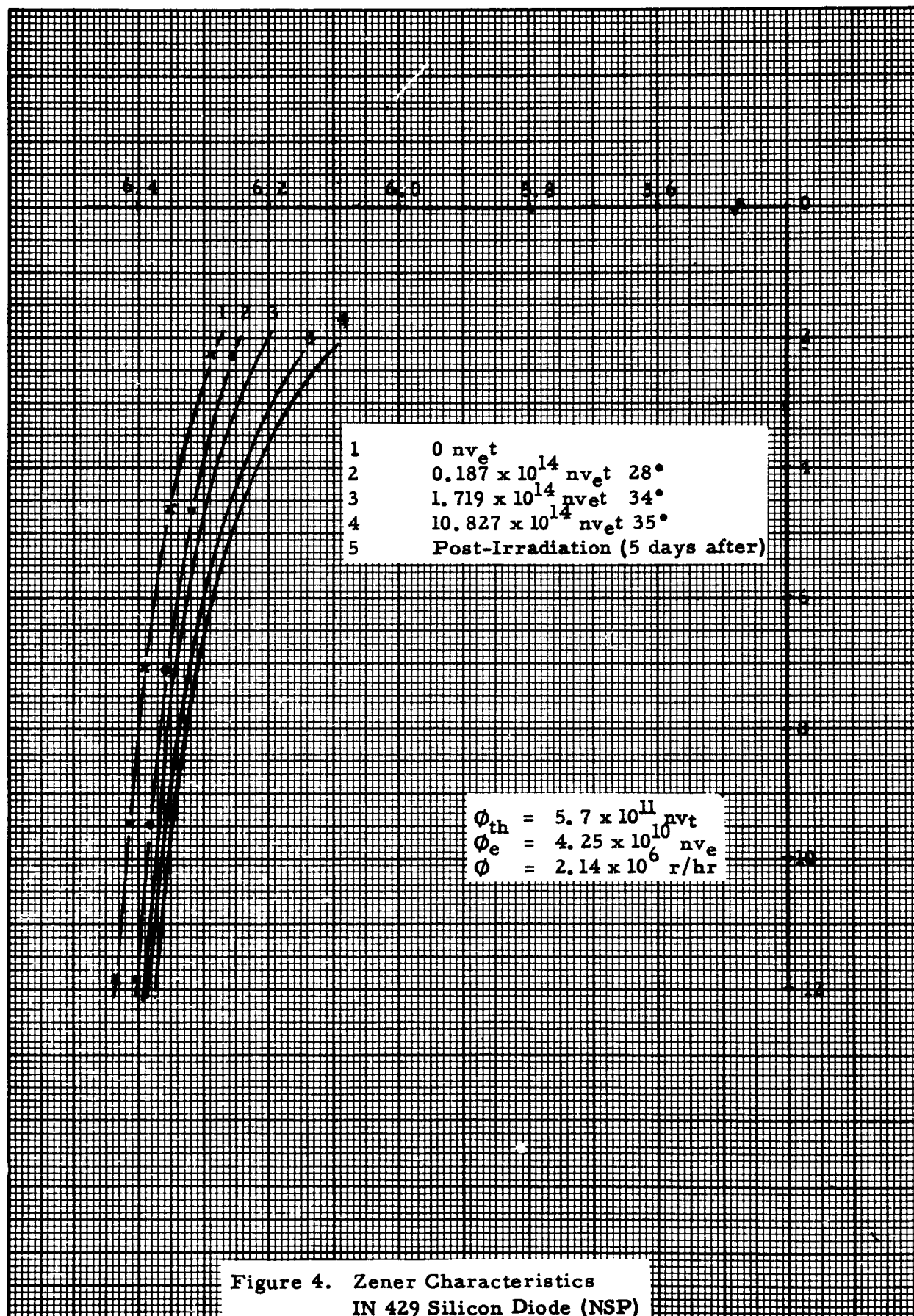


Figure 4. Zener Characteristics
IN 429 Silicon Diode (NSP)
Reactor Irradiation PD 488

TABLE I

VARIATION OF IN429 REFERENCE VOLTAGE WITH RADIATION

Unit Case Temperature No.	$\phi_e \times 10^{15}$ nvt	0.05 28°C		0.4 31°C		0.8		1.0		Maximum Change Post During Irradiation (%)
		0	0.2	3	0.6	0.8	1.0	1.0	1.0	
1	V _Z	6.172	6.144	6.132	6.125	6.123	6.119	6.120		-0.85
	I _Z	7.44	7.44	7.42	7.42	7.42	7.39	7.39		
2	V _Z	6.092	6.063	6.044	6.022	6.012	5.996	5.983		-1.78
	I _Z	7.46	7.47	7.45	7.45	7.45	7.43	7.440		
3	V _Z	6.461	6.426	6.421	6.423	6.426	6.436	6.435		-0.40
	I _Z	7.31	7.32	7.30	7.29	7.28	7.26	7.25		
4	V _Z	6.014	5.981	5.964	5.950	5.943	5.931	5.920		-1.56
	I _Z	7.49	7.50	7.48	7.48	7.47	7.46	7.46		
5	V _Z	6.275	6.234	6.224	6.214	6.209	6.203	6.198		-1.28
	I _Z	7.39	7.38	7.37	7.37	7.36	7.36	7.35		
6	V _Z	6.226	6.196	6.183	6.174	6.170	6.164	6.168		-0.93
	I _Z	7.41	7.41	7.38	7.38	7.37	7.36	7.36		
7	V _Z	6.091	6.054	6.038	6.025	6.019	6.010	6.005		-1.41
	I _Z	7.46	7.46	7.44	7.44	7.44	7.43	7.42		
8	V _Z	6.257	6.222	6.207	6.198	6.198	6.191	6.190		-1.07
	I _Z	7.40	7.40	7.37	7.37	7.36	7.34	7.35		

Radiation Conditions: $\phi_{th} = 2.7 \times 10^{11}$ nvt $\phi_e = 1.5 \times 10^{10}$ nve $\phi_x = 2.1 \times 10^6$ r/hr

TABLE 2

VARIATION OF IN429 REFERENCE VOLTAGE WITH RADIATION

Unit No.	Case	Temperature $\phi_e \times 10^{15} \text{ nvt}$	28°C		32°C		34°C		34°C		Maximum Change During Irradiation (%)
			0	0.05	0.2	0.4	0.5	1.0	Post		
9	V _z	Volts	6.305	6.269	6.257	6.250	6.247	6.237	6.249	-1.08	
	I _z	ma	7.15	7.16	7.17	7.16	7.16	7.18	7.23		
11	V _z	Volts	6.444	6.402	6.383	6.369	6.382	6.330	6.352	-1.78	
	I _z	ma	7.09	7.11	7.11	7.11	7.11	7.12	7.18		
12	V _z	Volts	6.378	6.341	6.330	6.324	6.320	6.306	6.316	-1.19	
	I _z	ma	7.12	7.13	7.13	7.13	7.12	7.15	7.20		
13	V _z	Volts	6.293	6.250	6.236	6.226	6.222	6.198	6.215	-1.51	
	I _z	ma	7.15	7.16	7.17	7.16	7.16	7.19	7.24		
14	V _z	Volts	6.269	6.232	6.224	6.220	6.221	6.208	6.221	-0.97	
	I _z	ma	7.16	7.17	7.17	7.16	7.16	7.16	7.23		
15	V _z	Volts	6.082	6.044	6.037	6.036	6.036	6.025	6.039	-0.93	
	I _z	ma	7.23	7.24	7.24	7.23	7.23	7.26	7.30		
16	V _z	Volts	6.235	6.218	6.215	6.215	6.213	6.211	6.222	-0.34	
	I _z	ma	7.17	7.170	7.17	7.16	7.16	7.18	7.23		
17	V _z	Volts	6.303	6.265	6.252	6.242	6.237	6.212	6.227	-1.44	
	I _z	ma	7.15	7.15	7.15	7.15	7.15	7.16	7.23		

Radiation Conditions: $\phi_{th} = 5.7 \times 10^{11} \text{ nvt}$ $\phi_e = 4.3 \times 10^{10} \text{ nve}$ $\phi_r = 2.1 \times 10^6 \text{ r/hr}$

TABLE 3

VARIATION OF IN430B REFERENCE VOLTAGE WITH RADIATION

Unit No.	Case	Temperature $\phi_e \times 10^{15} \text{nv} \cdot \text{t}$	28°C	34°C	45°C	52°C	52°C	52°C	Post 15 hrs	Maximum Change During Irradiation (%)
1	V_z I_z	Volts ma	8.350 8.88	8.270 8.93	8.236 8.96	8.215 8.98	8.210 8.92	8.210 8.96	8.223 8.44	-1.68
2	V_z I_z	Volts ma	8.323 8.89	8.239 8.93	8.206 8.97	8.196 8.98	8.189 8.93	8.190 8.95	8.201 8.44	-1.66
3	V_z I_z	Volts ma	8.315 8.93	8.148 8.97	8.116 9.00	8.087 9.02	8.074 8.98	8.074 9.00	8.076 8.49	-2.9
4	V_z I_z	Volts ma	8.353 8.88	8.317 8.90	8.294 8.92	8.275 8.94	8.268 8.90	8.268 8.92	8.273 8.41	-1.01
5	V_z I_z	Volts ma	8.418 8.86	8.328 8.90	8.301 8.92	8.285 8.94	8.280 8.89	8.282 8.91	8.297 8.40	-1.64
6	V_z I_z	Volts ma	8.395 8.92	8.309 8.91	8.283 8.93	8.265 8.94	8.256 8.90	8.255 8.92	8.268 8.41	-1.67
7	V_z I_z	Volts ma	8.492 8.88	8.421 8.86	8.397 8.88	8.376 8.89	8.366 8.86	8.360 8.88	8.371 8.37	-1.55
8	V_z I_z	Volts ma	8.302 8.95	8.249 8.92	8.225 8.94	8.209 8.96	8.194 8.93	8.196 8.94	8.201 8.44	-1.28

Radiation Conditions: $\phi_{th} = 5.7 \times 10^{11} \text{nv} \cdot \text{t}$ $\phi_e = 4.25 \times 10^{10} \text{nv} \cdot \text{e}$ $\phi_r = 2.14 \times 10^6 \text{r/hr}$

TABLE 4

VARIATION OF IN430B REFERENCE VOLTAGE WITH RADIATION

Unit No.	Case Temperature $\phi_e \times 10^{15} \text{nv} \cdot \text{et}$	28°C	36°C	43°C	48°C	50°C	50°C	Post 39 hrs	Maximum Change During Irradiation (%)	
9	Volts	8.281	8.211	8.195	8.176	8.171	8.161	8.19	-1.45	
	I_z ma	8.57	8.60	8.60	8.64	8.65	8.67	8.78		
10	Volts	8.358	8.181	8.163	8.141	8.131	8.124	8.145	-2.8	
	I_z ma	8.53	8.60	8.61	8.64	8.66	8.68	8.80		
11	Volts	8.278	8.281	8.266	8.247	8.241	8.236	8.256	-0.51	
	I_z ma	8.56	8.56	8.57	8.60	8.61	8.64	8.76		
12	Volts	8.405	8.359	8.345	8.331	8.331	8.327	8.352	-0.91	
	I_z ma	8.50	8.53	8.54	8.56	8.58	8.60	8.72		
13	Volts	8.271	8.185	8.171	8.157	8.150	8.150	8.182	-1.46	
	I_z ma	8.56	8.60	8.60	8.63	8.65	8.66	8.80		
14	Volts	8.407	8.309	8.295	8.280	8.270	8.270	8.296	-1.63	
	I_z ma	8.50	8.54	8.56	8.58	8.60	8.60	8.75		
15	Volts	8.386	8.310	8.296	8.281	8.271	8.271	8.291	-1.39	
	I_z ma	8.51	8.54	8.56	8.57	8.59	8.61	8.76		
16	Volts	8.361	8.265	8.251	8.234	8.231	8.225	8.250	-1.62	
	I_z ma	8.52	8.56	8.57	8.60	8.61	8.63	8.77		
Radiation Conditions:										
		$\phi_{th} = 5.7 \times 10^{11} \text{nv} \cdot \text{et}$	$\phi_e = 4.2 \times 10^{10} \text{nv} \cdot \text{e}$	$\phi_g = 2.1 \times 10^6 \text{r/hr}$						

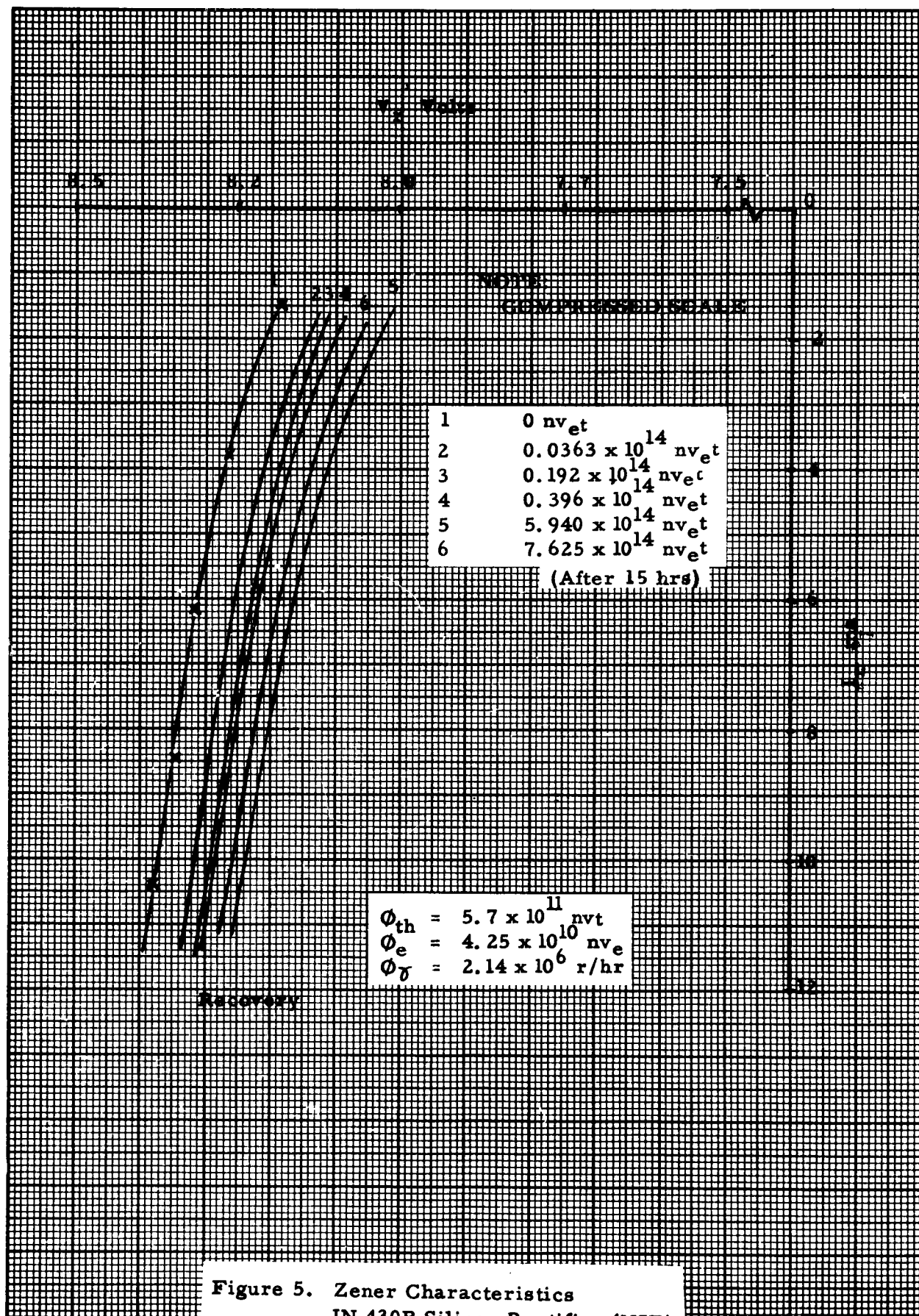


Figure 5. Zener Characteristics
IN 430B Silicon Rectifier (NSP)
Reactor Irradiation PD 502

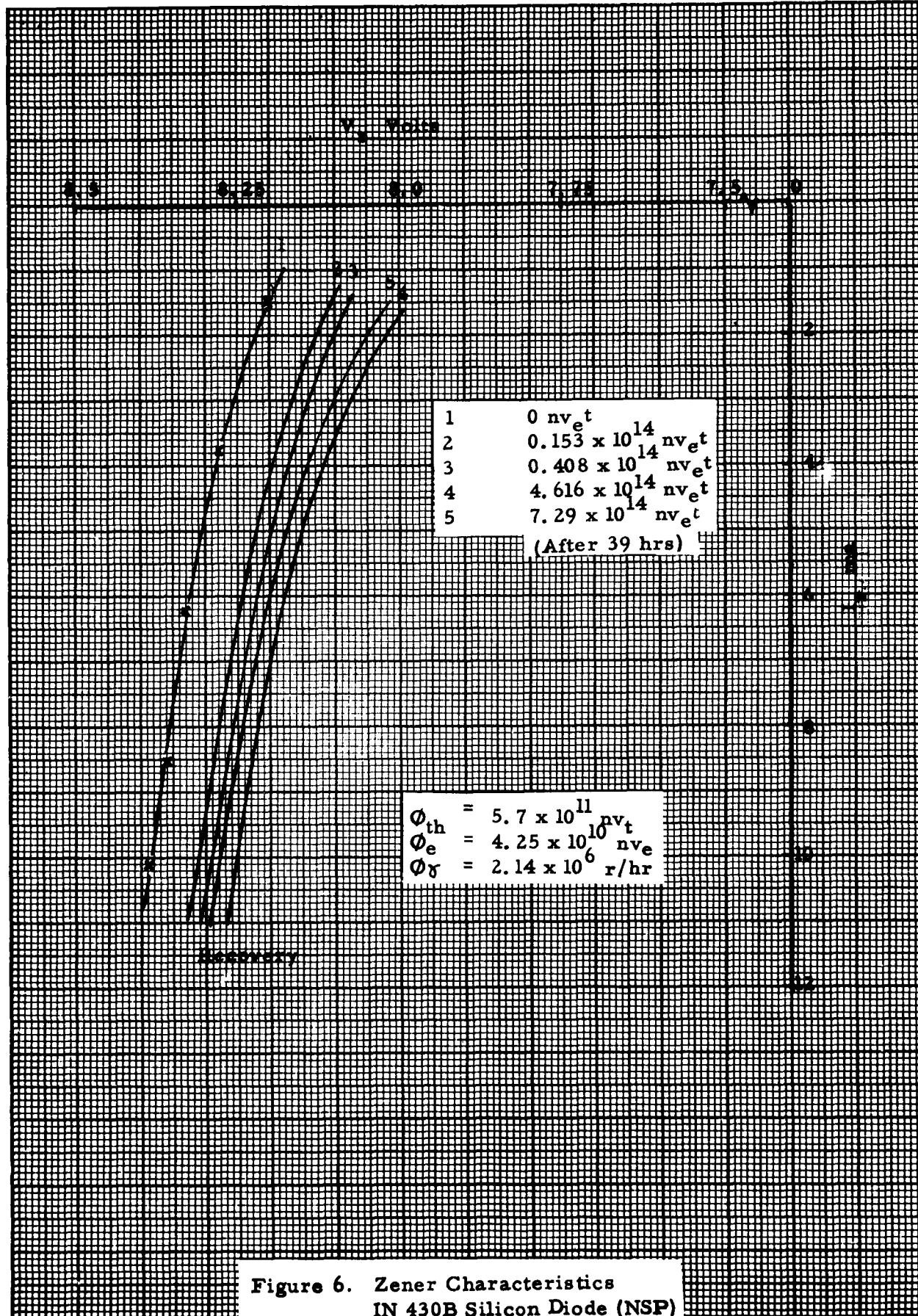


Figure 6. Zener Characteristics
 IN 430B Silicon Diode (NSP)
 Reactor Irradiation PD 515

reference voltage ranged from 0.51 to 2.90 per cent with a mean change of 1.57 per cent. The case temperature of the reference elements have risen from the preirradiation value of 28°C to approximately 45°C at 10^{14} nvt (gamma dose rate $2 \times 10^6 \text{ r/hr}$) and 50°C after a neutron dose of $5 \times 10^{14} \text{ nvt}$ was reached.

DISCUSSION OF TEST RESULTS

1. General Diode Behavior

The changes observed in reference element voltages are small, but the behavior can be semiquantitatively explained by examination of semiconductor material and device behavior during irradiation.

The two types of Zener reference elements studied consist of forward-biased p-n junction diode elements in series with the junctions reverse-biased into the avalanche breakdown region. The forward-biased elements provide temperature compensation for the reference elements. In order to explain the behavior of the types 1N429 devices during exposure to nuclear radiation, it is necessary to examine the behavior of forward-biased silicon diode elements during irradiation, as well as the behavior of the avalanche voltage of reverse-biased elements.

A voltage applied across a silicon p-n junction diode in the forward-direction is divided into three parts:

$$V = V_P + V_J + V_N \quad (1)$$

where V_P and V_N are the voltages across the P and N regions, respectively, and V_J is the voltage across the junction. V_P (or V_N) can be written as:

$$V_P = I(R_P C_M) \quad (2)$$

where:

I = the current through the diode

R_P = the equilibrium resistance of the P region

C_M = conductivity modulation factor which includes the effect of minority carrier lifetime (injection), the width of the region and the level of carrier injection.

Conductivity modulation is effective when the density of minority carriers injected into the body of semiconductor becomes of the order of magnitude of the equilibrium majority carrier density.

The voltage across the junction V_J can be written as ³:

$$V_J = \frac{2KT}{q} \ln \left(\frac{J}{J_d} \right) \quad (3)$$

where:

K = Planck's Constant

T = Junction Temperature in degrees Kelvin

q = Electronic charge in coulombs

J = Junction current density = amps/cm²

$$J_d = \frac{qn_i s}{\tau}$$

s = Width of junction (intrinsic region)

τ = Mean hole-electron lifetime in the intrinsic region

n_i = Density of hole or electrons in intrinsic region

The avalanche breakdown voltage of the reverse-biased diodes used in the reference elements can be calculated from the empirical relationship⁴

$$V_z = 75 \rho_n^{0.71} \quad (4)$$

where:

ρ_n = the N-region resistivity

2. Variation of Semiconductor Properties with Radiation

It is known that the carrier densities and minority carrier lifetimes are affected by nuclear radiation. ^{5, 6, 7, 8} It has been shown that the rate of majority carrier removal in p and n type silicon is of the order of 2 per incident epicaldium neutron. The maximum neutron doses reached were of the order of 10^{15} epicaldium neutrons per square centimeter,

so that approximately 2×10^{15} carriers/cm³ are removed. The avalanche breakdown voltages of the diodes used were in the range of 5 to 6 volts, indicating an electron density of 2×10^{17} carriers/cm³ in the n-region. The change in the resistivity of the region and therefore of the breakdown voltage is an increase of approximately 1 per cent.

The minority carrier lifetime in silicon is drastically affected by radiation⁸

$$\frac{1}{\tau} = \frac{1}{\tau_0} + K_{\theta} \Sigma \theta_e \quad (5)$$

where:

τ = the minority carrier lifetime after exposure to a dose θ_e

τ_0 = the preirradiation minority carrier lifetime

K_{θ} = damage constant

$\Sigma \theta_e$ = integrated epicaldmium neutron flux

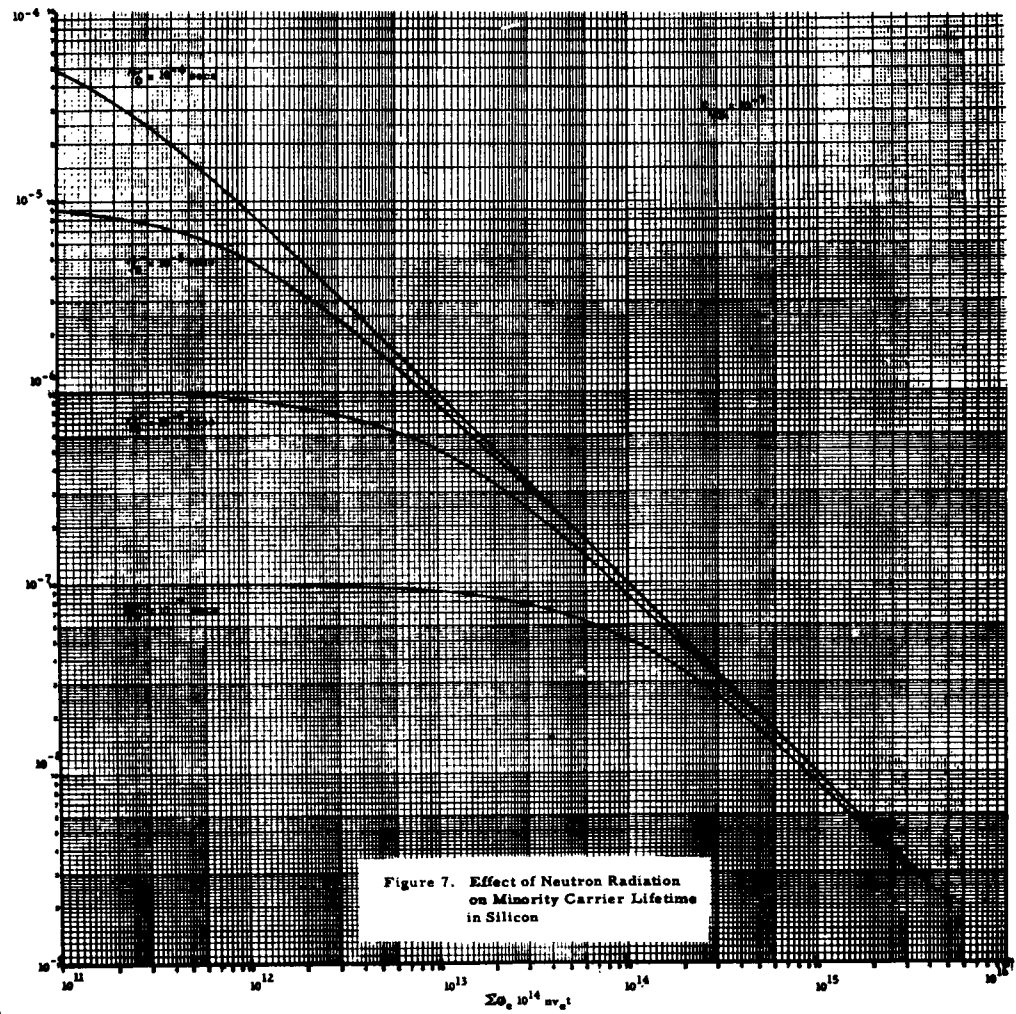
A simple plot of the changes in τ with neutron dose is shown in Figure 7. The relationship (5) is not rigorously followed but the trend is relatively well established.

The damage constant K_{θ} for silicon has been found to be approximately 3×10^{-7} (sec⁻¹ neutrons⁻¹ cm²) by Messenger and Spratt⁹. A calculation from previous work on transistors by the author¹⁰ has yielded a damage constant of 10^{-7} (sec⁻¹ neutron⁻¹ cm²). This is relatively good agreement in view of comments by Messenger and Spratt on the possible effects of material resistivity and the possible difference in the neutron spectra used by different investigators. The lifetime of minority carriers in the completed devices is not known accurately, so that the difference in these damage constants is not alarming since only semiquantitative analyses of radiation damage to diodes are possible.

The avalanche breakdown characteristic as defined by Equation (4)

$$V_z = 75 \rho_n^{0.71}$$

shows that the avalanche voltage will tend to increase with radiation, since ρ_n will increase as the majority carriers are removed with increasing neutron doses.



In the forward characteristics, the junction voltage will tend to decrease with radiation.

For a given device current density J , the junction voltages can be written:

$$J = J_{D1} \exp \left[\frac{q V_{J1}}{2KT} \right] = J_{D2} \exp \left[\frac{q V_{J2}}{2KT} \right]$$

or

$$\exp \frac{q}{2KT} \left[V_{J1} - V_{J2} \right] = \frac{J_{D2}}{J_{D1}}$$

$$V_{J1} - V_{J2} = \frac{2KT}{q} \ln \frac{J_{D2}}{J_{D1}}$$

The change in junction voltage is then

$$\Delta V_J = \frac{2KT}{q} \ln \frac{\tau_1}{\tau_2} \quad (6)$$

Since τ_2 is less than τ_1 , ΔV_J is greater than zero; that is the junction voltage decreases with increasing radiation doses. Semiquantitative analyses of the changes in properties of the 1N429 and 1N430B reference elements can now be discussed.

DISCUSSION OF TYPE 1N429 REFERENCE ELEMENT BEHAVIOR

This type of reference element is made up of one P region formed on each side of an N-type wafer in a P-N-P arrangement. One junction is therefore forward-biased and the other reverse-biased into the avalanche breakdown region. The minority carrier lifetime in the N region is very low, probably less than 10^{-7} seconds, so that the unit can be considered as two independent diodes in series.

Assuming a preirradiation minority carrier and lifetime of 10^{-7} seconds and $K_0 = 10^{-7}$, from Equation (5), the minority carrier lifetime decreases to 7×10^{-8} seconds after a neutron dose of $5 \times 10^{13} \text{ nv}_e \text{ t}$. The majority carrier density changes are negligible ($\sim 10^{13} \ll 10^{17} \text{ carrier/cm}^2$).

From Equation (6), it is seen that, for the same current, the junction voltage will decrease by the order of 19 millivolts after a neutron dose of $5 \times 10^{13} \text{ nv}_e \text{ t}$. After a dose of $10^{14} \text{ nv}_e \text{ t}$, this junction voltage change would be of the order of 36 millivolts. After $10^{15} \text{ nv}_e \text{ t}$, the decrease in junction voltage should be about 120 millivolts. The change in junction voltage is much slower than the decrease in minority carrier since V_J is related to the minority carrier lifetime as the logarithm of the lifetime.

It is to be noted that by $10^{15} \text{ nv}_e \text{ t}$, the resistivity of the N region and therefore the avalanche voltage has increased by about 1 per cent for 5 volt diodes (approximately 50 millivolts) so that the net decrease in 1N429 reference element voltage will be 70 millivolts. (This represents approximately 1 per cent of the reference element voltage).

Reference to Tables 1 and 2 shows that at $5 \times 10^{13} \text{ nv}_e \text{ t}$, the decreases in reference voltage were from 17 to 41 millivolts for the 16 units tested. After exposure to $2 \times 10^{14} \text{ nv}_e \text{ t}$, from 20 to 50 millivolts. After $10^{15} \text{ nv}_e \text{ t}$, the reference element voltages had decreased by 25 to 90 millivolts. These values are in relatively good agreement with the calculations made above.

The effects of decreased forward conductivity will tend to change V_P and V_N across the P and N regions but these changes will be of the order of 1 per cent of the voltage of the forward-biased elements, yielding about 10 millivolts after a dose of $10^{15} \text{ nv}_e \text{ t}$ is reached.

The above discussion indicates that the consistent decreases in 1N429 reference element voltages with neutron irradiation is due to changes in the forward-biased element behavior.

As stated earlier, the type 1N429 diode has a reference voltage between 5.9 and 6.5 volts. The reference voltage, at 7.5 milliamperes, will not vary by more than 0.100 volt (± 0.050 volt) when the ambient temperature changes from -65°C to $+100^\circ\text{C}$. The changes noted in the reference voltages of the 16 elements which were irradiated show that these specification limits are exceeded in most cases. The mean change in reference voltage after exposure to approximately $10^{15} \text{ nv}_e \text{ t}$ was a decrease of 1.11 per cent of the preirradiation values. After $0.4 \times 10^{15} \text{ nv}_e \text{ t}$, the mean change was a decrease of 0.895 per cent. These

values are of the order of magnitude that can be accounted for by the mechanisms described above.

Post-irradiation measurements on 8 units showed recovery, i. e., increase in reference element voltage of approximately 1/3 per cent. The mechanism of recovery is not clearly understood, but it is probable that the recovery is due to the transient effects of radiation on the junction proper since the changes are too consistent for the small temperature variations which were encountered.

The performance of 1N429 elements during radiation exceeds the specified limits in practically all cases after an epicadmium neutron dose of $10^{15} \text{nv}_e \text{t}$, even though the temperature of the devices is only 6 degrees above ambient or room temperature.

DISCUSSION OF TYPE 1N430B REFERENCE ELEMENT BEHAVIOR

Over a range of -65°C to $+150^{\circ}\text{C}$, the reference element voltage of the type 1N430B at 10 milliamperes does not change from its 25°C value by more than ± 0.001 per cent per degree Centigrade. This temperature compensation is accomplished by use of two selected forward-biased diodes in series with a third diode which is biased into the avalanche breakdown region. These three units are press-fitted into an aluminum slug before encapsulation.

From the discussions on the behavior of the forward-biased element of the type 1N429 device, it is to be expected that this device type will suffer larger changes in the reference voltage since there are two forward-biased diodes in series. The avalanche voltages (and hence the resistivities) of the reverse-biased diodes of the 1N429 and 1N430B are approximately the same value.

Examination of the test results presented earlier in Figures 3 and 4 and Tables 3 and 4 show this to be indeed the case.

Assuming again a preirradiation minority carrier lifetime of 10^{-7} sec, the 1N430B reference element voltage should decrease by $(2 \times 36) = 72$ millivolts after an epicadmium neutron dose of $10^{14} \text{nv}_e \text{t}$. Examination of the results tabulated in Tables 3 and 4 show that changes of 60 to 170 millivolts were recorded in the units tested. After a dose of $5 \times 10^{14} \text{nv}_e \text{t}$, the computed decrease in reference element voltage, with a case temperature of 52°C , will be 109 millivolts minus the change in the avalanche voltage which is less than 20 millivolts. This computed value corresponds to a decrease of approximately 1.1 per cent in the reference voltage. The actual values of changes in 1N430B reference element voltage after the dose were decreases ranging from 0.51 to 2.9 per cent, with a mean value of

approximately 1.5 per cent. Again, the agreement between calculated and measured changes due to radiation is relatively good. Note that the percentage and millivolt decreases for the 1N430B are higher than those for the 1N429, as expected. These values are considerably outside the specified limits. The forward-biased diodes which provide excellent temperature compensation cause the departure from specified performance. Recovery of 5 to 15 millivolts is noted in the eight units on which post-irradiation data were recorded.

GAMMA IRRADIATION

A gamma irradiation was performed at the Cook Electric Company Cobalt-60 facility in Morton Grove, Illinois. A dose of 2×10^6 roentgens at a flux of 0.75×10^6 roentgens per hour caused no changes in two 1N429 and two 1N430 devices. The temperature of the cases rose a few degrees.

CONCLUSIONS

Changes in temperature stabilized silicon reference elements due to neutron irradiation can cause the reference voltage to fall outside the specified limits even at normal temperature conditions.

The actual doses at which the departure occurs will depend on the type of units used. Tests during irradiation are necessary since partial recovery is noted several hours after the irradiation is terminated.

BIBLIOGRAPHY

1. Xavier, M. A., First Semiannual 125A Radiation Effects Symposium
2. Xavier, M. A., The Behavior of Semiconductor Junction Rectifying Devices Exposed to Nuclear Radiation, Ph. D. Thesis, Illinois Institute of Technology (January, 1958)
3. Hall, R. N., Power Rectifiers and Transistors, Proc.IRE. 40, (November, 1952) 1512-1518
4. Prince, M. B., Personal Communication
5. Cleland, J. W., et al, Fast Neutron Bombardment of N-Type Germanium, Phys. Rev. 98 (June 15, 1955) 1742-1750
6. Cleland, J. W., et al, Fast Neutron Bombardment of P-Type Germanium, Phys. Rev. 99 (August 15, 1955) 1170-1181
7. Pigg, J. C. and Robinson, C. C., Effects of Radiation on Semiconductors, Elec. Mfg. (April, 1957) 116-124
8. Curtis Jr., O. L., Cleland, J. W., Pigg, J. C., Effect of Irradiation on the Lifetime of N-Type Germanium, Bull. Amer. Phys. Soc., Vol 2, No. 3, 157A (1957)
9. Messenger, G. C and Spratt, J P., The Effects of Neutron Irradiation on Germanium and Silicon, Proc.IRE, 46, No. 6 (June, 1958) 1038-1044
10. Xavier, M. A., Scientific Report No. 2, Research to Determine the Effects of Nuclear Radiation on Semiconductor Electronic Components, AF Contract 33(616)-3776

EFFECTS OF ELECTRON BOMBARDMENT ON CADMIUM SULFIDE WHISKERS

by

B. A. Kulp and D. C. Reynolds
Aeronautical Research Laboratory
Wright Air Development Center

ABSTRACT

Edge emission normally found in large crystals of CdS is not found in CdS whiskers and platelets in the as-grown condition. Bombardment of these whiskers by 700 and 500 kev electrons has brought out this emission. The threshold for producing the effect is being determined.

INTRODUCTION

Absorption spectra of semiconducting materials is characterized by a rather sharp absorption edge at a wavelength characteristic of material. For CdS the edge occurs at about 5200 Å at room temperature. The fluorescent emission spectra of those materials when excited by ultra violet light and observed at liquid nitrogen temperature generally has a band of radiation at the long wavelength side of the absorption edge. This band is commonly referred to as edge emission. In cadmium sulfide it consists of six lines and is green in color. Edge emission has been observed in many semiconductors including silver halides², germanium³, ZnS and ZnO⁴.

The mechanism of edge emission is uncertain. An early theory attributed it to recombination of excitons⁵ (coupled electron hole pairs which are capable of transmitting energy through the lattice⁶). More recently a study by Lambe, Click and Dexter⁷ suggests that edge emission occurs as a result of the recombination of a free hole with an electron trapped at some imperfection. However, with the present information no conclusive statement can be made as to the identity of the recombination center. The results of the experiments described here should contribute greatly to the understanding of this phenomena.

EXPERIMENTAL PROCEDURE

Figure 1 shows the crystal growing furnace used to grow Cadmium Sulfide Crystals by the vapor deposition method⁸. CdS powder is placed in a ceramic boat in the center of the furnace. The CdS is evaporated and deposits as single crystals on the seed plates at either end of the furnace. A temperature gradient exists between the center of the furnace and the seed plates. When it is desired to grow whiskers, the seed plate at the left is removed and the CdS deposits in the form of whiskers and platelets in the vicinity of the tube formerly occupied by the seed plate.

Figure 2 shows some of the large crystals after polishing. The crystals vary in size but commonly are $1/2 \times 1/2 \times 1/2$ inches or larger. Figure 3 shows a whisker which is about 3 microns in diameter and several cm. long. It has a perfect hexagonal cross section. The two parallel faces are very evident in the figure.

Figure 4 shows a platelet as grown, and Figure 5 shows a platelet with a twin fault. The whiskers and platelets do not show edge emission in the as-grown condition except at the twin fault line shown in Figure 5.

Brenner and Sears⁹ have postulated that whiskers are the result of crystal growth from a single screw dislocation. Figure 6 shows the etch pattern of such a dislocation. Crystal growth takes place along the spiral edges. Such a crystal should be dislocation free except for the one down the axis of the crystal and should have tensile strength approaching the theoretical limit. Figure 7 shows a 2.7 micron whisker bent to a radius of about six microns. This represents a strain of 2.4 percent and strength near the theoretical limit. Figure 8 shows the same whisker after release showing no permanent strain in the crystal.

The first bombardment experiments were carried out with a Van de Graaff generator with electron energies of 700 Kev and 500 Kev. Bombardments were made below room temperature and edge emission was observed at liquid nitrogen temperature after both bombardments. Current experiments are being carried out with the Cockcroft-Walton accelerator shown in Figure 9 and are expected to show a threshold for the production of edge emission below 250 Kev. In these experiments the sample is held at liquid nitrogen temperature during the bombardment and observation.

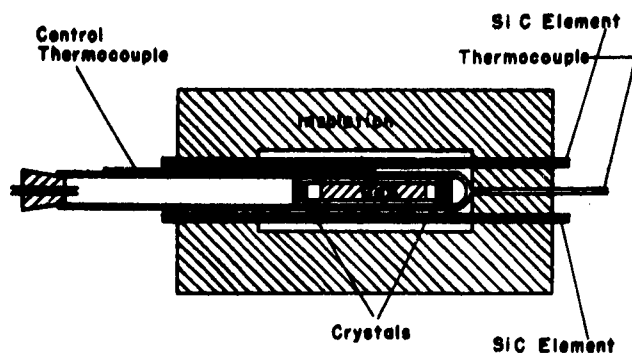
DISCUSSION

If it is assumed that a sulfur vacancy is responsible for edge emission in CdS, then a 250 Kev threshold energy would indicate a displacement energy of 21.4 ev for a sulfur atom. This compares with a reported 25 ev for copper¹⁰, 12.9 ev for the displacement of a germanium atom¹¹ and 6.2 ev for the displacement of an antimony atom in the InSb lattice.¹²

Further work is being directed toward a more accurate measurement of the threshold energy and a thorough investigation of the effect of electron bombardment on cadmium sulfide.

REFERENCES

1. C. C. Klick, J. Opt Soc Amer., 41, 816 (1951).
2. Farnell, Burton and Holloman, Phil Mag., 41, 157 (1950).
3. J. R. Haynes and H. B. Briggs, Phys Rev., 86, 647 (1952).
4. J. Ewles, Proc. Roy. Soc London, A 167, 34 (1938).
5. F. A. Kroger, Physica, 7, 1 (1940).
6. N. F. Mott and R. W. Gurney, Electronic Processes in Ionic Crystals, (Oxford, Clarendon Press (1936)).
7. J. J. Lambe, C. C. Klick and D. L. Dexter, Phys Rev., 103, 1715, (1954).
8. D. C. Reynolds, and S. J. Czyzak, Phys. Rev., 79, 543 (1950).
9. S. S. Brenner and G. W. Sears, Acta Metallurgica, 4, 268 (1956).
10. D. T. Eggen and M. J. Laubenstein, Phys Rev., 91, 238 (1953).
11. J. J. Loferski and P. Rappaport, Phys Rev., 98, 1861 (1954).
12. F. H. Eisen, P. W. Bickel, and A. Sosin, Third Progress Report on Contract AF 33(616)-3924 (Jan 31, 1958).



CROSS SECTIONAL VIEW of CRYSTAL FURNACE

Figure 1. Crystal Growing Furnace

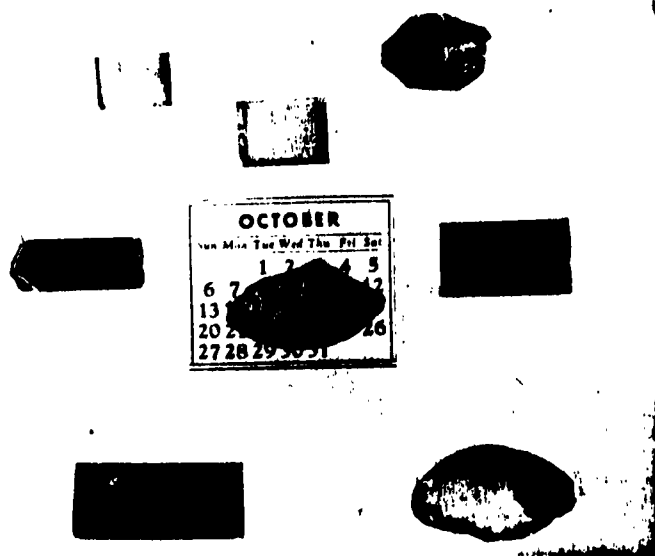


Figure 2, Cadmium Sulfide Crystals



Figure 3. Cadmium Sulfide Whiskers

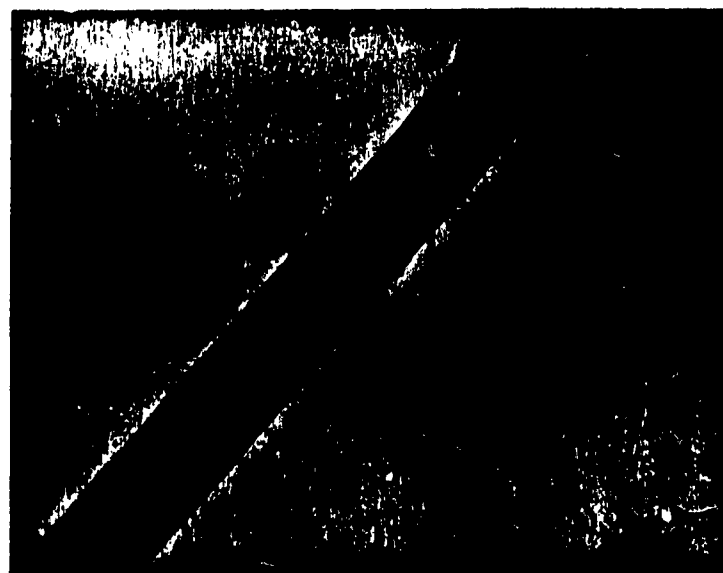


Figure 4. Cadmium Sulfide Platelet

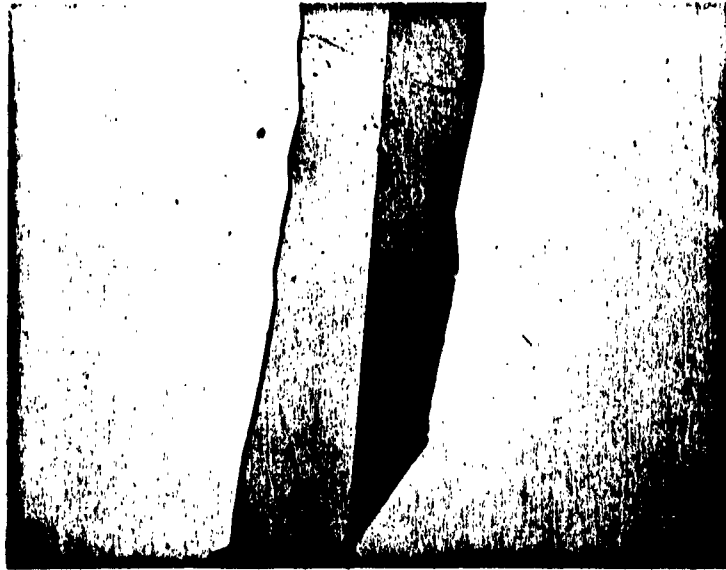


Figure 5. Twin Cadmium Sulfide Platelet



Figure 6. Crystal Growth About a Single Screw Dislocation



Figure 7. 2.4 Percent Strain in CdS Whisker



Figure 8. Whisker of Figure 7 and Removal of Constraints

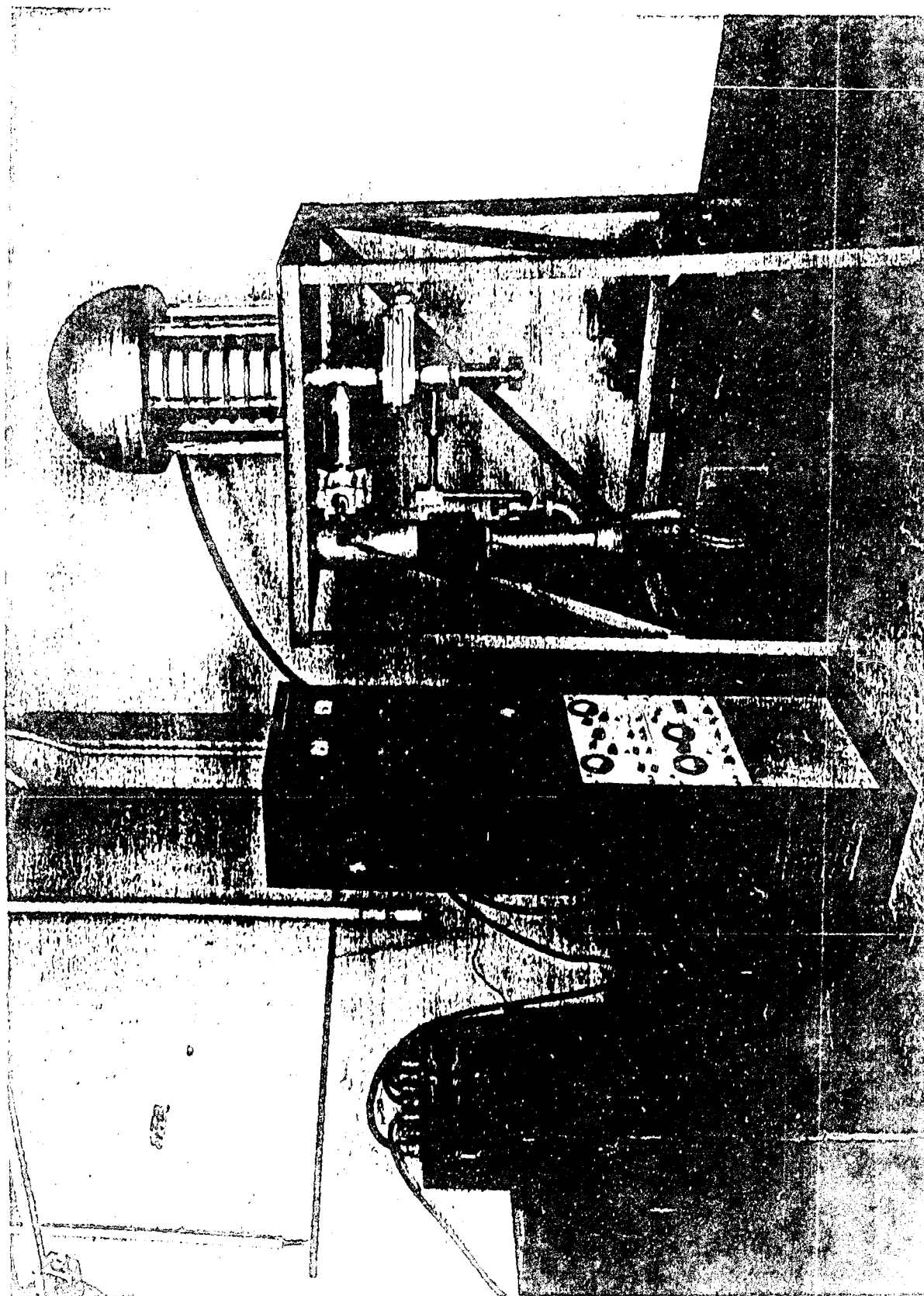


Figure 9. 250 KeV Cockcroft-Walton Accelerator